Structural studies of the thick filament positions in the A-band of vertebrate striated muscle

Thesis

STRUCTURAL STUDIES OF THE THICK FILAMENT POSITIONS IN THE A-BAND OF VERTEBRATE STRIATED MUSCLE.

Thesis submitted for the degree of Doctor of Philosophy in the Discipline of Biophysics.

by

Richard John Ward, BSc

Open University

March 1987

Date of Submission: 13.3.87
Date of Award: 3.6.87

ABSTRACT.

Equatorial X-ray diffraction analysis has been largely concentrated on spacing changes alone, although it is widely acknowledged that the reported observations showing broadening and weakening of these reflections seen on a change of physiological state (eg relaxed to contracted), or on changed conditions in the bathing solution (eg addition of high molecular weight polymer) are due to filamentary disorder.

Using electron microscopy (EM), the thick filament positions in the A-band were traced, digitized and compared to the ideal computer generated positions of the filaments. The analysis showed a systematic distortion corresponding to a bowing of the filaments at short sarcomere lengths in rigor. This bowing decreased with addition of 5mM pyrophosphate (PPi) to the rigor solution, and increased when the pH of the solution was reduced to pH5, or on transition from the relaxed to contracted state.

Comparison of the EM data to the width of the (1,0) reflection as seen with X-ray diffraction show that under conditions where the bowing increases, the width of the peak also increases. Fourier transforms together with optical diffraction studies of the EM pictures show that the bowing has a broadening effect on the peak width.

At longer sarcomere length (S), the X-ray diffraction results show that peak width is increased, and this increase is reduced by 5mM PPi. EM results show that the bowing at longer S is reduced or absent, but that there is an increase in the short range liquid type disorder between filaments, and this is reduced by PPi. Fourier transforms and optical diffractograms of the EM pictures at these longer sarcomere lengths confirm the X-ray diffraction observation.

These results show that the X-ray diffraction peak width is

determined by both the degree of the bowing and the short range local disorder within the A-band lattice.

A model to explain the bowing effect is suggested in which the thick filaments are bent by a bending couple formed from repulsive electrostatic forces acting over the whole thick filament but whose point of action is the M-line, and attractive cross-bridge restraining forces acting over the overlap region whose point of action is at the centre of the overlap zone. These two forces will be equal, opposite and separated by a given distance, so will constitute a bending couple. The point at which the two forces are equal and opposite will vary under changing conditions so the spacing of the filaments will change under the varied conditions, and so is in agreement with the idea that the filaments will be at a spacing where the resultant force over the whole filament is zero.

ACKNOWLEDGEMENTS.

I would like to thank Prof. Gerald Elliott for the many ideas and discussions over the three years, Drs R.A. Bergman and K.A.P. Edman for kindly providing electron micrographs of contracting muscle. I would also like to thank Dr Jonathan Kentish for collaboration with the mechanical studies, and Dr Finn Poulsen for advice with the X-ray and Fourier analyses and for reading the manuscript. I also thank Drs Else Bartels and Keith Meek for their advice and discussions over the years, and who with Dr Peter Cooke and Mr Tony King taught me the skills of the electron microscopist. I further thank Mrs Dawn Collins and Mrs Rosemary Hughes for technical assistance and general lab training (quite an achievement!). I thank Ingrid White for her help with the JEOL CX-100 at Oxford University, Dr Colin Nave for assistance at Daresbury, and Dr Derek Cummings for tolerating my fulminations over various computer terminals. Finally, I thank everybody at the ORU for encouragment in the lean times and enthusiasm in the good.

CONTENTS.

INDEX OF TABLES.

INDEX OF FIGURES.

INTRODUCTION.

It is more than three decades since the sliding filament model for length changes in striated muscle was proposed, simulataneously and independently in two articles in the same issue of Nature, by A.F Huxley and R. Neidergerke (1954), and H.E Huxley and Jean Hanson (1954).

There is now an abundance of evidence for this model; evidence from biochemistry, from light- and electron-microscopy, from X-ray diffraction and from mechanical studies of the properties of intact muscle. I do not propose to repeat this evidence in this Introduction, it has been the subject of several teaching and review monographs of which the most recent include A.F Huxley (1980), Harrington (1981) and Bagshaw (1982). An older, but very comprehensive, review is Bendall (1969). The model is also the subject of an Open University Course Unit, Unit 12 of S324, Animal Physiology (1985). The sliding filament model will be taken as axiomatic in this thesis.

Current interest in the model centres on the actual means of force production within it. Majority opinion favours the swinging cross-bridge theory, proposed in slightly different forms by H.E Huxley (1969) and by A.F Huxley and Simmons (1971). The tension generation according to this theory arises from a conformational changes in the mysoin head (S1) as it attaches to and detaches from the thin filament in a cyclic manner. Chemical energy, from ATP hydrolysis, is converted to mechanical energy to fuel the contraction. For balance, the critical review by Pollack (1983) analyses some of the aspects of the theory from a different viewpoint. Other theories have also been proposed, amongst them that of Elliott et al (1970) who proposed that tension in a contracting muscle derives from electrostatic repulsion between filaments, raising the possibility that

radial forces may be important in axial force generation. It is also approriate to mention the theory of Harrington (1971), which suggests that the tension might arise from mechanical effects in the S2 link between the myosin head and the myosin filament backbone.

1.1. The effects of radial forces.

Previous work on striated muscle has usually concentrated on the spacing changes seen under various conditions eg relaxed, rigor states, intact or skinned fibres, ionic strength, pH etc (eg Matsubara and Elliott (1972), April Brandt and Elliott (1971),(1972), Rome (1966),(1968)). The interpretation of the spacing changes has been based round the idea of a balance of attractive and repulsive forces between filaments in the myofilament lattice (Elliott (1968)). In many of these studies, it has been pointed out in passing that equatorial or meridional reflections become more or less diffuse with changing conditions (eg Yagi and Matsubara (1977), Magid and Reedy (1980)), and this has usually been attributed to changes in "filamentary disorder". In only one study, by Yu et al (1985), where peak broadening is seen going to the contracted state from the relaxed, is this effect specifically described as due to a liquid type disorder. In early experiments in our laboratory it was noted that pyrophosphate (PPi) caused the equatorial and the meridional reflections to sharpen up; this observation has also recently been repeated by Brenner et al (1986). In this thesis parallel X-ray and EM studies have been pursued to try to shed light on this effect.

Many EM pictures in the literature showed the thick filaments in the sarcomere to be bent, resulting in a barrel or cone-shaped appearance (see Fig 1.1). These bowed sarcomeres are apparent in striated muscle from a wide variety of phyla, and the phenomenon is

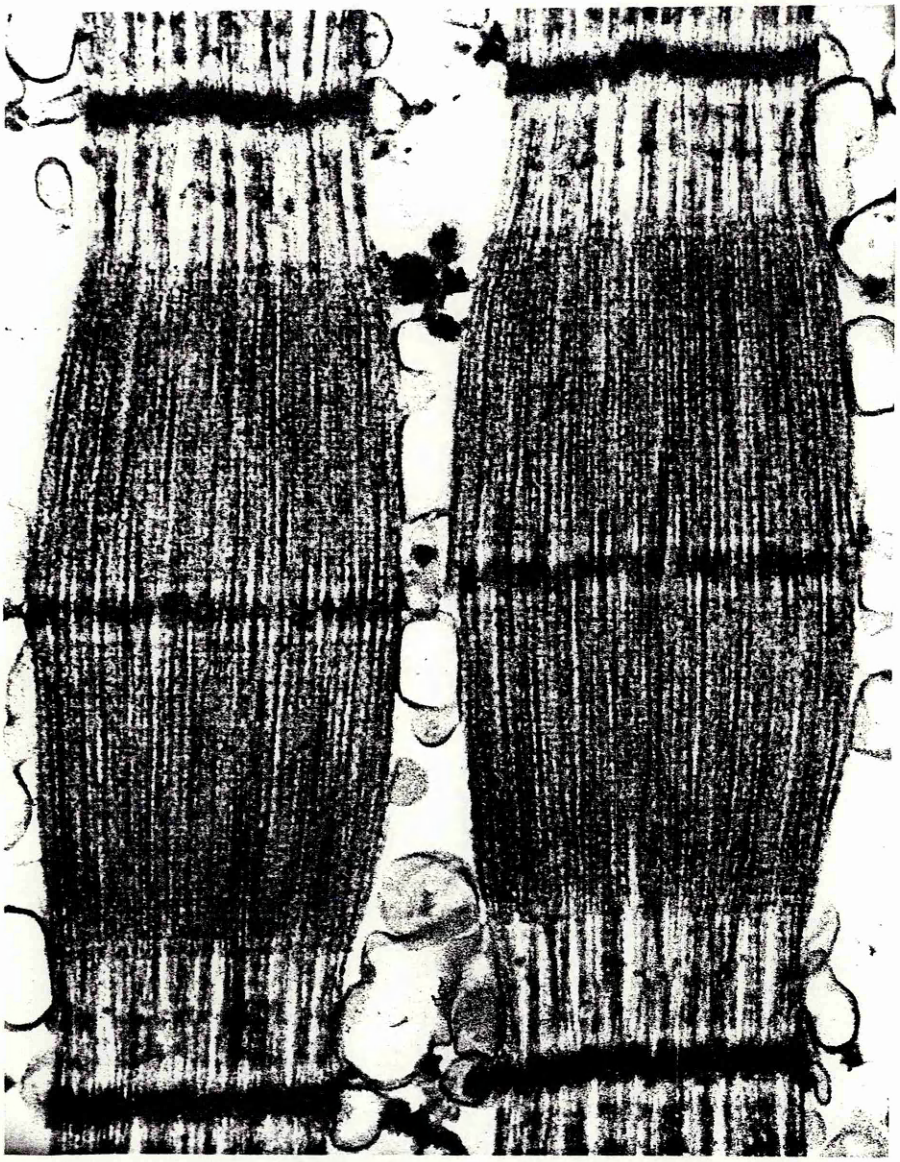

Fig 1.1 Sarcomeres of glycerinated rabbit psoas muscle in rigor at pH5 (S=2.6 μm). Under these conditions, the bowing in the A-bands of the sarcomeres is particularly clear. (x51500).

seen in both skeletal and cardiac muscle. The bowing has also been observed in the long sarcomeres of a crab muscle under the light microscope (Maeda (1978)).

A systematic electron microscopy study of the bowing phenomenon was carried out by Bergman (1979) in frog, and it is a pleasure to acknowledge that this paper was the seed from which this thesis project grew. This paper will be considered in detail at the beginning of Section 1.4.

The bowing has also received some attention from Goldspink (1972) who supposed that the lateral force on the Z-line might be increased during contraction and enhanced by bowing so leading to a splitting of myofibrils. He argues that this force would be greatest in the wider sarcomeres and so there will be a tendency for wide fibrils to split into smaller ones. He further supposes that not only does this facilitate a more rapid excitation of filaments (since the cross sectional area of the fibrils is always small), but also that fibrils splitting is the mechanism by which the number of myofibrils increases in growing muscle.

The preliminary results from our own EM study showed that bowing was indeed reduced by PPi, and this prompted a closer examination of EM pictures together with a thorough X-ray investigation. Whatever the reason was for the effects seen, the change in bowing had to be caused by radial forces, and so it seemed likely that the bowing was in some way related to spacing. A wealth of data already existed on the response of the myofilament lattice spacing to changes in bathing solutions, and these data too had to be explained in terms of the changes in balance of radial forces between filaments, so the rest of this introduction will be devoted to a review of the nature of these forces.

The forces acting on thick filaments in the A-band can be

divided into those acting to bring filaments closer together (attractive forces) and the opposite repulsive forces. These are listed in Table 1.1.

Table 1.1 Attractive and repulsive forces between filaments in the A-Band of striated muscle.

(a) Repulsive forces.

1. Electrostatic. Derived from the repulsion between the negatively charged thick and thin filaments. These forces have an exponential force law, to a first approximation (eg see Elliott (1968)).

2. At high compression, resistance to further compression appears, which has been suggested to arise from mechanical collision of lattice components (Millman and Nickel (1980)).

(b) Attractive forces.

1. London - Van der Waals forces. A long range attractive force between all filaments. These forces have an inverse fifth power force law, to a first approximation (Elliott (1968)).

2. Cross-bridges; these are physical links between thick and thin filaments, and may act as a mechnical constraint.

3. A possible radial component of the longtitudinal force in a contraction.

4. M-line/Z-line mechanical elastic force.

5. Other elastic elements, these probably comprise the third or intermediate filament lattice.

6. Osmotic forces, important in intact preparations, ie those with plasma membrane (Matsubara and Elliott (1972)) and shown to be active in demembranated preparations also (Elliott (1973b)).

Let us consider each of these forces in turn.

(a) 1.2. Repulsive forces acting on the filament.

(1) 1.2.1. Electrostatic forces.

Elliott (1968) showed that in theory, a balance between repulsive electrostatic double layer forces arising from charges on filaments and attractive London-Van der Waals forces could be achieved at a separation of 37 nm assuming a thick filament radius of 10 nm for non-overlap thick filaments. Later, Elliott (1973a) realised that the Van der Waals forces were probably too weak to be the major attractive constraint, and Matsubara and Elliott (1972) suggested that mechanical constraints, M- and Z-line, etc, probably were the major forces which opposed the electrical repulsive force.

This extented array of charged filaments in an ionic solution will cause the creation of a two phase system. The one phase inside the lattice is charged, and so will cause ions of the opposite charge to move inwards from the solution (which will be the other phase) to create an ionic imbalance between the two phases. This will give rise to a potential difference between the two phases which is called a

Donnan potential. Collins and Edwards (1971), using 3M KCl filled microelectrodes, showed that a Donnan potential could be measured between a glycerinated muscle preparation and a bathing solution, and using the Nernst equation, a value for the fixed average charge on a muscle protein could be calculated. It is this charge on the filament together with the attendant double layer which determines the magnitude of the electrostatic repulsive force. The original observations showed charge on the muscle proteins as a whole; subsequent studies have isolated two different Donnan potentials and so two separate charged regions in the A- and I-bands. These two charge systems have been shown in barnacle and rabbit (Bartels and Elliott (1981)), rat (Bartels and Elliott (1982)) and crayfish (Aldoroty and April (1984)), and are subject to change on varying the chemical composition of the bathing solution.

Increasing the pH increases the negative charge on the filaments by altering the charges on the amino acid side chains of the proteins in thick and thin filaments (Naylor et al (1985), Elliott et al (1985)). Increasing the ionic strength of the bathing solution (Naylor et al (1985)) also increases the charge on the filaments. The effect of changing ionic strength will be twofold, one will be to cause a change in the ions bound to thick filaments (Naylor et al (1985)), the other will be to change the concentration of the counter ions which form the double layer down to the filament. Both these will alter the effect of the electrostatic force between filaments. Decreasing sarcomere length has been shown to increase the Donnan potential measured, though it is likely this is a result of an increase in negative charge concentration within the A-band lattice brought about by an increase in overlap (Elliott (1973), Aldoroty et al (1985)). Further charge changes from the filaments can be caused by more physiological means. Adding ATP (or its analogue PPi) causes a reduction in charge (Bartels

and Elliott (1983),(1985)). Inducing the muscle to contract with raised pCa in the presence of ATP will cause the charge to increase from the observed relaxed value (Bartels and Elliott (1984a), Bartels and Elliott (1984b)).

(2) 1.2.2. Resistance to compression.

This effect appears under conditions of moderate to extreme lattice compression. Umazume et al (1986) in skinned frog fibres at a fixed S show that increasing osmotic pressure on the filament by soaking in solutions of high Mwt Polymer causes both fibre diameter and interfilament distance to decrease. At an interfilament spacing of ~35 nm there is a marked dislocation, and the size of shrinkage for a given increase in osmotic pressure is reduced beyond this point, indicating the action of a repulsive force resisting compression. Millman (1981) sees inflexion points in the rigor state in frog at ~38 nm and in relaxed rabbit muscle at ~40 nm (rigor rabbit data is unclear as to the inflexion point). A similar effect was seen by a Krasner and Maughan (1984) in rabbit muscle, though the dislocation was less well defined in this study. The explanation offered by Umazume et al is that compression of filaments brings about mechnical collision between S1 heads and actin filaments at about the ~35 nm spacing. Krasner et al also used the geometric relationship between S1 and thin filaments to explain their data. In the discussion, however, I will review other results indicating the effect maybe the result of double layer interaction, and so be of an electrostatic origin.

(b) 1.3. Attractive forces.

(1) 1.3.1. London-Van der Waals forces.

An attractive force between molecules was first postulated by Van der Waals who considered the attractive forces between two dipole molecules. The opposite charged regions of these molecules will attract each other, and furthermore each molecule will induce an enhancement of the dipole on the other by repelling like charges from the region nearest to it, so the nearer the molecules are to each other the greater the attraction. Expanding the theory, London in 1930 explained the liquefaction of He and H_2 by proposing universal attractive forces between all molecules, atoms, ions etc. Consider two atoms.

The basis of the expanded theory is that these atoms, due to the mobility of their own electrons are subject to fluctuations in the charge "cloud" surrounding the nucleus. These will cause fluctuating dipoles to be present which induce a dipole in the other atom, thereby causing attraction between the two. This effect also occurs in the other atom, and the result is a mutual influencing of the eletronic motions of both atoms causing the enhancement of the dipoles, and so enhancement of the attraction. Although this attraction is small between two atoms, the theory includes attraction in all particles, so in a system composed of aggregations of large molecules, the attractive force can be significant (Verwey and Overbeek (1948), Winterton (1970)). Elliott (1968) has shown that in theory, London-Van der Waals forces can balance the repulsive electrostatic double layer forces between thick filaments in striated muscle, the equilibrium position was at 37 nm using assumptions pluasible at that time. (Though note the later modification of the argument described above).

(2) 1.3.2. Cross-bridge attachment.

This involves the elastic constraining action of the cross-bridges; Tawada and Kimura (1986) have estimated that the compliance of cross-bridges is split twofold, 35% in the S2 link, but the major compliance (65%) is in the S1 head. Several studies have shown that as muscle passes from the relaxed state to the rigor state, a decrease in spacing of between 7-11% is seen at low sarcomere lengths (Matsubara and Elliott (1972), Matsubara et al (1984a), Matsubara et al (1984b), Goldman et al (1979) and Maughan and Godt (1981)). A decrease in spacing of 8-15% is also seen in contracting muscle (Shapiro et al (1979), Matsubara et al (1985), Brenner and Yu (1985)), and Krasner and Maughan (1984) report a small decrease in the skinned fibre diameter on activation. Goldman et al (1979) from studies of the transition of muscle from the relaxed to the rigor state concluded that cross-bridges exerted a radial force due to their elasticity. Matsubara et al (1984b) and Matsubara et al (1985) induced rigor tension in mouse muscle, measured the d(1,0) lattice spacing and released the muscle to remove the tension. On removal of the tension they found no change in spacing, and from this they concluded the change in spacing was due solely to the cross-bridge elasticity. Notice that this attractive force is a passive elastic force due to cross-bridges being strained, rather than the radial component of the axial force generated during contraction.

(3) 1.3.3. Radial Component of Axial Tension.

Due to the angle that S2 is thought to make to the thick and thin filaments, axial force generated during contraction will have a radial component. Schoenberg (1980) has calculated that in skinned

muscle this radial component will cause a 1-2% lattice shrinkage, but will cause no change in intact muscle contraction. Maughan and Godt (1981) subjected rigor muscle to stretches, and found a decrease of 4% in fibre width per $1x10^5$ Nm, somewhat larger than that predicted by Schoenberg. Elliott (1967) sees no spacing change in intact sartorius muscle on contraction, in keeping with the Schoenberg model. Other studies involving activation see much larger spacing changes, Shapiro et al (1979) report a 15% d(1,0) decrease on activation. This decrease was shown to be sarcomere length dependent. A smaller decrease was seen with increasing S, and since the force generated decreased with S this indicated that a decreased tension caused a decreased spacing shift. Other studies using Ca^{2+} activated fibres in frog (Brenner and Yu (1985)) and mouse (Matsubara et al (1985)) both show that the decrease in lattice spacing on contraction is related to tension. Both studies show that the radial force is not a constant fraction of axial force. The spacing changes in both these studies show larger spacing shifts than predicted by Schoenberg, 6% for the mouse on maximum activation and 15% for the frog.

(4) 1.3.4. M-line/Z-line Elasticity.

Using relaxed skinned fibres, April et al (1972) in crayfish and Rome (1968) in toad have both shown that there is an upper limit to the degree of expansion of the muscle lattice (175% and 150% respectively of the spacings in normal Ringer solutions). In other polyelectrolyte gel systems such as demembranated cornea where the diameter of collagen filaments and the charge they carry is similar to that in a muscle, the inter-filament spacing shows no upper limit on increasing hydration (Elliott et al (1982)). A comparison of the two systems indicates that in a muscle there must be a restraining force

constraining the swelling of myofibrils.

It has been suggested, that this restraining force arises from a mechanical elastic constraint in the M- or Z-line (Matsubara and Elliott (1972), Elliott (1968), Elliott et al (1980), Miller and Woodhead-Galloway (1971), April et al (1972)). Stromer et al (1967) extracted the M and Z-lines with very low salt concentration solutions, and an electron microscope analysis of 10 sarcomeres at the M-lines showed a small increase in spacing from 33.2 ± 2.2nm in intact muscle to 34.1 ± 2.3nm with extracted M- and Z-lines. However, the sarcomere lengths differed between the two samples, the extracted sarcomeres were at S equals 2.25 μm, the intact at 2.6 μm. This decrease in S will also tend to increase the spacing in the glycerinated muscle preparation used (Rome (1968)). The extreme extracting conditions may also have removed more than just M- and Z-lines.

(5) 1.3.5. Other elastic elements - intermediate filaments.

Apart from the thick and thin filaments in striated muscle, the existence of a third set of filaments has been the subject of debate since the earliest studies of myofilaments with EM (see Eremia (1985) for review), and the original hypothesis suggested that these filaments formed connections between Z-lines and thick and thin elements. A variety of combinations of connections have been suggested (see Eremia (1985)). Due to their size (7-10 nm in diameter), Wang (1983) has named them "intermediate filaments". The earlier models all concentrated on axial filaments, and Horowits et al (1986) have shown that low doses of radiation destroys the proteins titin and nebulin shown to make up these filaments (Wang (1984)). This destruction is accompanied by a large decrease in both active and passive tensions. Together with EM studies showing a drastic axial disordering of

filaments in the radiated samples in contraction, they suggest that the filaments are responsible for passive tension seen on stretching relaxed muscle, and keep the filaments in the centre of the sarcomere on contraction.

This network, however, is more extensive than simple axial connections. Loewy et al (1983) and Wang and Ramirez-Mitchell (1983) have shown that the intermediate filaments run throughout the sarcomere having a large number of radial fibres. The radial component of the system even extends to connections to the perimysium and extra cellular matrix, the level of the Z-line it links up with radial filaments from neighbouring fibres. Magid et al (1984), using an etching technique with EM, have seen a series of radial cross-struts as well as fibres extending from the end of the thick filaments to the Z-lines, and suggest, as do Maughan and Godt (1981), that these structures are responsible for radial stability under conditions of high fibre swelling. Interactions between axial and intermediate fibres has been invoked by Higuchi and Umazume (1986), who see a decrease in lattice spacing which is directly proportional to the passive tension imposed by stretching the mechanically skinned frog fibres. The decrease in d(1,0) increases even beyond thick/thin filament overlap, and they explain this as due to axial intermediate filaments pulling on radial intermediate filaments whose lateral force component causes the lattice to shrink. Cooke (1985) has characterised lateral structures in frog with a periodicity of 23nm at S=2.3 μm, the periodicity of these structures changes with the sarcomere length in a manner consistent with that of the *Neben* (commonly abbreviated to N) lines (Page (1968)). Since Wang (1984) has identified these points as sites of accumulation of Titin and Nebulin by antibody labelling, it is likely that these have a role in maintaining order within the sarcomere, as suggested by Cooke. They

may also be laterally linked and so play a part in regulation of radial lattice spacing.

(6) 1.3.6. Osmotic forces.

The muscle lattice with an intact sarcolemma exhibits an isovolumetric behaviour with increased sarcomere length, so a decrease in the lattice spacing compensates for an increase in S (Elliott et al (1963)). On skinning the fibres mechanically or chemically this constant volume behaviour disappears (Matsubara and Elliott (1972), April et al (1976)). Matsubara and Elliott (1972) proposed that the isovolumetric behaviour is preserved in intact muscles due to a combination of the Donnan effect and osmosis. The muscle proteins in thick and thin filament act as a polyelectrolyte gel with negative charge and in the presence of the sarcolemma the number of mobile ions will be closely regulated around a fixed level so that concentration may also be considered constant. As S is increased, the thick and thin element overlap decreases so effectively reducing the concentration of charges within the fibre. The Donnan effect will be reduced for such a decreased charge concentration, so mobile counter ions will leave the lattice, which will osmotically draw water from and so shrink the lattice. Removal of the sarcolemma by skinning removes the barrier which regulated the passage of ions. Now the ions may move into the lattice, drawing water in with them so leading to the swelling observed. Changing S now will mean that ions will enter from an extra cellular source, so the constant numbers of ions round the filaments is removed, allowing ions and water to enter the lattice causing it to swell. Whereas the phase boundary in the intact muscle is the permselective plasma membrane, in the demembranated rigor frog and rabbit preparation, it is now the A-band lattice since the

I-band is probably too incoherent to act as a boundary (Elliott (1973b)). In these preparations, a change in S will still alter the charge concentration in the A-band, and so some degree of osmotic effect will be expected in determining filament separation.

The skinned fibre does not lose its response to osmotic forces, and will shrink in response to concentrations of high molecular weight polymers in the bathing solution (eg Millman and Nickel (1980), Umazume et al (1986), Higuchi and Umazume (1986), Goldman et al (1979), Matsubara et al (1984a)). These changes in lattice spacing are reflected in changes in fibre width (eg Gulati and Babu (1985), Umazume et al (1986) and Krasner and Maughan (1984)). This increased shrinkage with increased polymer concentration has been used by many authors to measure the radial resistance to osmotic pressure compression and so allowed estimates of radial stiffness of the fibres to be made. These estimates can be used as a measure of the resultant radial forces operating in the myofilament lattice.

1.4. Bergman's results, and the initiation of this thesis project.

Bergman (1983) made a detailed electron-microscope (EM) comparison of passive (relaxed) and contracted sarcomeres for sarcomere lengths between 1.4 μm and 3.07 μm. He found that sarcomeres fixed in glutaraldehyde alone had no detectable tension during fixation, and were invariably rectangular in shape in longitudinal section, at all sarcomere lengths. If he added osmium tetroxide to the fixative, and at the same time stimulated the muscle electrically, he was able to prepare muscles fixed under active (contractile) tension. These muscles showed barrel-shaped distortion (bowing) for sarcomere lengths greater than 1.6 μm, and the degree of this bowing increased with sarcomere length in the range 1.6 $\rightarrow$ 3 μm.

In this range he suggested that the bowed sarcomeres could be approximated by a model based on a truncated cone.

For completeness we should mention that at shorter sarcomere lengths (S < 1.6 μm) Bergman showed that the sarcomere fixed under active tension bowed inwards at the centre, to produce a wheatsheaf-shaped distortion. Since it is not possible to produce such short sarcomeres consistently in glycerinated muscle, this range is not considered in this thesis.

At the time that Bergman (1983) paper appeared we had already seen in our work on the Daresbury synchrotron that glycerinated rabbit psoas muscles pseudo-relaxed with PPi showed much sharper equatorial X-ray reflections than those fixed in rigor conditions. In addition, for some time data from microelectrode measurments in A- and I-bands of striated muscle had been accumulating which showed large charge changes occuring under a variety of conditions (Bartels and Elliott (1981→1985), Elliott and Bartels (1982) and Aldoroty et al (1984)(1985)). In particular, it was found that the addition of ATP or PPi caused a large charge reduction in the A-band.

Taken together with the observation of the change in the sharpness of the equatorial reflections in the presence of PPi, it was an obvious question as to whether the charge change on the filaments affected the A-band structure, and whether any change could be correlated to the sharpness differences. Bergman's (1983) paper provided a clue to ways in which filaments might be distorted within the A-band, and this prompted an initial EM study with the changing PPi conditions.

The work proved promising, so the study was extended to include other conditions where charge or equatorial reflection sharpness showed significant changes, such as altered ionic strength, pH and S. Charge changes were also seen when fibres were activated (Bartels

and Elliott (1984a,1984b)), and so to find out whether or not the effects had any physiological significance, the analysis of X-ray and EM data was extended to include some of Bergmans EM pictures, which were kindly lent to us by Dr Bergman. We also made a literature search for data from activated frog fibres.

1.4.1. The objective of this thesis.

The objective of the project has been to compare EM data to X-ray diffraction data from striated muscle fibres, in conditions where the charge on the filaments in the A-band varied, in an attempt to find structural evidence correlating this charge change to changes in the equatorial reflection sharpness in X-ray diffraction and to filament bowing seen in the EM.

THE EFFECT OF CHANGING IONIC STRENGTH AND SARCOMERE LENGTH ON THE INTERFILAMENT SPACING IN RABBIT PSOAS MUSCLE.

Section 2.1 - Methods.

Adult rabbits (both male and female) were killed by cervical dislocation. All procedures were started within 1/2 hr and were completed within 1 hr of the rabbit's death. Bundles of psoas were removed and stretched to various sarcomere lengths (S). Resting length was about 2.4→2.6 μm in the intact animal. Other bundles were contracted in warm ringer solution to produce shorter S. All bundles were tied securely to perspex rods and glycerinated according to the method of Rome (1968). Samples were stored at -15 → -20°C. The period of use of each preparation ranged from within 1 to 4 months of glycerination, over which time no change was seen in response to the experiments performed.

Small ribbons of glycerinated muscle ~0.5 → 1 mm across were taken from the larger bundles and soaked for 1/2 → 1 hr in the experimental solution. Solutions were prepared by dilution from a stock (solution A), and the compostions are shown in Table 2.1.1. Ionic

Table 2.1.1. Composition of solutions of varying ionic strength used in the experiments.

SOLUTION	KCl (mM)	$MgCl_2$ (mM)	PO_4 BUFFER (mM)	I (mM)
A (Stock)	100	5	20	0.139

Dilutions of these solutions was as follows:-

SOLUTION	PARTS STOCK	PARTS DIST H_2O	I (mM)
A/2	1	1	0.071
A/5	1	4	0.029

strengths are calculated using the Perrin program (Perrin (1967)). The phosphate buffer was made using the potassium salts K_2HPO_4 and KH_2PO_4.

After soaking, samples were tied to perspex rings with cotton ligatures and placed in sealed cells with fresh soaking solution. The cells had mylar windows and narrow interwindow distance (~1-2 mm) to minimise X-ray absorbtion (see Rome (1967), PhD thesis, University of London). These were then placed in the X-ray beam of either a rotating anode GX6 or GX13 X-ray generator (Elliott Automation, Borehamwood, England) focussed by Franks cameras (Franks (1955)), with operating conditions as shown in Table 2.1.2.

Table 2.1.2. Operating conditions for rotating anode X-ray generators.

CURRENT (mA)	22	34
VOLTAGE (KV)	35	60
POWER (KW)	0.77	2.04

Exposure time used varied between 1/2 → 2 hrs depending on the sample and conditions (a long S generally needed a longer exposure time than a short S).

Equatorial patterns were recorded on film, developed and fixed after which (1,0) and (1,1) reflections were usually quite clear. The (1,0) spacing was measured using a Nikon 6C profile projector with 10x magnification, which allowed measurement of spacings to better than 0.1 mm. From the spacing of the (1,0) reflections, the d(1,0) could be calculated. The accuracy of the measurement depended to a large extent on the camera length of the system used to take the picture. Over the whole series of experiments 3 cameras were used with three different camera lengths; these are shown in Table 2.1.3. The values

given are for optimum conditions. Weak or diffuse reflections were measured with far less certainty, especially with the short camera where scatter from the backstop overlaps to a large extent with the (1,0) reflection.

Table 2.1.3. Camera lengths and ideal accuracy from those camera used in the ionic strength studies.

CAMERA	CAMERA LENGTH (m)	ACCURACY (%)
1 (GX6)	0.22	0.6
2 (GX6)	0.27	0.5
3 (GX13)	0.42	0.3

Pictures were taken over a wide range of S (1.8 → 4.2 μm) at three ionic strengths and these data were added to those already available from previous work to give sample sizes in all cases between 150 and 250. These equatorial X-ray data are stored on an ongoing data base and are taken from different studies undertaken by E.M.Rome, G.R.S Naylor, A.C Elliott, B.M Millman, T Racey, Jane-Anne Horne, J Ilowski, Tom Irving and Else Bartels. In these component Figures, my own data points comprise 1/3 → 2/3 of the total number. With this large amount of data it was possible to perform an accurate analysis of results. For each I, the data were divided according to S into 0.1 μm groups. This resulted in each group having between 10 and 20 points from which the mean ± SD was calculated. The results of a S vs d(1,0) plot are shown in Figs 2.2.1 → 2.2.3.

Meridional pictures were taken solely at the synchrotron radiation source at the SERC Daresbury laboratory. The specimen preparation was identical, as was film use and development, though the beam was here focussed by a monochromator. Exposure times were of the order 20 → 30 mins at typical operating conditions of 1.8 → 2.0 GeV.The

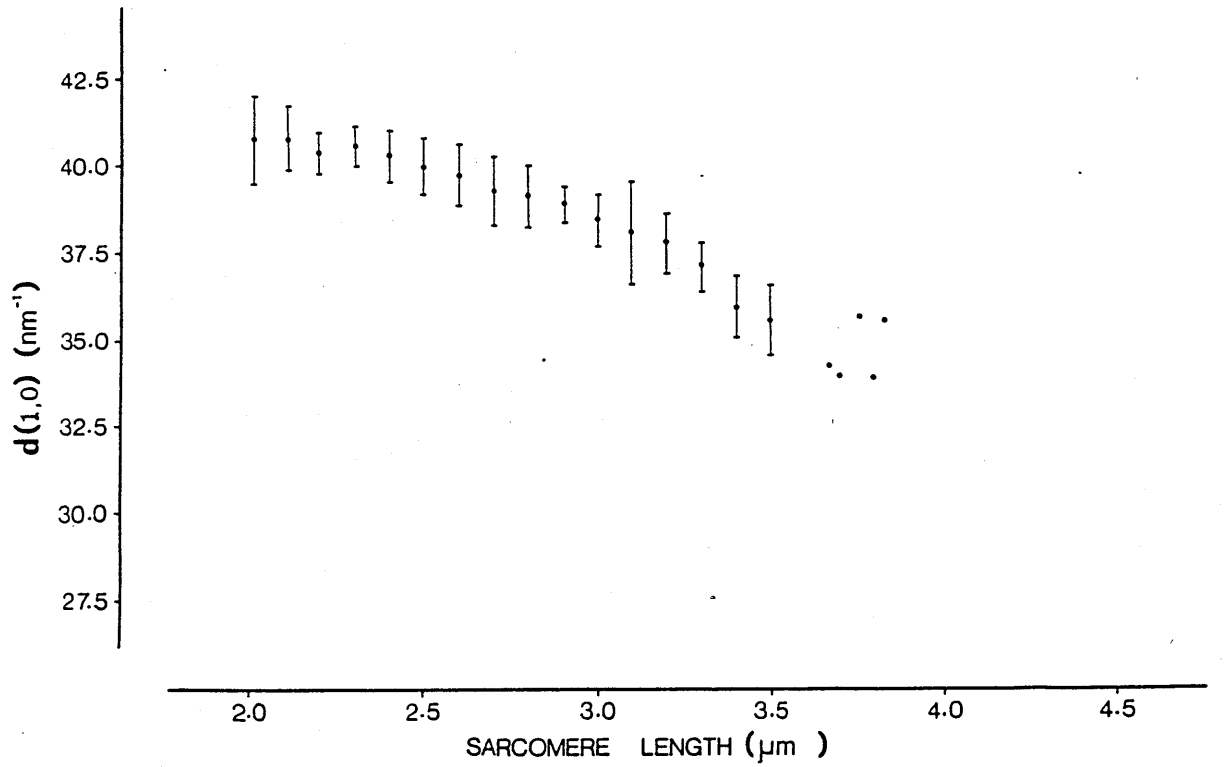

Fig 2.2.1 - d(1,0) vs S for I = 0.139 (A solution).

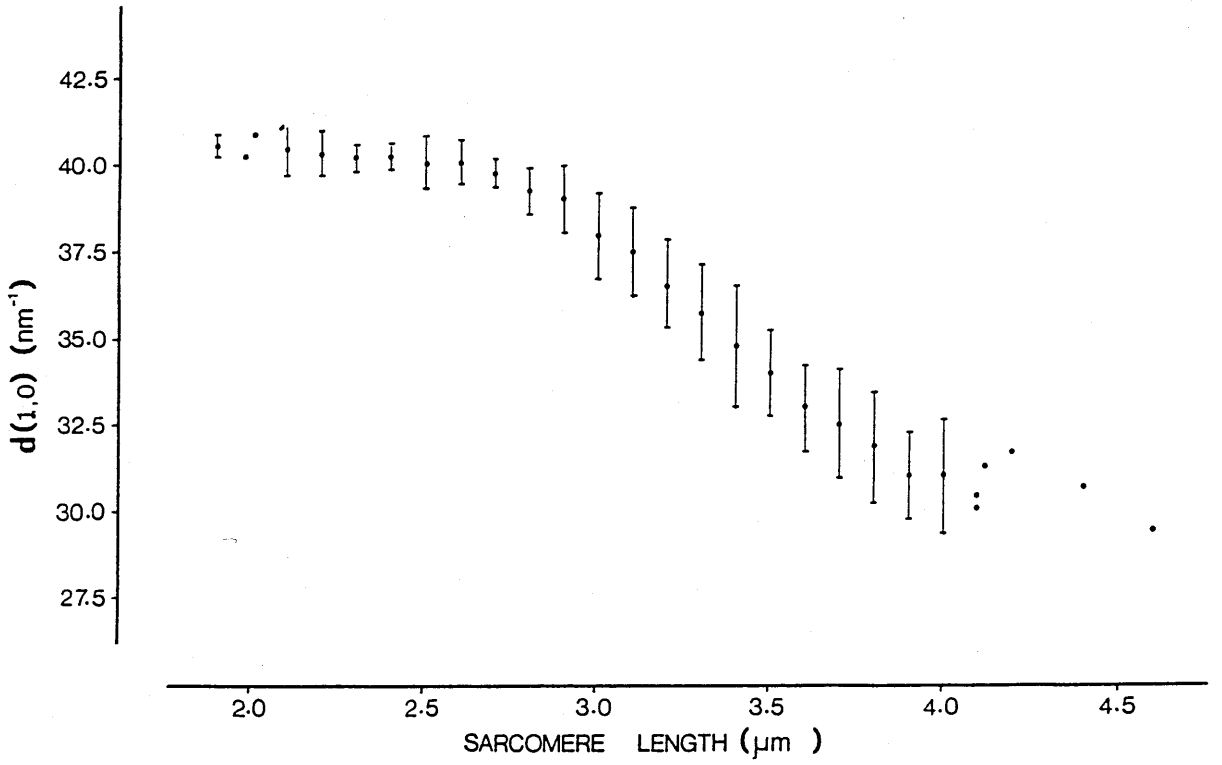

Fig 2.2.2 - d(1,0) vs S for I = 0.071 (A/2 solution)

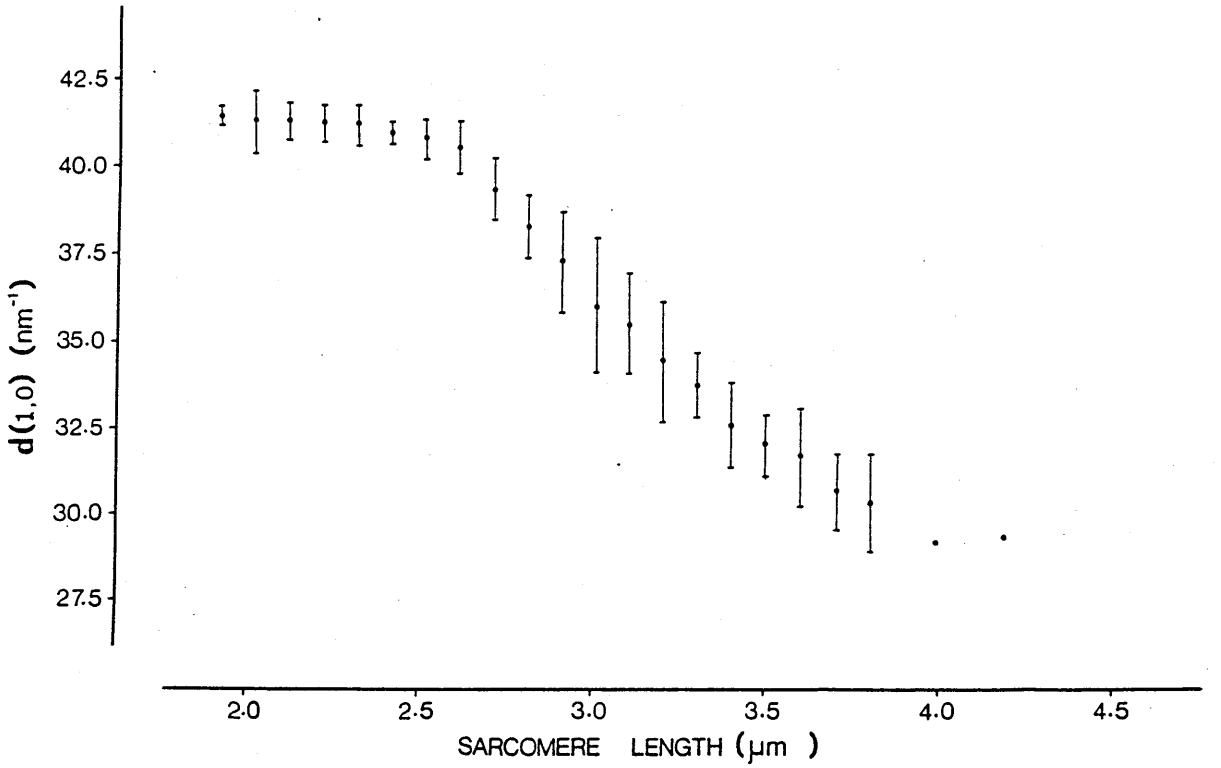

Fig 2.2.3 - d(1,0) vs S for I = 0.029 (A/5 solution)

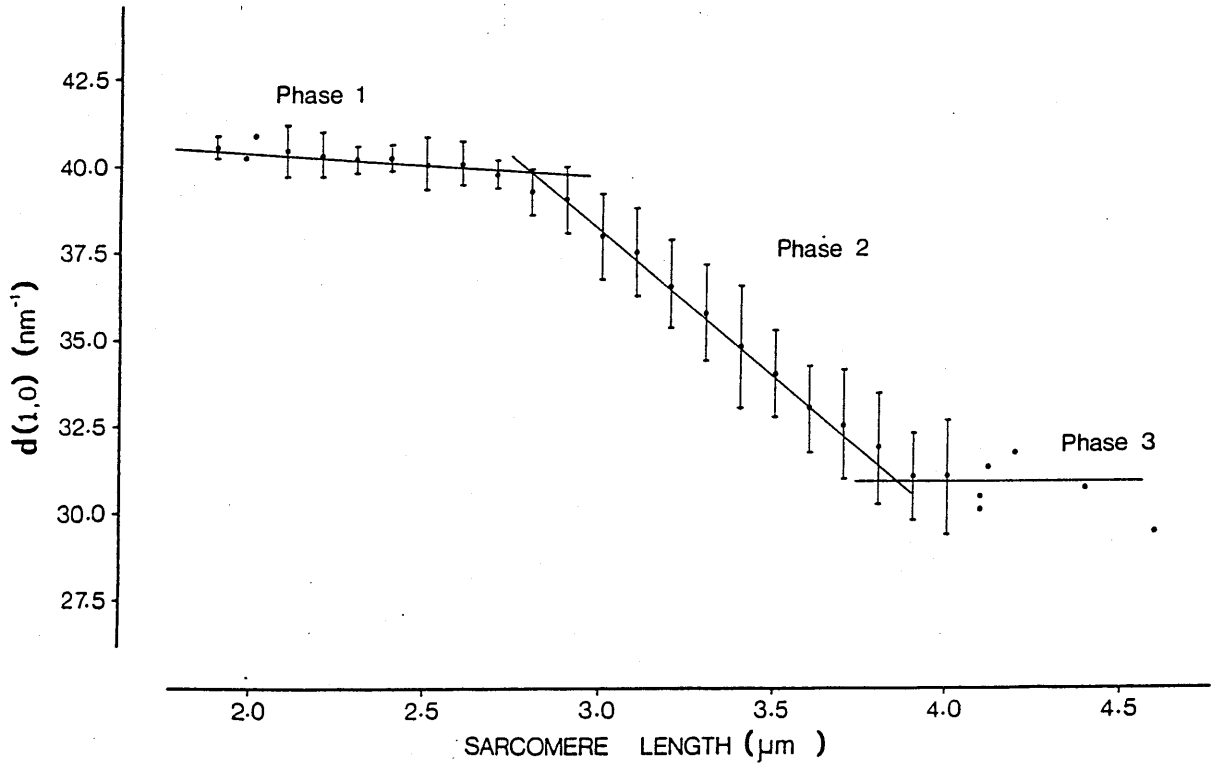

Fig 2.2.3.1 - Curve for I = 0.071 showing the division into three phases for analysis.

spacings in these pictures were calibrated by a wet rat tail tendon control which was assumed to have repeating orders of 67 nm. Spacings were measured using a travelling microscope to an accuracy of ~0.1 mm. This made it possible to measure spacing with a very high accuracy (0.2% or better was routine, even for poor pictures).

Section 2.2. Results.

The overall results of three experiments at various ionic strengths show that at short sarcomere lengths (S), *increasing* ionic strength *decreases* myofibrillar spacing as measured by the 1,0 reflection, whereas at long S the converse relationship holds true (see Table 2.2.1).

Table 2.2.1. Examples of variations of d(1,0) with ionic strength and sarcomere length. (n=10 → 20 for each point).

IONIC STRENGTH	d(1,0) (nm)			
	S = 2.1 μm	S = 2.6 μm	S = 3.2 μm	S = 3.8* μm
0.139 (A)	40.89 ± 0.81	39.69 ± 0.80	37.85 ± 0.83	≈ 35
0.071 (A/2)	40.52 ± 0.67	40.15 ± 0.66	36.59 ± 1.02	≈ 32
0.029 (A/5)	41.32 ± 0.56	40.60 ± 0.75	34.50 ± 1.70	≈ 30

* Values at this S are approximate due to lack of data.

These results are in general agreement with those obtained by Rome (1968), who varied ionic strength at a limited number sarcomere lengths, including 2.1 and 3.2. Plots of S vs d(1,0) for all three experiments give three curves showing a triphasic decrease of d(1,0) as S increases (see Figs 2.2.1, 2.2.2 and 2.2.3). The curves have been analysed assuming each of the three phases is a straight line (see Fig 2.2.3). Taking each phase separately and using a linear regression

Table 2.2.2. Linear regression results for phase 1 at three ionic strengths.

IONIC STRENGTH	S RANGE (μm)	EQUATION OF LINE	CORR. COEFF	GRADIENT
0.139 (A)	$\approx$2.3 → 2.9	d = 47.73 - 3.11s	0.99	- 3.11
0.071 (A/2)	< 2.6	d = 42.10 - 0.79s	0.92	- 0.79
0.029 (A/5)	< 2.3	d = 42.43 - 0.53s	0.91	-0.53

Table 2.2.3. Linear regression results for phase 2 at three ionic strengths.

IONIC STRENGTH	S RANGE (μm)	EQUATION OF LINE	CORR. COEFF	GRADIENT
0.139 (A)	3.1 → 3.8	d = 52.75 - 4.79s	0.85	- 4.79
		d = 57.88 - 6.34s*	0.99	- 6.34
0.071 (A/2)	2.9 → 3.6	d = 64.37 - 8.67s	1.00	- 8.67
0.029 (A/5)	2.6 → 3.4	d = 65.07 - 9.51s	1.00	- 9.51

* Since data at long S is incomplete, and therefore the point at which phase 2 ends poorly defined, data which may be contributing to phase 3 is excluded to obtain this second fit.

Table 2.2.4. Linear regression results for phase 3 at three ionic strengths.

IONIC STRENGTH	S RANGE. (μm)	EQUATION OF LINE	CORR. COEFF	GRADIENT
0.139 (A)	-	-	-	-
0.071 (A/2)	> 3.8	d = 32.07 - 0.27s	0.1	- 0.27
0.029 (A/5)	-	-	-	-

- Due to lack of data at long sarcomere lengths, only the A/2 curve was analysed - note even here the low correlation coefficent.

routine on data judged to fall within that phase, all three curves were analysed resulted in a series of equations describing each phase (see Tables 2.2.2, 2.2.3 and 2.2.4).

As ionic strength is increased, the gradient of phase 1 becomes *more* negative, whereas that of phase 2 becomes *less* negative. This behavior shows itself in the original data as a less pronounced "hump" as ionic strength increases. Data are lacking at longer S, so phase 3 analysis was only possible for the A/2 curve. This showed a small gradient with a low correlation coefficient, so assuming a horizontal straight line above S ≈ 3.8 μm does not seem unreasonable.

In phase 2 an additional line can be drawn from the data for experiments at lower ionic strengths (see Table 2.2.5).

Table 2.2.5. A more detailed analysis of the phase 2 data for experiments at lower ionic strengths.

IONIC STRENGTH	S (μm)	EQN OF LINE	CORR. COEFF.	GRAD.	DIFFERENCE BETWEEN LINES
0.071 (A/2)	2.9→3.6	d=64.37-8.67s	1.00	-8.67	d=11.32-3.13s
	3.6→4.0	d=53.05-5.54s	0.97	-5.54	
0.029 (A/5)	2.6→3.4	d=65.07-9.51s	1.00	-9.51	d=10.27-3.09s
	3.4→3.8	d=54.80-6.42s	0.99	-6.42	

The difference between the two lines (found by subtracting the additional line equation from the main phase 2 line) shows they have a similar gradient (3.13 and 3.09) but differing intercepts (11.32 and 10.27), indicating they are very nearly parallel.

Since all three curves have been broken down into straight lines of varying slope, there will be points on the curve where the lines intersect and a change in gradient will occur. The most conspicuous of these dislocations, or "break points", occur between phases 1 and 2 and between phases 2 and 3. They have been characterized both by

reading values directly from the graph after fitting lines by eye, and by solving simultaneous equations of the lines involved. Considering first the break point between phase 1 and 2 (see Table 2.2.6);

Table 2.2.6. The position of "break-points" between phase 1 and phase 2, as found by solving simultaneous equations of the lines and as measured by eye.

IONIC STRENGTH	CALCULATED		BY EYE	
	S (μm)	d(1,0) (nm)	S (μm)	d(1,0) (nm)
0.139 (A)	2.98,3.14*	37.61,38.55*	3.05 (2.95→3.16)#	38.5 (37.8→38.8)
0.071 (A/2)	2.83	39.8	2.81 (2.66→2.94)	39.8 (38.8→40.0)
0.029 (A/5)	2.52	41.1	2.52 (2.35→2.59)	40.8 (40.3→41.1)

* The two values shown correspond to the calculated intercepts of the two lines previously fitted for phase 2 in solution A (see Table 2.2.3).

See text below.

There is good agreement between the calculated values and those obtained by eye (the range of values given in Table 2.2.6 reflect the range over which one line merges into the other - the point of intersection is not as clearly defined as the calculated data may suggest). This shows that as ionic strength *increases*, the sarcomere length at which the break point occurs also *increases*. However, the d(1,0) at the dislocation *decreases* as the ionic strength is raised.

At low S (<2.2 μm) and high ionic strength (solution A), the phase 1 line levels off at a lattice spacing of ≈ 40.6 nm, this causes a minor inflection in the phase 1 at a S.L of ≈ 2.25 μm and d(1,0) of ≈ 40.5 nm.

The break point between phase 2 and 3 is, with the exception of

A/2, less well defined due to lack of data. The values in Table 2.2.7 are therefore only approximate.

Table 2.2.7. Characterization of the dislocation between phases 2 and 3 under conditions of increasing ionic strength.

IONIC STRENGTH	CALCULATED		BY EYE	
	S (μm)	d(1,0) (nm)	S (μm)	d(1,0) (nm)
0.139 (A)	-	-	≈ 3.8	≈ 33.7
0.071 (A/2)	3.98	31.0	4.0	30.8
0.029 (A/5)	-	-	3.9	29.3

Dislocations between these two phases all lie within the S range 3.8 to 4.0, but as ionic strength is *increased*, lattice spacing also increases; note this is the reverse behaviour to the situation between phases 1 and 2.

As noted earlier, in phase 2 at low ionic strength (A/2 and A/5), an additional line may be described (see Table 2.2.5). The intersection of this line with phase 3 gives the data in Table 2.2.7. Table 2.2.8 shows the the results of the analysis of the minor dislocation between the line and the main segment of phase 2.

Table 2.2.8. Characterization of the minor dislocation between the major segment of phase 2 and the additional line described in Table 2.2.5.

IONIC STRENGTH	CALCULATED		BY EYE	
	S (μm)	d(1,0) (nm)	S (μm)	d(1,0) (nm)
0.071 (A/2)	3.62	33.0	3.60	33.1
0.029 (A/5)	3.32	33.5	3.35	33.0

Here the d(1,0) at which the dislocation occurs is in both cases between 33 and 33.54 nm, but at the higher ionic strength the intersection is at a longer S.

2.2.1. SUMMARY.

Increasing ionic strength of the bathing media *increases* d(1,0) at long S, yet *decreases* d(1,0) at short S. The change in d(1,0) is essentially triphasic at all ionic strengths. The gradients of phase 1 *increase* with *increasing* ionic strength, whereas those of phase 2 *decrease* - from the limited data available at very long S it is assumed phase 3 has a negligible gradient.

Dislocations or "break points" from one region of the curve to another show that as ionic strength *increases,* the intersection of phases 1 and 2 occurs at a *longer* S, but a *smaller* d(1,0). However at the dislocation of phases 2 and 3, the S is roughly the same but the d(1,0) *increases* with *increasing* ionic strength.

A small but noticable discontinuity in phase 2 is observed at low ionic strength, which occurs in both cases at a d(1,0) of ≈ 33 nm. The gradients of these lines when subtracted from the main phase 2 data are also similar (≈ 3.1), but *increasing* ionic strength *increases* the S at which the intersection occurs.

THE EFFECT OF PYROPHOSPHATE ON X-RAY DIFFRACTION PICTURES OF RABBIT PSOAS MUSCLE IN THE RIGOR STATE.

Section 3.1 - Methods.

Bundles of glycerinated rabbit psoas were prepared as described previously in the ionic strength (I) experiment methods (Section 2.1). Small strips 0.5 → 1 mm were taken after 4-12 weeks, mounted in a perspex holder and soaked in control solution (see Table 3.1.1) which corresponded to the A/2 solution in the I experiment. A sequential soak method was adopted; the protocol followed was that one specimen was passed through A/2 solution to a 1mM pyrophosphate (PPi) and finally to a 5mM PPi solution. At each stage an X-ray picture was taken after a 1/2 → 1 hr soak in the solution. The 1mM and 5mM PPi solutions are shown in Table 3.1.1. All chemicals were obtained from BDH, except for PPi which was from Sigma chemicals, and were of "Analar" grade. Since the K_4 salt of PPi was used for the experiments, the I of the PPi solutions varied significantly, and so a number of experiments were conducted with a set of isosmotic PPi solutions, in which the K_2 salt was used and the I was kept constant at 0.071 by

Table 3.1.1. Composition of solutions used in sequential soak Δ[PPi] experiments.

SOLUTION	KCl	$MgCl_2$	PO_4 BUFFER	PPi	I
A/2	50	2.5	10	-	0.071
A/2 + 1mM PPi	50	2.5	10	1	0.076
1mM PPi isosmotic	48	2.5	10	1	0.071
A/2 + 5mM PPi	50	2.5	10	5	0.098
5mM PPi isosmotic	28	2.5	10	5	0.071

altering the level of KCl. Results obtained from the two set of solutions were the same.

X-ray pictures were taken using GX6 or GX13 rotating anode generators run at the same powers as for the I experiments (see Table 2.1.2). These pictures were used for measuring equatorial spacing changes only. The spacing of the (1,0) reflections were measured with a Nikon 6C travelling microscope for ~60 specimens which were subjected to the sequential soak for a range of S from ~1.8 → 3.5 μm. The difference in d(1,0) between control and the two solutions used was calculated and graphs plotted of S vs Δd(1,0).

Sharpness measurements were taken from equatorial data obtained at the synchrotron radiation source at the SERC Daresbury laboratory. In some instances film was used to record the patterns in which case the exposure time was ~15 → 30s. In other cases a linear counter was used - for these patterns it was necessary to attenuate the beam roughly 10 fold with Al filters to prevent counter overload, so longer exposure times of 2 → 3 mins were used. Data were analysed in two ways depending on whether film or counter was used.

(a) Film - The pictures were densitometered using an LKB ultroscan or Joyce-Loebl microdensitometer (Mk IIIc), a background was fitted by eye and the half height width (full width half maximum, FWHM) of the (1,0) reflection measured directly from the trace with calipers. Thespacing was measured again with calipers and the 'sharpness' of the peak defined as FWHM Δd/d(1,0) spacing.

(b) Counter - A slightly more complex method was employed here. All routines used were available on the Daresbury VAX in a package called OTOKO. The background was fitted by eye using a series of inputted points and interpolating a series of straight lines between them. The resulting trace was simply treated by drawing a straight line beneath the (1,0) peak joining the intersection at the x-axis of the trace, and

a point chosen to be the inflection point of the trace between the (1,0) and (1,1) peaks. The rest of the trace was subtracted leaving the (1,0) peak. This was subjected to a Gaussian curve fitting routine, and the value of the FWHM found. The spacing was found by counting the number of channels between the (1,0) peaks, and so FWHM/d could be found. More complex methods of isolating the (1,0) peak were tried which attempted to reduce the inaccuracies of the straight line and polygonal backgrounds used. These made little difference to the final result, and were very time consuming. Since reruns of the same procedure gave results consistent to within 5%, the more rapid method was chosen.

Various sarcomere lengths were used, and paired measurements of A/2 → A/2+5mM PPi were made by sequential soaking. This resulted in the paired data points seen in the graphs of $\Delta d/d$ vs S.

Meridional patterns were also taken for a number of specimens. In these cases film only was used, and an exposure time of 20 - 30 mins was sufficient to produce good resolution of meridional reflections as far out as the 14.4 nm as well as the first actin layer lines. Measurments of these films, together with those taken on previous trips to Daresbury, were made using a travelling microscope or calipers on a light box as previously described in Section 2.1 for the I experiments.

Section 3.2. Results.

Overall examination of patterns from experiments in A/2+1mM pyrophosphate (PPi) and A/2+5mM PPi compared to the control in A/2, showed less background scatter around the backstop region and a "sharpening up" of reflections with PPi, i.e faint reflections become stronger and all reflections become less diffuse. Table 3.2.1 shows the

Table 3.2.1. Meridional reflection spacings and qualitative assessment of intensities from rabbit glycerinated psoas muscle in control (A/2) and control + 5mM PPi solution.

A/2					PPi				
SPACING	n	S = 2.4	S = 2.84	S = 3.1	SPACING	n	S = 2.45	S = 2.76	S = 3.1
551.5 40.7	3				550.6 7.3	7			
443.8 2.1	10	Fairly weak	Weak	N.P*	443.7 1.5	20	Strong	Weak	V.weak
385.1 1.0	14	Strong	Less strong	Same as at 2.8	384.6 1.1	21	Strong	Less strong	Same as at 2.8
227.6 2.1	5	V.weak & diffuse	V.weak & diffuse	B.V@& v.diffuse	224.2 0.4	9	Fairly weak but sharp	Weak & diffuse	Weak & v.diffuse
213.3 1.6	8	Weak & diffuse	V.weak & diffuse	B.V & v.diffuse	213.6 1.2	9	Fairly weak & diffuse	V.weak & diffuse	V.weak & diffuse
192.0 1.0	8	Weak & v.diffuse	V.weak & v.diffuse	N.P	192.7 1.1	14	Weak	V.weak	V.weak
144.7 0.4	14	Strong	Weak	V.weak & diffuse	144.4 0.2	18	Strong	Fairly weak	Weak & diffuse
128.4 0.6	8	Weak & diffuse	B.V & v.diffuse	B.V & v.diffuse	128.2 0.3	11	Weak & diffuse	V.weak & diffuse	V.weak & v.diffuse
110.1 0.4	2	B.V & v.diffuse	N.P	N.P	109.8 0.6	5	V.v.weak	N.P	B.V
72.7 0.1		V.weak, sharp	B.V	B.V	72.4 0.3	11	Weak, sharp	V.weak, sharp	V.weak & v.diffuse
					64.9 0.3	9	B.V	B.V	B.V
					58.9 0.3	9	Weak & diffuse	V.weak & v.diffuse	V.weak & v.diffuse

* N.P - Reflection not visible

@ B.V - Reflection barely visible

measured spacings and qualitative assessment of the intensity of the reflections.

Since in all experiments the resulting picture showed the 38.4 nm reflection to be the most intense, and since differing exposure times were used, the intensity of the reflections is discussed in each picture relative to the 38.4 nm. In both the control and PPi experiments, an increase in sarcomere length causes a decrease in intensity of all reflections, including the 38.4 nm reflection. This effect is most striking in the 14.4 nm and 44.3 nm reflections. In all cases, the weaker and strong layer line reflections become more diffuse with increasing sarcomere length (in the case of the control this resulted in most of the weaker reflections becoming barely visible or even disappearing altogether e.g 19.2 nm and 11.0 nm).

Looking in more detail at the stronger reflections, the 44.3nm in both experiments decreased in intensity with increasing sarcomere length. However, with PPi the intensity relative to 38.4 nm increases so much that at short sarcomere lengths with 5mM PPi, the 44.3 nm and 38.4 nm reflections are approximately equal. Figs 3.2.1.1 and 3.2.1.2 show the densitometer traces at S=2.4 μm for control and PPi experiments and illustrates this increase in the intensity of the 44.3 nm reflection. The effect of PPi on the 22.4 nm reflection is similar; at short sarcomere length it is very weak and diffuse, and an increase in sarcomere length reduces its intensity and sharpness even further. However, with PPi both its intensity and sharpness increases.

The 14.4 nm reflection intensity decreases with increased sarcomere length, as does the sharpness in all cases, but with PPi the reflection retains a higher degree of sharpness than in the control A/2, though adding PPi appears to have little effect on the intensity of this reflection.

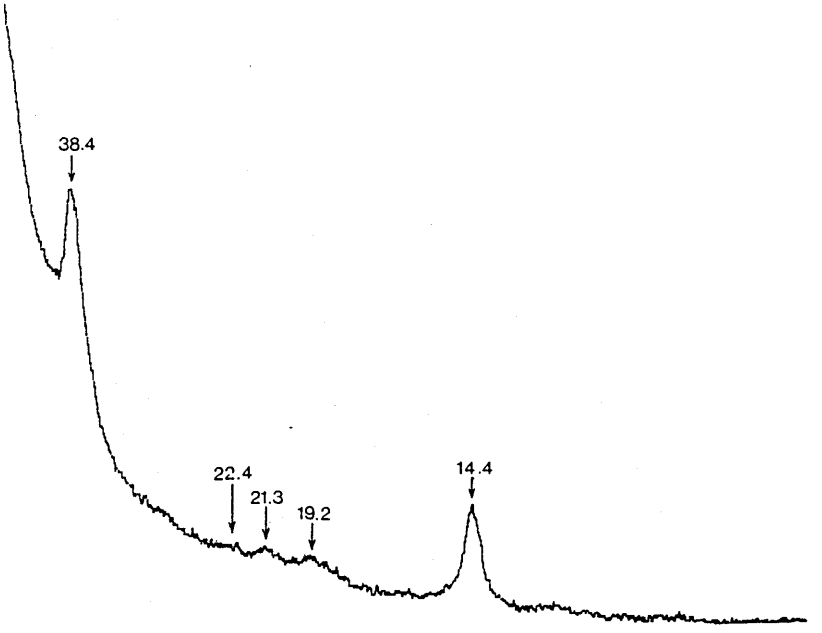

Fig 3.2.1.1. Densitometer trace of meridional reflections of rabbit psoas muscle in control (A/2) solution at S=2.4 μm. All spacings in nm.

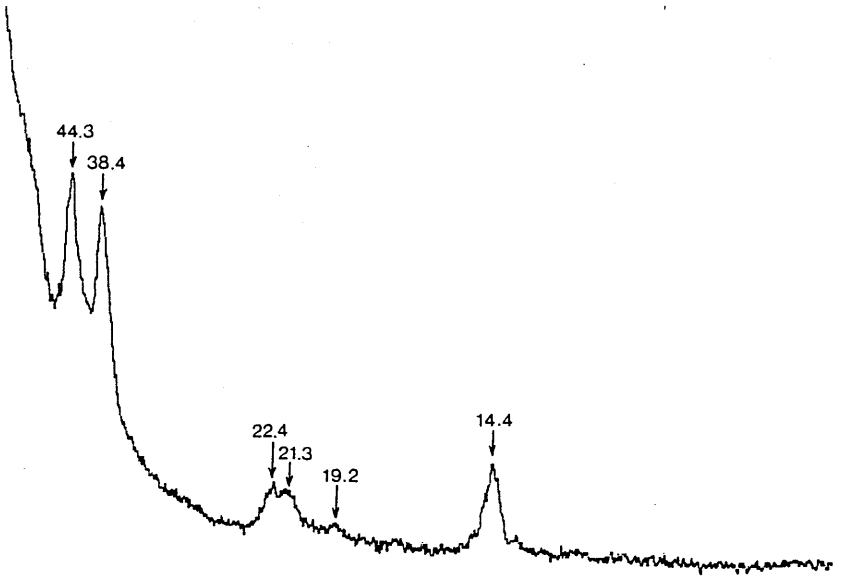

Fig 3.2.1.2 Densitometer trace of meridional reflections of rabbit psoas muscle in A/2-5 mM PPi solution at S 2.4 um. Note the increase in 44.2, 22.3, and 21.3 nm reflections. All spacings in nm.

3.2.1. Layer lines.

In the control solution (A/2) at short sarcomere lengths, strong layer lines appear at ~38 and at 14.4 nm together with a barely visible layer line at ~19 nm (the actin reflections can be seen, off the meridian, forming a layer line at ~5.9 nm, but in pictures taken under these camera conditions this is not strong enough for accurate measurement). All these layer lines become less intense, and in the case of 14.4 nm less diffuse, with increased sarcomere length.

3.2.2. Axial measurements.

Measurement of layer lines was made using densitometer tracings, since the pattern was generally faint and difficult to see in a travelling microscope. In the control, the layer lines have a slightly greater axial spacing on the film than the meridional reflection, showing that the structure giving rise to the layer line has a smaller axial repeat than that giving rise to the meridional reflection (see Table 3.2.2). On addition of 5mM PPi to the solution the meridional reflection shows little or no change, whereas the layer line shows a slight decrease in axial spacing (37.8 → 37.4 nm - see Table 3.2.2).

The densitometric data correlate with spacings measured using a travelling microscope, but the actual values are 0.3 → 0.4 nm less. Withmicroscope measurement, the standard deviation from the mean is slightly higher for the meridionals but a factor of 1.5 → 2 times greater for the layer lines, illustrating the difficulty of accurate measurement of the diffuse reflections in these regions of the picture.

Table 3.2.2. A comparison between densitometer and microscope measurment of meridional and layer line axial spacing in rabbit psoas muscle. (Spacing ± standard deviation).

REFLE-CTION	SPACING (nm)			
	A/2		A/2 + 5mM PPi	
	MIC	DEN	MIC	DEN
"384" MER	38.51±0.10	38.16±0.15	38.46±0.11	38.20±0.18
"380" LL	-	37.81±0.24	-	37.40±0.27

MER - Meridional reflection

LL - layer line

3.2.3. Off-meridional measurments.

In the control, weak sampling is seen on the 37.5 nm layer line, this effect being strongest at short sarcomere length, though even under these conditions the only other layer lines visible are 14.4 nm and a very faint 5.9 nm. With PPi however, all layer lines are stronger and considerably less diffuse. Other very faint layer lines appear, though these are too weak to measure. The most striking change in the layer line pattern occurs in the 37.5 nm region. From being broad and weakly sampled in the control, it becomes well sampled at ~1/230 → 1/250 nm (n=6) and further out at ~1/120 → 1/140 nm (n=3). An increase in sarcomere length causes a much reduced intensity and sampling both in the control and PPi experiments, but with PPi at long sarcomere length the layer line pattern remains visible, even if much weakened. The spacings of the maxima of the off-meridional reflections were measured more accurately using densitometric traces with subsequent digitization. The reflections in each quadrant were

digitized, backgrounds were subtracted by eye and averaged, giving a trace with its origin on the meridian, and its x-axis corresponding to distance from the meridian parallel to the equator. This procedure was carried out on two films at short S, one in the control (A/2) and the other in A/2+5mM PPi. Both the "38 nm" and 14.4 nm layer lines were treated this way.

3.2.4. 38 nm layer line.

Off-meridional measurements were continued on the 38 nm layer line by comparing the densitometer tracings along the equator and the layer line from synchrotron pictures. Fig 3.2.2 shows the half trace from the equatorial reflections and the trace from one quadrant of the 38 nm layer line at S~2.0 → 2.2 for A/2 and A/2+5mM PPi.

The results show that the position of the first maximum along the first actin layer line correlates well with the equatorial spacing of the (1,1) reflection (see also Table 3.2.3). The close correlation (>1.0% difference in both cases) has added weight after considering the potential errors in the method used to obtain the data. These are:

(a) Two separate pictures were used for equatorial and off-meridional measurements (though these were taken sequentially at the synchrotron on the same specimen). Since the beam was focused to a line, two different orientations of the specimen were used to take the two pictures. The meridional pattern was taken with the specimen perpendicular to the beam, so all reflections recorded will be lines perpendicular to the specimen axis. In terms of measuring layer lines, this means a scan perpendicular to the axis measures a series of end to end lines, if the reflections are diffuse and overlapping; this introduces some uncertainty in determining the positions of a maxima.

(b) Slight differences will arise between traces during densitometry

Table 3.2.3. Results of analysis of the 38 nm layer line using densitometer/ digitization at low sarcomere length.

	A/2	A/2+5mM PPi
Sarcomere Length (μm)	≈ 2.0	2.25
d(1,0) (nm)	41.11	44.61
d(1,1) (nm)	23.98	25.76
2nd order d(1,1) (nm)	≈11.9	≈12.9
1st layer line max	≈23.9	≈25.9
2nd layer line max*	12.0 → 13.0	13.0 → 14.0

* Value calculated from d(1,1)

and subsequent digitization due to purely mechanical effects in the densitometer and digital plotter. (See Appendix I for a discussion of the digitizing method).

The correlation between the second maximum along the layer line with the second order of the (1,1) is less exact due to the uncertainty of the position of the peak, however the spacing can be broadly estimated and the correlation is within 8-9%.

Note that at the short sarcomere length used in the analysis above, the control A/2 showed a degree of sampling. An increase of S to ≈2.4→2.5 μm results in the reduction of the observed sampling to a single broad, ill-defined peak. With 5mM PPi sampling reappears, though it is less intense than at the lower S (see Fig 3.2.2).

3.2.5. The 14.4 nm layer line.

In all patterns examined, a faint layer line is seen associated with the 14.4 nm meridional reflection. At short S it is stronger than at

Fig 3.2.2. Comparison of eqatorial intensity (—) with that along the 38 nm layer line (..) for A/2 and A/2+5 mM PPi at S 2.0→2.2 μm.

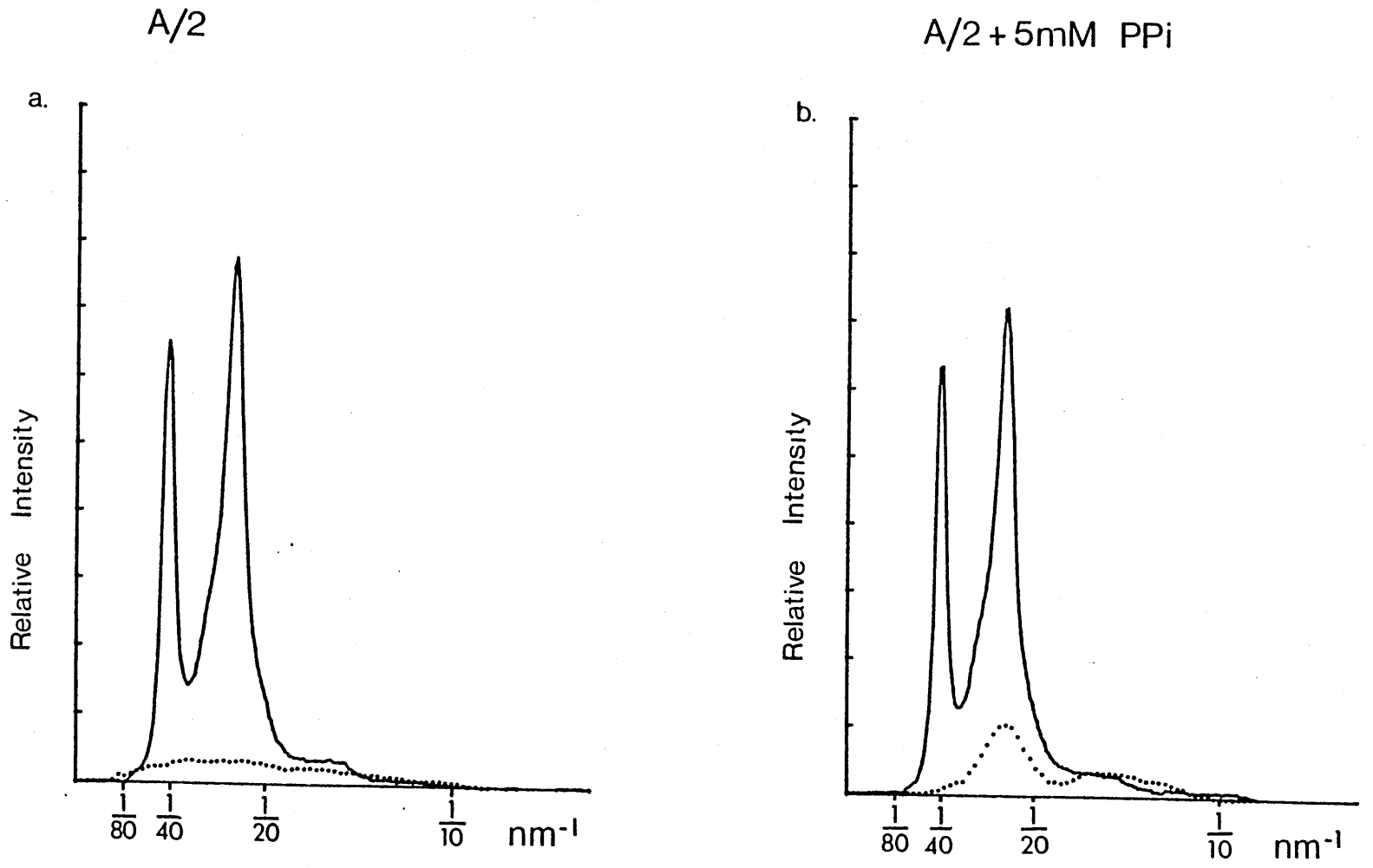

longer S, though at these lengths there appears to be little change with 5mM PPi. At short S a comparison between the two pictures available in control and PPi shows in the control a faint and diffuse layer line extending to ≈ 1/14.5 → 1/15.5 nm in the off-meridional direction. However, with PPi although the layer line remains faint, sampling is now seen, with maxima at ≈1/44.5 and ≈1/25.5 nm (see Table 3.2.3).

Table 3.2.3. Results of analysis of the 14.4 nm layer line using densitometer/digitization at low sarcomere length.

	A/2	A/2+5mM PPi
Sarcomere length (μm)	2.0	2.25
d(1,0) (nm)	41.11	44.61
d(1,1) (nm)	23.98	25.76
1st layer line max	-	≈44.5
2nd layer line max	-	≈25.5

From the pictures available there appears to be a good correlation between the equatorial (1,0) and (1,1) reflections and the two maxima seen on the 14.4 nm layer line with PPi treatment.

3.2.6. Intermediate [PPi].

All experiments so far discussed used A/2 or A/2+5mM PPi. A few pictures were taken with A/2+1mM PPi, the results were poor (due to misaligned specimens) but one good picture at sarcomere length 2.8 μm was produced. This shows similar changes to those seen with 5mM PPi, however the degree of sharpening is reduced, and intermediate sampling is found on the 38.4 nm layer line.

SECTION 3.3 - THE EFFECT OF PYROPHOSPHATE ON THE EQUATORIAL REFLECTIONS IN RABBIT PSOAS MUSCLE.

The analysis of the equatorial data concentrated on two properties of the reflection;

(a) The change in measured spacing, which yields the interfilament spacing.

(b) The "sharpness" of the reflection. A measure of this can be made using the Full Width Half Maximum (F.W.H.M) of the reflection. (This is the width of the reflection at half its maximum value).

Taking each of these in turn,

(a) 3.3.1. Changes in interfilament spacing on addition of pyrophosphate (PPi).

Figs 3.3.1 and 3.3.2 plot the results of a series of experiments using the sequential soaking method described in Methods (Section 3.1). The difference in d(1,0) between the control (A/2) and the chosen PPi solution is called $\Delta d(1,0)$;

$$\Delta d(1,0) = d(1,0)_{pyrophosphate} - d(1,0)_{control}$$

Figs 3.3.1 and 3.3.2 show this as a function of sarcomere length for both the change from control (A/2) to A/2+1mM PPi and to A/2+5mM PPi. In both cases the curve is fitted with a cubic spline routine. Both with 1mM and 5mM PPi the d(1,0) shows a biphasic change with increasing sarcomere length (S.L). In both cases at short S.L (<2.2 μm) the $\Delta d(1,0)$ *increases* with increasing S.L, but above this value the $\Delta d(1,0)$ *decreases*.

Table 3.3.1 includes a further analysis of the curves fitted to the

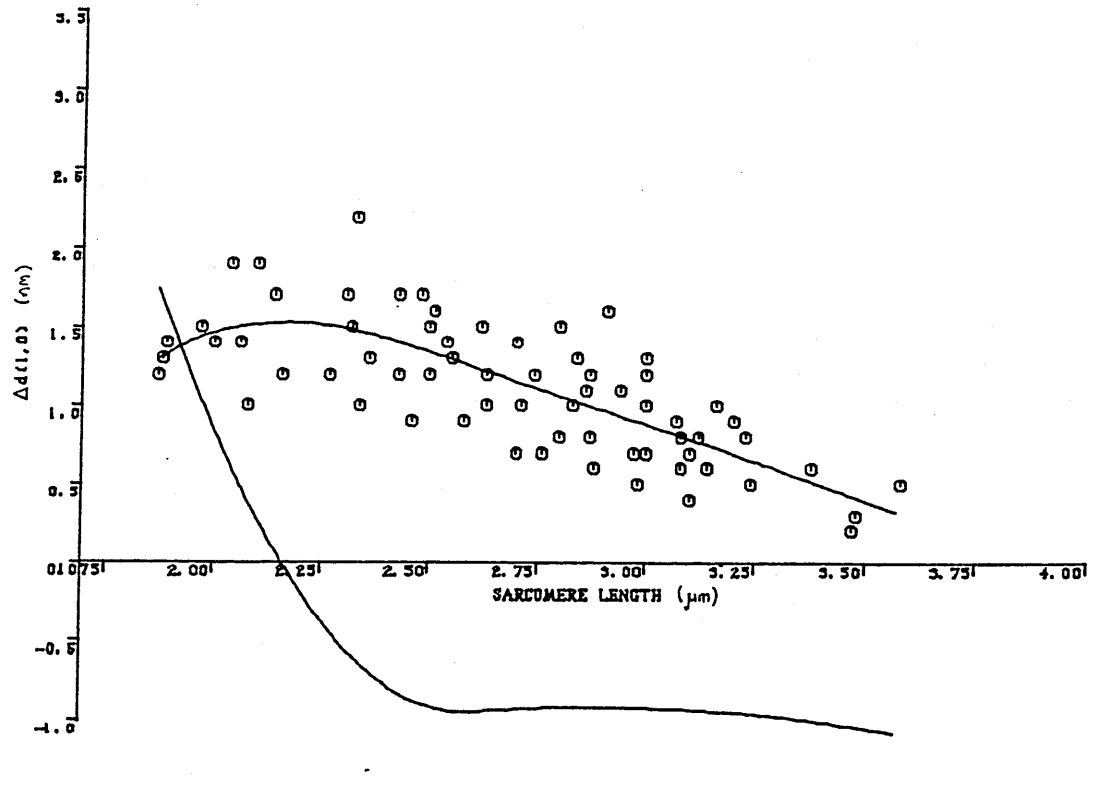

Fig 3.3.1. Δd(1,0) vs S for the change of solution A/2 → A/2+1 mM PPi. Upper curve cubic spline fit, lower curve first derivative of this fit.

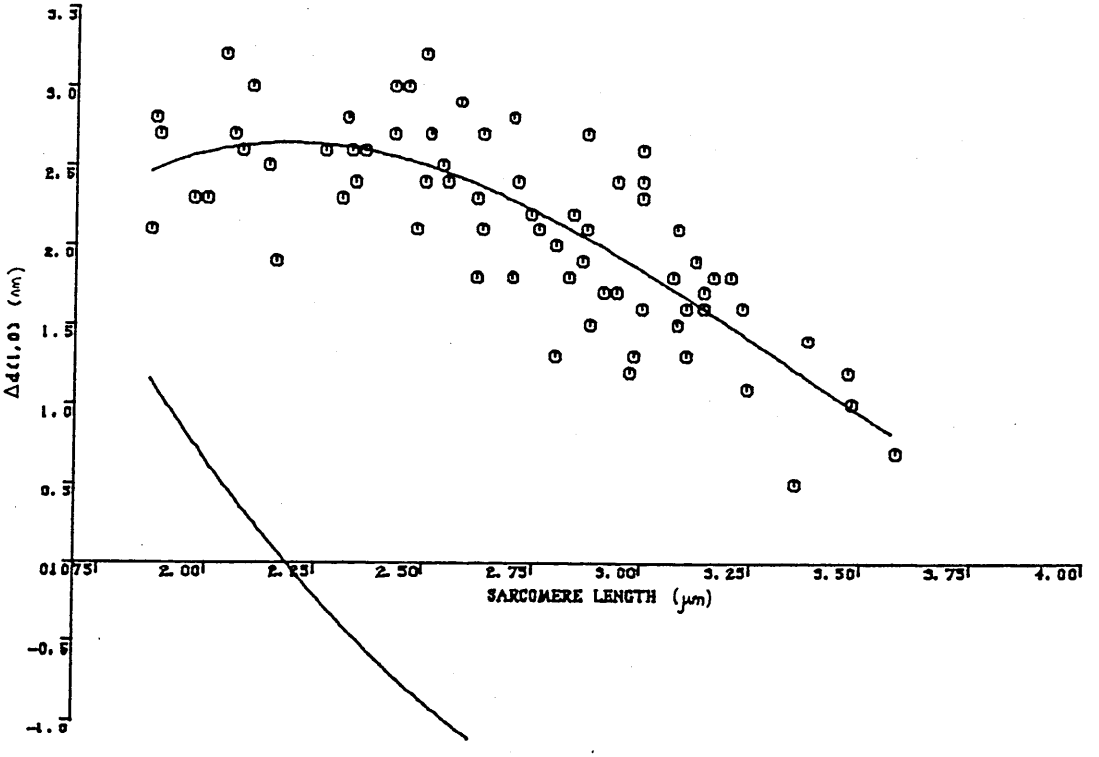

Fig 3.3.2. Δd(1,0) vs S for the change of solution A/2 → A/2+5 mM PPi.. Curves as above.

data. To calculate the parameters shown in row 1, the first derivative of the cubic spline fit was evaluated. The point of intersection of this new curve with the x-axis yielded the inflection point of the original fitted curve (i.e the point at which dy/dx=0). Furthermore the new curve flattened out to an approximately horizontal region at higher sarcomere lengths, showing the gradient of the curve in these regions was roughly constant (i.e essentially linear) in the original plot. The points in the original fitted curve which lay in these linear regions were used in a linear regression calculation to find the intercept at the x-axis of the original data.

Table 3.3.1. Analysis of the cubic spline fitted curve for both 1mM and 5mM pyrophosphate.

PARAMETER	A/2+1mM PPi	A/2+5mM PPi
Point of inflection (μm)	2.16	2.18
Equation of straight line portion of curve	y=3.67-0.93x	y=7.17-1.78x
Correlation coefficent of linear fit	0.99	0.99
Intercept (μm)	3.95	4.03

(b) 3.3.2. Changes in sharpness on addition of pyrophosphate (PPi).

Only synchrotron data was used in the sharpness analysis. Both film and detector traces were used, those from film being obtained by densitometry and analysed manually and those from detector analysed using the data manipulation software package "OTOKO" run on the VAX computer at the Daresbury laboratory.

Sharpness was quantified by measuring the full width half maximum of the (1,0) reflection (called here Δd), and dividing this by

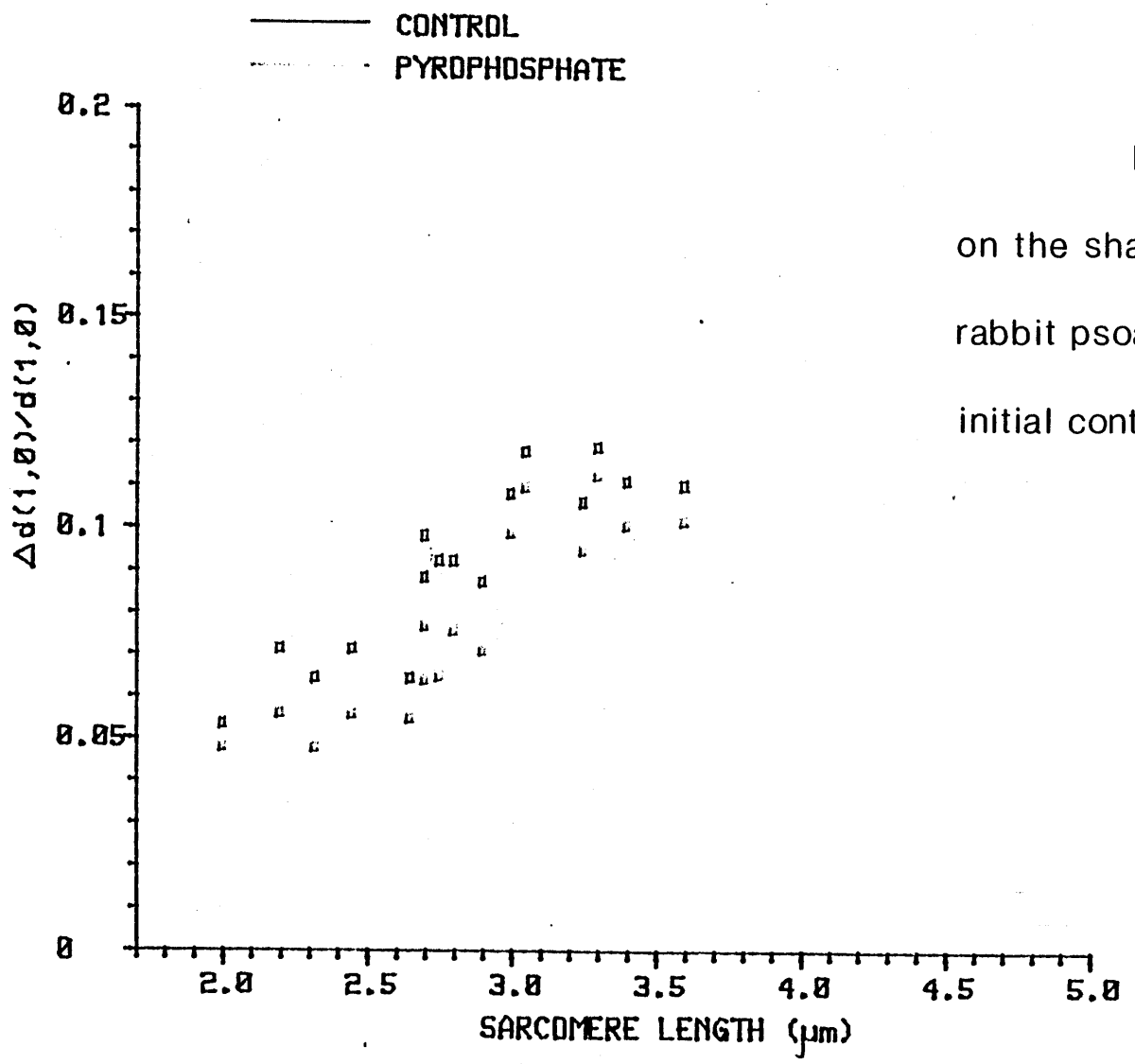

Fig 3.3.3. The effect of 5mM PPi on the sharpness of the (1,0) reflection in rabbit psoas muscle. (Paired data). The initial control is the muscle in the rigor state.

the by the measured peak spacing (d). To measure the parameter Δd, the background scatter was subtracted by eye and a straight line drawn beneath the (1,0) reflection from the point where the innermost arm of the peak is zero to a point where it was judged the outermost arm of the peak met the (1,1) reflecton. The area above this line was deemed to be arise from the (1,0) peak alone. Using this, the half maximum and so the width at this value was found. Thus for any given value of d, a *decrease* in Δd corresponds to an *increase* in sharpness. To check this somewhat crude analysis, one pattern was fitted several times varying the background and lines drawn, the results were consistent, with little or no change in the Δd measured. The value of d was taken as the spacing between maxima of the d(1,0) peaks.

Δd/d was plotted against sarcomere length (S) for both control (A/2) and A/2+5mM PPi (see Fig. 3.3.3). Since each specimen was exposed once in A/2, resoaked in PPi solution and exposed again. Fig. 3.3.3 represents paired data. In all cases the addition of PPi caused a decrease in Δd/d (Mean 0.013 ± 0.008 n=16).

Figs. 3.3.4 and 3.3.5 show Δd/d plotted against S for control (A/2) and A/2+5mM PPi these plots include all data available under the two conditions, this includes some unpaired points. The curves were fitted using a cubic spline routine (see NAG library) in which all data points weights were set equal to 1. This routine relies on a least squares fitting routine using a series of polynomial functions. As with all fitting routines based on polynomials the resulting curve has a tendency to "drift" at the extremes if the number of data points is low in these regions (note in the previous section the relatively large number of data points at short S, this eliminates the problem). To counter this drift dummy points were generated to lie beyond the range of the data as follows. The maximum and minimum values of S

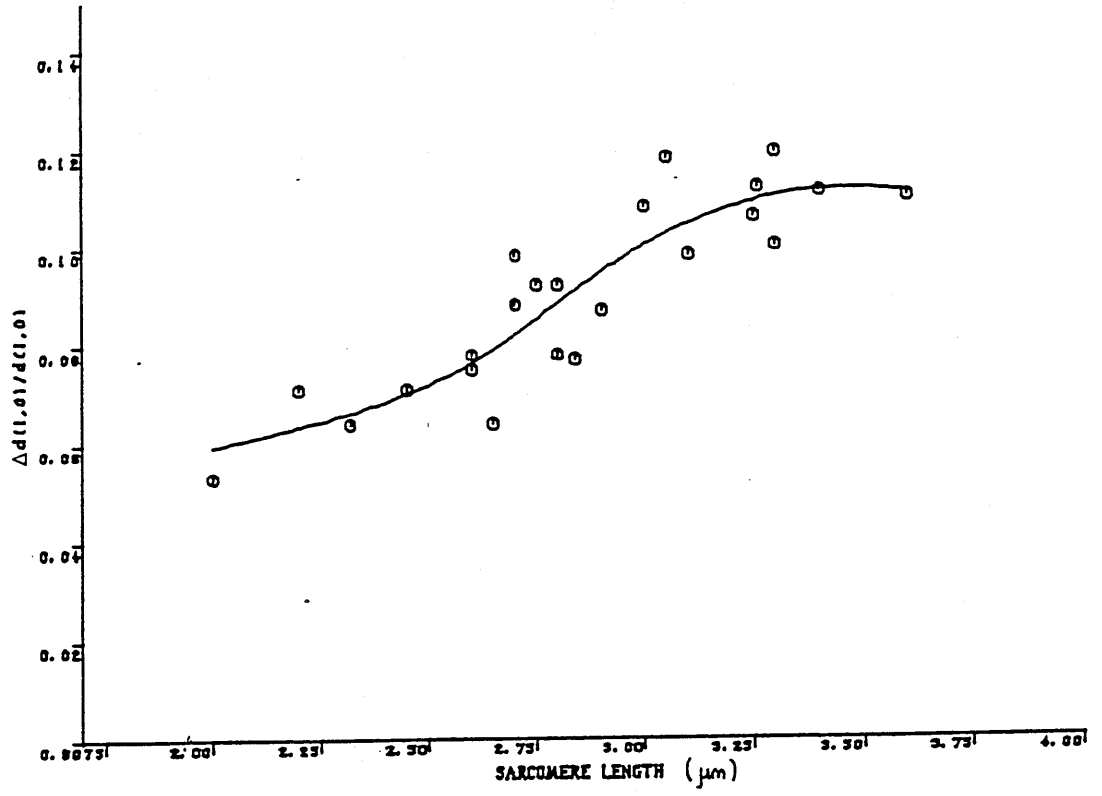

Fig 3.3.4. $\Delta d/d$ of the (1,0) reflection vs S in rigor solution.

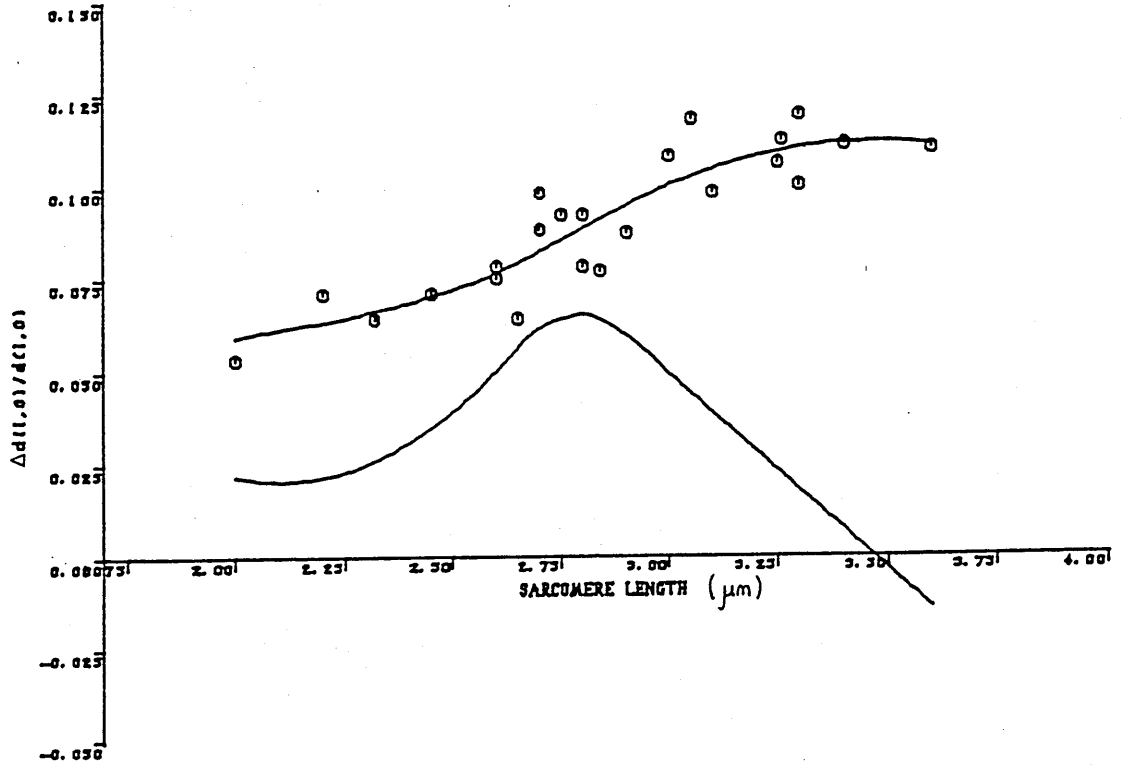

Fig 3.3.4.1. Upper curve as above , lower curve is the first derivative of the upper curve.

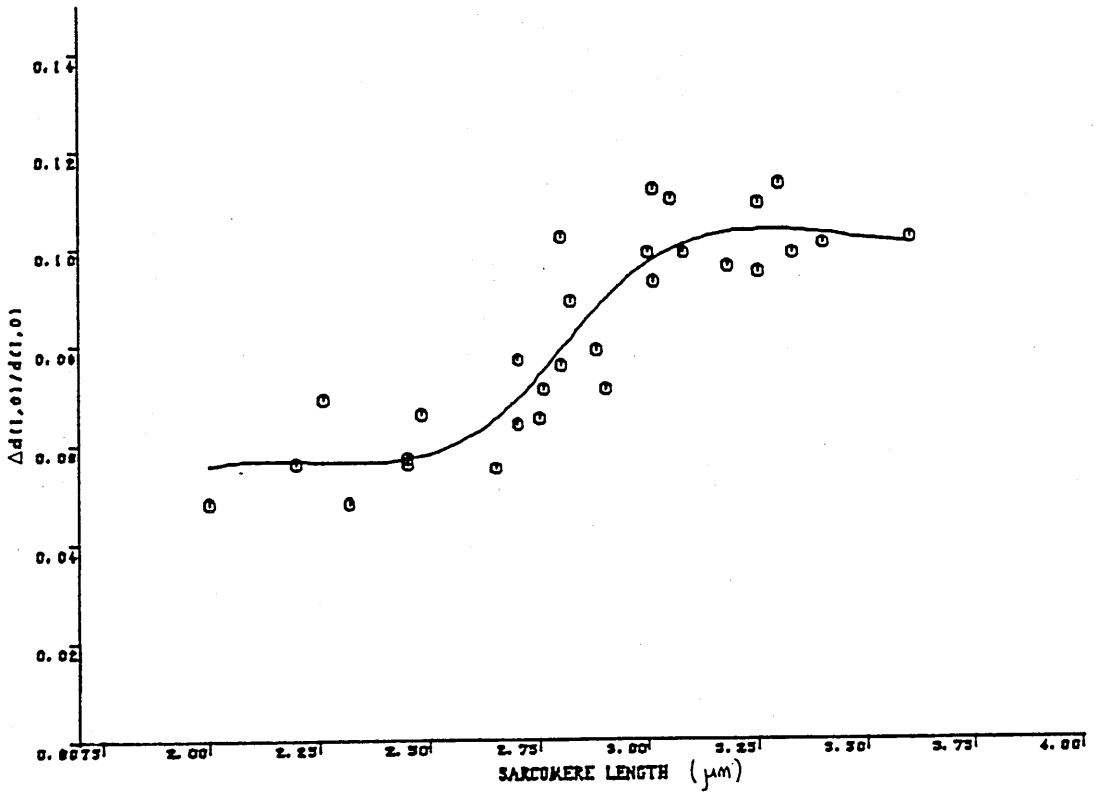

Fig 3.3.5. $\Delta d/d$ of the (1,0) reflection vs S in rigor - 5 mM PPi solution.

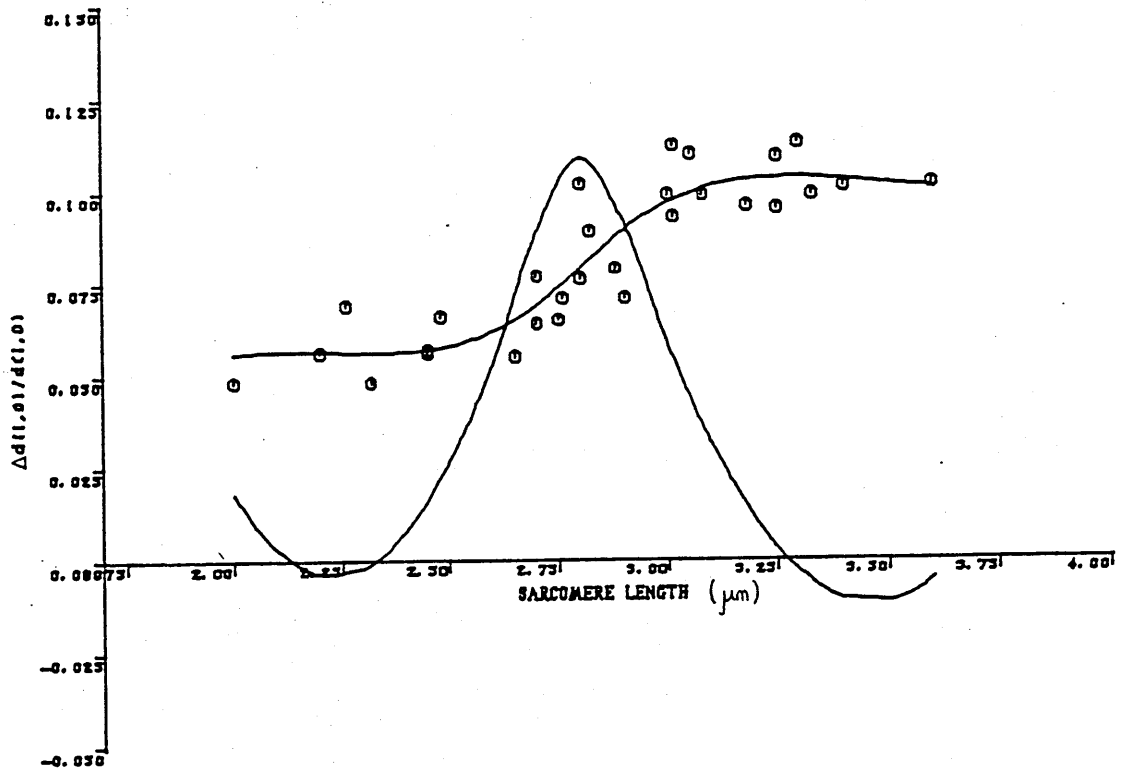

Fig 3.3.5.1. Upper curve as above, lower curve is the first derivative of the upper curve.

was taken and a small increment added or subtracted respectively (in this case 0.2 μm). The values of Δd/d at these points were generated by taking the maximum and minimum values of Δd/d from the data over the first or last 0.5 μm of the data scatter and a third point between the two. These dummy points were all given a low weighting of 0.3.

Both curves show a sigmoid decrease in sharpness with increasing SL (ie. an increase in Δd/d). The maxima and minima are summarised in Table 3.3.2.

Table 3.3.2. Maximum and minimum values for curves fitted to sharpness vs. sarcomere length data in Figs 3.3.4 and 3.3.5.

SOLUTION	MAXIMUM	MINIMUM
A/2 (Control)	0.111 (0.098 → 0.118)*	0.055 (0.051 → 0.071)
A/2+5mM PPi	0.102 (0.092 → 0.112)	0.055 (0.047 → 0.067)

* Values in brackets indicate the range of data spread in these regions

The PPi curve is consistently lower than the A/2 curve, both in the value of the fitted curve and in the range of data scatter (though the latter does show a high degree of overlap). Further differences are apparent between the PPi and A/2 curves. By taking the first derivative of of the curves the gradient changes may be quantified (see Figs 3.3.4, 3.3.5 and Table 3.3.3). The maximum gradient of the PPi curve the steeper by a factor of ≈ 1.7, though the SL at which the maximum gradient is seen is about 2.85 μm in both cases.

From Figs 3.3.4 and 3.3.5 it can also be seen that the rate of change of the gradient is also different for the two curves. By taking the second derivative the maximum rate of change may be found (see Table 3.3.4). Note that since the curves are sigmoid in shape there is

Table 3.3.3. Maximum gradients of curves fitted to Δd/d vs sarcomere length with control (A/2) and A/2+5mM PPi.

	A/2	A/2+5mM PPi
Maximum gradient (Δd/d μm^{-1})	0.065	0.109
S at max. gradient (μm)	2.84	2.85

Table 3.3.4. Rates of change of gradients for the 1st derivative of Δd/d vs SL for specimens in control (A/2) and A/2+5mM PPi solutions.

SOLUTION	RANGE OF LINEARITY (μm)	GRADIENT		MAX/MIN	S (μm)
A/2 (Control)	2.00 → 2.55	0.24	*		
				0.12	≈2.6
	2.67 → 2.87	-0.85			
				-0.10	≈2.9
	2.90 → 3.60	0			
A/2+5mM PPi	2.00 → 2.68	0.86			
				0.40	≈2.7
	2.70 → 2.87	-4.31			
				-0.37	≈2.9
	2.90 → 3.60	0.65			

* Maximum/minimum and S are taken at the points of inflection of the linear regions before and after as indicated by the brackets.

both a positive and negative rate of gradient change. The rates of change of gradient fell into three linear phases with marked discontinuities between them.

All rates of change of gradient are greater in the PPi curve than in the control. These steeper gradients give rise to the pronounced bell-shaped curve of the first derivative seen in Figs 3.3.4 and 3.3.5. The ranges over which the changes in gradient occurs are broadly similar however.

3.3.3. Summary.

The effect of pyrphosphate (PPi) on the equatorial refection in gycerinated rabbit psoas muscle is twofold,

(a) The d(1,0) *increases* with PPi treatment, this is a concentration dependent effect, the increase with 5mM PPi being greater than with 1mM PPi. The effect of increasing sarcomere length (S) results in a maximal change in d(1,0) (ie $\Delta d(1,0)$) at S $\approx$2.15-2.2, with a fall in $\Delta d(1,0)$ on either an increase or decrease S. This fall in $\Delta d(1,0)$ is approximately linear with S.

(b) An increase in sharpness (ie a decrease in $\Delta d/d$) is also seen with PPi treatment in every case in the paired experiments, and analysis of the control and PPi data shows that the plot $\Delta d/d$ vs S is sigmoid in both cases, with the PPi curve showing the more pronounced inflections.

THE EFFECT OF pH CHANGES ON THE EQUATORIAL (1,0) REFLECTION IN GLYCERINATED RABBIT PSOAS MUSCLE.

Section 4.1 - Methods.

Bundles of glycerinated rabbit psoas muscle were prepared as in Section 2.1. The preparation, soaking and X-ray exposure were similar to the sequential soak methods used for the PPi experiments, except that here, to shorten the time of the experiments, the specimen was divided into two, both of which were subject to an exposure in control (pH7) solution. It was found that the d(1,0) measured from these two twin specimens never differed by more than 1%, so in the analysis of the data the control value was taken as the average of these two spacings. One bundle was then put through the increasing pH series, which alternated between soaking and X-ray exposure in pH8 and pH9 solutions, and the other went through the decreasing pH series of pH6 and then to pH5. In this way whilst one specimen in one series was soaking, the other specimen in the opposite series was in the X-ray beam. This speeded up the experiment considerably. The experimental solutions are shown in Table 4.1.1. All chemicals were obtained from

Table 4.1.1. Compositions of solutions used in the ΔpH experiments (all concentrations in mM).

pH	KCl	$MgCl_2$	BUFFER	CONC	I
5	24.7	2.5	citrate	10	0.071
6	32.7	2.5	citrate	10	0.071
7	50	2.5	phosphate	10	0.071
8	50	2.5	borate	10	>0.095*
9	50	2.5	borate	10	>0.095*

* Estimate - no data available for accurate calculation.

BDH and were of "Analar" grade. Titration of 1M HCl or KOH to get the correct pH added K^+ or Cl^- ions, and these are included in the calculation of ionic strength.

X-ray pictures were taken on film using GX13 rotating anode run at 35 kV and 60 mA, exposures took 1/2 - 1 hr. After developing and drying the d(1,0) spacing was measured using a Nikon 6C travelling microscope, and the film densitometered using an LKB Ultrascan densitometer. The (1,0) reflection sharpness was found by the method described in Section 3.1 (PPi methods).

Some pictures in a pH5 solution had previously been taken at the SERC synchrotron radiation source at Daresbury, and these too were densitometered and the traces analysed for sharpness of the (1,0) reflection.

Section 4.2. Results.

The effect of changing the pH on the equatorial d(1,0) reflection was twofold.

(a) Change in measured spacing of the reflection

(b) Change in the sharpness of reflection.

Considering each of these in turn:

(a) 4.2.1. Changes in spacing of the d(1,0) reflection.

These experiments used a Franks camera on the GX13 X-ray set. Control pictures were taken in pH7 solution for each sample, and the average was taken to give the control value. The difference between the two d(1,0) readings was never more than ≈ 1%. The d(1,0) spacing was measured using a travelling microscope (Nikon 6C). Fig 4.2.1 shows the d(1,0) vs sarcomere length (S) for sequential soaks over pH range

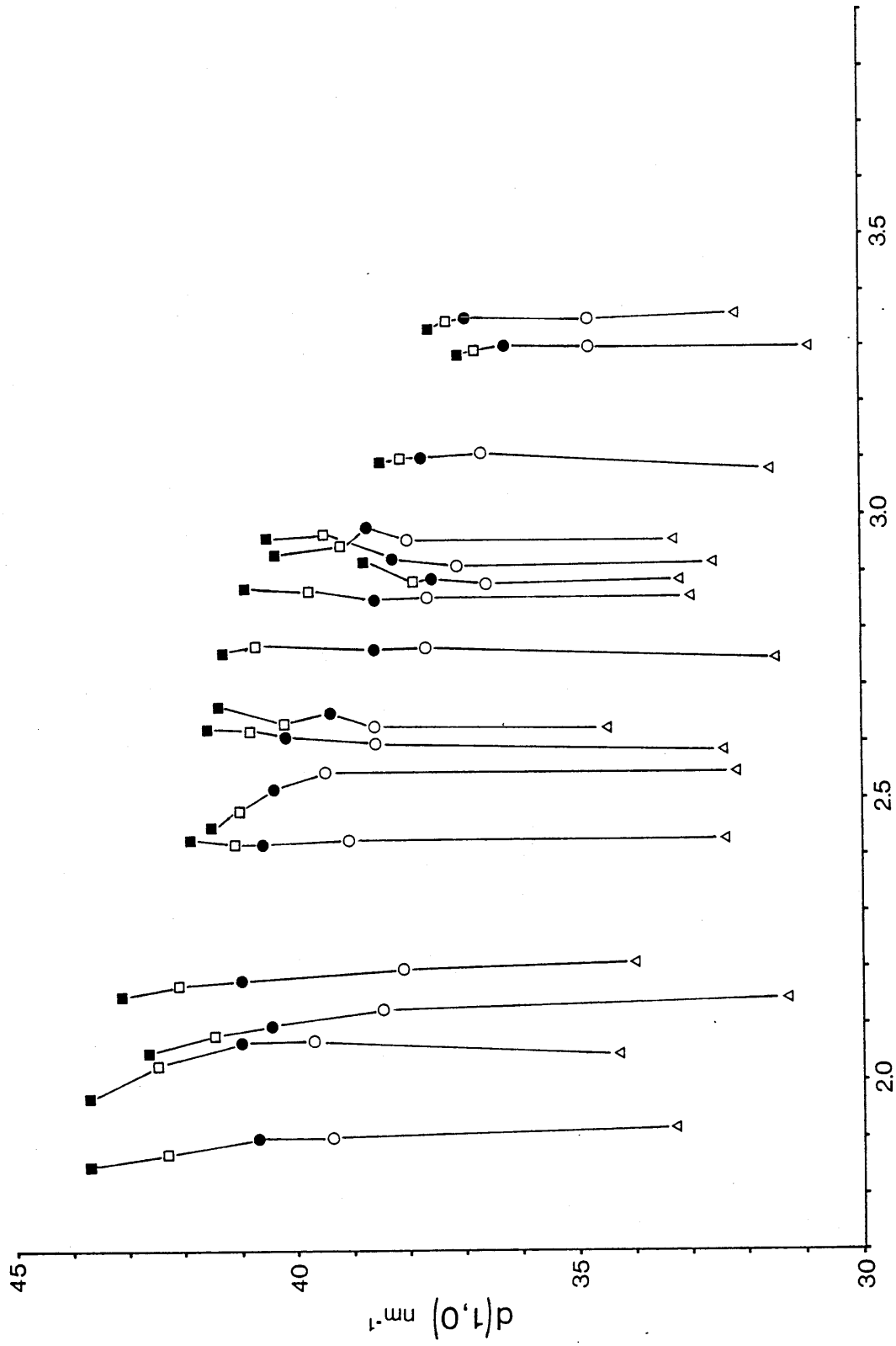

Fig 4.2.1 d(1,0) vs S for sequential soak experiments in various pH solutions

△- pH5 ○- pH6 ●- pH7 □- pH8 ■- pH9

5 to 9. All experiments show that as S is increased the d(1,0) decreases. This relationship holds true for all pH values used in this study. The decrease is non-linear, and this correlates with results from ionic strength (I) change experiments where a dislocation at S ≈ 2.8 μm was observed at ionic strength 0.071 (this being the I of all the pH solutions). Using this S as the dislocation point at all pHs, linear regression fits were performed on data either side of this point for each pH. The two lines resulting from the analysis correspond to the phase 1 and phase 2 of the I data. Table 4.2.1 shows the regression lines. The interpretation of linear regression for so few points is to show trends in the data.

The phase 2 regression coefficient (which is analogous to the gradient) of the line is between ≈ 2.6 and ≈ 4.5 times that of the phase 1, showing a marked dislocation in the region S ≈ 2.7 - 2.9.

Table 4.2.1. Linear regression fits to d(1,0) vs S for pH range 5 to 9.

pH	EQUATION OF PHASE 1 REGRESSION LINE	EQUATION OF PHASE 2 REGRESSION LINE	GRADIENT 1/ GRADIENT 2
5	d = 34.4 - 0.58s	d = 37.7 - 1.78s	3.07
6	d = 41.1 - 1.16s	d = 52.5 - 5.23s	4.51
7	d = 43.5 - 1.32s	d = 51.0 - 4.31s	3.27
8	d = 46.2 - 2.04s	d = 55.3 - 5.52s	2.71
9	d = 48.5 - 2.58s	d = 59.7 - 6.73s	2.61

Furthermore, the gradient of the line of both phases shows an increasing trend as pH is raised from 5 to 9. At any given value of S, increasing the pH also results in an increase in d(1,0). Fig 4.2.2 shows the difference Δd, between d(1,0) at pH7 and d(1,0) at raised pH (8+9) or lowered pH (5+6) vs S with linear regression lines fitted (see Table 4.2.2). At every pH the greatest Δd is seen at the shortest S. At any

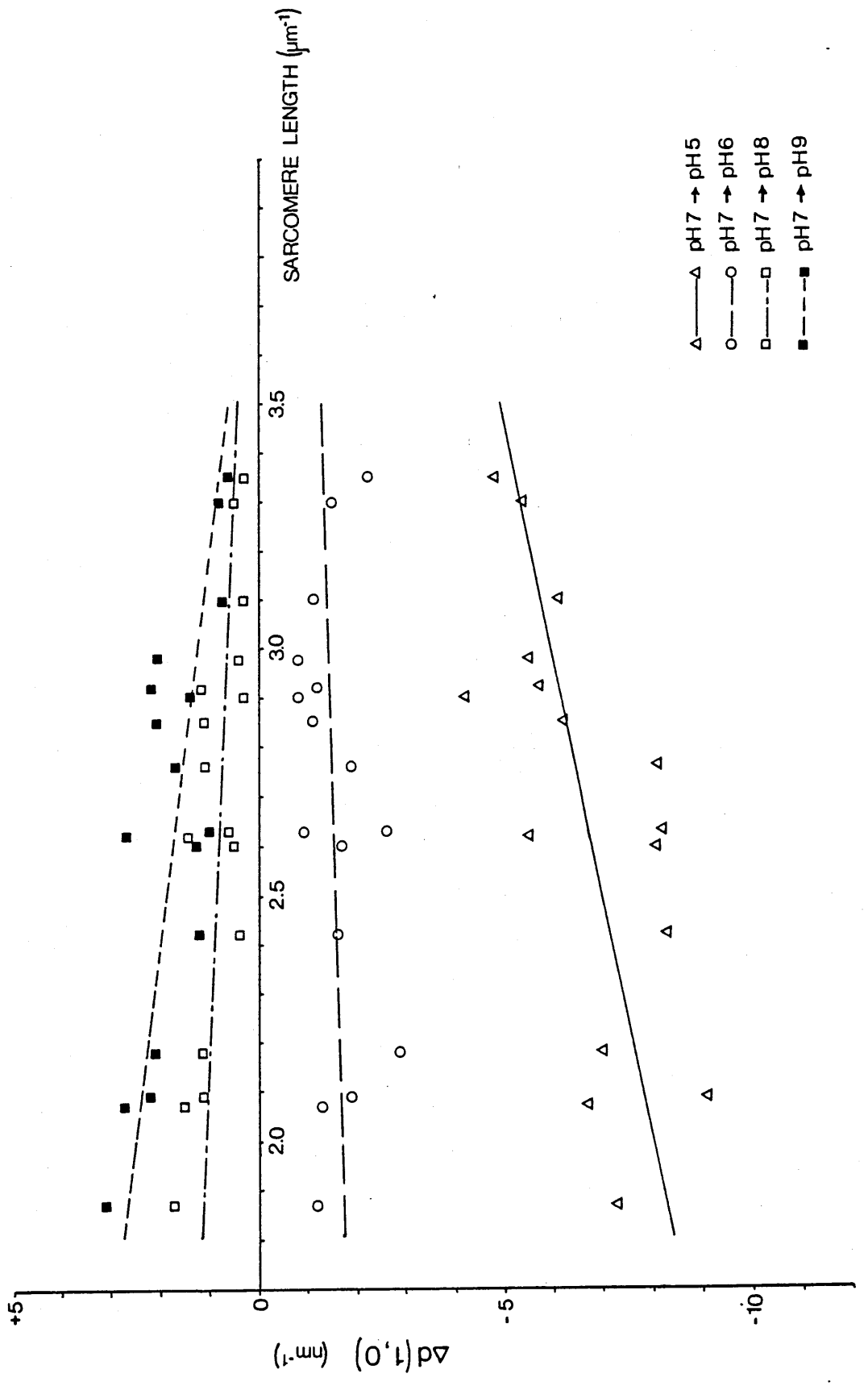

Fig 4.2.2. Changes in d(1,0) spacing from the control at pH7 vs S over the pH range 5 to 9.

given S, the Δd is always negative as pH is lowered and positive as pH is raised, the increase or decrease in Δd being proportional to pH change. However, as S increases, the effect of pH is reduced for every pH (ie Δd decreases). Table 4.2.2 shows linear regression fits for Δd vs S for the pH changes studied.

The trend illustrates the changes in Δd with S and pH, the larger changes being seen with the highest or lowest pH and shorter S. Lowering the pH has a greater effect on Δd than an increase in pH by the same increment, this is reflected in the intercepts of the lines which range from -12.11 in pH5 to 4.97 in pH9. The regression coefficient gives a measure of the effect of S on the Δd and shows again that decreasing pH by a given amount results in an increased response to S over the response to the same increase in pH (range 2.06 at pH5 to -1.20 at pH9 - note the opposite signs in the gradient

Table 4.2.2. Linear regression fits for Δd vs S as pH is increased from pH7 to either pH8 or 9, or decreased to pH5 or 6.

ΔpH	EQUATION OF REGRESSION LINE	REGRESSION COEFF.
7 → 5	Δd = -12.11 + 2.06s	2.06
7 → 6	Δd = - 2.28 + 0.27s	0.27
7 → 8	Δd = 1.89 - 0.41s	0.41
7 → 9	Δd = 4.97 - 1.20s	1.20

since lowering pH decreases d(1,0), and so increasing S will cause a reduction in the decrease seen, leading to a positive gradient. The reverse holds true for increasing pH).

(b) Section 4.2.2. The effect on sharpness of pH changes.

The peak width analysis was performed in the same way as for

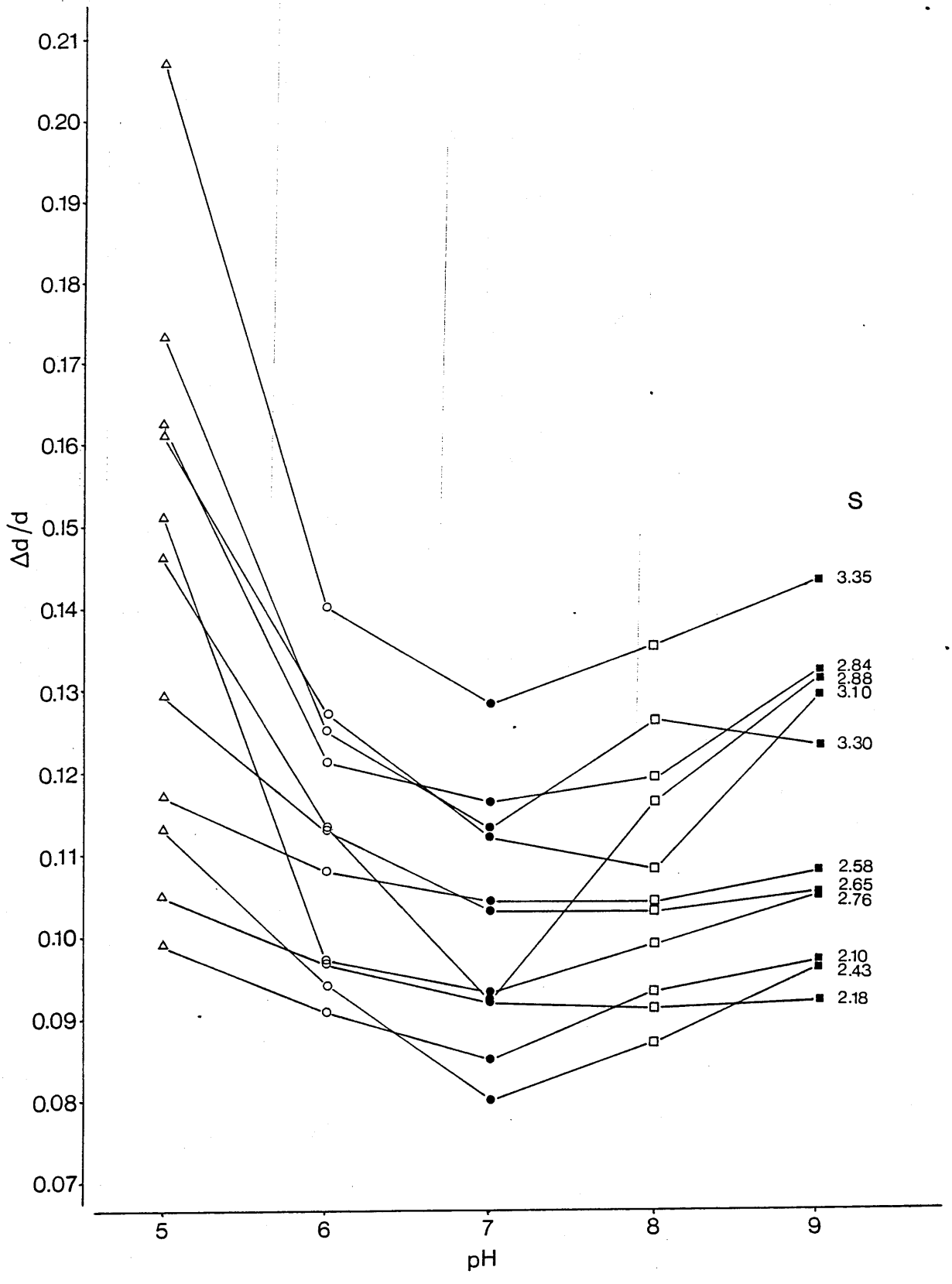

Fig 4.2.3. Δd/d vs pH over a range of S in seqential soak experiments.

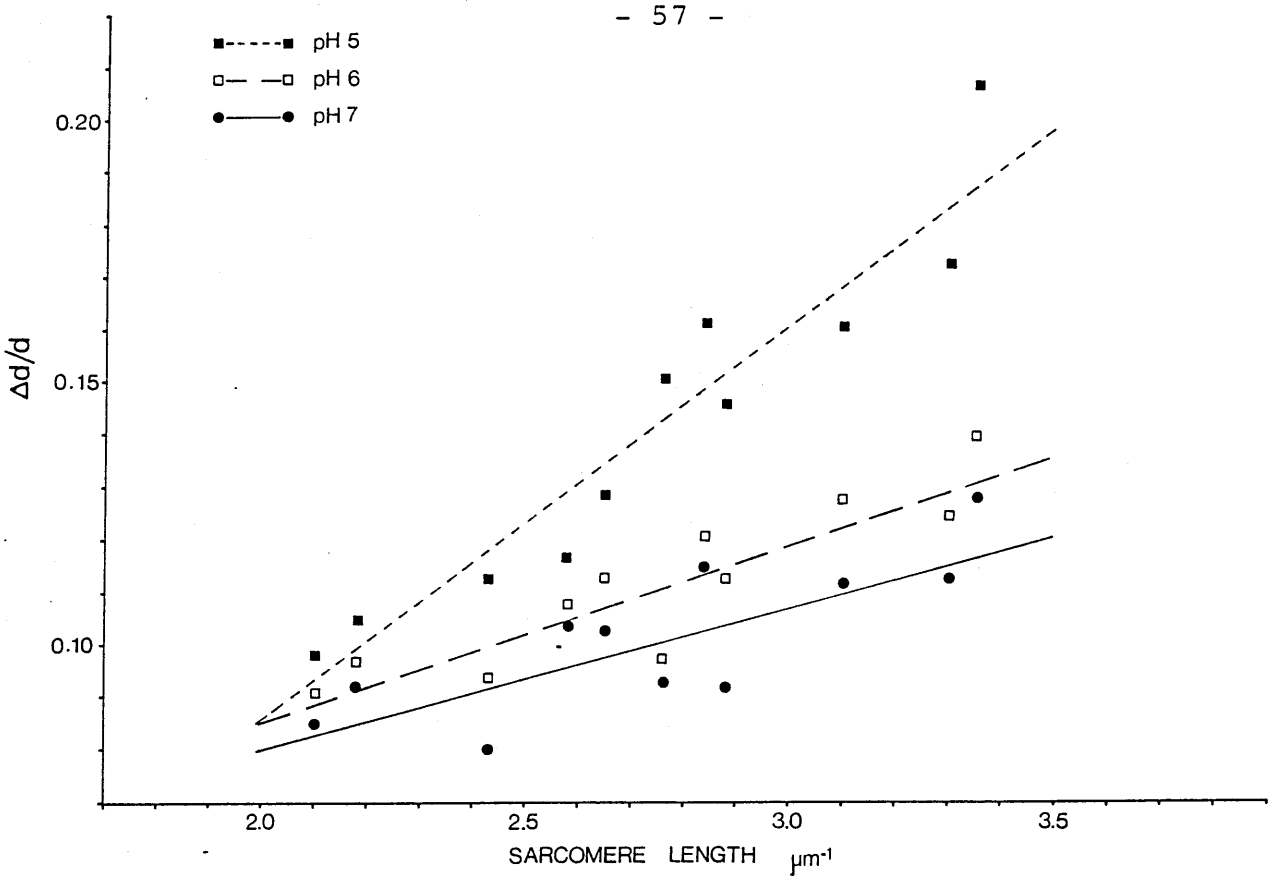

Fig 4.2.4 $\Delta d/d$ changes vs S for pH 5 to 7.

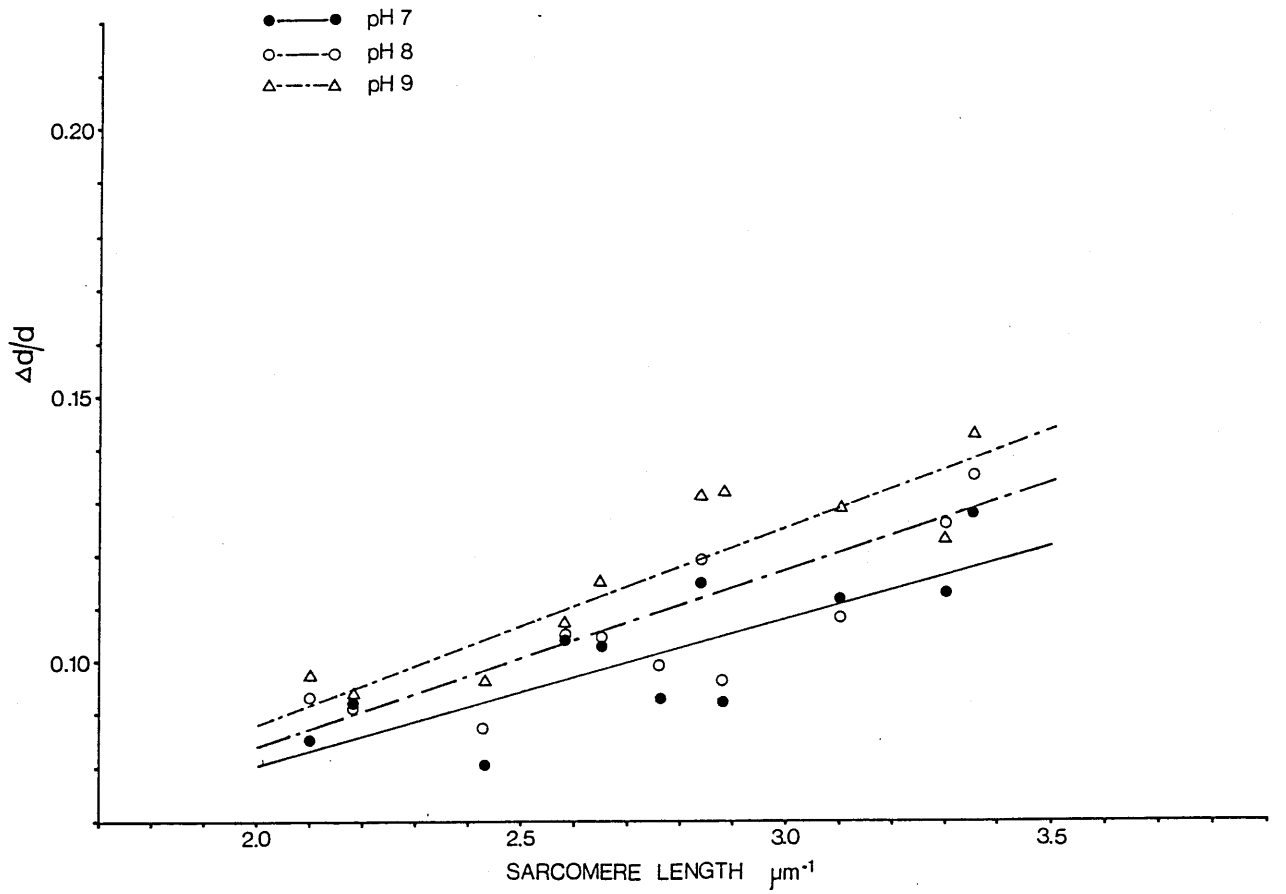

Fig 4.2.5. $\Delta d/d$ changes vs S for pH 7 to 9.

that in the PPi experiments, so a value for Δd/d was again generated. Fig 4.2.3 shows the result of sequential soaks for specimens in changing pH from 5 to 7 and from 7 to 9 as a continuous line. The overall trend shows that Δd/d falls rapidly as pH is increased from pH 5 to pH 7 and rises again by a small amount from pH 7 to pH 9. Furthermore as the sarcomere length (S) increases, the changes in Δd/d with pH become greater, and at any given pH the Δd/d increases with increasing S. Both these latter trends become clearer in Figs 4.2.4 and 4.2.5. Note that the absolute value of Δd/d in the GX13 pictures is higher than that measured from the synchrotron pictures. This is probably a consequence of the differences in direct beam widths between the synchrotron (where reflection width/beam width is greater than 10) and rotating anode (where reflection width/beam width ~3-4). This will result in higher Δd/d values for the data from the GX13. Although the values are higher, the trend at pH7 still shows the increased Δd/d at increased S.

Since comparatively few data points at each pH were available for analysis, a simple linear regression was chosen to fit the data. The result of such a fit of Δd/d vs S for the series of pH values is shown in Table 4.2.3.

Table 4.2.3. Results of linear regression fit to Δd/d vs S data with changes in pH at ionic strength of 0.071.

pH	EQUATION OF REGRESSION LINE	REGRESSION COEFFICIENT	CORRELATION COEFFICIENT (r)
5	Δd/d = - 0.067 + 0.076s	0.076	0.95
6	Δd/d = 0.017 + 0.034s	0.034	0.90
7	Δd/d = 0.024 + 0.028s	0.028	0.80
8	Δd/d = 0.018 + 0.033s	0.033	0.88
9	Δd/d = 0.014 + 0.037s	0.037	0.89

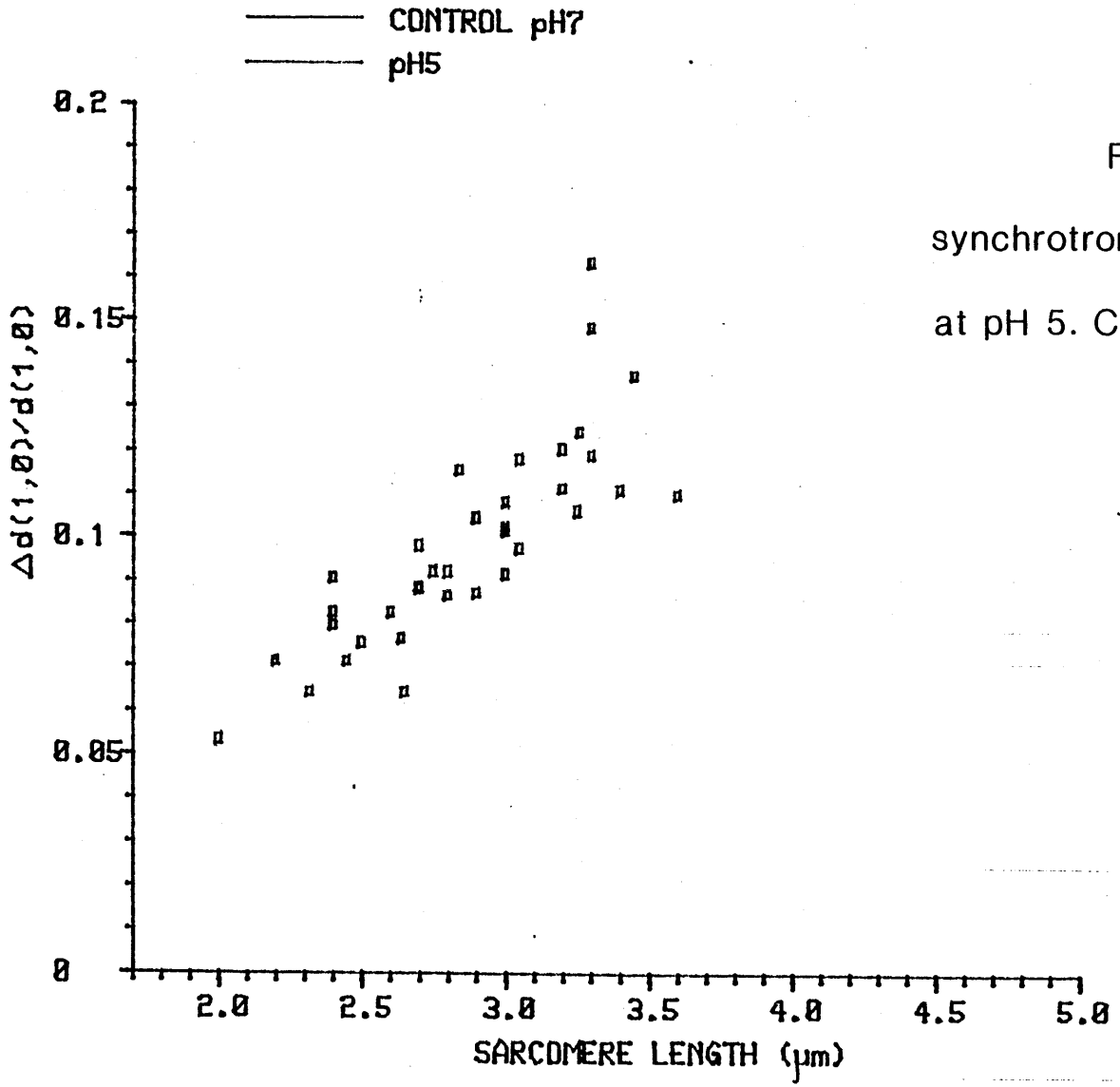

Fig 4.2.6. Sharpness vs S from synchrotron pictures of rabbit psoas muscle at pH 5. Control data at pH7 shown in red.

The gradient of the line at pH 7 is lower by a factor of ≈2.7 compared to pH 5, and by ≈1.3 compared to pH 9. Figs 4.2.4 and 4.2.5 also show the regression lines fitted. Note that an increase in $\Delta d/d$ corresponds to a decrease in sharpness. The analysis assumes that,

(a) The means of the distribution of $\Delta d/d$ for the range of given S and pH fall on a straight line.

(b) The variance of the distributions at any given pH and S is constant.

There is insufficient data to either support or disprove either of the above assumptions in this case, so the results of the fit can only be interpreted as trends of sharpness with S and pH. The correlation coefficient is a measure of the departure of the data from the fitted curve, so the fall in r from 0.95 with pH 5 to 0.80 with pH 7 and slight rise to 0.89 with pH 9 could either indicate an increase in data scatter or an increased departure of the true fit from a straight line. In the PPi experiments, the control (A/2) solution was the same as the pH7 solution in these pH experiments, and the synchrotron data were fitted with a cubic spline and do not result in a straight line. Synchrotron data were also available in the form of film for pH 5. Fig 4.2.6 shows $\Delta d/d$ vs S at this pH for these data. The results of a cubic spline fit to this scatter shows the points do not fall on a straight line either, though the gradient of the curve fitted is steeper than in A/2. The difference between pH 7 and pH 5 is much greater in the paired pH expts (on GX13) than with the separate experiments in the synchrotron data. This could be due to differences in solutions used, or that the peaks in the synchrotron data are better defined above the background, thereby making the analysis less sensitive to errors in background subtraction.

4.2.3. Summary.

Graphs of d(1,0) vs S show that the d(1,0) decreases with increasing S in a biphasic manner over the range of S and pH studied, and that the point of transition between one line and the other occurs at about S ≈ 2.7 to 2.9. The response of the d(1,0) spacing to a raised pH is always an increase, and to a lowered pH a decrease in spacing. These changes become smaller as S increases.

Changing pH from 5 to 7 results in an increase in sharpness (ie a decrease in $\Delta d/d$). A smaller decrease in sharpness is seen when pH is raised from 7 to 9. Sharpness is maximal at about pH 7. Increasing S results in a decrease of sharpness at every pH, though in serial exposures the effect becomes increased (ie greater decreases in sharpness either side of pH 7). The $\Delta d/d$ vs S for pH is not linear at pH 7 or pH 5, as shown by cubic spline fits of synchrotron data. However by approximating the data of the serial experiments to a straight line in a linear regression analysis, the trend in the results illustrate both the larger decrease in sharpness as pH is changed from 7 to 5 over the decrease from pH 7 to 9 and the overall decrease in sharpness at any pH with increasing S.

SECTION 5.1. ELECTRON MICROSCOPY OF RABBIT PSOAS MUSCLE - METHODS.

The EM studies were undertaken to directly examine the changes in shape of the A-band, and the positions of the thick filaments in rigor and with 5mM PPi at increasing values of S, and with changing pH. It was hoped these changes could be correlated to the changes seen in the equatorial X-ray reflections seen in Sections 3 and 4.

(a) 5.1.1. Preparation of samples.

Bundles of glycerinated muscle fibres ~1 mm in diameter were stripped from previously prepared samples that had been stored at -20 → -30°C for between 1 and 3 months. The bundles were trimmed to ~2 cm in length, ligatured at both ends and held in a U-shaped stainless steel mount by the friction of the ligatures on cuts in the metal. This allowed samples to be manipulated to remove twists, and held at a tension just above slack. This ensured straight and parallel fibres, which made sectioning the final blocks a good deal easier. To vary S, different bundles from samples that had been stretched or contracted prior to the initial glycerinating process were used (see X-ray methods). The bundles were soaked in the relevant solution for 1/2 → 1 hr at 20°C. The solution was changed for the the same experimental solution with 2.5% glutaraldehyde. Chemicals for EM were all from Agar Aids, except where indicated. The following method was then adopted for all samples, on the advice of Drs K.M.Meek and P Cooke.

(a) 4 hrs in experimental solution + 2.5% glutaradehyde. At the end of this time, samples were chopped into 1-2mm lengths. This allowed more rapid entry of chemicals and allowed them to fit into the polymerizing

trays.

(b) 1/2 hr rinse in experimental solution.

(c) 2 hrs in a 1:1 mixture of 4% OsO_4 and 0.1 M s.collidine at pH 7.4. In some experiments this post-fixation/staining was performed at 2-4°C, since Maupin-Szamier and Pollard (1979) showed that at this temperature the destruction of actin filaments by OsO_4 was reduced. In practice, the lower temperature post-fixation made no difference to the final result, and Maupin-Szamier and Pollard suggest that tropomyosin has a stabilizing effect during osmium treatment.

(d) Thorough wash in distilled water.

(e) 1/2 hr en bloc stain in 1-2% uranyl acetate at 60°C in sealed vials to prevent dehydration.

(f) Repeated washes in distilled water.

(g) 1 hr in 1% aqueous tannic acid (Aldrich Chemicals) solution.

(h) Distilled water wash.

(i) Ethanol dehydration. 15-20 mins in each of a 30, 50, 80 and 95% solution. Finally 2 washes in 100% ethanol for 15-20 mins each.

At this point either Araldite or Spurr resin was used as the embedding medium, and slight differences in method were employed for each. Spurr resin proved easier to use since early experiments showed infiltration with Araldite was very slow so leading to a very lengthy procedure.

5.1.2. <u>(1) Araldite.</u>

(j) 5-10 mins in 1:1 mixture of ethanol and propylene oxide.

(k) 2 washes in 100% propylene oxide for 20 mins each.

(l) 10% resin in propylene oxide for the rest of the day (usually 1-3 hrs)

(m) Evaporate down to 50% resin/propylene oxide and leave to infiltrate overnight (~12 hrs).

(n) Fresh 100% resin for 4-5 hrs.

(o) Change for more fresh 100% resin for another 4-5 hrs.

(p) Embed in fresh resin, polymerize at 40°C for 1 day, 60°C for another day and leave to cure at 40°C for a final day.

5.1.3. (2) Spurr.

(j) 1/2 hr in 1:1 mixture of ethanol and resin.

(k) 100% resin for the rest of the day (1-3 hrs).

(l) Replace with fresh 100% resin overnight (~12 hrs).

(m) Embed in fresh resin, polymerize at 40°C for 1 day, 70°C or another day and cure at 40°C for a final day.

The choice of resin had no effect on the results, though as mentioned previously Spurr was most often used, to save time.

After polymerization the blocks were left to cure for 1-2 days at room temperature in a dessicator, so the whole process from fixation to a block ready for sectioning could be done in under a week. Sections were cut using either a Sorvall MT-2 or Reichert Ultracut E with glass knives (rectangular or rhomboid made with an LKB knifemaker) or a Dupont diamond knife. Grey or silver/grey section were cut (~30-40nm), relaxed with chloroform vapour and collected on G400 Cu or Cu/Pd grids. The sections were checked for orientation of fibres and only those sections which were parallel to the plane of cut were accepted. The criterion for judging if the fibre was parallel was if 15-20 adjacent sarcomeres in a fibril had the same width. If the sections failed this test, the block was realigned and sections cut until the condition was met.

Sections were stained with Reynolds lead citrate for 20 mins in petri dishes with NaOH pellets present to prevent precipitation of lead carbonate. The grids were examined and photographed in either a JEOL JEM T-7, Philips EM-300 or JEOL CX100 at high voltage/low current settings. Only those pictures from the EM-300 or CX 100 were used for digitization and optical diffraction studies.

(b) 5.1.4. Calculation and computation.

The measurement of bowing was performed using pictures taken on the JEOL JEM T7 microscope at approximately 10000x magnification. The width of the myofibrillar sections were measured at both the M-line and the A/I junction for individual sarcomeres. The number of thick filaments in the section was noted, to provide a measure of depth into the fibril. The ratio of the sarcomere width at the A/I junction (W_{ai}) to M-line width (W_m) was taken and incorporated into an equation to get a percentage measure of the bowing;

$$\text{bowing} = 100\left[\frac{W_m - W_{ai}}{W_m}\right] \quad ----- \quad (1)$$

About 200 separate measurements were made, and the mean ± standard deviation was calculated for each value of number of filaments in the cross section. For the more detailed analysis pictures were taken of silver/grey sections (≈30 → 40 nm thick) using a JEOL CX 100 at 10000x magnification. The micrographs were placed in a photographic enlarger at 10x magnification and the pattern of thick filaments traced onto A4 sized paper. The tracings were digitized using a Tektronix 4662 digital plotter with the platen calibrated for A4 paper. The software used was written in Tektronix 4051 BASIC and

performed the following routine:

(a) The number of filaments in the sarcomere under consideration were counted and the mean spacing between them calculated. The angle which the filaments make to the horizontal axis of the plotter was also measured. Since the M-line was often not perpendicular to the filaments, the difference between the measured M-line angle and the perpendicular was also calculated. This difference was used to generate the vectors to move the cross-hairs during digitization.

(b) The length of the thick filaments was measured and divided into 10 equal segments, the cross-hairs were moved to the M-line, for each filament in turn, and moved along the filament 10 times, so covering one half filament from M-line to A/I junction in 10 jumps. At each jump the X/Y coordinates at the position were recorded.Since the filaments were disordered, movements in a second dimension of the cross-hairs were necessary at each jump to locate the traced line. This was achieved by moving the cross-hairs in repeated small segments of an arc centered on the previous point and of radius filament length/10. The point of intersection of arc and filament was the point input for that jump. This routine was repeated for all filaments in the half sarcomere.

The data were transmitted directly to a Tektronix 6130 where the calculation was performed. The basis of this was to generate an "ideal" lattice from the two angles measured at the plotter, assuming the filaments to be perfectly straight and separated by the same distance (the mean spacing measured at the plotter), this resulted in a 2-dimensional lattice of parallel lines. Other types of lattice were generated, based on longitudinal sections through truncated cones and ellipses. The "ideal" points from all three lattice types were then subtracted from the digitized lattice points of the micrograph tracing, to generate a figure for the distortion of the experimental result from

the theoretical lattice at each point in the half sarcomere. This treatment is clearer if one imagines the experimental tracing (eg, results Fig 5.2.4.1) superimposed on another 2D tracing of the positions of the filaments in the calculated "ideal" lattice. The match will not be perfect, and so there will be differences between experimental and ideal lattices over the whole half sarcomere. The lateral distance which separates a point on a filament in the experimental lattice from its corresponding position in the same filament in the ideal lattice is the numerical value of the distortion. Since the filaments in the ideal lattice are either to the right or the left of the experimental lattice, then a subtraction of the cartesian coordinates of analagous points will result in the distortion having a positive value if the value of a given experimental point is to the right of the corresponding ideal point (since in cartesian space values increase to the right) and a negative value in the reverse case. The resulting graphs plot the value of distortion against position of the point in the filament for all filaments in the section, and so show the distortion along each filament from M-line to A/I junction, giving a representation of distortion over the whole half sarcomere.

The digitized data were further analysed using a one dimensional Fourier summation;

$$F(k) = \Sigma\ 2\pi k f(x) \qquad ------ \quad (2)$$

where k is the point in reciprocal space. In this case the summation was carried out over the range of k=0 to k=5 nm^{-1} and this was reached in 1000 steps of 0.005 nm^{-1}; this was found to give acceptable resolution of peaks.

Programs to calculate F(k) were written both in tBASIC (run on a Tektronix 6130) and in Tops 10/20 FORTRAN (run on a DEC-20). The

only difference was the time taken to obtain the result (~90 mins for the Tektronix, ~50 seconds for the DEC-20). Both digitized and ideal lattices were subjected to this summation, the sum of the squares of the F(k) were calculated for points over the whole half sarcomere to give an approximation of the optical diffraction pattern expected from each half sarcomere.

The predicted result from the Fourier summation was checked by taking optical diffractograms (OD) of the half sarcomeres, using a diffractometer as shown in Fig 5.1.1. All components of the system were on mounts fully adjustable in 3 dimensions, and securely clamped to a 4m long optical rail. In operation it was found that careful initial adjustment of the laser to the horizontal with a spirit level saved considerable time later on when aligning the optical axes of the lenses to the instrument axis. Pinholes (b) and (d) were very crucial; initially 1mm aluminium sheet was used as the pinhole material (the low laser power meant that heating and subsequent distortion of pinholes was not a problem). This gave poor results as drilling small symmetrical holes was in practice impossible. Also, the depth of hole was greater than or equal to its width, and this gave rise to indistinct diffraction rings from the pinhole. Both these problems would adversly affect the final picture, and were eliminated by using 50 μm steel foil as the pinhole material. Assiduous cleaning of the pinholes to remove dirt and swarf was also very important. Positioning of the lenses was a trade-off betweem size of diffraction pattern and area of micrograph illuminated, the settings in Fig 5.1.1 giving a circle of even illumination ~2 cm in diameter at the micrograph, and a resolution of ~0.1 - 0.2 mm on the film. The double lens system (e) and (g) ensured that the light beam at the micrograph was parallel. The optical axes of the lenses were aligned using the diffraction of a fine muslin cloth reflected back to the Boys point, so that the cloth acted as both

Fig 5.1.1. Schematic diagram of the optical diffractometer used in Electron Micrograph analysis.

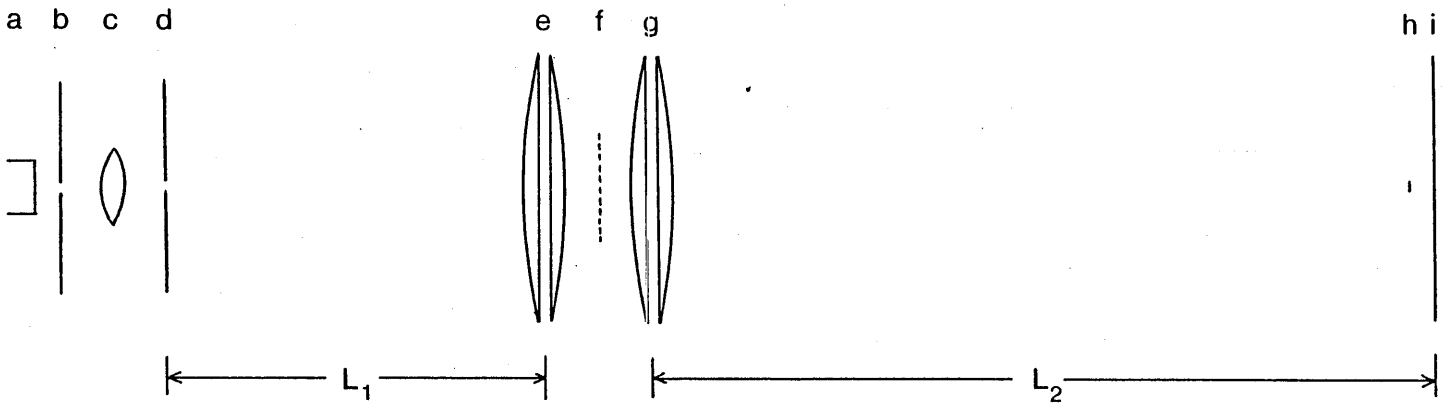

L_1 = 1.12 m

L_2 = 2.32 m

a 5 mW He/Ne laser (λ = 632.8 nm - NEC GLG5022)

b 1 mm apeture

c Light microscope objective lens (0.03 NA, f=60 mm - Beck)

d 350 μm pinhole

e + g Double plano convex lenses (Diameter 102 mm, f=1.5 m - Unitron)

f Electron micrograph in U-shaped perspex mount

h Aluminium foil backstop

i White paper screen or photographic film (Ilford FP4)

source and screen, allowing adjustment of the lens optical axis to better than 10' of arc. The diffractometer was calibrated using a computer-generated sine wave to simulate a helical diffraction pattern. This was punched out on aluminium foil with a pin mounted on a pen holder in an X–Y plotter. This produced imperfect diffraction patterns because the action of the plotter resulted in tearing rather than punching the foil. This gave rise to rectangular rather than circular holes, and caused the layer line reflections to broaden considerably. However, the axial positions of the holes were very accurate, so for calibration purposes the resulting diffraction patterns were adequate.

The micrographs were masked off with thick black paper until all that was showing was the half-sarcomeres under study. They were mounted in a U-shaped clamp which held three edges of the micrograph to ensure they were flat and perpendicular to the beam between the lenses. Pictures were taken using Ilford FP4 mounted in the plane of the screen, and an exposure of <1 s was sufficient to produce high contrast diffractograms. Spacings were measured using a Nikon 6C profile projector with underneath light source.

The OD results were compared to X-ray diffraction results of specimens both in solution and after embedding. These latter specimens were treated as in Section 5.1 except that cutting into small blocks was omitted so that a substantial length of muscle was prepared and embedded; this made mounting in the X-ray beam very simple. The sample was kept to a small width (<1 mm) so penetration of stains and resin was no different than for the EM specimens. The exposure times for these embedded specimens was about half that for the untreated muscle (~10–20s). Despite the fact that more material was present in the sample, the increased scattering from the heavy metal stains more than compensated for the increased density.

SECTION 5.2. RESULTS OF ELECTRON MICROSCOPE STUDIES WITH RABBIT PSOAS MUSCLE.

(i) The effect of Sarcomere length (S) and pyrophosphate (PPi).

(a) 5.2.1. Analysis of micrographs.

In this section the results of the analysis of electron microscope (EM) pictures is presented. It will be shown that distortions within the A-band lattice fall into two categories: (1) a gross distortion of the A-band which is apparent as a bowing, and (2) a local disorder over a smaller distance between individual filaments or groups of filaments which form domains within the sarcomere.

The results of the simple measurements of M-line width and A/I junction width were used to calculate the the overall bowing as defined by equation (1) in the (see Methods Section 5.1.4). The mean was calculated for each value of the number of filaments over the whole range measured, and the values obtained are shown plotted as mean vs number of filaments in section (N) for S=2.1 μm (see Fig 5.2.1). This value of N for the abcissa gives a crude measurement of the position of the section within the sarcomere, assuming that all the myofibrils are roughly cylindrical and of similar diameter. Fig 5.2.1 shows the mean + or - S.D for successive numbers of filaments in the sections, the rest of the data (Figs 5.2.2 and 5.2.3) show just the mean values. Consider first the graphs of the control experiments with rigor muscle at various S (Figs 5.2.2 and 5.2.3). For the sake of brevity, only graphs at S=2.1 μm and 3.3 μm are presented. Overall the bowing decreases with increasing S, the decrease having reached zero at S$\geq$2.9; this disagrees with Bergman (1983). In the experiments where bowing is present, (ie S=2.1 and 2.6) addition of PPi caused a

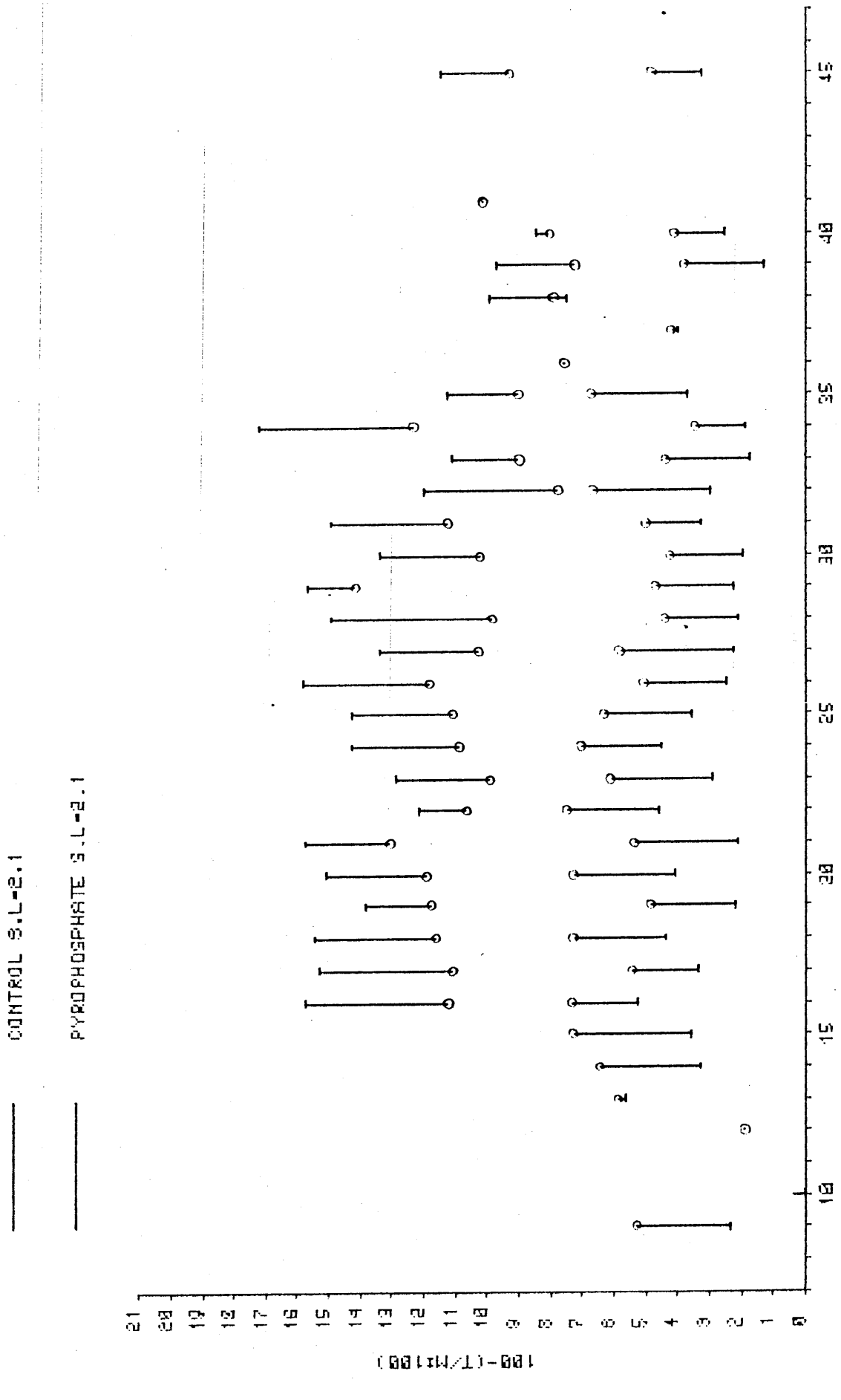

Fig 5.2.1. Mean and standard deviation bowing for control and PP1 at S=2.1 µm.

reduction in the degree of bowing. At higher S this simple measurement of distortion shows that bowing increases slightly with addition of PPi at S=2.9, and that at S=3.3 for low N (ie towards the edge of the myofibril) a small "negative" bowing is present. This means that the A/I junction has a greater width than the M-line in rigor under these circumstances. This effect is abolished by PPi.

An attempt was made to fit a theoretical curve to the data. The half sarcomere was modelled on successive sections of a truncated cone, as suggested by Bergmans' (1983) constant volume model. Figs 5.2.3.1 and 5.2.3.2 give the fit at S=2.1 μm, Figs 5.2.3.3 and 5.2.3.4 give the fit at S=3.3 μm. The full range of values fitted to the bowing data curves using the truncated cone model are shown in Table 5.2.1. These values give the percentage decrease in diameter between the M-line and the A/I junction at the maximum N, i.e at the point in the fibril of maximum diameter.

Table 5.2.1. The degree of bowing for specimens in control and in PPi solution modelled by a truncated cone. These values of the model parameters give best fit for the experimental data.

SARCOMERE LENGTH	BOWING IN CONTROL (%)	BOWING IN PPI (%)
2.1	8.50	4.25
2.6	7.00	4.00
2.9	0	2.00
3.3 *	No fit possible	0 (?)

The asterisk by S=3.3 denotes that with the model used no fit was possible. The curve showed a negative bowing at low N and no bowing at higher N - with all the models used, a fit of 0% would result in a horizontal line equal to 0, and not curve downward. Addition of PPi considerably reduced this effect and allowed a

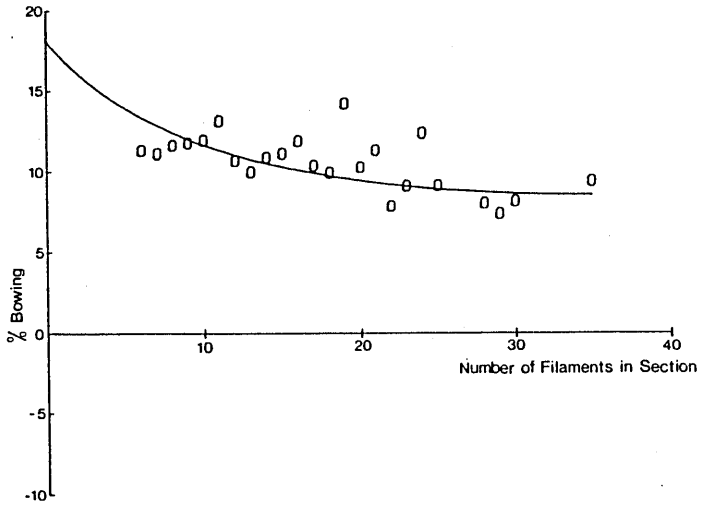

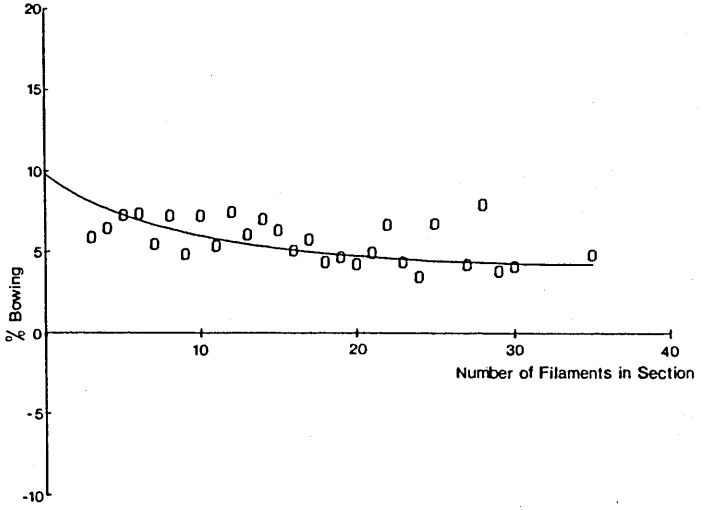

Fig 5.2.2.1. (left) and Fig 5.2.2.2 (right). Bowing measured vs level of the section in the fibril (as measured by the number of filaments in the section) for rigor (left) and 5mM PPi at S=2.1 μm. Circle shows best fit with a truncated cone model.

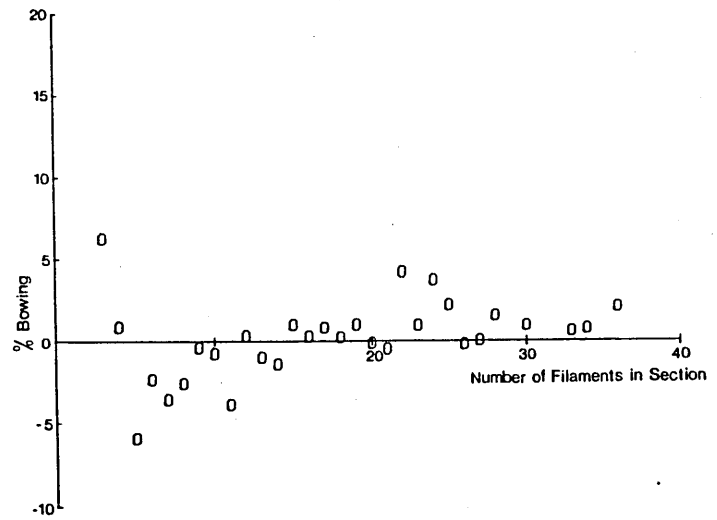

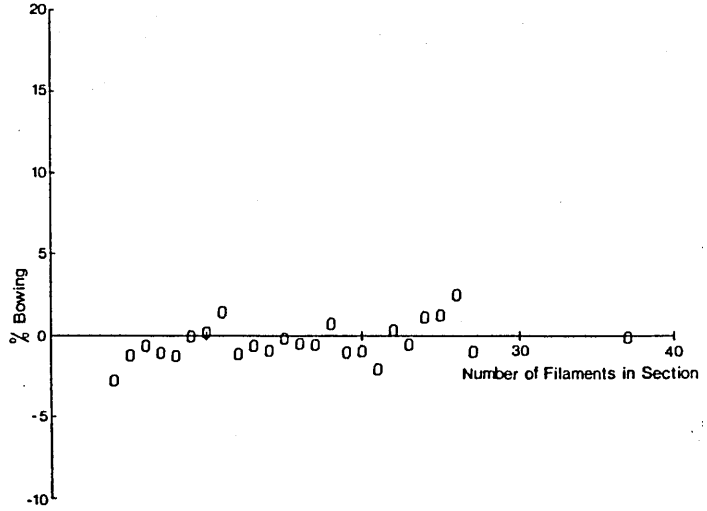

Fig 5.2.2.3. (left) and Fig 5.2.2.4 (right). Bowing measured vs level of the section in the fibril (as measured by the number of filaments in the section) for rigor (left) and 5mM PPi at S=3.3 μm.

tentative fit of 0%.

The curves so generated are at best only an approximate fit and this fact, together with the anomalies at long S, suggested that the simple analysis based on the truncated cone is good only as a first order estimate of distortion in the A-band of rabbit psoas. Consequently, randomly chosen individual sarcomeres were analysed by digitizing the filaments in a half sarcomere and comparing the result to a computer generated "ideal" rectangular A-band (see Figs 5.2.4.1 and 5.2.4.2) for results at S=2.1 μm in the rigor and PPi states and Figs 5.2.4.3 and 5.2.4.4 for S=3.3 μm.

In these diagrams the distortion from the ideal lattice at any given point is represented by the value of the ordinate. The overall pattern of distortion in the control solution shows marked changes as S is increased. However, it also illustrates the major limitation of the analysis that direct comparison between any two graphs is not strictly valid. The reasons for this are:

(a) With EM, the preparation of specimens involves a series of irreversible physical and chemical changes, so one specimen cannot be subjected to a series of experiments to provide paired data. This disadvantage can be offset by (experimentally) making conditions between two separate samples as similar as possible. In the present case this was achieved by using the same stock solution on different fibres from the same pre-soaked sample.

(b) The sample size of the data is always one, since each half sarcomere is treated independently. This contrasts directly with the previous simple analysis with its sample size of $\geq$200.

(c) The mean and standard deviation values in Fig 5.2.1 show that the range of data values overlaps for control and PPi experiments, and that the calculated means and standard deviations themselves exhibit considerable scatter. So at least for measurements of bowing, the

result of one experiment may well lie within the range of the other. For any other analysis this scatter should be taken into consideration when comparing two experiments under different conditions.

Bearing in mind the points made above, an overall qualitative description of the distortion between pairs of graphs at the same S in control and PPi shows that where distortion increased with increasing distance along the filament, addition of PPi caused a reduction in the magnitude of this distortion, (see Figs 5.2.4.1 and 5.2.4.2). In the graphs where this increase toward the A/I junction occurs, there is a symmetry round an axis roughly at the lateral mid-point of the half sarcomere i.e a positive distortion is matched by a negative distortion at the corresponding position in the opposite side of this axis - it is observed that this distortion is reduced by PPi. This is a direct measurement of the degree of reduction in bowing and is clearest at S=2.1 μm.

A further effect of PPi was an overall smoothing of the graph at all distances along the filament. This was apparent at all values of S. Also, over the whole range of S studied, areas of local distortions were present within the graph (see Fig 5.2.4.3). These domains were less clear at short S and with PPi. At longer S in the control experiment the local domains have a greater magnitude of disorder than any differences between M-line and A/I junction. Addition of PPi at these longer sarcomere lengths results in a reduction in the magnitude of these local distortions (see Figs 5.2.4.3 and 5.2.4.4)

To get a more quantitative measure of the overall distortion of the half sarcomere, the root mean square distortion (RMSD) for all points in the graph was taken. Table 5.2.2 shows the results for the RMSD calculation for all value of S in control and PPi solutions. In keeping with the model used in the simple analysis performed earlier, an attempt was made to fit the experimental lattice to an "ideal"

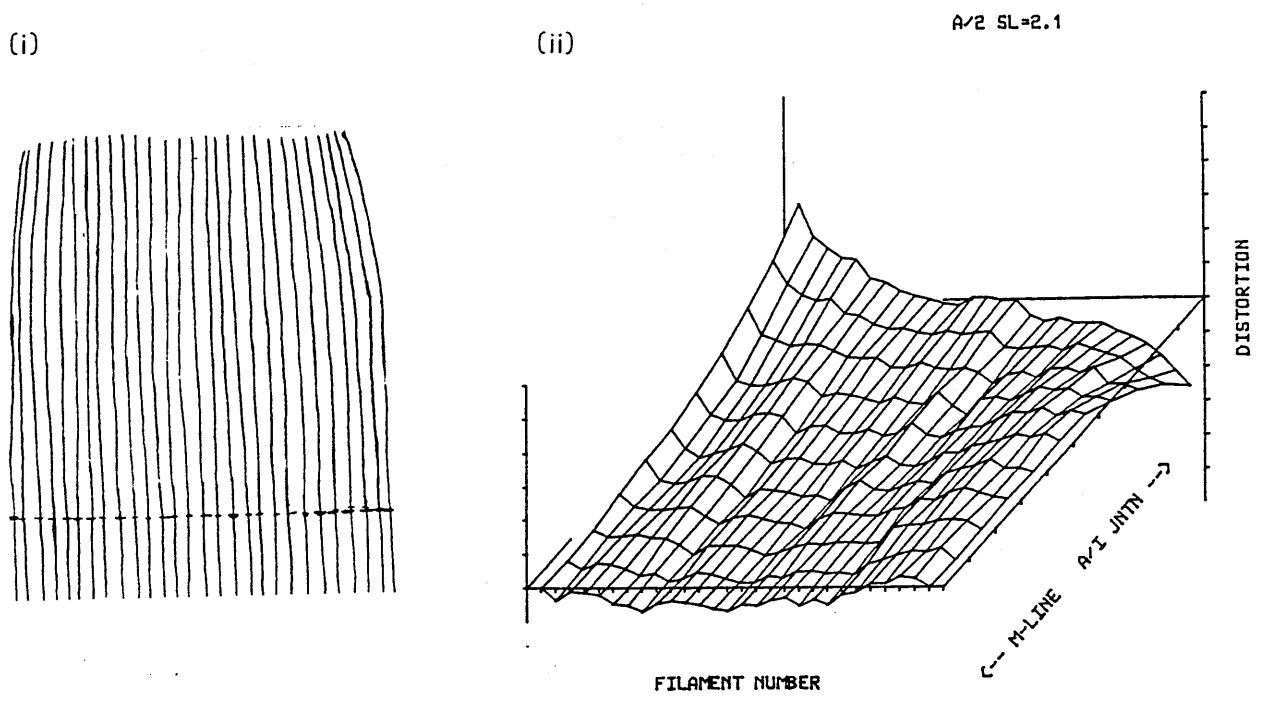

Fig 5.2.4.1 (i) Tracing of thick filaments in a half-sarcomere at S=2.1 μm in control rigor solution. (M-line downwards).

(ii) Distortion from an ideal rectangular lattice of the half-sarcomere in (i).

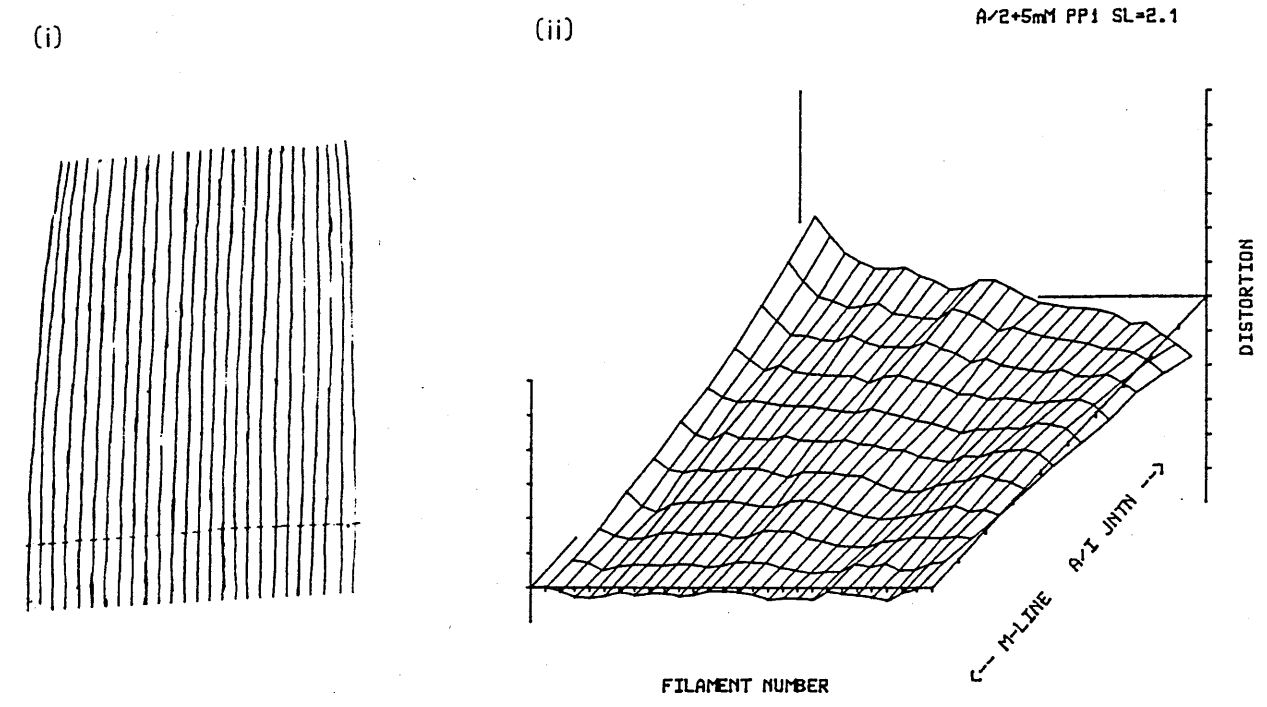

Fig 5.2.4.2.(i) Tracing of thick filaments in a half-sarcomere at S=2.1 μm in 5mM PPi solution. (M-line downwards).

(ii) Distortion from an ideal rectangular lattice of the half-sarcomere in (i).

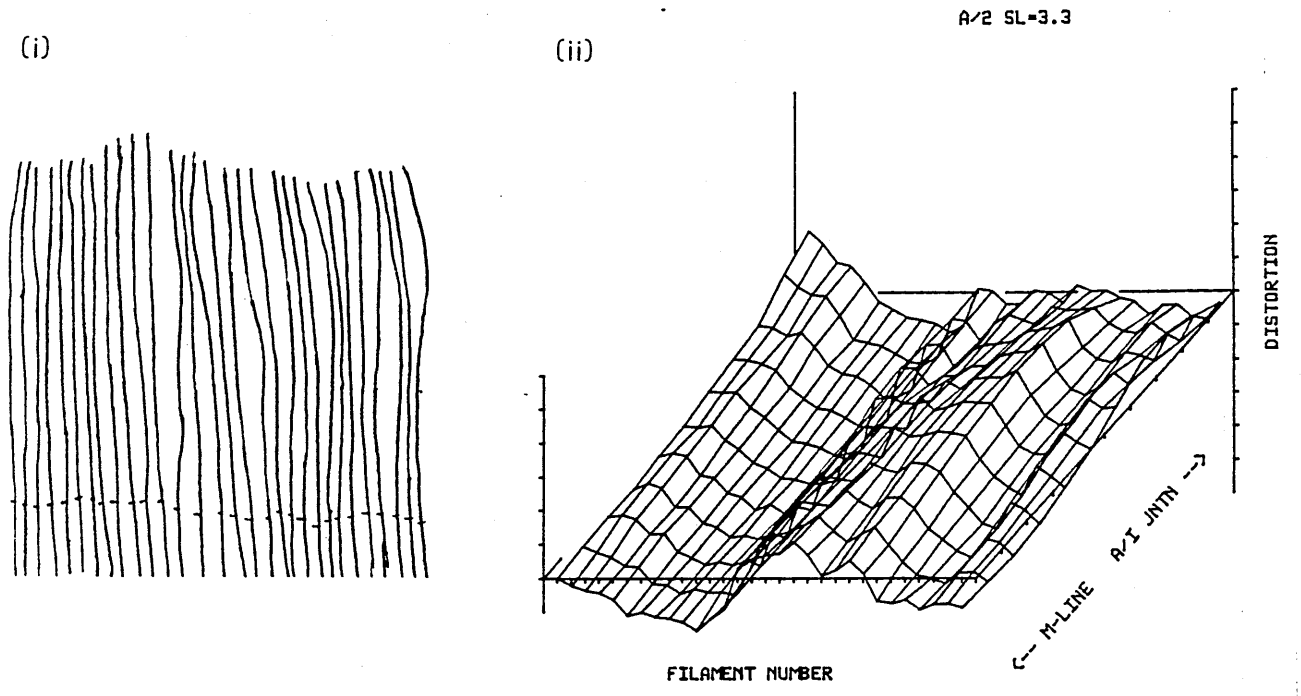

Fig 5.2.4.3.(i) Tracing of thick filaments in a half-sarcomere at S=3.3μm in control rigor solution. (M-line downwards).

(ii) Distortion from an ideal rectangular lattice of the half-sarcomere in (i).

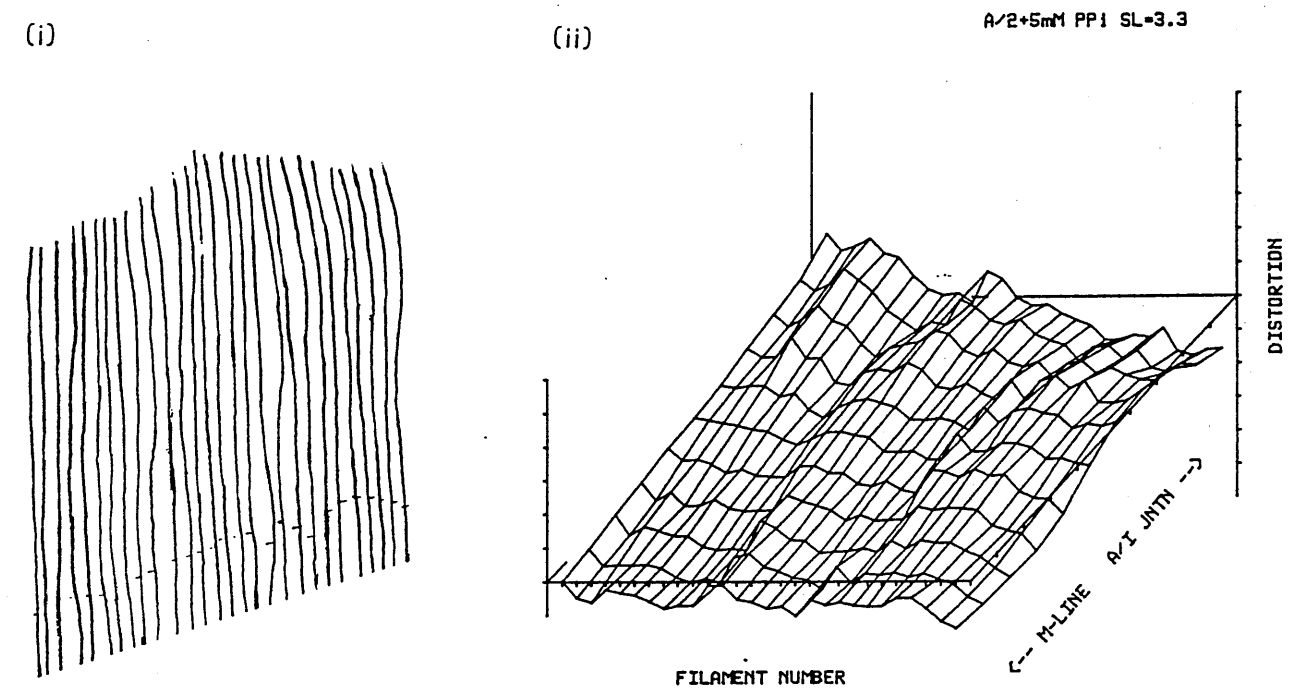

Fig 5.2.4.4.(i) Tracing of thick filaments in a half-sarcomere at S=3.3μm in 5mM PPi solution. (M-line downwards).

(ii) Distortion from an ideal rectangular lattice of the half-sarcomere in (i).

truncated cone lattice. If the distortion were a perfect truncated cone then a regular change in distortion would be seen at short S. Fig 5.2.5 shows the distortion of a perfect truncated cone lattice from the "ideal" rectangular lattice using data from the control experiment at S=2.1 μm. The changes seen are all linear, but the overall result shows regions of high distortion in the areas at the edge of the A/I junction similar to that seen in the results shown in Figs 5.2.4.1 for S=2.1 μm and also seen at S=2.6 μm. Figs 5.2.6.1 and 5.2.6.2 show the distortion from the truncated conical model at S=2.1 μm. The fit shows considerable deviation, but now the distortion at the A/I junction is in the opposite direction, indicating that the distortion from the cone is the reverse to that of the rectangle. If the cone were a better overall fit to the data then there should be a reduction in the RMSDs of the fits, these values are also given in Table 5.2.2 for control and PPi experiments (a perfect fit would result in a completely planar graph and an RMSD of 0) From Figs 5.2.4.1 and 5.2.4.2 together with Figs 5.2.6.1 and 5.2.6.2 at S=2.1 μm, it is apparent that the increase in distortion is not linear and so the simple truncated cone does not model the distortion seen. For this reason, an "ideal" truncated ellipse was fitted to the data. Fig 5.2.7 shows the distortion of the generated "ideal" ellipse from the rectangular lattice, again using data from the control at S=2.1. Fig 5.2.7 differs from Fig 5.2.5 in that the distortion along the filaments is now curved and not linear. Figs 5.2.8.1 and 5.2.8.2 show the distribution from the elliptical lattice for S=2.1 μm, Figs 5.2.8.3 and 5.2.8.4 at S=3.3 μm. Again the fit is not perfect and the graph of distortion is similar in form to the conic fit, however there are differences in the RMSD (see Table 5.2.2).

That these distortions persist in the conic and elliptic models shows that the distortion in the experimental data is not fitted by the theoretical models. A more detailed examination of the distortion graphs

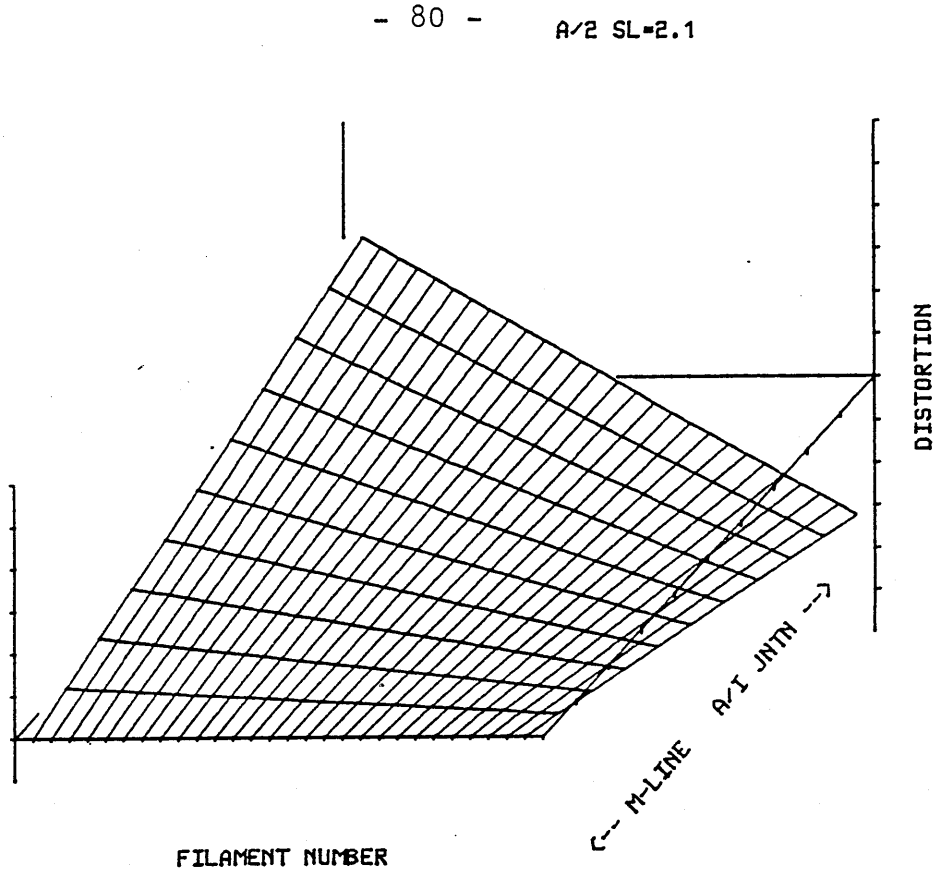

Fig 5.2.5. Distortion from a rectangular lattice of an ideal truncated cone.

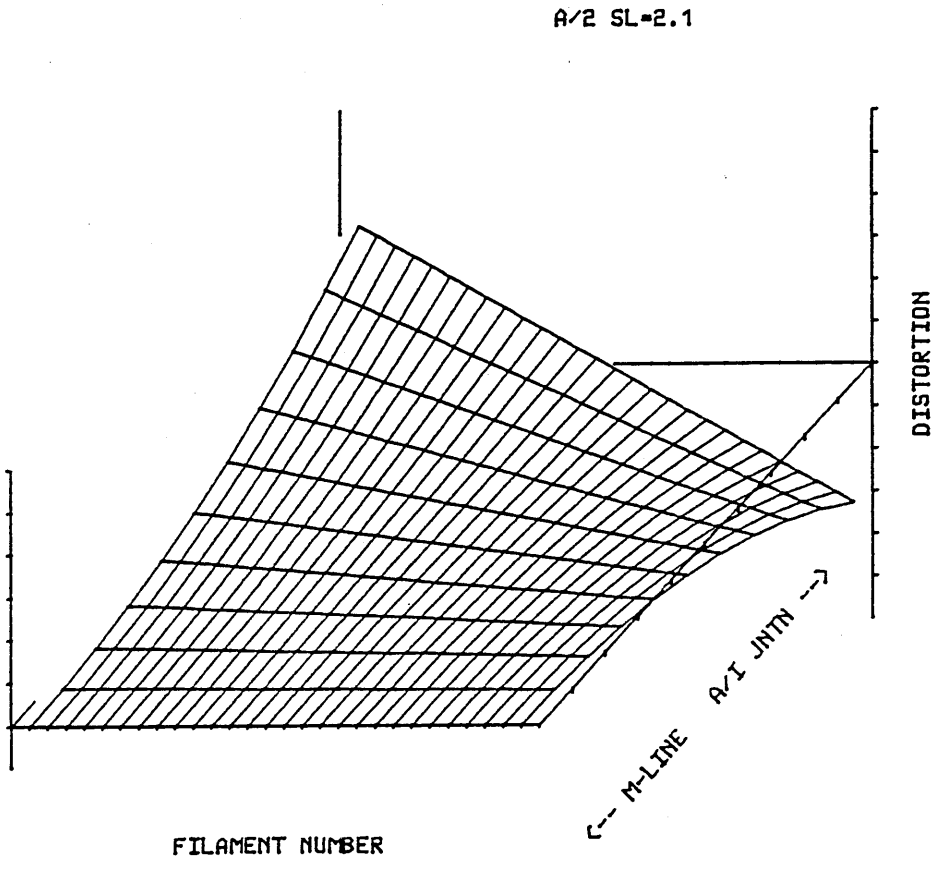

Fig 5.2.7. Distortion from a rectangular lattice of an ideal truncated ellipse.

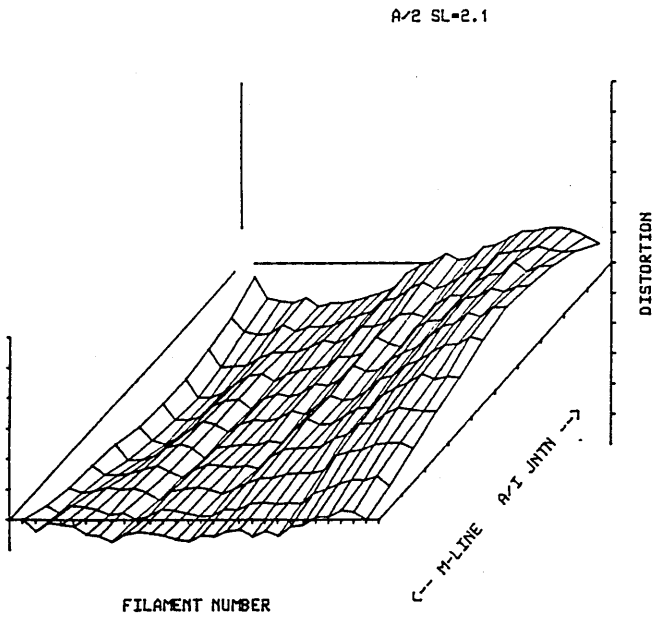

Fig 5.2.6.1. Distortion from an ideal truncated conical lattice of the half-sarcomere shown in Fig 5.2.4.1 in control rigor solution at S=2.1 μm.

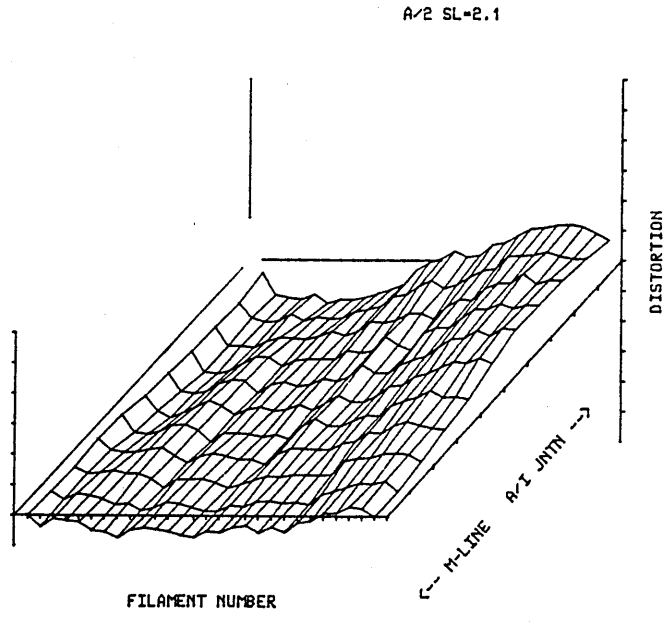

Fig 5.2.8.1. Distortion from an ideal truncated elliptical lattice of the half-sarcomere shown in Fig 5.2.4.1. in control rigor solution at S= 2.1 μm.

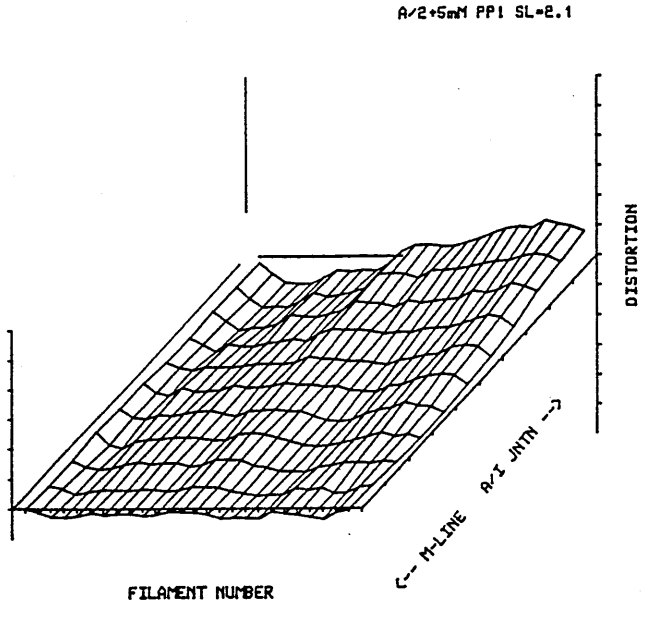

Fig 5.2.6.2. Distortion from an ideal truncated conical lattice of the half-sarcomere shown in Fig 5.2.4.2 in control + 5mM PPi solution at S=2.1 μm.

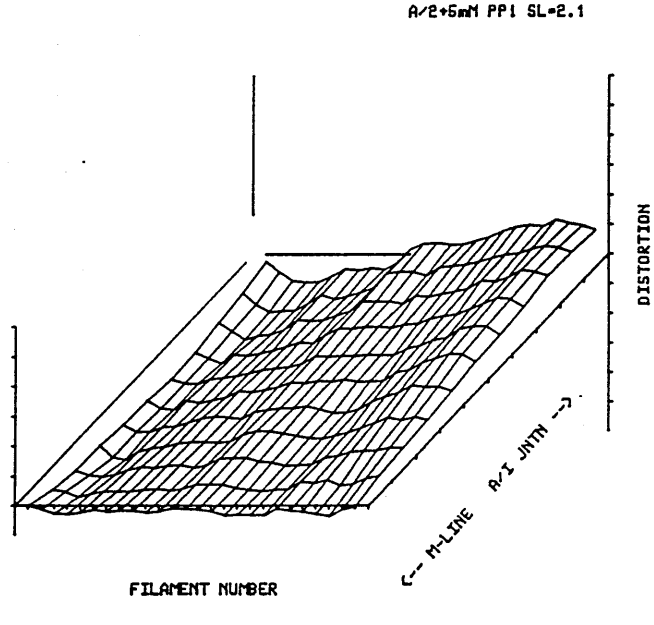

Fig 5.2.8.2. Distortion from an ideal truncated elliptical lattice of the half-sarcomere shown in Fig 5.2.4.2 in control + 5mM PPi solution at S=2.1 μm.

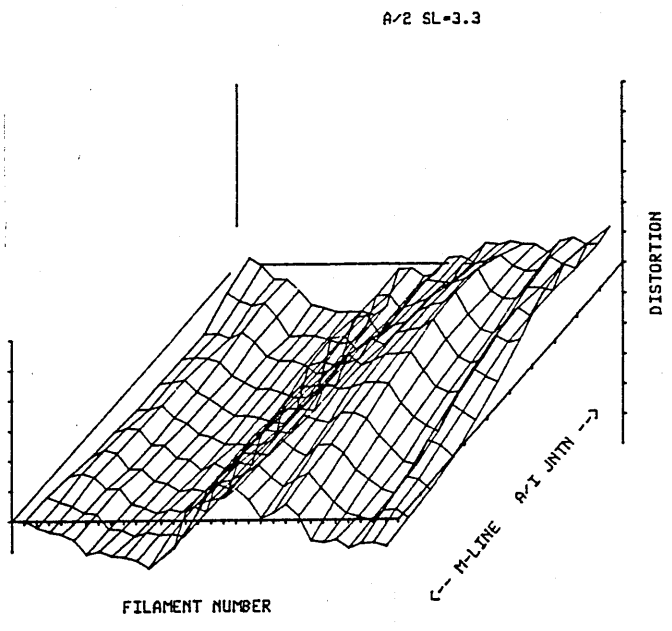

Fig 5.2.6.3. Distortion from an ideal truncated conical lattice of the half-sarcomere shown in Fig 5.2.4.3 in control rigor solution at S=3.3 μm.

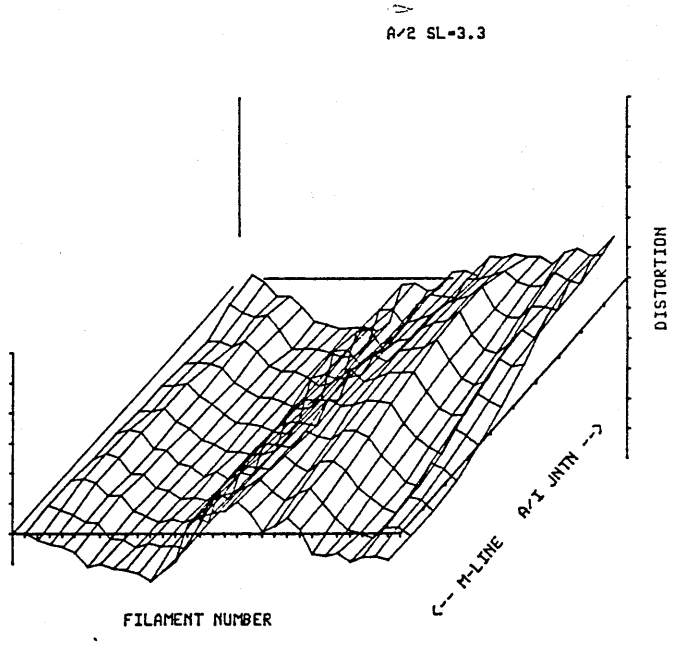

Fig 5.2.8.3. Distortion from an ideal truncated elliptical lattice of the half-sarcomere shown in Fig 5.2.4.3 in control rigor solution at S=3.3 μm.

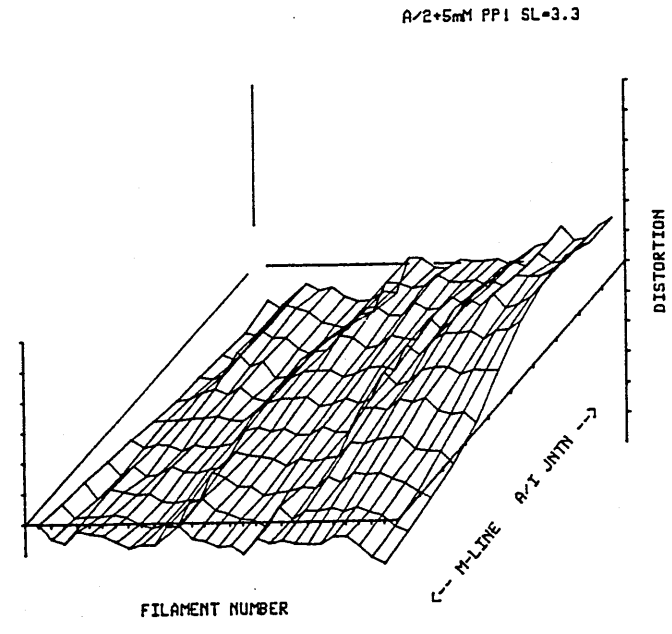

Fig 5.2.6.4. Distortion from an ideal truncated conical lattice of the half-sarcomere shown in Fig 5.2.4.4 in control + 5mM PPi solution at S=3.3 μm.

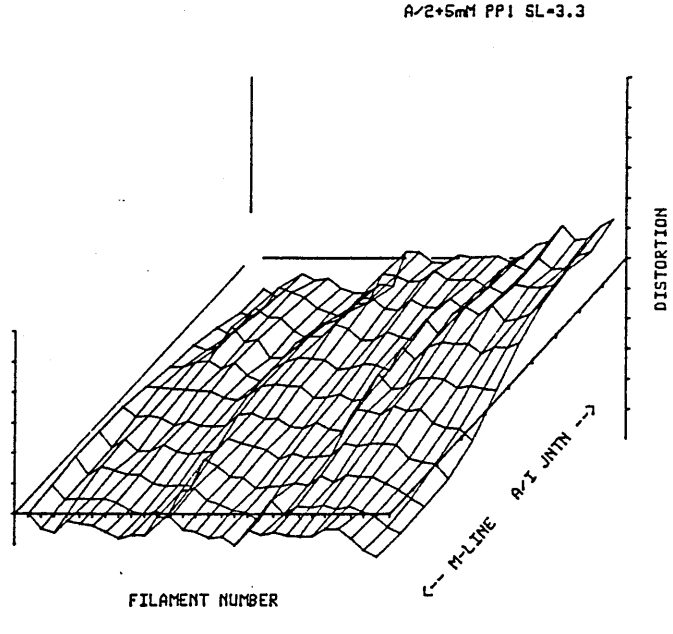

Fig 5.2.8.4. Distortion from an ideal truncated elliptical lattice of the half-sarcomere shown in Fig 5.2.4.4 in control + 5mM PPi solution at S=3.3 μm.

shows that in cases where there is pronounced bowing (i.e increases in distortion with distance along the filament and symmetry about a lateral mid-point) then the result of fitting a truncated cone or ellipse, which is simply a subtraction of "ideal" from experimental lattice, is to reverse that symmetry. Thus a positve distortion becomes negative, but the axis of symmetry remains roughly constant. Figs 5.2.6.3 and 5.2.6.4 show the distortion from the ideal conical and elliptical lattices and at these longer S, where local domains dominate the graph, then the change of model has a smaller effect on the form of graph (see Figs 5.2.4.3 and 5.2.6.3 for example) and little effect on RMSD of that particular fit (see Table 5.2.2). That the RMSD is not reduced to a relatively low value shows that generated lattice still does not fit the experimental data, and the symmetry shows that the distortion from the ideal lattice has some systematic component. Fig 5.2.9.1 shows the calculated position of the filaments at M-line and A/I junction at S=2.1 μm. The positions were calculated relative to the lateral mid-line of the half sarcomere (the origin on the graph), a negative distance corresponds to a distance to the left of the mid-point. The line joining the points at either extreme represents the line through the theoretical positions predicted by either the ideal truncated cone or the ellipse model, the difference between the point and the line represents the distortion seen in Figs 5.2.6.1 and 5.2.8.1 at M-line and A/I junction. At the M-line there is good correlation between experimental and theoretical, but at the A/I junction the curve shows a regular departure from the fit. This suggests that there is an ordered departure from the ideal filament spacing, resulting in a gradual change of spacing between filaments, as the distance from the mid-point increases. It is this gradual change in spacing which gives rise to the symmetrical distortions seen in the conic and elliptic model fits. Fig 5.2.9.2 shows a similar analysis with

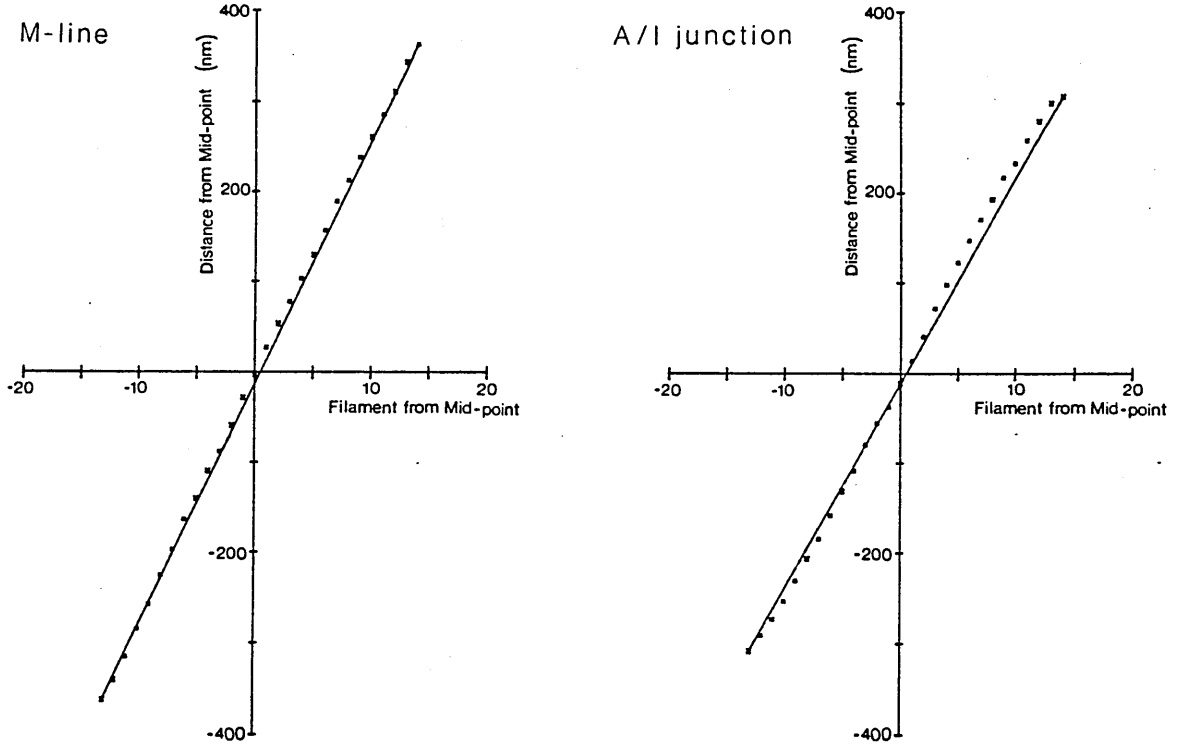

Fig 5.2.9.1. Distortion from an ideal linear separation of filaments in the M-line and A/I junction for rigor muscle at S=2.1 μm.

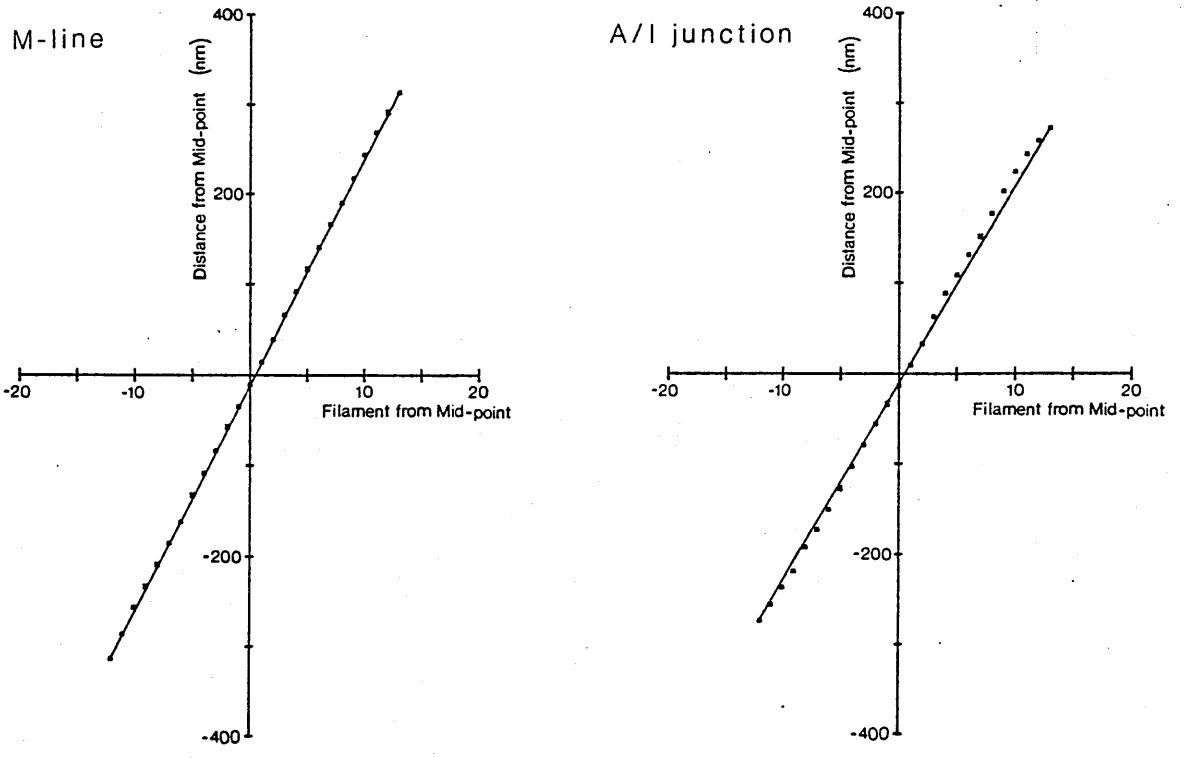

Fig 5.2.9.2. Distortion from an ideal linear separation of filaments in the M-line and A/I junction with control+5mM PPi at S=2.1 μm.

PPi at S=2.1 μm. The fit at the M-line is extremly good, and although the fit at the A/I junction shows the same effect of changing spacing as in the control, the magnitude is much reduced. Since the program used to generate the conic and elliptic lattices in the analysis bases the position of the calculated filament position on the mean spacing at the M-line and A/I junction, any regular departure from these positions will bias the fit produced, the bigger the spacing change the greater the bias. This positioning is not the only factor in determining the degree of fit, since examination of Table 2 shows the conic sections with PPi have a greater RMSD than the elliptical fit even though the values of the ideal lattice at the M-line and A/I junction are the same in both fits.

The overall result from Table 5.2.2, using the three models at all values of S, is that addition of PPi causes a reduction in the RMSD. This reflects the effects of PPi described earlier. However, there is a subtle relationship between the type of model lattice used and the

Table 5.2.2. Root mean square distortion (RMSD) from "ideal" rectangular, conical and elliptical lattices for single half sarcomeres at various sarcomere lengths in control and pyrophosphate solutions.

S (μm)	EXPT	$RMSD_{rect}$ (nm)	$RMSD_{cone}$ (nm)	$RMSD_{ellipse}$ (nm)
2.1	CON	8.4	16.1	11.4
	PPi	7.1	8.4	5.8
2.6	CON	12.1	10.9	9.0
	PPi	7.0	9.3	6.1
2.9	CON	23.2	25.2	24.6
	PPi	18.9	14.8	14.4
3.3	CON	12.2	15.6	14.4
	PPi	11.0	12.6	9.3

RMSD obtained. Only with PPi does it appear that the elliptical model fits the experimental lattice slightly better than the others, and even then the level of distortion from the theory is not minimal. As mentioned earlier in the closer examination of the different model graphs, the pictures which showed bowing (i.e those at short S) underwent a symmetrical reversal in distortion and relatively large changes in RMSD, whereas those with predominantly local domains (at longer S) showed little difference in RMSD with a change in model and less change in appearence of the distortion graph. This indicates that the total distortion as measured by RMSD has two components;

(a) A local disorder which manifests itself in the form of domains which may be several filaments across, and either a whole filament or a fraction of a filament long. These distortions tend to be of greater magnitude at longer S and are reduced with PPi. This local disorder results in the more constant RMSD values for various types of model, since no "ideal" lattice will allow for local distortions within the sarcomere. See for example Table 5.2.2, or the Figs at S=3.3 μm under control conditions where little variation in RMSD occurs

(b) A gross disorder over the whole half sarcomere which corresponds to a bowing. This bowing effect is reduced with increasing sarcomere length and by addition of PPi. The bowing results in the elliptical model being a slightly better fit with PPi when the effects of local disorder are reduced. In all cases where bowing is present, subtraction from a rectangular "ideal" lattice results in a symmetrical graph. (see Figs 5.2.4.1 and 5.2.4.2).

At shorter S an additional source of disorder can be identified;

(c) A regular change in spacing from the ideal positions within the major bowing distortion as shown in Figs 5.2.9.1 and 5.2.9.2. This shows itself in the reversed symmetry with conical/elliptical fits at short S. The fact that at longer S there is little or no reversal shows that this effect is diminished at these values as local disordering becomes more predominant.

(b) 5.3. Further analysis using digitized data.

Section 5.2 gave the results of the analysis of the EM pictures relative to ideal structures to show how distortions within the A-band are reduced by PPi treatment. In an attempt to draw a clearer correlation between these distortion changes and changes seen in the X-ray pattern, the analysis was continued along two main lines :-

(i) A mathematical treatment using Fourier summation and cubic spline fitting to estimate the widths of peaks arising from a diffraction experiment on EM pictures. In practice the cubic spline fit was the first derivative of a cumulative total of the data. By using this method a function of k with large magnitude and no sharp dislocations was generated, this type of function is better suited to a polynomial fit than the direct and "noisy" result of the Fourier summation.

(ii) An optical analysis using an optical diffractometer (OD) to measure directly any changes seen in patterns from the sarcomere studied.

(i) 5.3.1. Fourier summation of digitized EM data.

As described in the Methods Section 5.1.4, 11 1D transforms were

taken at regularly increasing distances from the M-line and averaged to produce the final graph. This was converted to a cumulative amplitude trace and the first derivative of a cubic spline taken as the fitted curve.

Figs 5.3.1 to 5.3.4 show the following curves :-

Green trace - result of the averaging of the 11 1D Fourier summations - note the average is squared to get this trace. A qualitative assesment of the trace shows an uneven distribution of peaks. At S=2.1 μm it is readily seen from the grouping of the peaks where the overall maximum lies within the trace (see Figs 5.3.1 and 5.3.2), at the longer S of 3.3 μm this maximum is more difficult to resolve (see Figs 5.3.3 and 5.3.4).

Red trace - Result of taking the first derivative of cumulative data. This results in a smooth trace through the green summation trace. At short S peaks are apparent which encompass the peak groupings and show some degree of symmetry. At longer S, the identification of these peaks becomes more difficult, though the red trace is still an improvement on the summation data.

Black trace - The mean spacing of the filaments was calculated from all points in the half sarcomere and the value used to generate this "ideal" curve. The result shows a typical theoretical pattern which would be expected from an extended array of equally spaced diffracting objects. Only the first two orders of the pattern are shown, but for those traces where the peak resolution is high the correlation between the ideal peak spacing, the summation data and the fitted data is good.

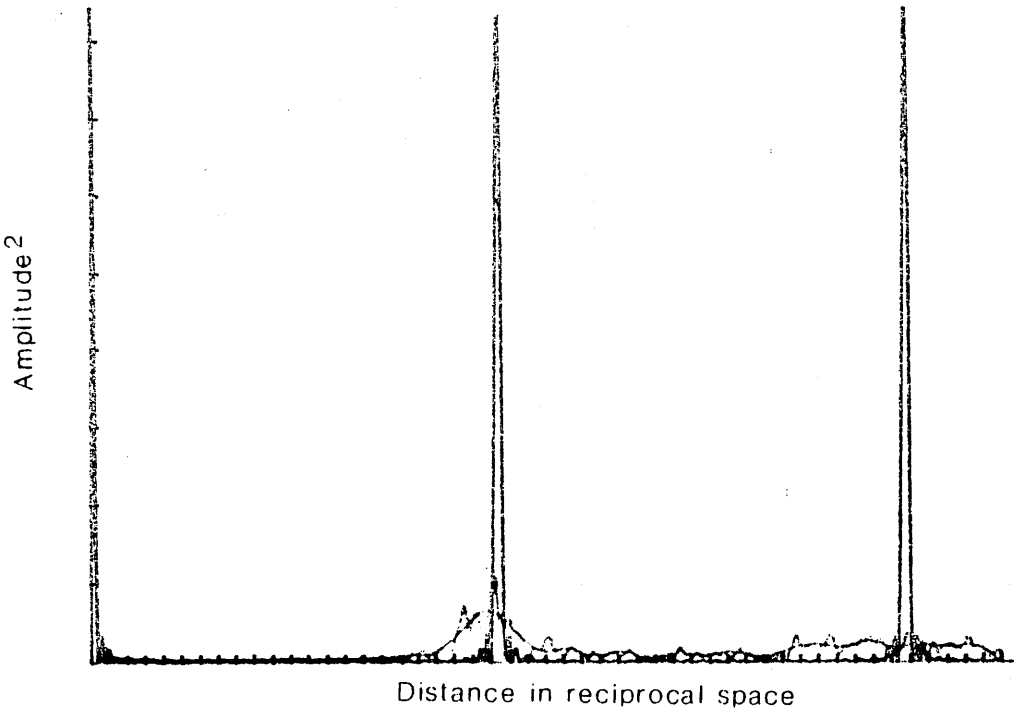

Fig 5.3.1 Fourier summation of the half-sarcomere shown in Fig 5.2.4.1 of control (A/2) at S=2.1 μm^{-1} The black curve shows the ideal result, the green the experimental and the red the fitted curve (see text).

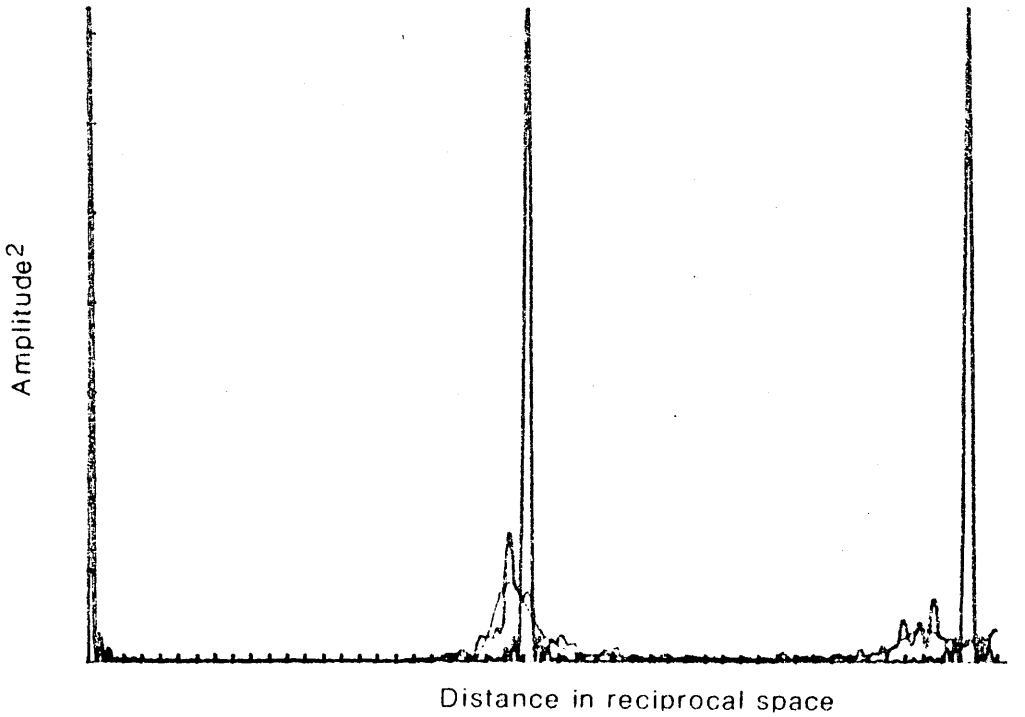

Fig 5.3.2 Fourier summation of the half-sarcomere shown in Fig 5.2.4.2 of A/2-5mM PPi at S=2.1 μm^{-1}. (See above for details).

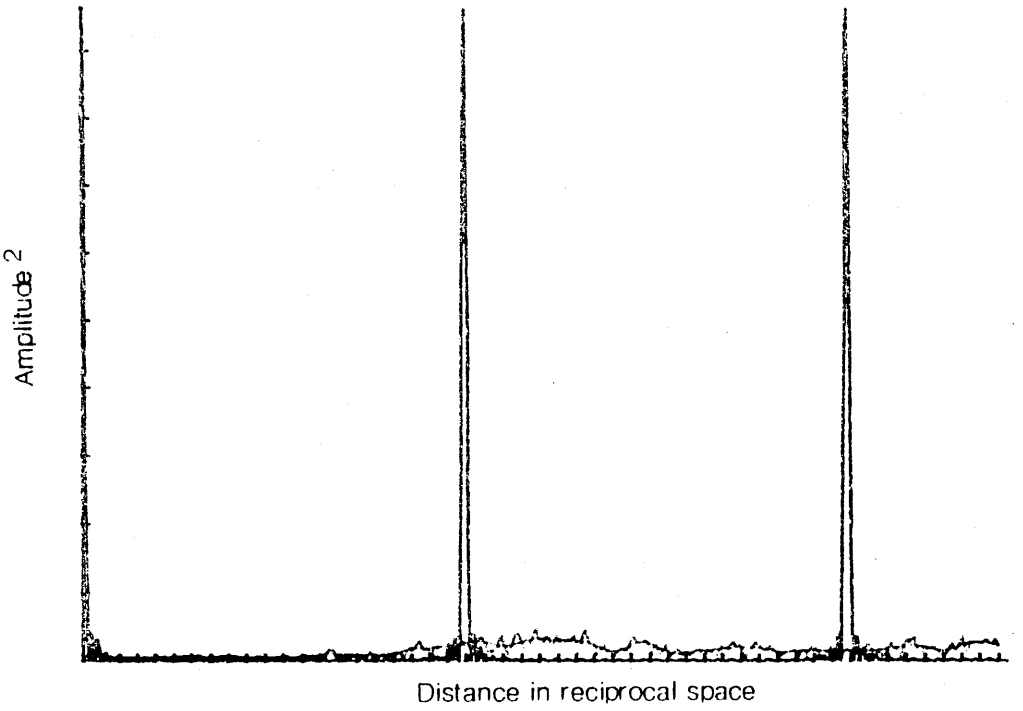

Fig 5.3.3. Fourier summation of the half-sarcomere shown in Fig 5.2.4.3 of control (A/2) at S=3.3 μm. The black curve shows the ideal result, the green the experimental and the red the fitted curve (see text).

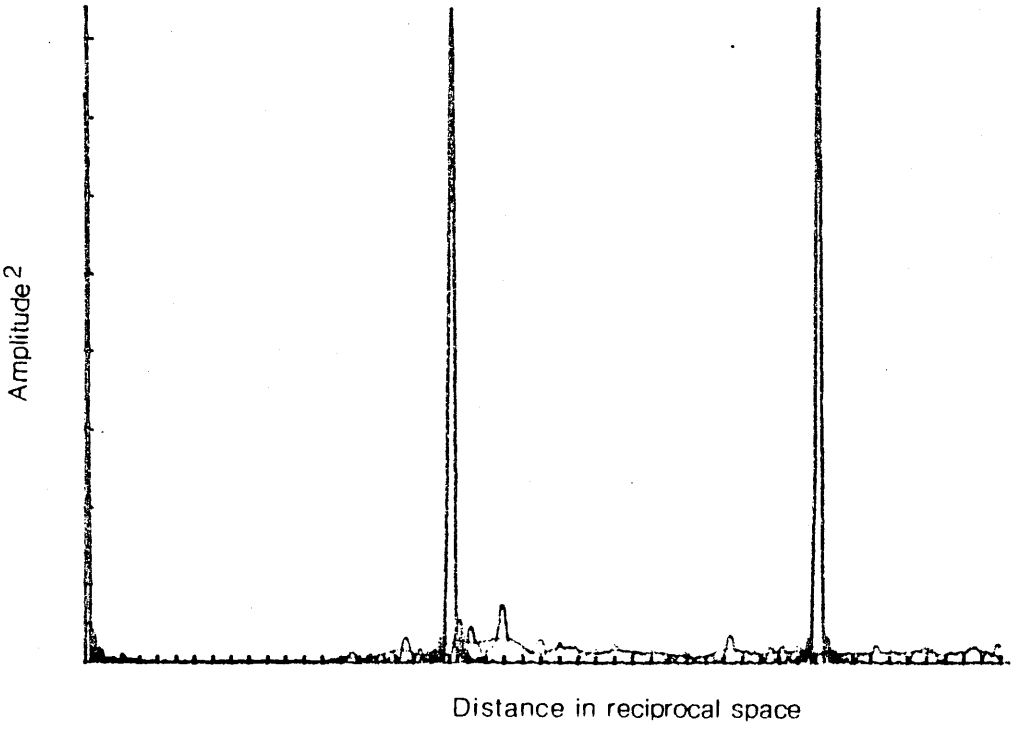

Fig 5.3.4. Fourier summation of the half-sarcomere shown in Fig 5.2.4.4. of A/2+5mM PPi at S=3.3 μm. (See above for details).

Table 5.3.1 shows the results of a simple analysis of the cubic spline fit for Figs 5.3.1 to 5.3.4. This involved taking the full width at the half maximum point of the first major peak (FWHM) and normalising this to the peak separation so as to obtain a value relating peak width (Δs) to peak spacing (s). This gives a value $\Delta s/s$ which is analogous as a measure of sharpness to the $\Delta d/d$ measured for the equatorial reflections in the X-ray diffraction experiments, the greater the value of $\Delta s/s$, the broader the peak. R_{hw}, the ratio of the peak maximum to the FWHM, was also measured. This gave a crude estimate for the resolution of the peak. An R_{hw} of $\leqslant 0.25$ was considered too poorly resolved to be analysed.

Both a qualitative assessment by eye together with examination of Table 5.3.1 shows that as S increases in control solution the maxima in the fitted trace show an increase in $\Delta s/s$ and a decrease in R_{hw}. Both

Table 5.3.1. $\Delta s/s$ and R_{hw} for peaks of the cubic spline fitted trace with increasing S and addition of PPi.

S(μm)	CONTROL (A/2)		PPi	
	$\Delta s/s$	R_{hw}	$\Delta s/s$	R_{hw}
2.1	0.08	0.94	0.06	2.0
2.6	0.07	0.80	0.05	2.3
2.9	-	< 0.25 *	0.12	< 0.25
3.3	-	< 0.25	-	< 0.25

* The value of 0.25 is given here since attempts to quantify the peak which gave a result of > 0.25 were clearly unrealistic. Below this figure estimations were not possible with any accuracy. For this reason the corresponding $\Delta s/s$ were not given, except for PPi at S=2.9 μm where the R_{hw} was 0.22 so the value shown was estimated.

these observations are consistent with a decrease in sharpness of the peaks in the traces. At S$\lesssim$ 2.6 the peaks have roughly constant parameters but at S$\gtrsim$ 2.9 the peaks become difficult to resolve. Visual examination of Fig 5.3.3 shows a definite increase in the size of peaks in the Fourier summation curves which are translated to perceptible bumps in the fitted curves. There appear to be two groupings within the data, one at short S where peaks are well defined, and the other at longer S where peaks are poorly defined. This reflects well the sharpness data from X-ray diffraction studies which show greater and lesser sharpness over similar changes in S. Comparing actual values of $\Delta s/s$ from Fourier summation calculations and $\Delta d/d$ values from the (1,0) peaks in X-ray equatorial peak measurements, a good correlation is seen. Table 5.3.2 shows the values of each measure of sharpness.

Table 5.3.2. A comparison of $\Delta s/s$ values from the first major peak in the Fourier summation data with $\Delta d/d$ values from the (1,0) equatorial X-ray data.

S (μm)	A/2		PPi	
	$\Delta s/s$	$\Delta d/d$	$\Delta s/s$	$\Delta d/d$
2.2	0.08	0.063	0.06	0.057
2.6	0.07	0.076	0.05	0.062
2.9	-	0.094	0.12	0.088
3.3	-	0.110	-	0.102

Table 5.3.1 shows that with addition of PPi, the decrease in $\Delta s/s$ indicate the peak has become sharper at all values where measured. This is seen in all the Fourier summation figures as a more clearly resolved peak (this observation is supported by a increase in R_{hw} values). Table 5.3.2 shows that this change in sharpness seen in the Fourier summation is also seen in the sharpness of the (1,0) equatorial

peak in the X-ray picture. Again there are two distinct peak behaviours - the well defined short S and the ill-defined longer S. Where quantitative peak measurement was not possible qualitative examination of the summation curves shows that the improvement of peak resolution with PPi is still present and so is in agreement with the effects seen at shorter S.

The summation curves (the green traces) not only show a grouping of peaks round the first order position, but also further out round the second order. These second order peaks were only clearly resolved in the case of S=2.1 μm with PPi (see Fig 5.3.2). Under these conditions the second order fitted peak has a $\Delta s/s$ of 0.08 and R_{hw} $\approx$0.22 (just at the limit of reasonable measurement). These compare to 0.06 and 2.0 for the same parameters for the first order. With the other second order peaks it is not possible to asses either parameter. At S$\geqslant$2.9 μm, this second order is no longer visible above the background. The changes seen in these higher orders are very similar to those seen in X-ray diffraction pictures of the higher orders of the equatorial reflections.

As already mentioned the black line represents the summation based on the mean spacing of filaments over the whole half-sarcomere and gives a result typical of an extended diffraction grating (see any of Figs 5.3.1 to 5.3.4). The positions of the first and second orders correspond well, but not perfectly, with those from the fitted curve. With PPi the tendency is for the disparity between the spacing of the peak in the ideal trace (from mean filament separation) and that from the fitted curve to decrease (see Table 5.3.3). This difference is due partly to the way in which the ideal peak was generated. Taking the mean spacing of all the points first, and then calculating the ideal curve gives a single sharp peak but will not take into account the individual mean spacings at different levels in the half-sarcomere. An

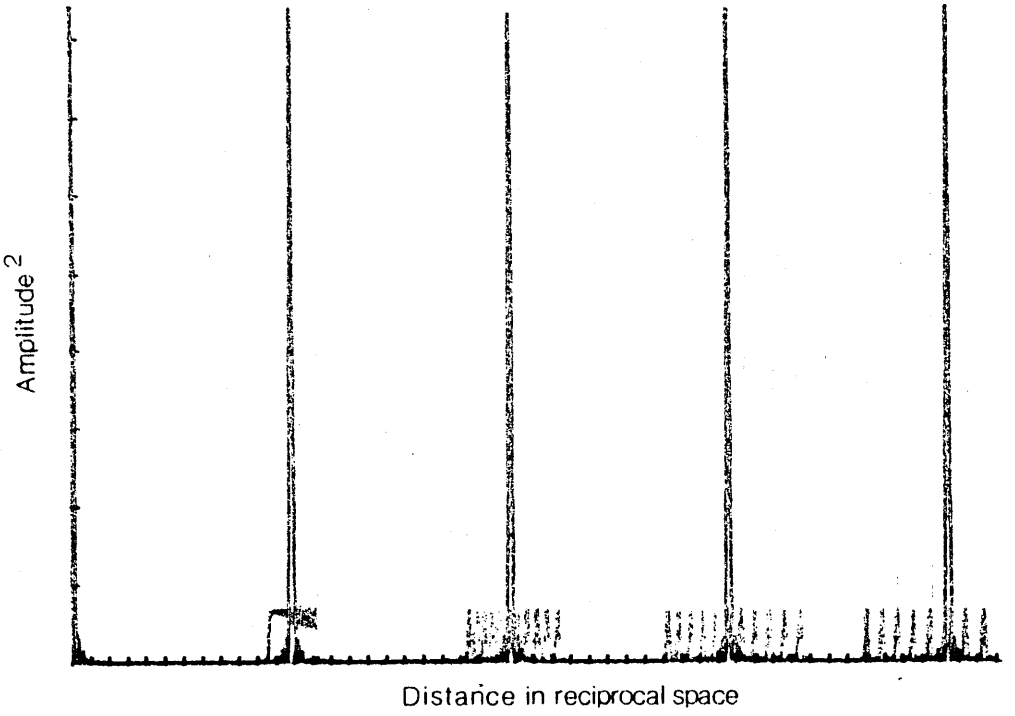

Fig 5.3.5. Fourier summation of the ideal conical lattice generated for the rigor half-sarcomere at S=2.1 μm. (First four orders shown).

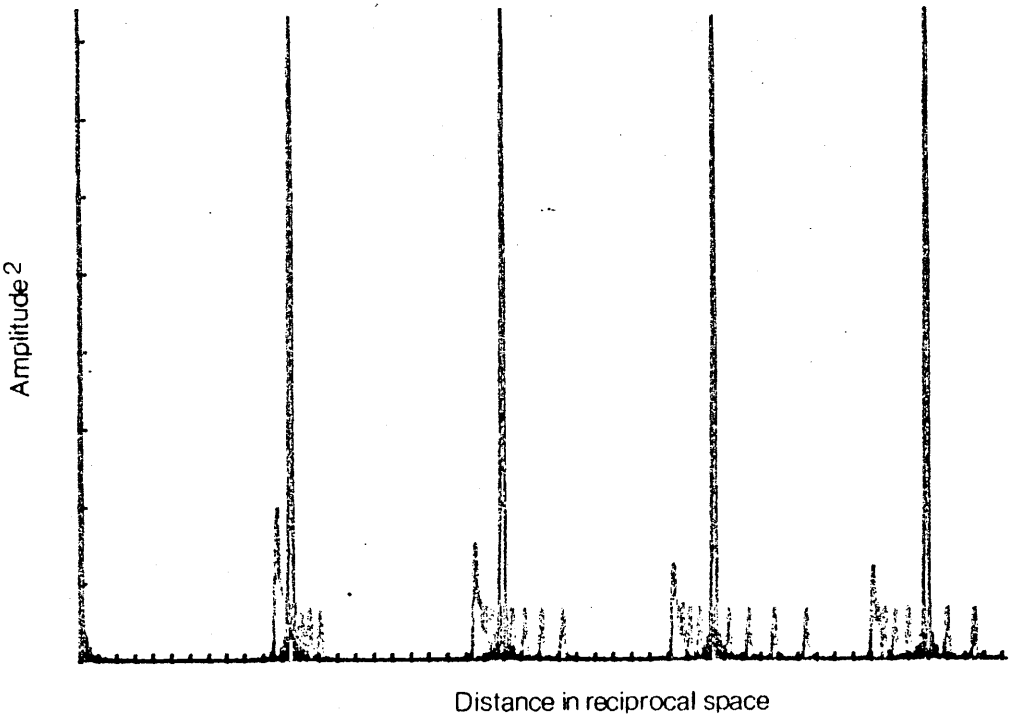

Fig 5.3.6. Fourier summation of the ideal elliptical lattice generated for the rigor half-sarcomere at S-2.1 μm. (First four orders shown).

average of a range of summations using the mean spacing at each level in the half-sarcomere would give a series of overlapping peaks but no clear overall mean - the green summation traces were generated by an averaging of individual traces taken over the 11 levels in the half-sarcomere, and so use an approach similar to this. In comparing the ideal and fitted traces, therefore, a correlation is being made between curves generated in these two different ways. PPi reduces the difference in spacing between the two peaks, so it is possible that a change in bowing or local distortion at the different levels could cause the apparent change in spacing. To check this possibility, the ideal lattices used to generate the graphs in Figs 5.2.8 and 5.2.9 in Section 5.2 were subjected to the Fourier summation. The results are shown in Fig 5.3.6 for the elliptical lattice

Table 5.3.3. Mean spacing over the whole half-sarcomere compared to spacing of peaks in the fitted curve. (All spacings in nm).

S(μm)	A/2			PPi		
	MEAN SPCNG	FITTED	DIFF	MEAN SPCNG	FITTED	DIFF
2.1	29.2	29.8	+0.6	27.2	27.9	+0.5
2.6	29.8	26.3	-3.3	28.9	28.2	-0.7
2.9	27.2	24.4	-2.8	29.6	28.8	-0.8
3.3	27.4	-	-	29.6	-	-

and Fig 5.3.5 for the conical lattice. Both graphs show individual peaks whose spacings effectively corresponds to the mean spacing at the 11 different levels from M-line to A/I junction in the lattice over which the average was taken (see Section 5.2.1 for a more complete discussion of these computer generated lattices). The elliptical lattice summation in Fig 5.3.6 shows a predominant peak to the left of the mean spacing, corresponding to the curving in of the filaments

towards the A/I junction, and a wider spacing to the right of the mean peak. The conical lattice summation, however, gives a more evenly distributed pattern though even in this latter case, the distribution is not symmetrical about the mean.

From these graphs it is apparent that changes in shape of the lattice will have an effect on the position of the maximum of the fitted peak relative to the mean purely as a result of a change of shape of the peak. A reduction in the degree to which the ellipse bowed toward the tip or the cone moved inwards would result in there being less spread in the mean filament separations at the various levels and so would result in a narrower and higher peak. In fact anything which caused a reduction in the variation of filament spacing would be expected to both reduce peak width and increase peak height. These changes are exactly those seen with increasing S (an increase in $\Delta s/s$ and decrease in R_{hw}) and PPi (a decrease in $\Delta s/s$ and increase in R_{hw}).

In Section 5.2 it was shown that at short S a major contributor to distortion was a shape change from the ideal rectangular lattice in the A-band, whereas at longer S, local distortions predominated, both types of distortion would increase variation in filament spacing and so decrease summation peak sharpness. PPi was seen to reduce both these types of distortion and so be expected to increase sharpness. Changes in the degree of local disorder are also likely to change the position of the peak since they will introduce a wider distribution of spacings so increasing the disparity between the ideal and experimental data, leading to a shift in the experimental mean.

In this section it has been shown in calculations using "ideal" lattices that the types of distortion seen in Section 5.2 can affect peak sharpness in the Fourier summation, and calculations using Fourier summations with experimental data show changes in $\Delta s/s$ and R_{hw} with

increasing S and PPi that correlate with those expected.

(ii) 5.3.2. Optical diffraction (OD) studies.

Section 5.3.1 dealt with calculated Fourier transforms from digitized EM pictures. In this section a more direct method of finding the Fourier transforms is employed. This uses the diffraction of laser light by the EM picture directly, in the optical diffractometer.

The half-sarcomeres analysed by Fourier summation in Section 5.3.1 were used for the OD experiments, the rest of the micrograph was masked off with thick black paper (see Methods Section 5.1.4). Figs 5.3.7.1 and 5.3.7.2 show the half-sarcomeres used and the diffraction pattern obtained with diffractometer at S=2.1 μm in rigor and with PPi. Figs 5.3.8.1 and 5.3.8.2 show the pictures and diffractograms under the same conditions at S=3.3 μm. All pictures taken showed a high intensity of "grainy" background noise, so a quantitative assessment by densitometry was not possible, but a qualitative survey of the pictures shows peaks on the equator, the meridian and in some cases on layer lines and it was possible to measure the spacings of these reflections using a travelling microscope. Table 5.3.4 shows the spacings of reflections present in control and with PPi. Comparing the values for the first peak on the equator of the diffractogram (Table 5.3.4 row 1) with the mean spacings measured directly from the EM pictures and from the Fourier summation peaks in Section 5.3.1 Table 5.3.3 shows a good correlation. The values for mean spacings measured directly from the film are in good agreement with the position of the first peak in the fitted curve in Fourier summation. Both these values correlate well with the inner reflection from the OD, so it is clear the inner reflection seen in the OD arises from the thick filament lateral repeat, making it analagous to

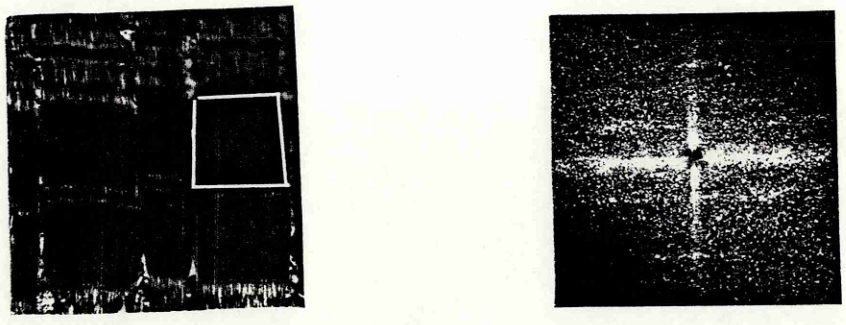

Fig 5.3.7.1. Electron micrograph and its optical diffractogram of the half-sarcomere in control rigor solution at S=2.1 μm. (Picture mag x18000).

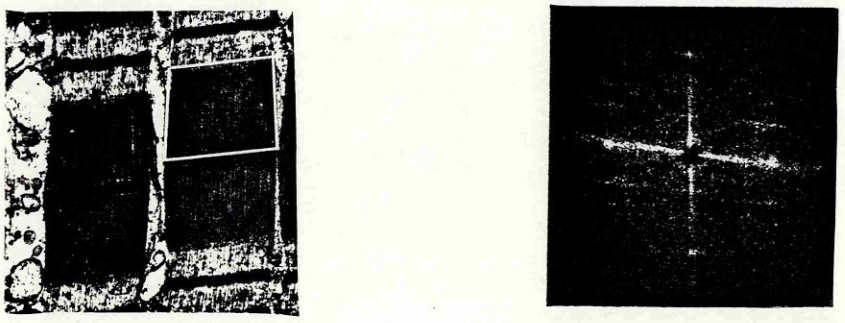

Fig 5.3.7.2. Electron micrograph and its optical diffractogram of the half-sarcomere in control +5mM PPi solution at S=2.1 μm. (Picture mag x18000).

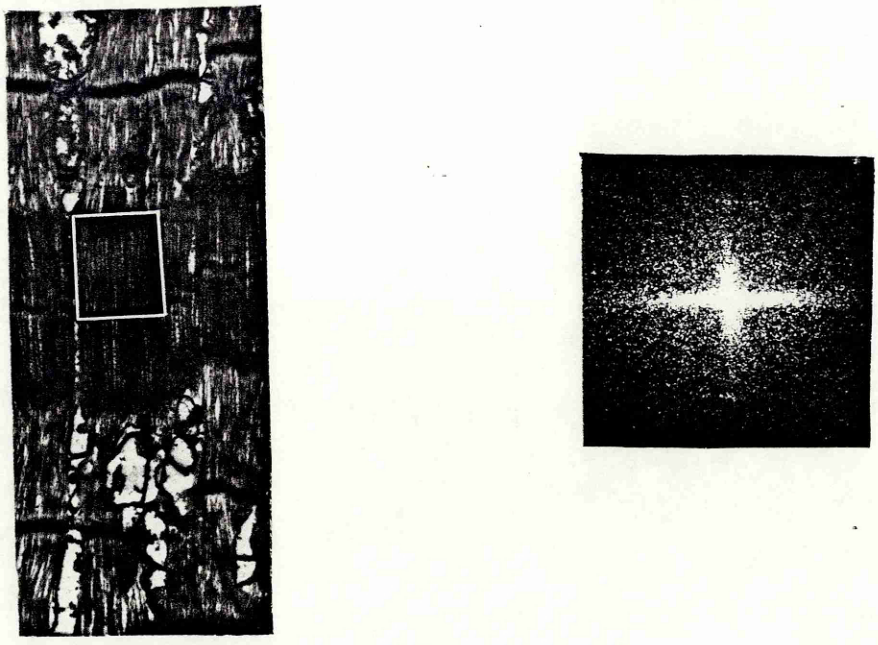

Fig 5.3.8.1. Electron micrograph and its optical diffractogram of the half-sarcomere in control rigor solution at S=3.3 μm. (Picture mag x18000).

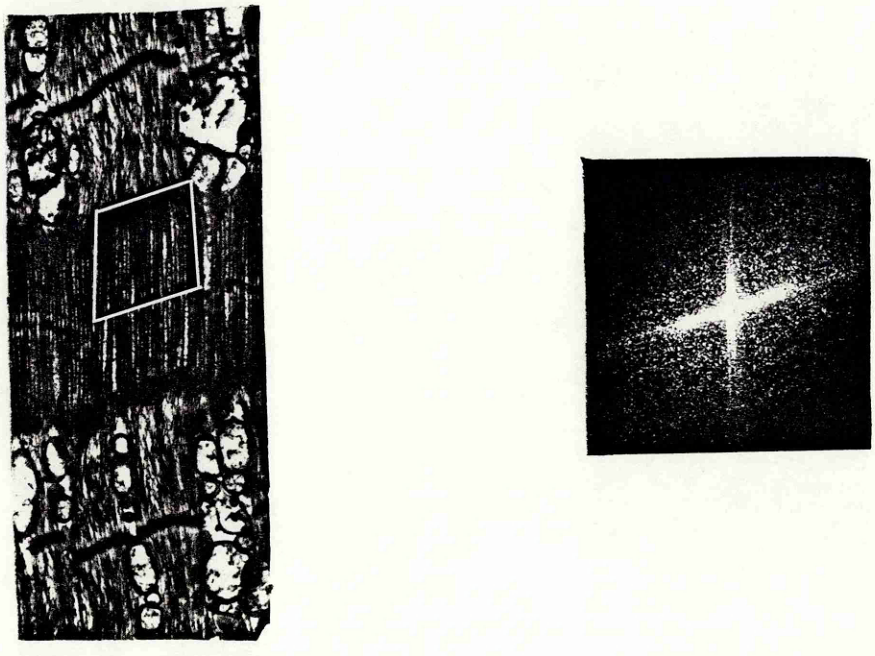

Fig 5.3.8.2. Electron micrograph and its optical diffractogram of the half-sarcomere in control +5mM PPi solution at S=3.3 μm. (Picture mag x18000).

Table 5.3.4. Measured spacings from optical diffractograms in Control (A/2) and A/2 + 5 mM PPi solutions. (All spacings in nm).

REFLECTION	2.1		2.6		2.9		3.3	
	A/2	PPi	A/2	PPi	A/2	PPi	A/2	PPi
EQUATORIAL	28.0	-	27.9	28.9	27.6	27.0	-	27.7
	15.6	15.7	-	-	-	-	-	-
MERIDIONAL	35.1	35.8	NP	NP	-	-	-	-
	14.0	13.2	NP	NP	13.5	13.9	13.2	-
LAYER LINES								
MERIDIONAL	33.9	33.7	36.1	35.1	36.2	33.8	NP	NP
	14.0	22.0	-	-	13.5	13.9	13.2	NP
EQUATORIAL SAMPLING								
350 -> 360 LL	16	16	18	21	Too Faint		NP	NP
220 LL	NP	16	NP	NP	NP	NP	NP	NP

Although the quality of the individual diffractograms varied (NP denotes where a measurement is not possible), there is a general trend towards loss of data at the higher sarcomere lengths.

the (1,0) reflection seen with X-ray diffraction.

Since the only criterion used to select the half sarcomeres studied was linearity of M-line, the filament lattice planes which the sections cut in longitudinal section vary, so a variety of equatorial spacings will result. eg at S=2.1 μm there are 2 peaks on the equator at 28.0 nm and 15.6 nm. Taking the 28.0 nm reflection as the (1,0), the calculated (1,1) spacing is 16.2 nm, which is a reasonable approximation to the other reflection seen. Since the sections are 30-40 nm thick, the material in the section can be at most about 1.5x a (1,0) plane thickness. This is thick enough to include more than one layer of thick filaments together with a layer of thin filaments. The EM picture is 2-dimensional as opposed to the rotation diagram of the 3D lattice exposed to X-rays, so in the EM there might be some effect of filaments in the third dimension.

For example, in the EM diffractogram it is possible that the two reflections seen arise from differing lateral repeats of thick filaments introduced by the offset of adjacent (1,0) planes. This would require the lattice in the picture to be very well ordered to maintain the same offset across a significant region of the half-sarcomere which Section 5.2 has shown not to be the case. It would also require that the plane cut during thin sectioning be perfectly along the (1,0), to ensure both sets of filaments were included. Since thick filament spacing is unlikely to account for the outer reflection seen, thick-thin filament spacing must. Since both reflections are seen and the outer reflection is so near to the calculated (1,1) and bearing in mind the thin filaments are superimposed on the thick, this implies the section cut is nearer the (1,0) plane than the (1,1). However with PPi at the same S, the only reflection seen clearly is at 15.7 nm. This implies the cut is more on the (1,1) plane. The meridional and layer line peaks will be dealt with later in Section 5.4.

Concentrating now on a qualitative treatment of the peaks, it is seen that as S increases it becomes more difficult to resolve both individual peaks on the equator and in the rest of the pattern (ie the meridional reflections and the layer lines). This decrease in the sharpness of peaks in the pattern is reflected in the decrease in the number of measurements possible from each picture in Table 5.3.4. The fewer the number of readings possible, the less clear the picture, and in Table 5.3.4 the left hand columns at shorter S contain more information than the right hand columns at longer S. This decrease in sharpness with increased S is in agreement both with the Fourier transforms of Section 5.3.1 and the observed X-ray data. In general, the Fourier summation peak amplitudes correlate well with the intensity maxima seen in the OD, though the differences in how the pictures are sampled can result in differences between the two methods. This is most apparent at S=2.1 μm with PPi. As already noted, the section is cut close to the (1,1) plane so OD will pick out thick-thin filament periodicities. But with the Fourier summation method only thick filaments were traced, so the summation shows a peak corresponding to the (1,0) whereas in OD the thick filament contribution is included in the (1,1) and no (1,0) is seen.

With PPi the sharpness of the peaks is improved, this is most obvious on the equator and on the layer lines. Again this agrees with the observed X-ray diffraction and the Fourier analysis. Note that although there may be differences in the position of the peaks between the summation and OD, in all cases the PPi causes a sharpening. With S=2.6 μm, although it was not possible to obtain good diffractograms, it did mean that the tracing of filaments for Fourier summation was not seriously affected, so the summation shows a clearer distribution along the equator than does the diffractogram.

Section 5.3.2 has shown the changes seen in the Fourier analyses

are in good agreement with those seen with OD. Changes in the Fourier summation were correlated with changes in the disorder of the EM, so changes in the OD peaks can be linked to the EM changes too. In the course of presenting the results the changes seen with OD have been linked to changes seen in the analogous reflections in X-ray diffraction under more physiologial conditions. In Section 5.3.2 the relationship between OD and X-rays is analysed further by direct comparison of pictures, and since EM procedures of fixing, staining and embedding may inevitably introduce artefacts, the comparison includes pictures from embedded material in an attempt to trace artefactual distortions.

(c) 5.4. Direct comparison of X-ray and EM results.

The previous section made the point that the amplitude of the Fourier summation and the intensities of the equatorial OD are analogous to reflections seen with X-ray diffraction. In this section the position of peaks and spacings are directly compared between the various EM techniques and X-ray diffraction. This is done bearing in mind differences in which will arise due to EM artefact. For this reason X-ray pictures of embedded material are included in the comparison.

First, the equatorial reflection spacings in the X-ray and OD experiments are compared to the mean thick filament spacing measured directly from the electron micrographs in the control and PPi experiments over the range of techniques used. Table 5.4.1 shows the summary of this. Columns 1 and 2 show S and the experimental conditions, the other 5 columns show the following :-

(i) Column 3 - Mean spacing over the whole half sarcomere measured

from tracings used in the analysis of Section 5.2 and the summation in Section 5.3 (reproduced from Section 5.3 Table 5.3.3 cols 2 & 5).

(ii) Column 4 - Spacing of the first major peak of the curve fitted to the summation curve with the cubic spline (taken from Section 5.3 Table 5.3.3 cols 3 & 6).

(iii) Column 5 - Spacing of the first peak in the optical diffractogram (from Section 5.3 Table 5.3.4 row 1).

(iv) Column 6 - Since the mean spacing for the whole half-sarcomere as given in column 3 is subject to the filamentary distortions of one sarcomere, and since this distortion varies with S and PPi, filament spacing was also measured at the M-line in 10 different sarcomeres and the total was used to calculate a further figure for mean spacing. This value gives a better estimate of measured spacing over the whole sample. A comparison of these figures will show trends between experiments, though the actual values may not be an accurate assessment of true spacing since data were collected from the M-line only, and not over the whole half-sarcomere.

(v) Column 7 - The (1,0) spacing, measured by equatorial reflection seen in the X-ray diffraction in the solution used in the EM experiments prior to fixation, dehydration and embedding (mean ± SD given).

Discussion of comparisons within cols 3 to 5 are included in previous Sections 5.2 and 5.3. Taking the results in these columns as a whole and comparing them to col 6 shows the two groups of results are in general agreement.

Table 5.4.1. Summary of thick filament spacing in increasing S and with PPi by the range of techniques used.(All spacings in nm).

S	EXPT	3	4	5	6	7
2.1	A/2	29.2	29.8	28.0	28.9 ± 6.6 (n=290)	40.5 ± 0.7 (n=6)
	PPi	27.2	27.9	-	28.4 ± 6.5 (n=290)	42.4 ± 0.7 (n=5)
2.6	A/2	29.8	26.3	27.9	28.5 ± 7.5 (n=209)	40.2 ± 0.7 (n=10)
	PPi	28.9	28.2	28.9	28.0 ± 7.0 (n=300)	42.3 ± 0.8 (n=6)
2.9	A/2	27.2	24.4	27.6	26.7 ± 8.3 (n=231)	39.2 ± 0.7 (n=10)
	PPi	29.6	28.8	27.0	24.2 ± 6.8 (n=290)	41.9 ± 1.3 (n=7)
3.3	A/2	27.4	-	-	24.3 ± 8.7 (n=292)	35.9 ± 1.2 (n=12)
	PPi	29.6	-	27.7	25.4 ± 6.9 (n=260)	36.9 ± 2.1 (n=5)

Column 6 shows the overall spacing change as S is increased, to be small, bearing in mind the large values of SD. Any change is a slight decrease in spacing, and this corresponds to the direction of the change seen with X-rays in column 7 (the X-ray changes are clearly significant when SD's are compared between the two sets of data). There is also a small increase in SD as S increases which indicates that the increases in disorder are apparent even at the M-line. Addition of PPi results in little or no change in the EM spacingcompared to the control, but again the decreasing trend is observed. This contrasts with the result of the X-ray experiments, where the addition of PPi causes a clear increase in spacing at all S. In the EM the values for SD are all lower with PPi, indicating a decrease in disorder. The value of the spacings measured from

electron micrographs (columns 3 to 6) is lower by 25 → 30% than those measured from X-ray pictures (column 7), showing that a considerable shrinkage in the lattice has occured during the EM preparation procedure. Table 5.4.2 shows d(1,0) spacings and Δd/d for embedded material at S≈2.2 for comparison with columns 6 and 7 in Table 5.4.1.

Table 5.4.2. Values for equatorial spacing and sharpness from embedded material at S≈2.2 μm.

EXPERIMENT	d(1,0)(nm)	Δd/d
Control (A/2)	33.9	0.075
A/2 + 5mM PPi	34.2	0.065

Table 5.4.2 shows that the lattice expansion effect of PPi is removed when the specimen is fixed stained and embedded. This is in keeping with the result from the OD spacings seen (Table 5.4.1 col 5). The spacing value is intermediate, 15-17% smaller than the solution spacing and 11-13% greater than that seen in the micrographs. This indicates that the preparation process for EM accounts for roughly only half the shrinkage seen. Further differences could be due to a treatment during sectioning or section staining (eg chloroform treatment) or to shrinkage of the specimen under the electron beam (see EM artefact discussion). Another source for the disparity could be a low estimate for mean spacing due to sampling differences similar to those discussed in the OD results in Section 5.3: the X-rays will sample a series of 3D lattice planes by Bragg diffraction whereas all the EM techniques are based round a 2D image of filaments. If as a result of section thickness thick filaments from more than one plane are present, they will be superimposed and increase the number of filaments per section width, thus giving a low estimate for mean spacing. Other errors which may contribute to the difference could be

a small calibration error in the electron microscope magnification or small changes in magnification with focusing due to lens hysteresis.

The d(1,0) equatorial reflections from the embedded specimens were analysed to give a measure of $\Delta d/d$. These too are shown in Table 5.4.2. The values for $\Delta d/d$ are slightly higher than those for the control and PPi solutions (compare Table 5.4.2 to $\Delta d/d$ range of ~0.05-0.07 in control solution and ~0.045-0.065 in PPi solution), indicating that the preparative proceedure for EM disorders the filaments to some extent. However, with PPi a similar decrease in $\Delta d/d$ is seen in the embedded specimen as well as in the specimen in solution at $S \approx 2.2$ μm. It has already been mentioned that the OD pictures have too high a background scatter to be analysed by densitometry, so the peaks seen in the embedded specimen have to be correlated to changes seen in $\Delta s/s$, as measured in the Fourier summations (Section 5.3.2 shows the summation is a reasonable approximation of the equatorial OD pattern seen). Section 5.3 Table 5.3.2 shows values of $\Delta s/s$ for the first peak of the Fourier summation, and demonstrates the good correlation between the $\Delta d/d$ from the embedded specimens and that from the calculation. Note the embedded specimen is at $S \approx 2.2$ μm and the half-sarcomere undergoing summation is at $S \approx 2.6$ μm, this may result in the two numbers having slightly different values (see Table 5.4.1 which shows the effect of S on the measured spacing seen in EM pictures).

Thus the original change in sharpness of the d(1,0) equatorial reflection is maintained in the embedded state. This change can be reproduced by OD of electron micrographs. The OD are themselves Fourier transformations of the micrographs, and calculated Fourier summations using digitized filaments from the EM pictures fit the observed OD well. Perturbations from the ideal lattice cause changes in the shape of the peak in the calculated transform, and these

perturbations have been measured and shown to be a bowing or a change in local disorder. In this way, changes in shape and relative alignment of groups of filaments in the sarcomere have been shown to influence the sharpness of equatorial reflections in X-ray diffraction.

In Section 5.3 Table 5.3.4 values are given for measurements of meridional and off-meridional peaks and layer lines in the OD experiments. It would be expected that these might correlate with reflections seen in similar positions in the X-ray diffraction pattern. Table 5.4.3 shows a comparison of meridional reflection spacings from solution, embedded material and OD experiments (the mean spacings where appropriate are given).

The clarity of the X-ray pictures decreased as the specimen is prepared for EM, showing that the filaments have become more disordered in the sample. The decrease in the number of measurable peaks is indicative of this. The pictures also show an increase in the amount of background scatter - in the case of the embedded specimen, a large increase in the scatter round the backstop was observed. This is most likely due to scatter from the electron dense material added during EM processing (eg. OsO_4,UAc), which has become associated with the filaments. The meridional spacing changes showed a slightly different behaviour than the equatorial reflections. The embedding process decreased the meridional reflection spacings by 6-8% compared to 15-17% in the equatorial spacings. This smaller shrinkage indicates the lattice is much more stable in the axial than in the lateral direction. A comparison between the values obtained in the embedded specimen and those from the OD showed that the lattice spacings changed little with sectioning, staining and exposure to the electron beam.

Table 5.4.3. A comparison of values for meridional reflection spacings in solution, embedded and OD experiments (all spacings in nm).

A/2			PPi		
SOLUTION	EMBEDDED	OD	SOLUTION	EMBEDDED	OD
55.15	-	-	55.06	-	-
44.38	41.60	-	44.37	-	-
38.51	34.93	35.1	38.46	35.43	35.8
22.76	21.59	-	22.42	~21.0	-
21.33	-	-	21.36	-	-
19.20	~18.0	-	19.27	17.97	-
14.47	13.79	13.6	14.44	13.74	13.6
12.84	-	-	12.82	-	-
11.01	-	-	11.98	-	-
7.27	-	-	7.24	-	-
-	-	-	6.49	-	-
-	-	-	5.89	-	-

Further comparison was possible between the layer lines in the OD and meridional X-ray pictures. In OD experiments it was seen that at low S, a fairly prominent layer line was present at a meridional spacing of 35-36 nm. This was correlated to the first actin layer line at 37.5-38 nm in the X-ray pictures. As with the X-ray picture, the intensity of this layer line decreased with increasing S. A further layer line was associated with the 13.5 nm OD meridional reflection. This too decreased with increasing S and was correlated to the 14.5 nm layer line in X-ray pictures. Table 5.4.4 shows a comparison of the 37-38 nm layer lines in X-ray pictures with the layer lines seen in OD together with the values for the layer lines seen in embedded

specimens. The layer line shows a similar behaviour to the meridional reflections in general, a moderate spacing decrease with embedding, and little change in the final micrograph.

Table 5.4.4. A comparison of layer lines in solution, embedded material and OD pictures. (All spacings in nm).

CONDITION	SOLUTION	EMBEDDED	OD
Control (A/2)	37.81	34.4	35.4
A/2 + 5mM PPi	37.40	34.9	34.2

Off-meridional sampling in the 37 nm layer line was also compared. Whereas in solution at S$\leqslant$2.8 μm clear sampling was present, in the embedded material it was possible only to measure a vague cut-off point where sampling ended since the layer line was so diffuse. In the OD of EM pictures the situation was improved, and peaks could again be distinguished. These were similar in form to those seen in the X-ray pictures, but sampling in the OD patterns was spread over a wide range along the layer line, so only approximate measurements were made. Table 5.4.5 shows the off-meridional sampling of the layer line in the three conditions.

As noted in Section 3.2 (meridional X-ray results), there is a good correlation in the X-ray patterns between the first two peaks sampled on the first actin layer line and the (1,1) and (2,1) reflectionspacings on the equator. This correlation between off-meridional layer line sampling and equatorial spacing appears to persist through the embedding to the OD. The value of the spacings in both Tables 5.4.4 and 5.4.5 corresponds with the magnitude of the relative changes in the other reflections in the meridional and equatorial directions as the conditions change.

Table 5.4.5. Off meridional sampling of first the actin layer line in solution, embedded and OD at S≈2.25 μm. (all spacings in nm).

CONDITION		1st PEAK	2nd PEAK	d(1,1)	d(2,1) ¤
A/2	Solution +	23.9	12.0 → 13.0	24.0	~11.9
	Embedded +	18.9 *	-	19.8	-
	OD o	~16.0	-	15.6	-
PPi	Solution	25.9	13.0 → 14.0	25.8	12.9
	Embedded	18.9 *	-	19.9	-
	OD	~16.0	-	15.7	-

¤ Calculated value fron (1,1)

* Cut off point beyond which intensity equals background

+ Measured from X-ray pictures

o Measured from OD of electron micrographs

The layer line at 14.47 ± 0.4 nm in the solution remains associated with the analagous reflections in the embedded specimen and also in OD throughout the spacing changes in that reflection. The behaviour of the layer line with increasing S is similar between the solution and OD (data is limited to 2 pictures for embedded). In both conditions increasing S reduces the intensity of the layer line. In the case at S≈2.2 μm in solution, sampling was seen on the 14.5 nm layer line; this is not apparent in either embedded meridional X-ray or OD patterns, again showing that some disordering has occured in the EM procedure.

This section has indicated that reflections seen in OD can be correlated with analagous reflections seen in X-ray diffraction, and changes seen in the one are apparent in the other. Since changes in the OD have been correlated to the changes in filament order as seen under EM, the link between filamentary bowing and disorder and the changes seen in X-ray diffraction is established.

5.5. Summary of EM results.

A simple measure of distortion within the sarcomere can be obtained by taking the ratio of sarcomere width at M-line to that at the A/I junction. This gives a crude measure of the degree of bowing over the half-sarcomere. The bowing measured in this way decreases with increasing S, this effect being in disagreement with the observation of Bergman (1983), who also saw a decrease in bowing over a similar range of S with frog muscle. A curve was fitted to the data in each experiment using a truncated cone model which resulted in a value for bowing under each experimental condition. Comparing the results at short S for control and PPi experiments shows that the addition of PPi also causes a reduction in the degree of bowing seen with EM.

However, the fit of the curve is only reasonable at short S, and at longer S anomalies between the data and the model curve increase. For this reason a more detailed analysis involving digitizing the filaments, and generating a series of theoretical "ideal" lattices based on a rectangle, truncated cone or truncated ellipse. The distortion in the lattice was found by subtracting the experimentally determined A-band lattice from the theoretical lattice, and the root mean square distortion (RMSD) calculated for the result of each subtraction. This gives a measure of total mean distortion of the experimental data from the ideal lattice. In all the model lattices used, RMSD is reduced by PPi, showing that the overall distortion in the A-band decreased. At short S where bowing was present, fitting a truncated cone or ellipse resulted in a transformation of symmetry of the distortion graph, indicating an underlying gross distortion of the half-sarcomere. These transformations were reflected in the RMSD values which showed no

regular pattern. At longer S the symmetry reversal was less pronounced indicating less gross disorder. The various models had little effect on RMSD, this is consistent with the form of the distortion graph which shows the local domains to be the predominant disordering factor that no "ideal" lattice could fit.

The analysis was continued using Fourier summations over the half sarcomere based on the digitized data used for the distortion graphs to examine the effects of disorder on the Fourier transform. The results show that where peaks could be measured they showed a decreasing height/width ratio and an increasing $\Delta s/s$ with increasing S and a decrease in these parameters with addition of PPi. Where measurement was not possible due to the diffuse peaks produced at long S, a qualitative assessment of the pictures showed consistent behaviour with the measured peaks.

Both the quantitative and qualitative methods give results that are consistent with the peaks observed in X-ray diffraction under similar conditions. A more direct comparison between EM and X-ray results was performed using an optical diffractometer on the same half-sarcomeres. These showed the same effects with increasing S and PPi as the Fourier summations and X-rays, again the decrease in sharpness with increasing S, and an increase in sharpness with PPi. Although differences are apparent in the actual positions of the peaks between OD and the Fourier summation, they are due to the inherent differences in sampling between the two methods and the overall changes in sharpness are consistent with the rest of the results.

Furthermore, the OD shows meridional reflections and, at the shorter S, layer lines. A comparison showed a good correlation between analagous reflections in the X-ray pattern and OD, although the measured spacings were quite different; axially a moderate decrease in lattice spacing (7-9%) in embedding was followed by little

or no change in spacing in the OD. Larger changes were seen laterally where embedding resulted in a 12-15% shrinkage, and the OD showed a further 10-15% decrease in spacing. This indicates a difference in lateral and axial lattice stabilities. However, the equatorial sharpness changes of the original X-ray pictures were present in the embedded material, and these were seen on the OD.

So a chain of evidence is established running from changes in the X-ray equatorial reflections, through sharpening in the reflections seen in embedded material to the changes seen in OD. The OD pictures are Fourier transforms of electron micrographs, so the chain is continued by calculating Fourier summations using digitized data from the micrographs. From these it is shown that changes in shape or internal order of the ideal lattice can influence the transform seen. The link between X-ray diffraction and EM is finally made by quantifying the changes seen in the micrographs, when changes in S or addition of PPi cause measurable changes in the overall bowing of the A-band lattice and in local disorder of filaments.

THE EFFECTS ON EM OF pH ON RABBIT GLYCERINATED PSOAS MUSCLE.

6.1. Methods.

The method used in the preparation, soaking and processing for EM of the samples were the same as for the PPi experiments described in Section 5.1. Note that the solutions used in fixation were as shown in Table 4.1.1 (with 2.5% glutaraldehyde added), and that only pH5, 7 and 9 were examined. All specimens were at an S=2.6 μm. The analysis of the pictures used the same computer routines and generated similar output as to those used for the PPi analysis.

(a) 6.2. Analysis of Electron Micrographs.

In Section 5, which dealt with the effect of PPi on rigor muscle, it was shown that changes in thick filament disorder measured in EM could be correlated to changes seen in the X-ray diffraction picture. Having now established the link, this section will examine the effect of pH on EM and X-ray pictures in terms of filamentary disorder.

Again the simple analysis involving measuring the M-line and A/I junction sarcomere widths and applying eqn (1) in Section 5.1.4 (EM methods) to determine a value for bowing is applied. This was repeated with ~150-200 sarcomeres for each of two specimens fixed in solutions at pH5 and pH9. All experiments were at S=2.6 μm. Figs 6.2.1.1 and 6.2.1.3 show the mean bowing over an increasing range of section thicknesses (as represented graphically by an increased number of thick filaments in the section). For comparison, Fig 6.2.1.2 shows the same graph for S=2.6 μm under the control conditions at pH7. The lines drawn in all three graphs shows the theoretical fit of the data based on the bowing expected from a truncated cone. Table

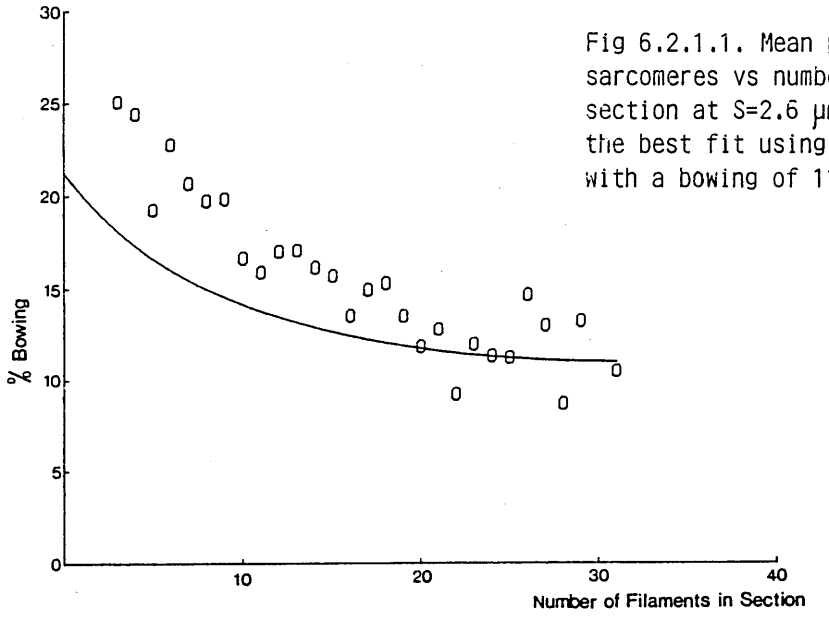

Fig 6.2.1.1. Mean percentage bowing of sarcomeres vs number of filaments in the section at S=2.6 μm and pH5. The line is the best fit using a truncated cone model with a bowing of 11%.

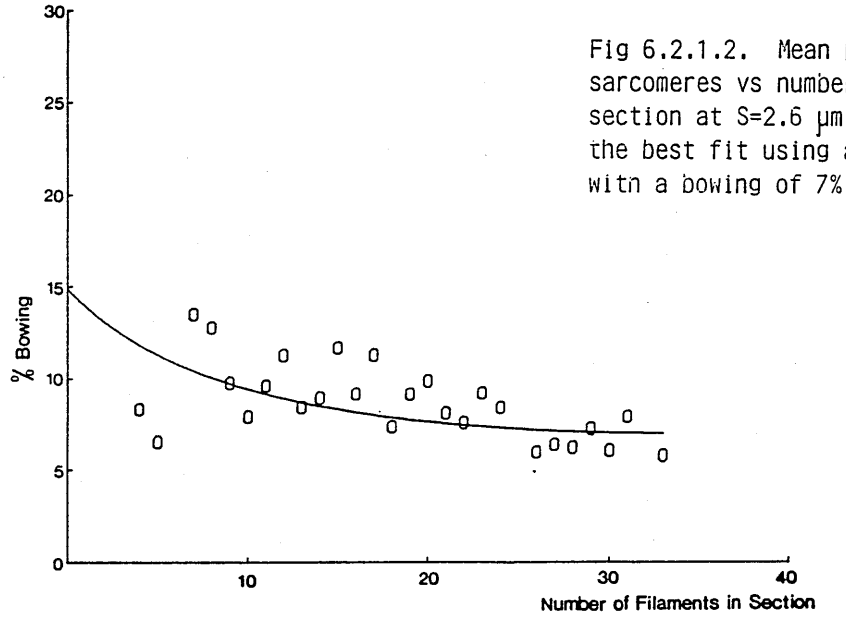

Fig 6.2.1.2. Mean percentage bowing of sarcomeres vs number of filaments in the section at S=2.6 μm and pH7. The line is the best fit using a truncated cone model with a bowing of 7%.

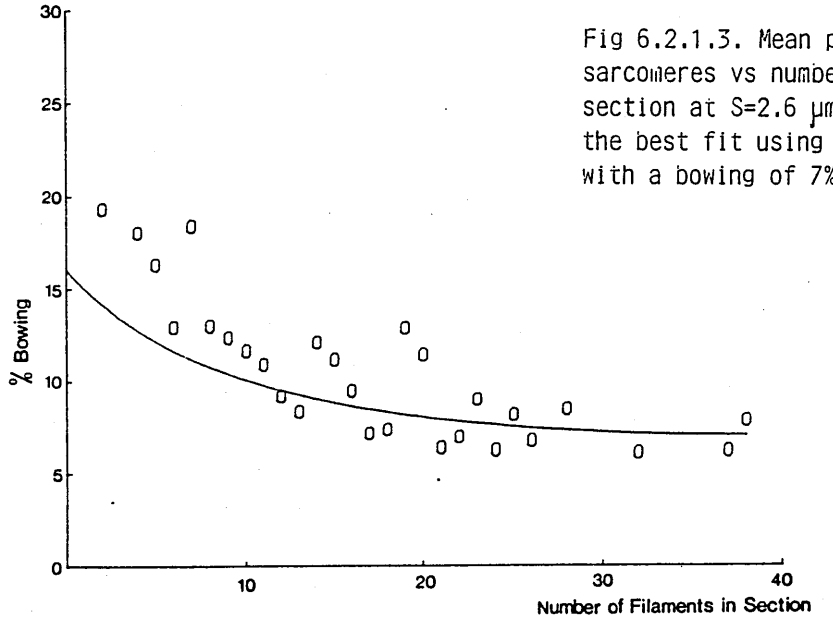

Fig 6.2.1.3. Mean percentage bowing of sarcomeres vs number of filaments in the section at S=2.6 μm and pH9. The line is the best fit using a truncated cone model with a bowing of 7%.

Fig 6.2.2.1. Distribution of number of filaments in a section at S=3.6 µm in PHE solution.

Fig 3.3.2.2. Distribution of screened beams at 2.5 µm in PPD solution

Fig 6.2.2.3. Distribution of filaments bearing at s=2.6 μm in pHG solution.

Table 6.2.1. Values used in the theoretical bowing curve to obtain the best fit to bowing graphs under varying pH at S=2.6 μm.

pH	BOWING (%)
5	11
7	7
9	7

6.2.1 shows these values used to obtain the best fit in Figs 6.2.1.1 → 6.2.1.3.

An overall examination of the graphs shows that the upward swing predicted from the simple truncated cone model is easily seen in both the pH5 and pH9 models. As with the sarcomere length change (ΔS) and PPi experiments, the theoretical curve is not a particularly good fit to the experimental data, but whereas the previous experiments showed a scatter above and below the fitted curve (see Fig 6.2.1.2), the trend in the pH result is for the experimental data to be above the fitted curve. This departure from the fitted curve is present only at lower number of filaments in the section ie towards the edge of the sarcomere (N>20 for pH5, N>10 for pH9). The sections with higher numbers of filaments is fitted reasonably well indicating again a more regular departure from the theoretical curve than the scatter in Fig (6.2.1.2).

Figs 6.2.1.1 to 6.2.1.3 show the distribution of all the points used to calculate the mean values. From pH5 to pH7 there is a significant decrease in the overall values of the points in the distribution. From pH7 to pH9, little difference is seen over most of the range, but at low section filament number the values of the points are higher, as would be expected from the mean. The maximum and minimum values at a given filament number also tend to be higher in the pH9 sample,

supporting the idea of a slight increase in bowing at pH9 over pH7. This effect is small, and a much greater sample size would be needed to quantify the difference with confidence. Table 6.2.1 shows that the overall bowing decreases from 11% to 7% as the pH is raised from 5 to 7. A further increase in pH from 7 to 9 has no further effect on the bowing as estimated by the fitted curve, though bearing the previous point in mind the curve is perhaps an underestimate.

As with the previous results from the study of ΔS in response to addition of PPi, the analysis was continued further by selecting a sarcomere with a straight M-line at each pH, tracing the thick filaments onto A4 paper using a photographic enlarger and digitising these traces. (See Figs 6.2.3.1 → 6.2.3.3 for traces at pH5, pH7 and pH9). The result of this treatment was an array of numbers representing the experimental 2D lattice of the half-sarcomere under study. Similar arrays for 2D lattices were generated for ideal rectangular, truncated conical and truncated elliptical models, and the experimental lattice subtracted from these, so generating a numerical value for distortion at each point in the lattice (see Section 5.1 (EM methods) for a more detailed description of the computational methods employed).

Figs 6.2.3.1 to 6.2.5.3 show the graphs of distortion over the whole half-sarcomere in the three pH solutions with the rectangular, truncated cone and truncated ellipse models. Figs 6.2.3.1 and 6.2.3.3 show the distortion in pH5 and pH9 respectively from the rectangular model. Comparing these with Fig 6.2.3.2, the distortion at pH7, then similar overall distortions of the half-sarcomere are seen; a gross regular distortion at the edges of the sarcomeres increasing as the filament runs from the M-line to the A/I junction is seen. These distortions are positive on the one side since the filaments curve inwards. This inward curvature also results in the distortion being

(a) Fig 6.2.3.1. pH5 S=2.6 μm

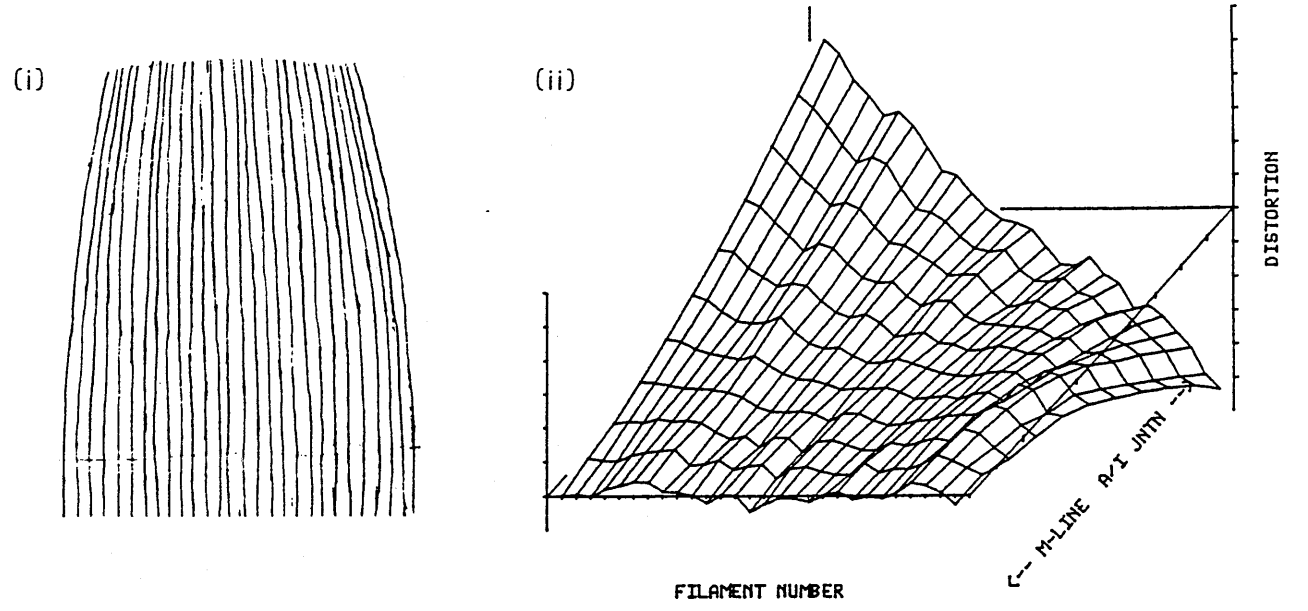

(b) Fig 6.2.3.2. pH7 S=2.6 μm

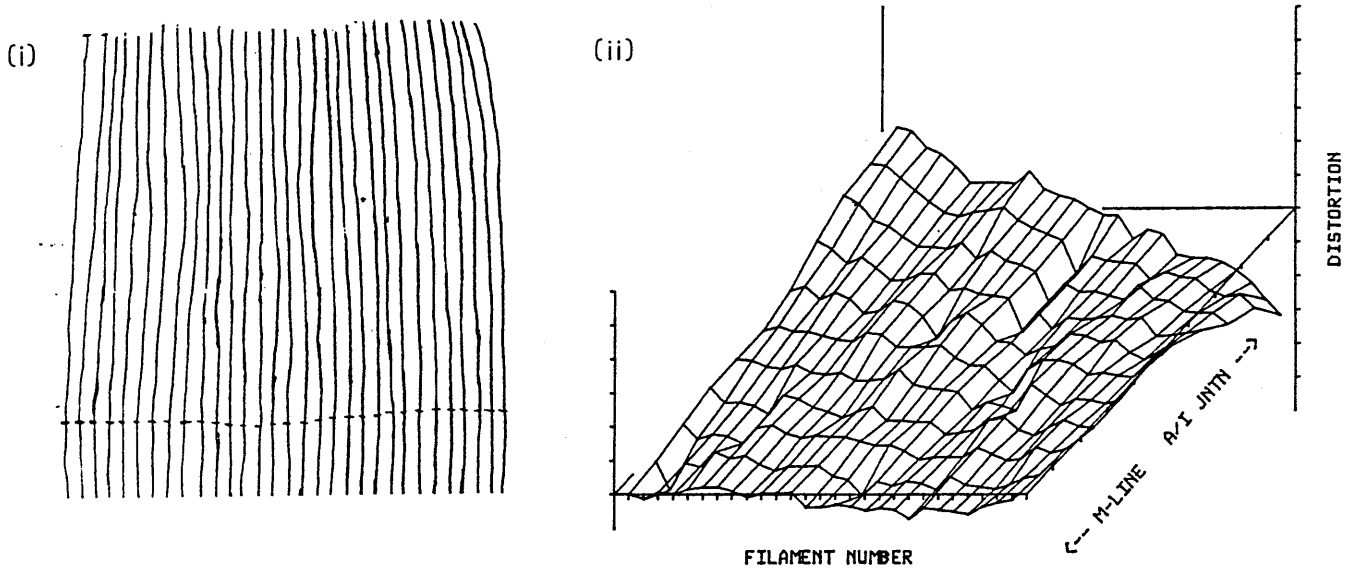

(c) Fig 6.2.3.3 pH9 S=2.6 μm

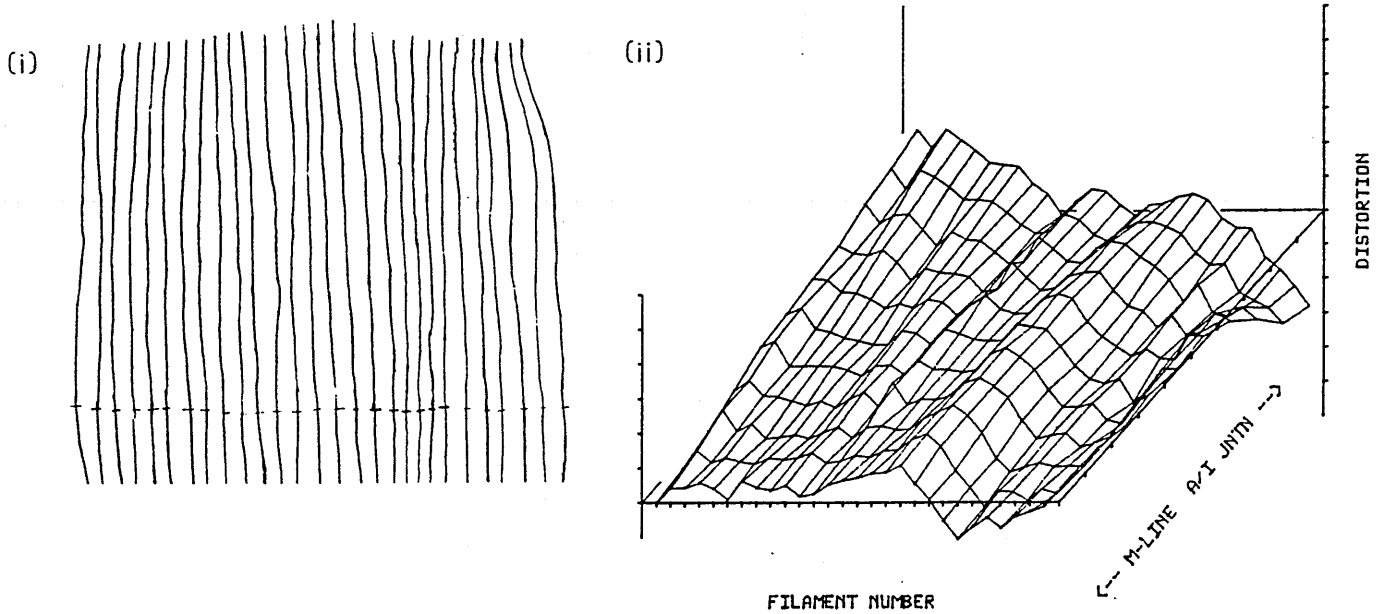

Guide to Figs 6.2.3 to 6.2.5 .

Preceeding page. (a) →(c)

Figs 6.2.3.1, 6.2.3.2 and 6.2.3.3 show,

(i) (left hand column) Thick filament tracings of half sarcomeres at S=2.6 μm in pH5, pH7 and pH9 rigor solutions respectively.

(ii) (right hand column) Distortion from an ideal rectangular lattice of the half sarcomeres in (i).

Following page.

(d) →(f).

Figs 6.2.4.1, 6.2.4.2 and 6.2.4.3 (left hand column of figures) show distortion from an ideal conical lattice of the half sarcomeres in Figs 6.2.3.1 → 6.2.3.3.

(g) →(i).

Figs 6.2.5.1, 6.2.5.2 and 6.2.5.3 (right hand column of figures) show distortion from an ideal elliptical lattice of the half sarcomeres shown in Figs 6.2.3.1 → 6.2.3.3.

(d) Fig 6.2.4.1 PH5 SL=2.6

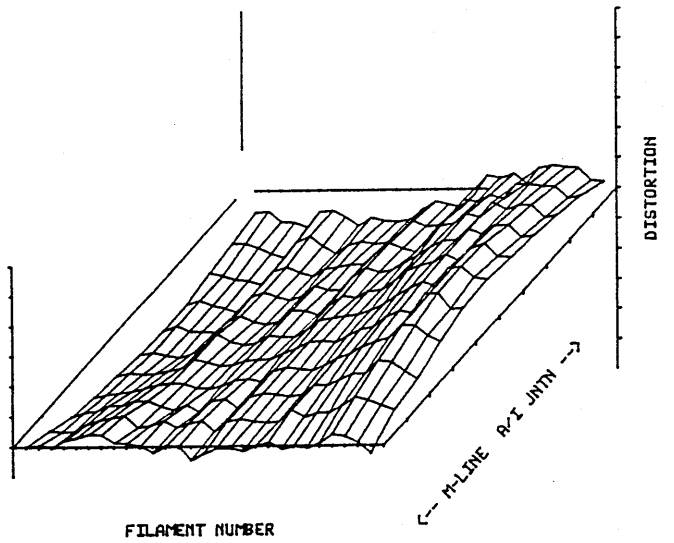

(e) Fig 6.2.4.2. α/2 sl=2.6

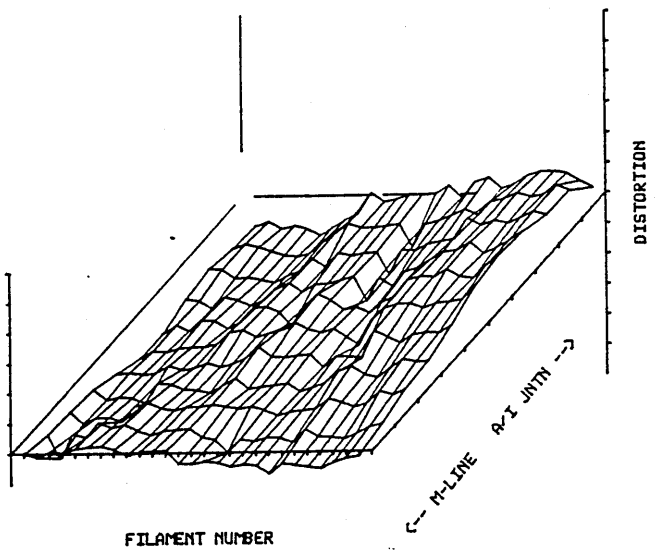

(f) Fig 6.2.4.3. PH9 SL=2.6

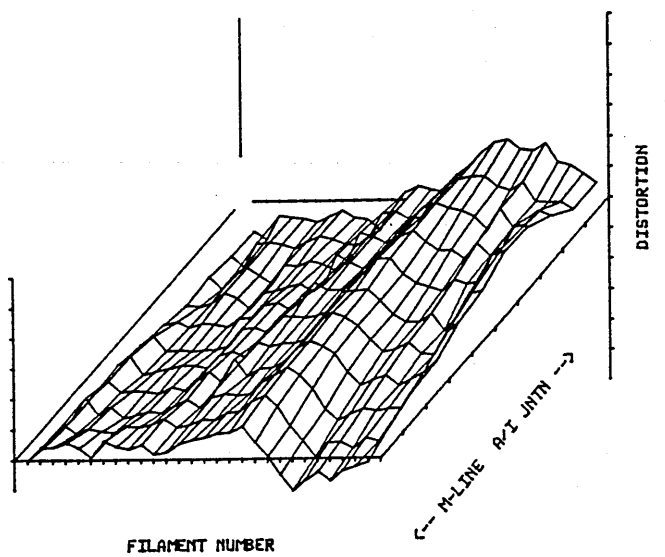

(g) Fig 6.2.5.1. PH5 SL=2.6

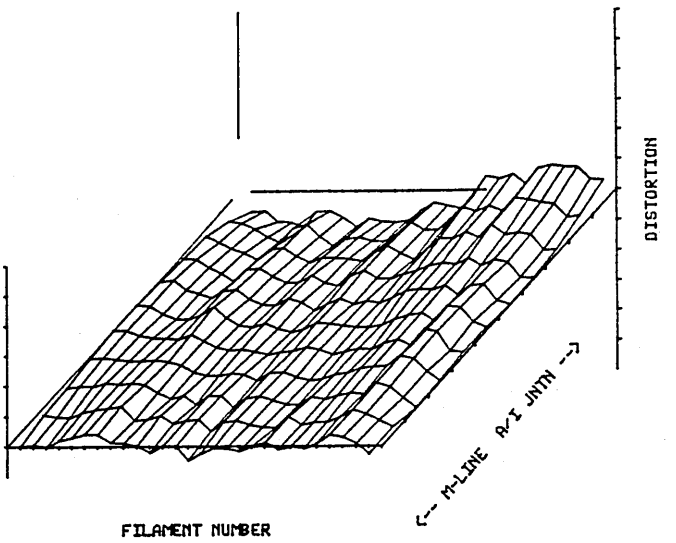

(h) Fig 6.2.5.2. α/2 sl=2.6

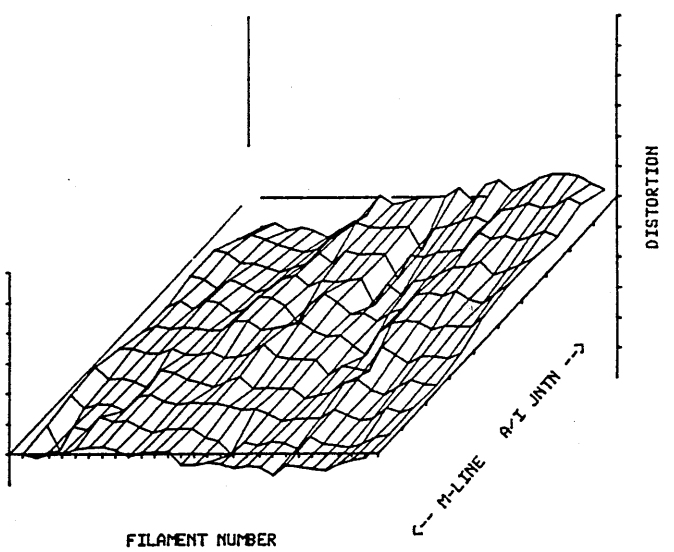

(i) Fig 6.2.5.3. PH9 SL=2.6

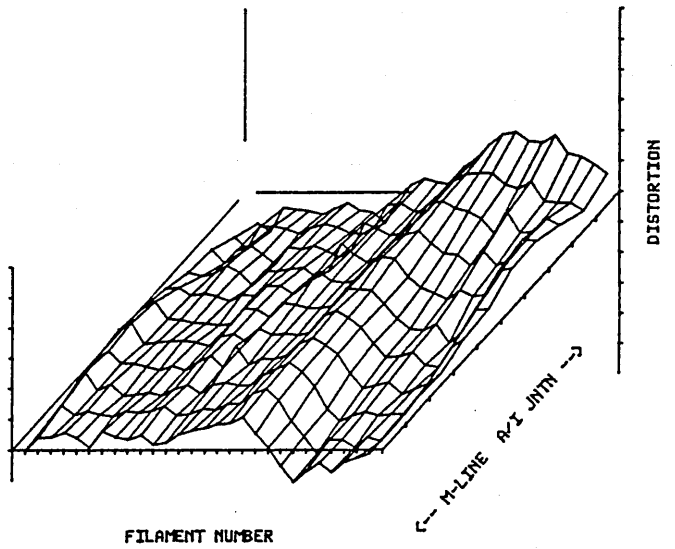

negative on the opposite edge as a result of the subtraction. This is the gross distortion introduced as a result of the sarcomere bowing, and is in agreement what is expected from the theoretical graphs (compare with Figs 5.2.8 and 5.2.9 from the ΔS and PPi results Section 5.2). The sarcomeres analysed show little change in the degree of bowing as the pH is raised from 7 to 9, as would be expected from the values shown in Table 6.2.1. Table 6.2.1 also shows a significant decrease in bowing as pH is raised from 5 to 7. It would be expected that this decrease is reflected in the degree of distortion seen at the edges of the sarcomere towards the A/I junction. A comparison of Figs 6.2.3.1 with 6.2.3.2 shows that this is the case. Furthermore, when the experimental data were subtracted from the ideal truncated conical and elliptical lattices, a similar symmetry reversal was noted as was seen at low S in control solution, confirming that the gross overall distortion was present. The root mean square distortion (RMSD) over the whole half sarcomere was calculated, and the results of this are given in Table 6.2.2.

The RMSD values given in Table 6.2.2 all show a decrease as the model used to fit the lattice changes from rectangular through conical to elliptical. This indicates that the elliptical model is a better fit to the experimental lattice, and correlates with data at short S both with and without PPi, where RMSD values for elliptical are also lower than

Table 6.2.2. RMSD values for S=2.6 μm for increasing pH with the rectangular, conical and elliptical model lattices. (All values are in nm).

pH	RECTANGULAR	CONICAL	ELLIPTICAL
5	18.8	12.4	5.7
7	12.1	10.9	9.0
9	13.7	11.9	10.1

for rectangular or conical models. As with ΔS and PPi experiments, the variability of RMSD values between the single sarcomeres makes a direct comparison difficult, but the large change in RMSD at pH5 is striking. The result at pH5 shows a low value for RMSD (a 3 to 3.5 fold decrease over that in the rectangular model) indicating a particularly close fit. Fig 6.2.5.1 is the graph of the distortion from the elliptial model at pH5 and shows over ~80% of the filament length that the fit is extremly good, as represented by the nearly flat plane parallel to the z-axis, and only the remaining 20% show the small but significant distortion. Fig 6.2.6 shows the distance from the centre of the sarcomere as plotted against filament number for M-line and A/I junction. The M-line shows a regular spacing (the straight line is the ideal situation), whereas the A/I junction shows regular departure as seen in ΔS and PPi experiments. This change in spacing at A/I tip is the cause of the effect seen, and is particularly clear in this case.

The sarcomeres analysed also show changes in the local disorder between the filaments. A qualitative assesment of this can be made from the smoothness of the graphs in Figs 6.2.3.1 → 6.2.3.3. At pH5 (Fig 6.2.3.1) the filaments are in reasonable lateral alignment resulting in an overall smooth appearance of the graph similar to that seen with PPi at low S. At pH7 (Fig 6.2.3.2) the degree of lateral order is less than at pH5 giving rise to a rougher appearance of the graph. Even though the local disorder has increased, the bowing is still obviously present. At pH9 (Fig 6.2.3.3), the bowing effect although still present, is reduced in comparison to the local disordering effect and the lateral register of the filament is significantly perturbed in a local manner giving rise to discrete domains within the A-band. In these regions, the distortion is higher or lower than a smooth plane showing groups of filaments with similar lateral spacings cluster together within the A-band.

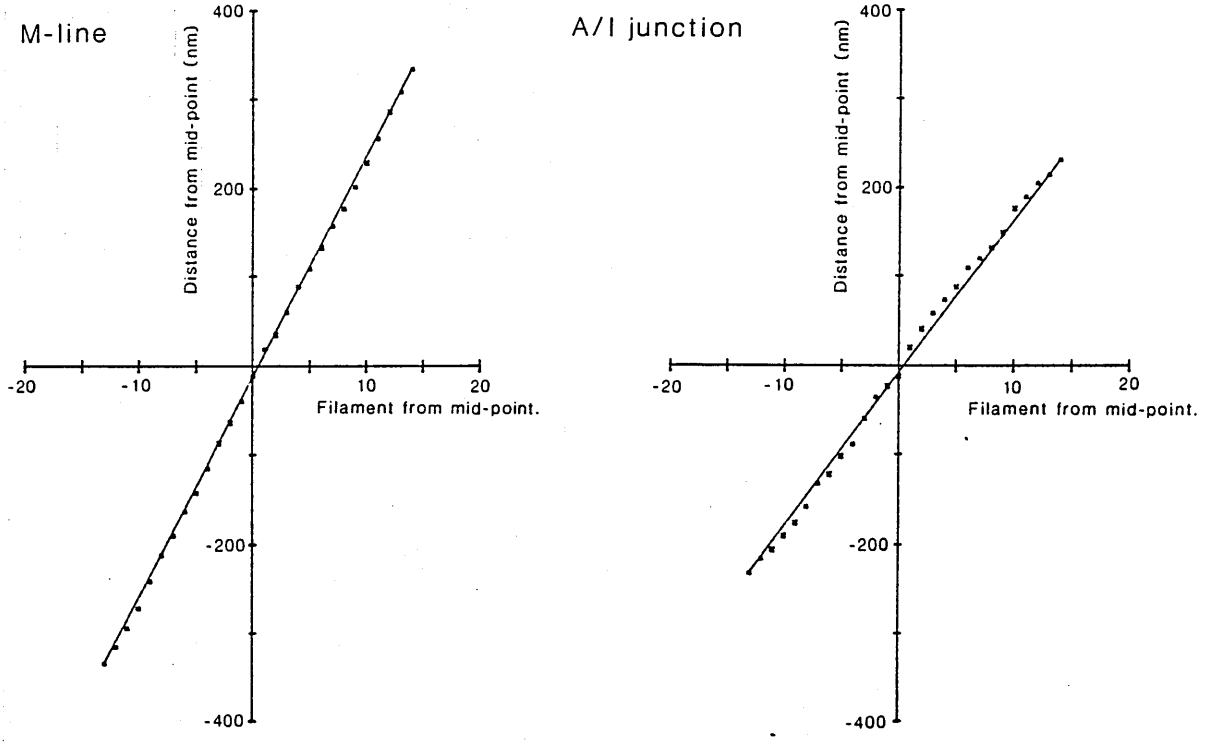

Fig 6.2.6. Distortion from an ideal linear separation of filaments in the M-line and A/I junction in rigor at S=2.6 μm and pH5.

So as with ΔS and PPi experiments, changing pH affects the distortions seen within the A-band lattice. The high local disorder seen at pH9 is similar to that seen at long S in the previous experiment, though in those experiments at long S no bowing was present, so the different fits had no effect on RMSD. The RMSD at pH9 shows a decrease with conical and elliptical fits, indicating bowing is still present. This implies at S=2.6 μm at pH9, the overall disorder seen is a combination of local disorder and bowing. This contrasts with the result at pH5 which shows very low local disorder but a high degree of bowing.

To assess how these distortions affect the X-ray pattern seen, the same half-sarcomeres are used to calculate the Fourier summations and these are compared to the OD patterns seen. Finally, the results from OD are compared directly to the X-ray results seen in the pH solutions.

(b) 6.3. Correlation of distortion seen under EM with X-ray results.

The Fourier summations were performed using the same data that were used to generate the distortion graphs. Figs 6.3.1, 6.3.2 and 6.3.3 show the results of the analyses for pH5, pH7 and pH9. The curves are as previously described (see Section 5.3, the results sections of the ΔS and PPi experiments, for further details).

(i) Black curve - The ideal curve from the same number of filaments as in the section, each separated by the mean spacing value.

(ii) Green curve - The Fourier summation curve from the experimental data.

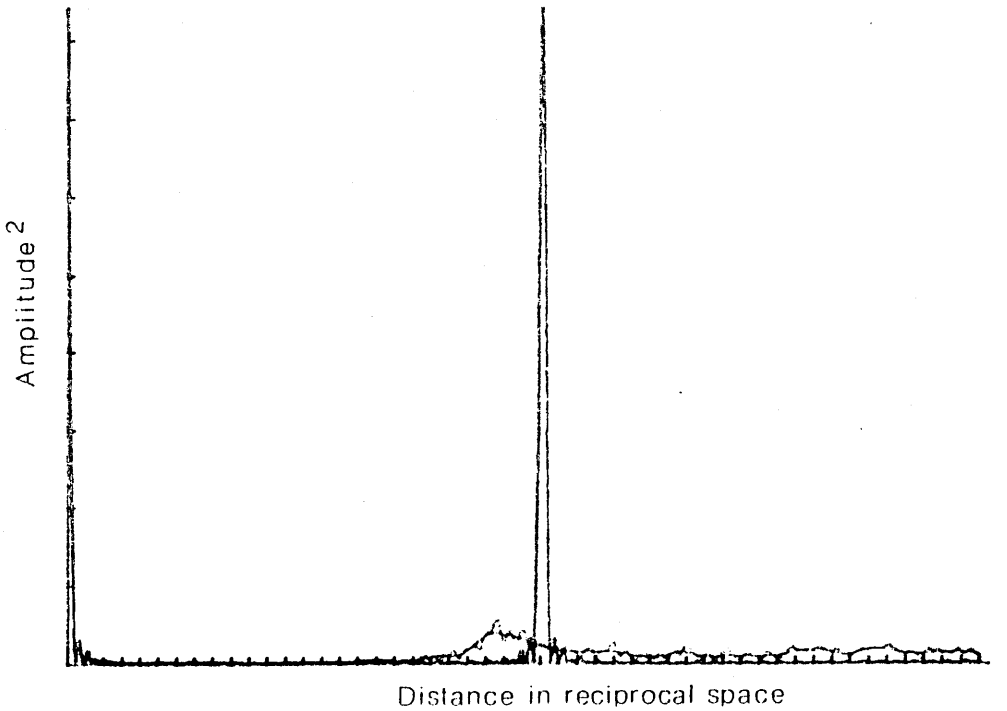

Fig 6.3.1. Fourier summation of the half-sarcomere shown in Fig 6.2.3.1 of pH5 solution at S=2.6 μm. The black curve shows the ideal result, the green the experimental and the red the fitted curve (see text).

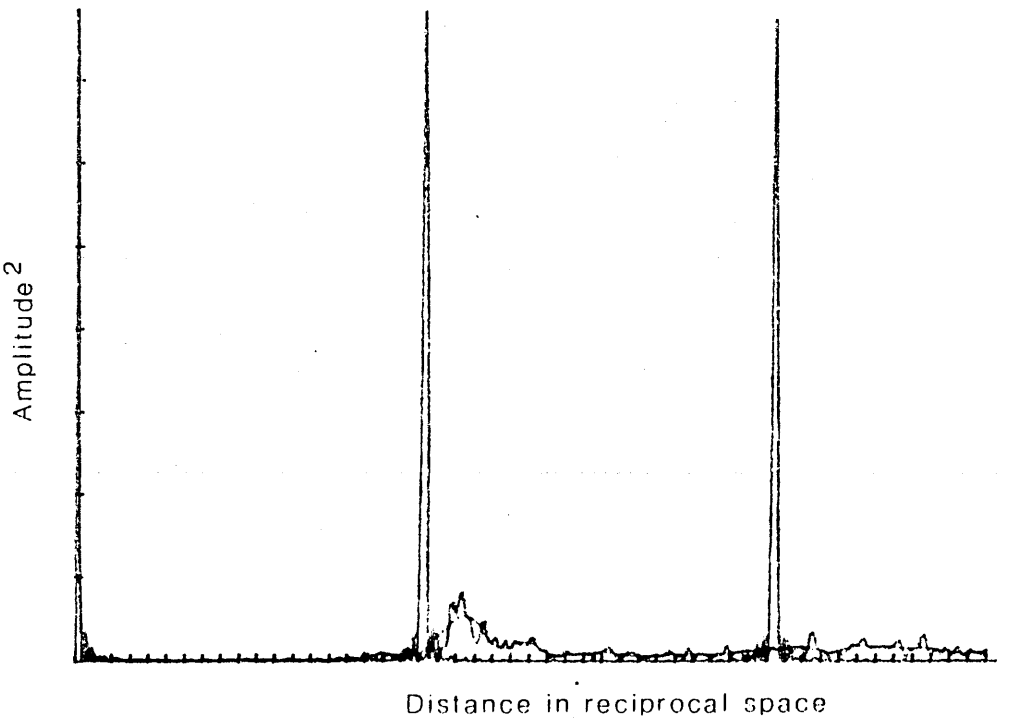

Fig 6.3.2. Fourier summation of the half-sarcomere shown in Fig 6.2.3.2. of pH7 solution at S=2.6 μm. (See above for details).

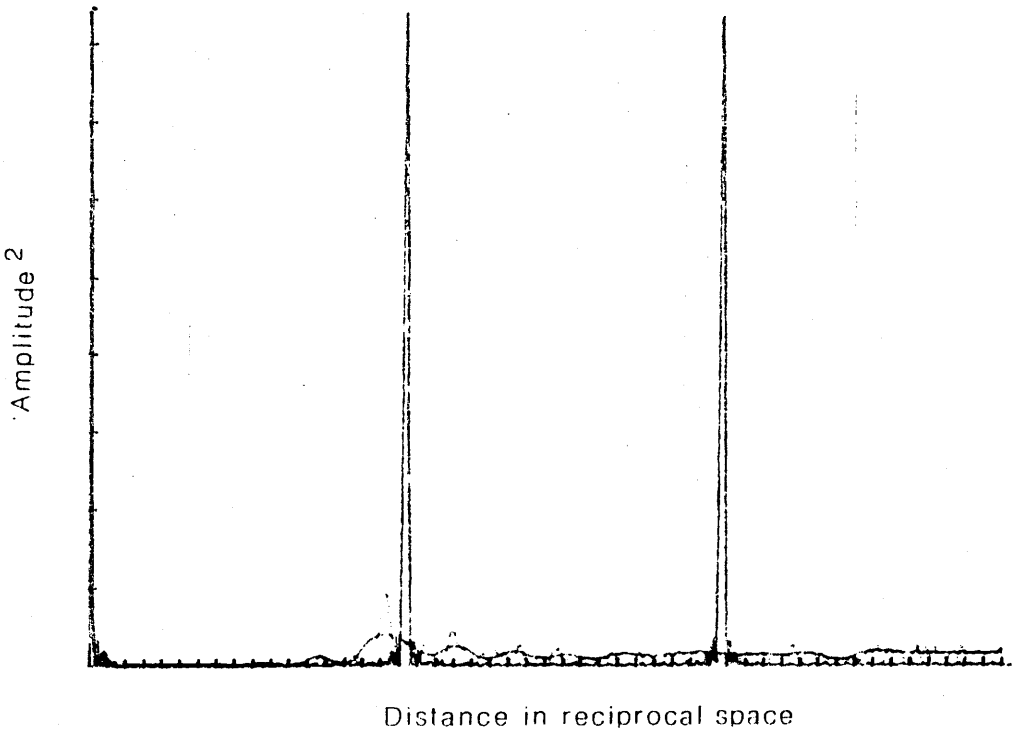

Fig 6.2.3. Fourier summation of the half-sarcomere shown in Fig 6.2.3.3 of pH9 solution at S=2.6 μm. (See previous page for details).

(iii) Red curve - Curve fitted to summation curve by taking the first derivative of the cubic spline of the cumulative total of the Fourier summation curve.

In both plots, a peak in the experimental (green) curve is clear around the same region as the first order peak in the ideal (black) curve. Table 6.3.1 shows the values of mean spacing over the whole half-sarcomere ie positions of peaks in the black curve, and the spacing of the first peak of the fitted curve (all spacings given in nm).

Table 6.3.1. Spacing of the fitted curve and of ideal curves at increasing pH at S=2.6 μm. (All spacings in nm).

pH	MEAN SPACING	1st PEAK SPACING
5	22.0	21.4
7	29.8	27.9
9	33.0	32.3

Table 6.3.1 shows that the values from the ideal mean spacing and the Fourier summation peak are in good agreement. As with the ΔS and PPi results (Section 5.3) the slight differences could be accounted for by shape changes in the peak and by sampling differences between the two methods. The red summation peaks seen were analysed to estimate the sharpness, as given by $\Delta s/s$. This is analagous to the $\Delta d/d$ seen with X-ray diffraction on the equator. The peak height to peak FWHM (R_{hw}) was also measured and Table 6.3.2 shows these values.

The values show that the $\Delta s/s$ increases as the pH is perturbed from pH7 to either pH5 or pH9, a concommitant increase in R_{hw} is also seen, and these two observations are in agreement in showing the

Table 6.3.2. $\Delta s/s$ and R_{hw} values for samples at S=2.6 μm with increasing pH.

pH	$\Delta s/s$	R_{hw}
5	0.083	0.38
7	0.070	0.80
9	0.080	0.71

sharpness of the fitted peak increases as pH is raised from 5 to 7, but decreases again as the pH is raised further from 7 to 9. This change in sharpness at pH5 and pH9 indicates that the distortion seen at pH5 (ie the bowing) and at pH9 (the local disorder) both contribute to the broadening of the peaks seen in the summation and so, by analogy with OD, broaden the reflections seen in the X-ray pictures. The actual values of the sharpness in the Fourier summation and in the X-ray diffraction in solution show a correlation, in both cases there is an increase in sharpness from pH5 to pH7 and a decrease in sharpness from pH7 to pH9, giving rise to the U-shaped curve in pH X-ray results (Section 4.2 Fig 4.2.3). Table 6.3.3 compares sharpness values from Fourier summation and X-ray diffraction.

Table 6.3.3. A comparison of sharpness of the first peak of the Fourier summation ($\Delta s/s$), and of the (1,0) X-ray equatorial reflection both measured with GX13 and at the sychrotron ($\Delta d/d$).

pH	$\Delta s/s$	$\Delta d/d$ (GX13)	$\Delta d/d$ (SYNCHROTRON)
5	0.083	0.115 → 0.130	0.070 → 0.085
7	0.070	0.095 → 0.110	0.060 → 0.075
9	0.080	0.105 → 0.115	Expt to be done

Values for $\Delta d/d$ give a range of values since relatively few points were available for a more rigorous statistical treatment.

The values in Table 6.3.3 show that the overall trend seen in the Fourier summation is the same as that seen in the X-ray experiments, the values obtained from the synchrotron source showing a very good correlation with $\Delta s/s$. The variation of values with pH is similar in all three measurements, an initial decrease of 0.01→0.02 as pH is raised from 5 to 7 followed by an increse of 0.01 as pH is increased from 7 to 9.

Table 6.3.1 shows the values of the mean spacing over the whole half-sarcomere and the spacing measured from the fitted curve. To analyse further the spacing changes seen by EM with the changes in pH, a comparison was made between the spacing measurements made in EM and with X-ray diffraction. Table 6.3.4 shows the summary of the results: the values shown are for the same measurments as in Table 5.4.1 of the ΔS and PPi experiments (Section 5.4). Briefly the columns are -

Column 3 - Mean spacing over the whole half-sarcomere used for the analysis of distortion and in the Fourier summation (Table 6.3.1 col 1)

Column 4 - Spacing of the first major peak of the fitted curve of the Fourier summation.

Column 5 - Spacing of the first peak in OD.

Column 6 - Mean spacing as taken over 10 M-lines of separate sarcomeres.

Column 7 - The (1,0) spacing as measured by X-ray diffraction.

Table 6.3.4. A summary of thick filament spacing changes with changing pH as measured by the range of techniques (all spacings in nm).

S	EXPT	3	4	5	6	7
2.6 μm	pH5	22.0	24.2	21.4	23.46 ± 6.99 (n=322)	32.9 ± 1.1 (n=4)
2.6 μm	pH7	29.8	26.3	27.9	28.50 ± 7.50 (n=209)	40.2 ± 0.8 (n=6)
2.6 μm	pH9	33.0	35.3	32.3	32.06 ± 7.84 (n=304)	41.9 ± 0.5 (n=4)

Columns 3,4 and 5 compare the calculated OD spacing to that seen experimentally. As with the ΔS and PPi experiments the two figures are in good agreement. The OD traces again show a high level of grainy background, and so the whole discussion of comparison between X-rays and EM has relied on the calculated summation. The agreement between columns 3 and 5 confirms that the spacings are a good approximation, and a qualitative examination of the OD prints shows that changes in sharpness are also similar to those predicted.

The values of calculated and experimental OD spacings in columns 3,4 and 5 are in agreement with the mean spacing as measured over 10 M-lines. The values of the spacing from EM showed a similar pattern to those seen with X-rays diffraction, an increase in pH results in an increased spacing. As Section 5.3 (ΔS and PPi results) the spacing with EM is reduced to 65 → 75% of the X-ray value, showing again that considerable shrinkage had taken place.

6.4. Summary.

Using the link established between distortion of the A-band lattice and changes in the X-ray pattern, EM pictures of samples in

either pH5 or pH9 solution at S=2.6 μm were compared to those seen at pH7. The simple distortion analysis, where bowing is assessed as a percentage decrease in width between A/I junction and M-line, shows that the change of pH from 5 to 7 is accompanied by a decrease in bowing from 11 to 7%, an increase to pH9 has little further effect, though a qualitative analysis of the scatter indicates a slightly higher value at lower numbers of filaments in the section.

A more detailed analysis, using digitized data fitted with varying "ideal" lattices, shows that at pH5 there is a reduction in local disorder within the A-band as well as the increase in bowing, but at pH9 there is an incease in this local disorder, but little change in the bowing. The effect of these distortions on the sharpness of the X-ray reflections was assessed both by calculated Fourier summation and by OD. The results show that both the bowing, which predominates at pH5, and the increased local disorder in evidence at pH9, both contribute to the decrease in sharpness seen in the summation and OD peaks, and so by analogy decrease the sharpness seen in the (1,0) peaks in X-ray diffraction pictures. This correlates well with the experimentally determined sharpness of the (1,0) reflection. Increases in sharpness with either an increase or decrease in pH give rise to the U-shaped curve seen. The changes in Fourier summation and OD from EM give rise to a similar result.

Again large changes ($\sim$ 25 $\rightarrow$ 35% decrease) are seen in thick filament spacings under EM as compared to X-ray diffraction spacings. However, the values of the spacings showed a far clearer relation to the original X-ray pictures than do those from ΔS and PPi experiments. The increase in X-ray spacing for a pH change of 5 to 7 and from 7 to 9 is reflected clearly in the EM results.

A COMPARISON OF RABBIT DATA TO DATA FROM CONTRACTING FROG STRIATED MUSCLE.

Section 7.1. Electron Microscopy of Glutaraldehyde fixed muscle.

The previous sections have been concerned with the effects of varying conditions on rabbit rigor muscle, and analysing changes in A-band distortion with EM and X-ray diffraction. This analysis has shown that changes in distortion seen under EM can be correlated with the sharpness of the X-ray diffraction reflections. This is true for both meridional and equatorial reflections, but the EM effect has been correlated largely with the equatorial reflection changes. In this section, the possible role of these distortions in muscle under physiological conditions is examined by the same methods used in the analysis of rigor fibres.

Bergman (1983) used relaxed or contracting frog fibres fixed in glutaraldehyde (GA) or OsO_4. Using prints kindly provided by Dr Bergman, negatives were made and analysed by the same tracing and digitizing method as were pictures of the rabbit fibres. The pictures show sarcomeres in various physiological states, but show only a limited number in each case. Because of this low sample size, the analysis of M-line to A/I junction width ratio was not performed, and the results presented are from the analysis involving fitting ideal rectangular, truncated conical and elliptical lattices to the experimental data. Table 7.1.1 shows the RMSD for all pictures analysed.

Taking the pictures of each state separately, the relaxed sarcomere distortions from the ideal lattices are shown in Figs 7.1.1.1 → 7.1.1.5. Fig 7.1.1.1 shows the traced filaments divided into two lattices. The left hand (unbounded lattice) contains 30 filaments, and its distortion from the ideal rectangular, conical and elliptical lattices

(a).

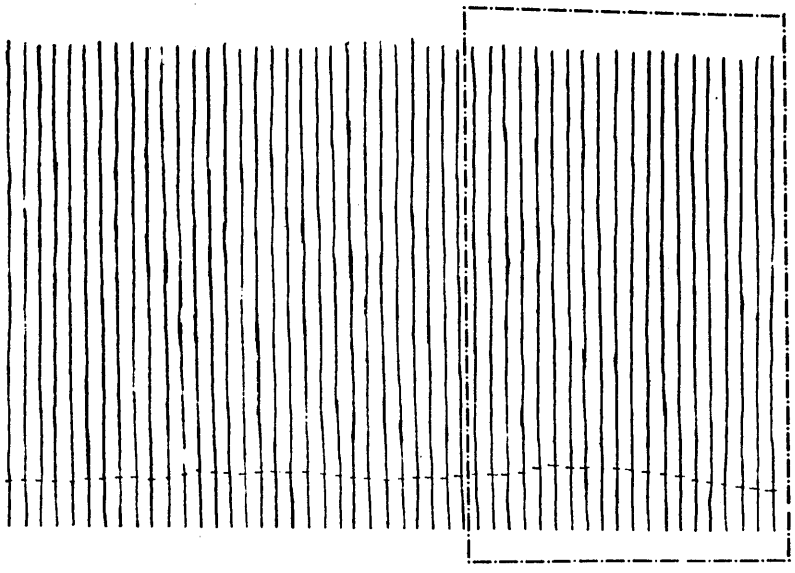

(b).

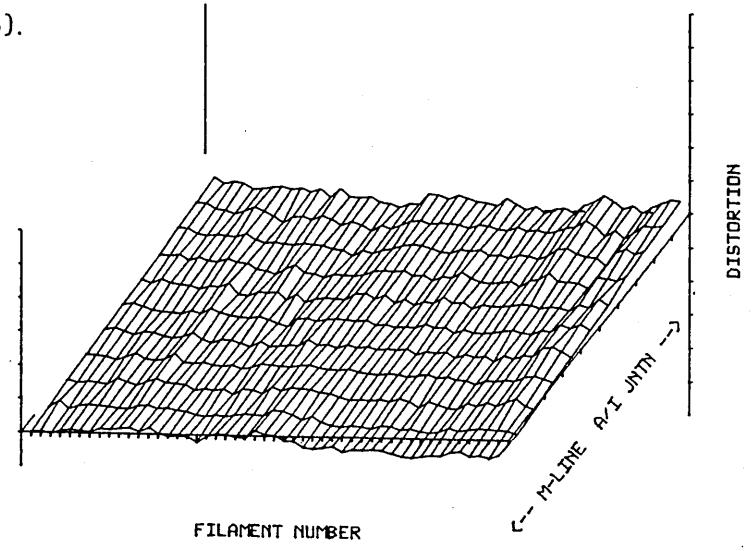

(c).

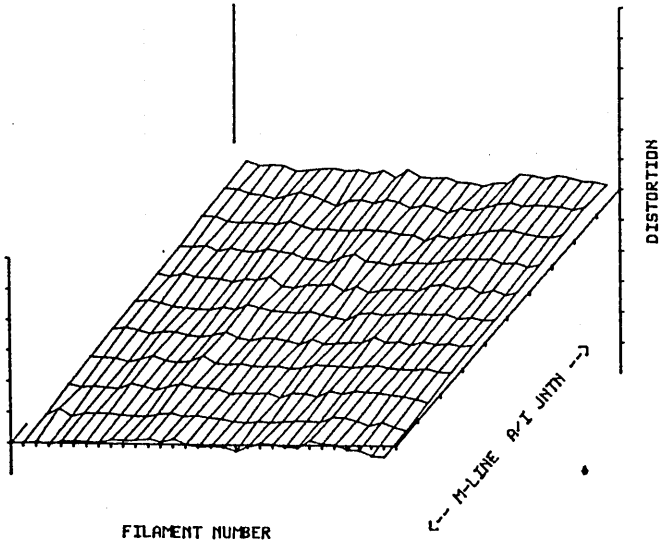

(a). Fig 7.1.1.1. Tracing of filaments from a relaxed sarcomere at S=2.77 μm. The area including that in the dashed box is 50 filaments in width, and excluding the box, 30 filaments in width.

(b). Fig 7.1.1.2. (Above) Distortion from the ideal rectangular lattice of the 50 filament lattice shown in Fig 7.1.1.1 of the relaxed half-sarcomere at S=2.77 μm.

(c). Fig 7.1.1.3. (Left) Distortion from the ideal rectangular lattice of the 30 filament lattice shown in Fig 7.1.1.1 of the relaxed half-sarcomere at S=2.77 μm.

are shown in Figs 7.1.1.3 to 7.1.1.5. Figs 7.1.1.2 shows the distortion taken over the broad sarcomere (the previous lattice plus the filaments in the dashed box) containing 50 filaments, at S=2.77 μm. The reasons for this division are discussed later. As shown in Table 7.1.1, the distortion from the ideal lattices are small, all RMSD values are ~4 nm which shows a good fit

Table 7.1.1. RMSD values for all pictures analysed in relaxed, contracting and rigor frog muscle at a variety of S.

CONDITION	S (μm)	$RMSD_{rec}$	$RMSD_{con}$	$RMSD_{ell}$
Relaxed (50)*	2.77	4.01	4.32	4.06
Relaxed (30)*	2.77	3.82	3.82	4.22
Contracted	2.67	15.19	14.00	13.94
Contracted	2.06	12.91	10.25	5.59
Rigor	2.06	12.17	9.84	7.56

* The figure in brackets denotes the number of filaments of the section used in the analysis - see text for details.

in all cases. There is little difference between the RMSD values for the different lattices. This consistency confirms Bergmans (1979) original observation that relaxed sarcomeres have an essentially rectangular shape. In the ideal rectangular lattice the M-line and A/I widths are the same and the filaments are straight lines between corresponding points at each end. For a truncated cone or ellipse where the M-line and A/I junction widths are also the same, the ideal lattice will again be a series of equally spaced points on the M-line and A/I junction joined by straight lines, so in this unique situation, there is no difference between the model lattices.

Fig 7.1.1.2 not only shows little overall gross distortion, but also a smooth appearance indicating that the local disorder in these relaxed

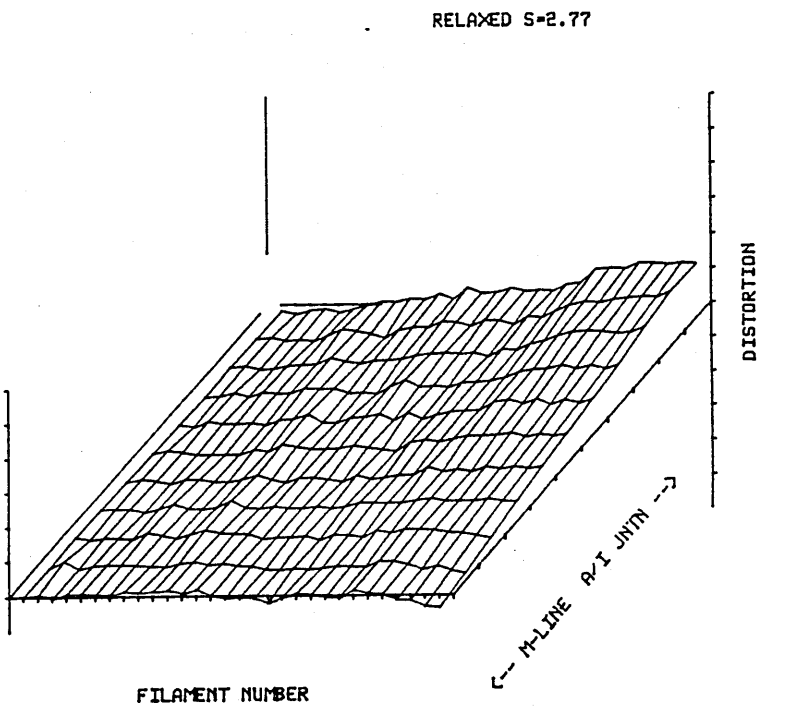

Fig 7.1.1.4. Distortion from the ideal truncated conical lattice of the 30 filament traced lattice in Fig 7.1.1.1 of the relaxed half-sarcomere at S=2.77 μm.

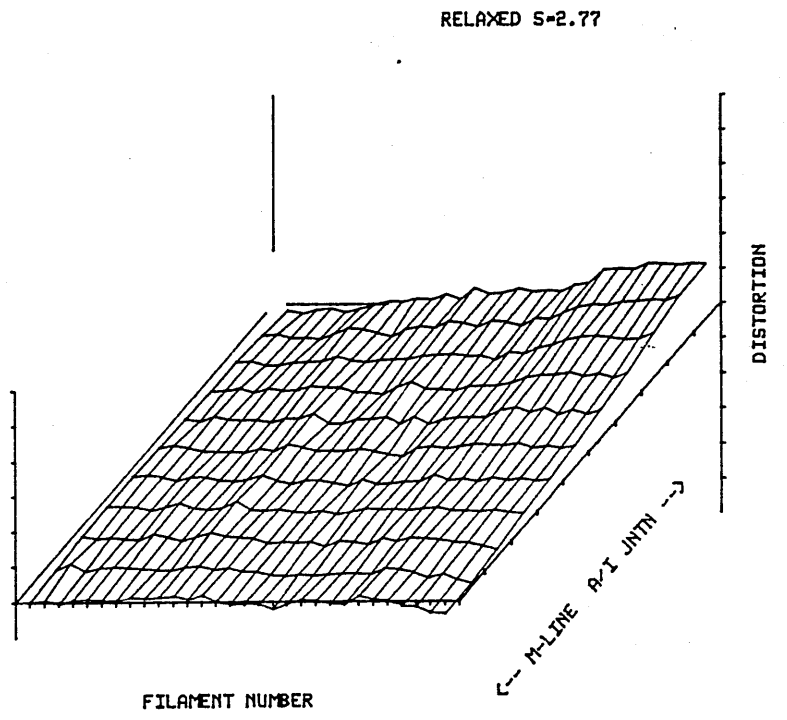

Fig 7.1.1.5 Distortion from the ideal truncated elliptical lattice of the 30 filament traced lattice in Fig 7.1.1.1 of the relaxed half-sarcomere at S=2.77 μm.

sarcomeres is small. The sarcomere section in Figs 7.1.1.2 contains 50 filaments, whereas the sarcomeres in the other states contain 25 → 30 filaments. Fourier theory predicts that the width of a peak from a series of equally spaced diffracting units is inversely proportional to the number of such units, so to reduce the error in peak width produced by these differences in filament number, the analysis was repeated for the first 30 filaments only (see Table 7.1.1 and Fig 7.1.1.1 - a more complete discussion of this point is given later). Figs 7.1.1.3 → 7.1.1.5 show the results of this second distortion analysis, and again little overall distortion is present as seen by the smoothness in the plane parallel to the Z-axis, where the low degree of local disorder gives a flat overall appearance. The RMSD given in Table 7.1.1 is not appreciably different between the three models, showing that the experimental lattice is very nearly a perfect rectangle, and is similar to the value for the full lattice. This indicates that the shortened lattice is representative of the full lattice. The shortened lattice is used to compare to the other (contracting) lattices which have a lower section filament number.

Figs 7.1.2.1 → 7.1.2.4 and 7.1.2.1 → 7.1.2.4 show the traced filaments, and the effect on the distortion graphs, of contraction at S=2.77 and 2.06 μm respectivly. Figs 7.1.3.2 and 7.1.4.2 show the distortion of the experimental data from the ideal rectangular lattice and the overall gross distortion typical of bowed sarcomeres is seen. The graphs also show a small but perceptible decrease in the smoothness of the trace, indicating that the local disorder has increased also, though this effect is fairly small. Because of the bowing effect, there should be a symmetry reversal round the lateral mid-point of the sarcomere, when the experimental data is compared to the ideal truncated conical or elliptical lattices. Figs 7.1.3 and 7.1.4 show the graphs of the distortion seen in such comparisons and

(a).

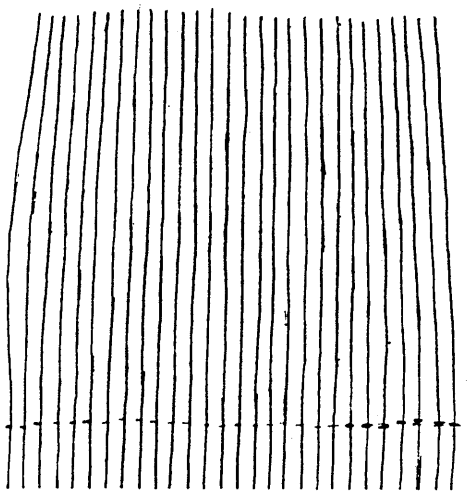

(d).

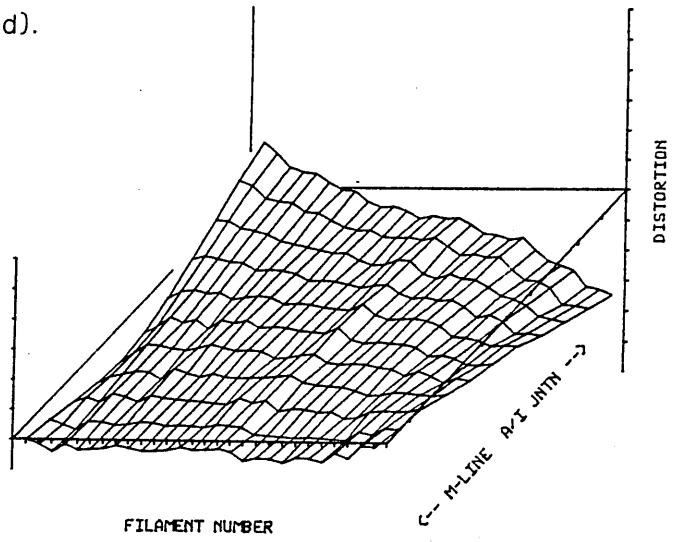

(b).

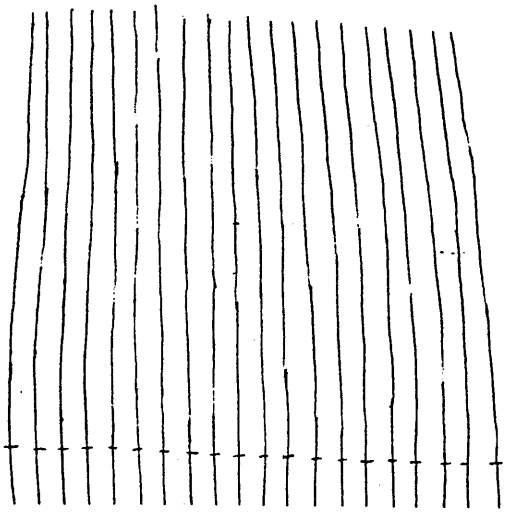

(e).

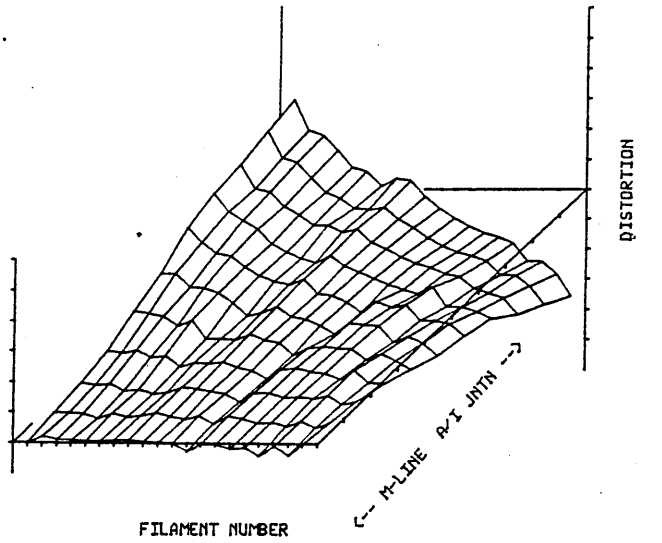

RIGOR S=2.86

(c).

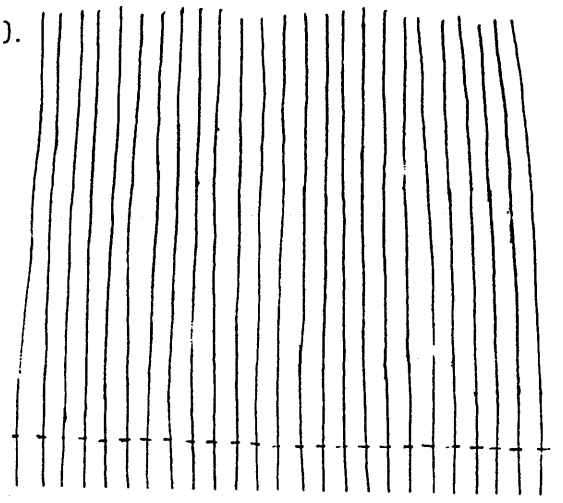

(f).

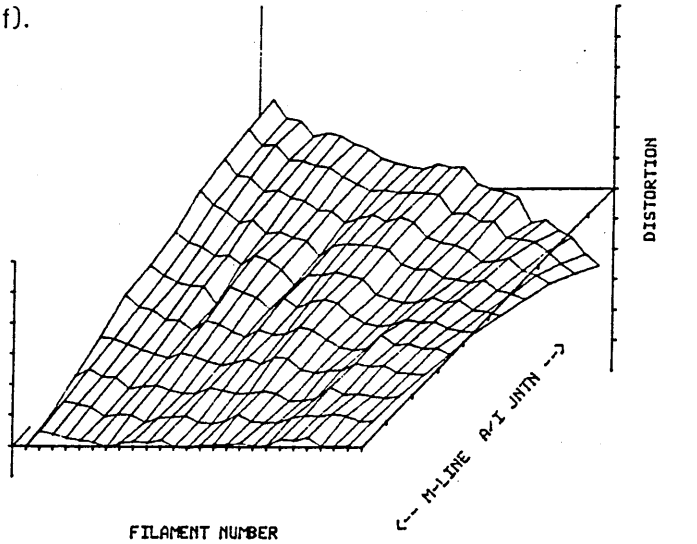

(See next page for captions).

Guide to Figs 7.1.2.1 to 7.1.4.2. (see previous page).

(a) Fig 7.1.2.1. Tracing of thick filaments in the A-band in the contracted state at S=2.77 μm.

(b) Fig 7.1.3.1. Tracing of thick filaments in the A-band in the contracted state at S=2.06 μm.

(c) Fig 7.1.4.1. Tracing of thick filaments in the A-band in the rigor state at S=2.06 μm.

(d) Fig 7.1.2.2. Distortion from the ideal rectangular lattice of the filaments shown in Fig 7.1.2.1.

(e) Fig 7.1.3.2. Distortion from the ideal rectangular lattice of the filaments shown in Fig 7.1.3.1.

(f) Fig 7.1.4.2. Distortion from the ideal rectangular lattice of the filaments shown in Fig 7.1.4.1.

Guide to Figs 7.1.2.3 to 7.1.4.4. (see next page).

(g) Fig 7.1.2.3. Distortion from the ideal conical lattice of the filaments shown in Fig 7.1.2.1.

(h) Fig 7.1.3.3. Distortion from the ideal conical lattice of the filaments shown in Fig 7.1.3.1.

(i) Fig 7.1.4.3. Distortion from the ideal conical lattice of the filaments shown in Fig 7.1.4.1.

(j) Fig 7.1.2.4. Distortion from the ideal elliptical lattice of the filaments shown in Fig 7.1.2.1.

(k) Fig 7.1.3.4. Distortion from the ideal elliptical lattice of the filaments shown in Fig 7.1.3.1.

(l) Fig 7.1.4.4. Distortion from the ideal elliptical lattice of the filaments shown in Fig 7.1.4.1.

(g).

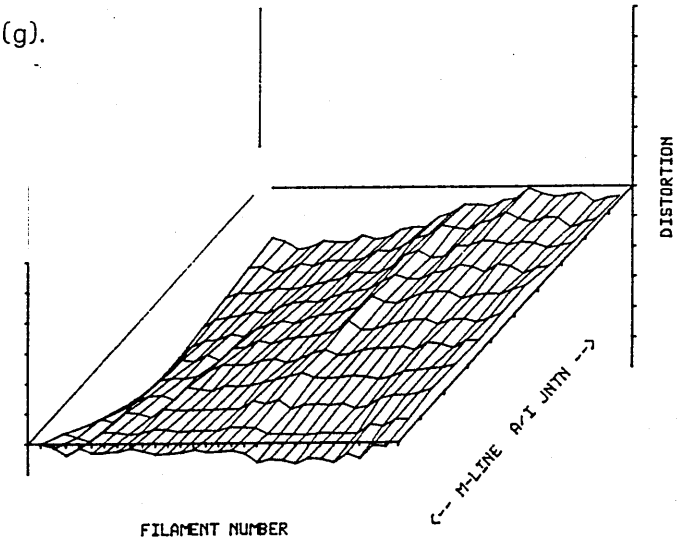

(j).

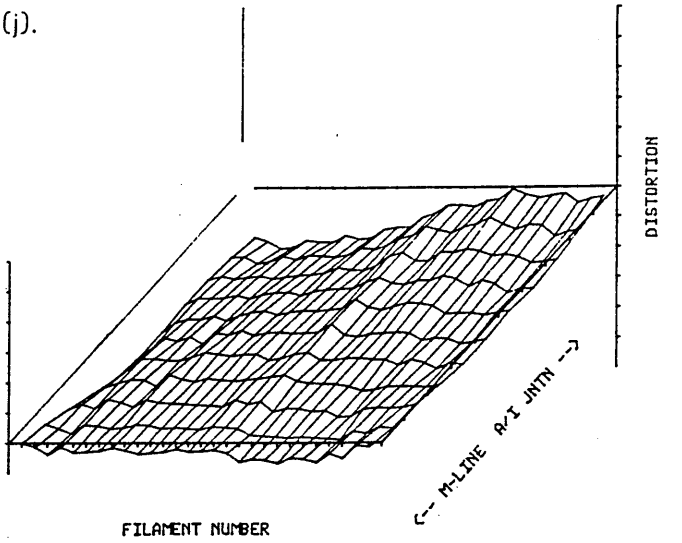

(h).

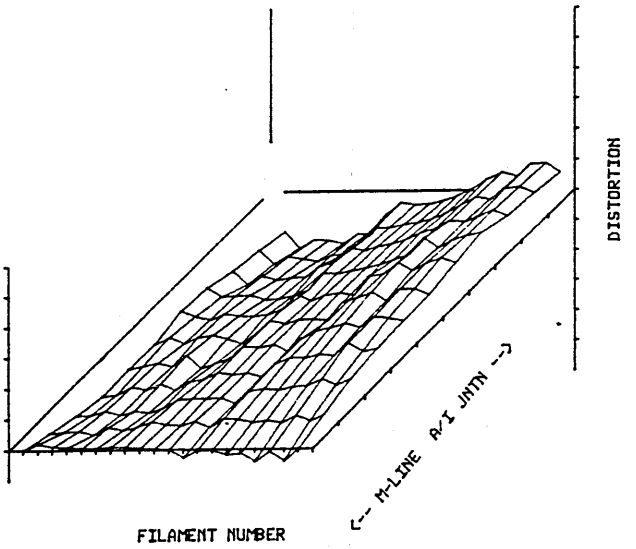

(k).

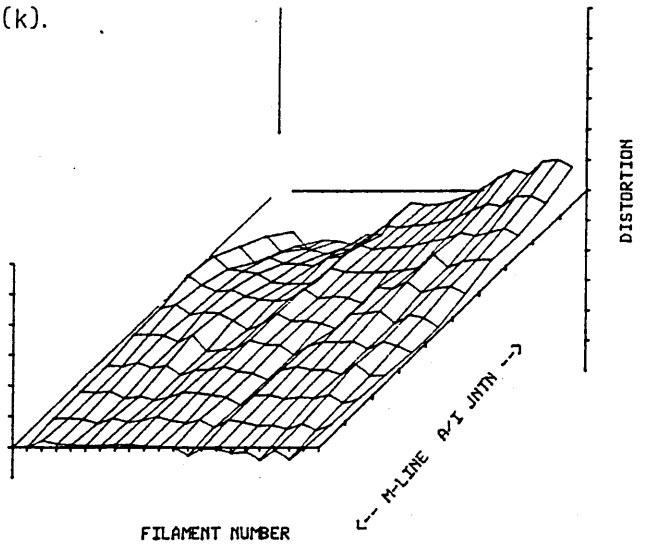

(i).

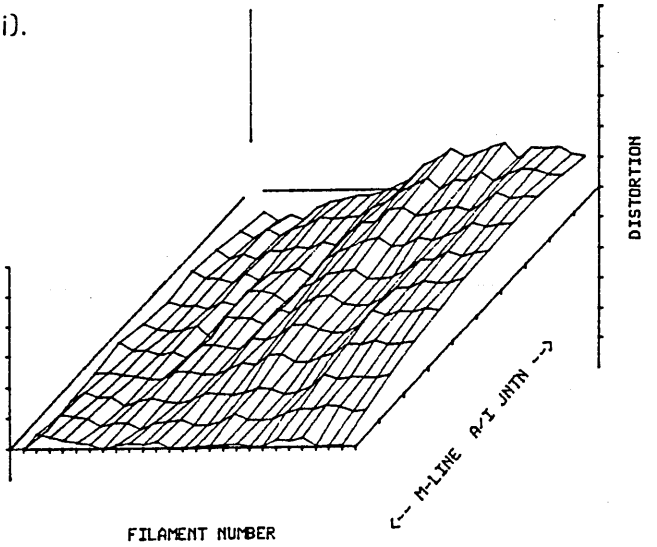

(l).

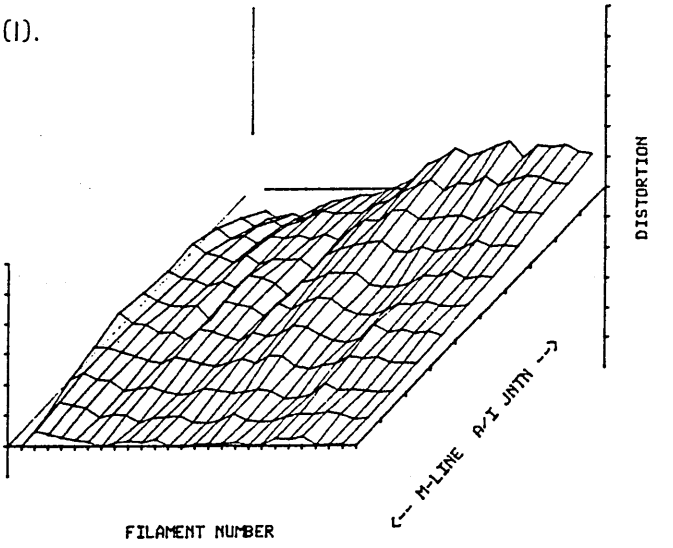

(See previous page for captions).

confirm the predicted symmetry reversal. Table 7.1.1 gives RMSD values for contracted sarcomeres and shows that for the sarcomere at S=2.67 μm there is a small decrease with the conical and elliptical lattice fits. At S=2.06 μm there is a small reduction in RMSD with the conical fit, but a significant reduction with the elliptical fit, showing that the truncated elliptical lattice is the best fit of these models.

The final picture, analysed in the series of prints provided by Dr Bergman, was that of a sarcomere in rigor at S=2.06 μm. Figs 7.1.4.1 → 7.1.4.4 show the tracing and the distortion from the ideal lattices. As with the contracted sarcomeres, the rigor section shows the typical overall bowing distortion with the ideal rectangular fit, and the symmetry reversal with the conical and elliptical lattices is also seen. The RMSD values again show a decrease with the conical fit and a further decrease with the elliptical fit, showing that as with the contracting sarcomeres, the truncated elliptical model was the best fit to the experimental data. The sarcomere shows a similar level of local distortion to the contracting sarcomere, as shown by the decrease in the smoothness of the trace in the graph.

7.1.1. Summary.

The EM analysis of GA treated muscle shows that in the relaxed state, the sarcomeres are very close to the ideal rectangular lattice at S=2.77 μm. This confirms Bergmans (1983) original observation. The distortion analysis further shows that local disorder is low in the relaxed state. When the sarcomere from contracted muscle at this S was examined, the rectangular lattice was replaced by a bowed lattice, which was best fitted by a truncated elliptical model. The local disorder in this case had also slightly increased. Bergman's experiments covered an extensive range of S, and he concluded that at

all S, the relaxed lattice maintained its rectangular shape, so it seems reasonable to predict a rectangular lattice with low local distortion at short S. At this low value of S in the contracted state, the bowed sarcomere is seen again, furthermore this bowed state is seen in the rigor sarcomere at the same S, and in both cases the best fit is with the truncated elliptical model.

As with the longer S, local disorder increases in both contracted and rigor sarcomeres. The rigor and contraction results correlate with those seen at short and intermediate S in rigor and PPi with rabbit muscle, where the best fit again tended to be the truncated elliptical model.

7.2. Fourier analysis of GA fixed muscle.

As before, the Fourier summations were taken at all 11 levels of the digitized data and averaged to get the final trace. Figs 7.2.1 and 7.2.2 show the relaxed sarcomeres at S=2.77 μm, the colours of the curves are the same as for Figs 5.3.1 to 5.3.4. As mentioned in the previous section, this sarcomere was treated in two ways, the first involved taking the transform of the full sarcomere (which was 50 filaments in width) and the second took the transform of the first 30 filaments of the same sarcomere to compare with the other sarcomeres (see later for the theory behind this decision). All sarcomeres in the other states had 25 → 30 filaments in the sections, and Figs 7.2.3 → 7.2.5 show their transforms. Table 7.2.1 shows the mean spacing given by the ideal lattice transforms and the spacing of the first and second orders of the transforms fo the experimental data.

The ideal and experimental data are in close agreement, better than that seen in the case of Fourier transforms from EM pictures of rabbit muscle (see Tables 5.3.3 and 6.3.3 for comparison). Examination

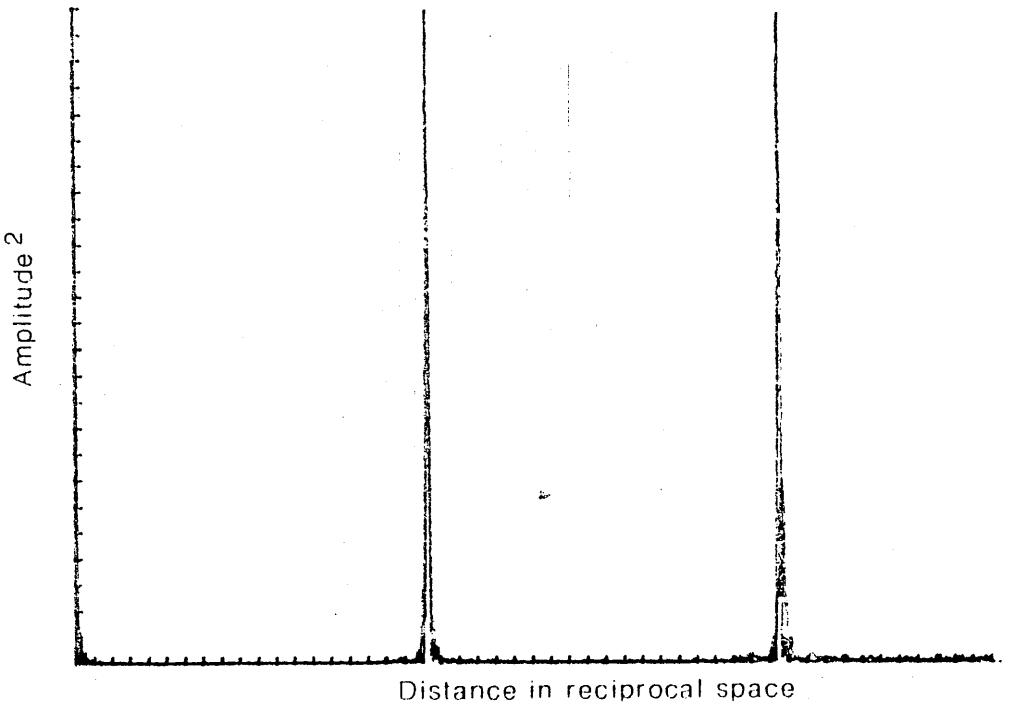

Fig 7.2.1. Fourier summation of the half-sarcomere shown in Fig 7.1.1.1 of relaxed frog sartorius. S-2.77 μm, results from 50 filament lattice (above) and 30 filament lattice (below in Fig 7.2.2.). The black curve shows the ideal result, and the green the experimental (see text).

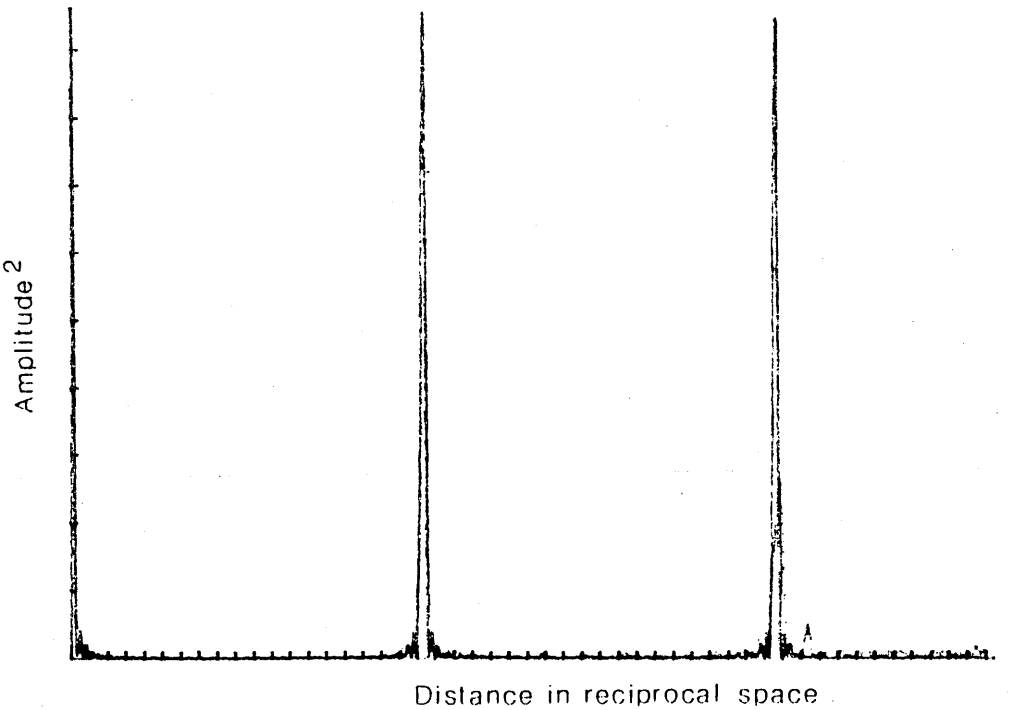

Fig 7.2.2. See above for details.

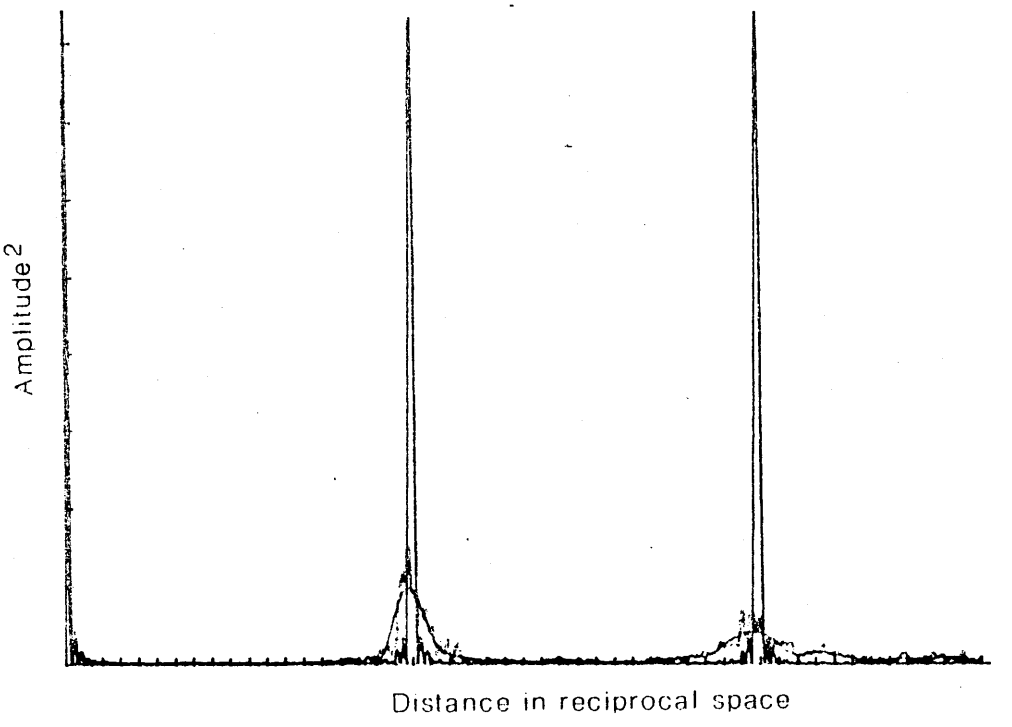

Fig 7.2.3. Fourier summation of the contracted half-sarcomere shown in Fig 7.1.2.1 at S=2.67 μm. The black curve shows the ideal result, the green the experimental and the red the fitted curve (see text).

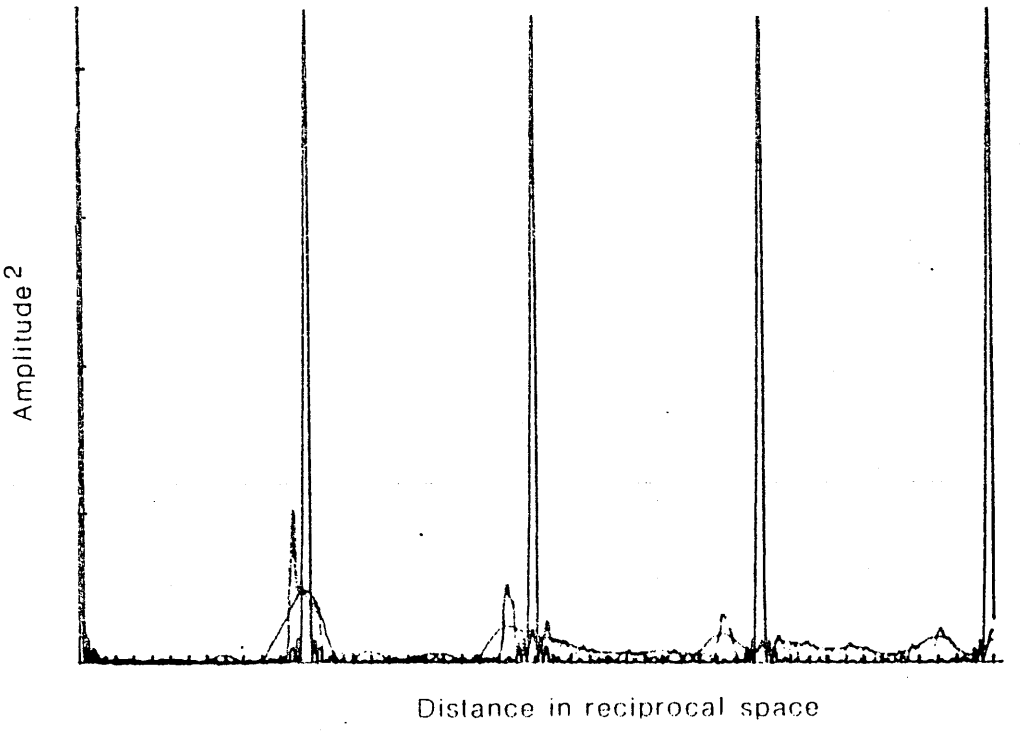

Fig 7.2.4. Fourier summation of the contracted half-sarcomere shown in Fig 7.1.3.1 at S=2.06 μm. (See above for details).

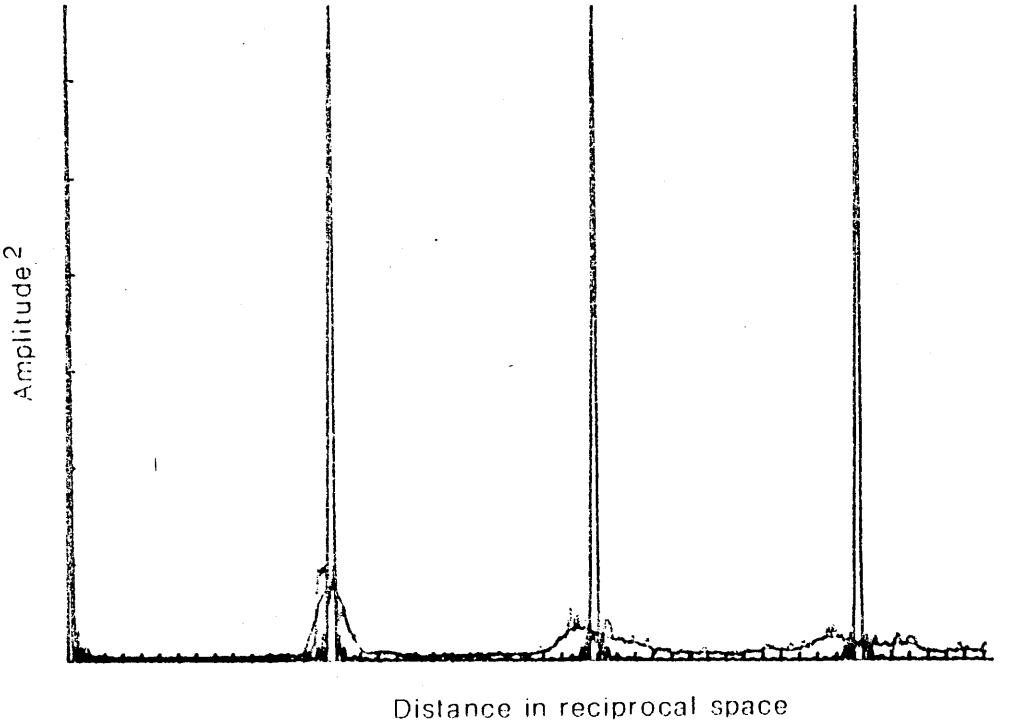

Fig 7.2.5. Fourier summation of the rigor half-sarcomere shown in Fig 7.1.4.1 at S=2.06 μm. (See text under Fig 7.2.1 for details).

of Figs 7.2.3 → 7.2.5 (those sarcomeres where bowing is present) shows that the uneven distribution of the green experimental curves are similar in shape to those seen in Fig 5.3.6 for the Fourier transform of the ideal truncated elliptical lattice. The peaks are also better defined than those from the rabbit where the effect of bowing is not seen as clearly. These two observations indicate that the A-band lattice in the frog has a lesser degree of local disorder than that in the rabbit. A high local disorder will tend to give a wider distribution of spacings, and thereby lead to both a reduction in the bowing effect on the summation curve, and greater variation between experimental and ideal data (see Section 5.3.1 for a more detailed discussion of some factors affecting peak widths and position).

Table 7.2.1 Ideal and experimental peak spacings of the first and second orders of the Fourier transforms together with equatorial spacings seen with OD (all spacings in nm).

CONDITION	S (μm)	IDEAL		EXPERIMENTAL		OD
		1st order	2nd order	1st order	2nd order	
Relaxed (50 filaments)	2.77	29.8	14.9	29.7	14.8	30.0
Relaxed (30 filaments)	2.77	29.7	14.9	29.5	14.8	-
Contracted	2.67	30.3	15.2	30.5	15.1	31.4
Contracted	2.06	46.1	23.0	46.1	24.2	24.6
Rigor	2.06	39.8	19.7	40.0	20.5	41.8

The OD spacing data also shows a good correlation with the first peak spacings in the Fourier transforms. In the contracted state at S=2.06 μm the plane of cut in the section is probably near the (1,1) lattice plane. The high values for the thick filament and OD spacings suggest that at this low S, thick filaments may have been mistaken for thin filaments crossing the M-line and so not have been traced. This

would not alter the validity of the data to be used for bowing and local disorder analyses, but would alter the mean spacing values appreciably. After processing the film to get negatives to use in OD, detail could just be made out of a short repeat cross-striation pattern in the A-band. These however did not produce any measurable meridional or layer line patterns with OD.

The peaks seen with the Fourier summation were further analysed for sharpness (given by $\Delta s/s$) and for ratio of peak height to peak width (R_{hw}). The results are shown in Table 7.2.2.

For the relaxed sarcomere at S=2.77 μm there were two analyses, one for the full 50 thick filaments and the other for the first 30. Differences in the number of thick filaments will affect the Fourier transform, and Figs 7.2.1 and 7.2.2 illustrate this clearly. Concentrating on the black ideal curve, which is given by calculating the summation over N filaments of mean spacing x_o, Fig 7.2.1 shows the result for N=50, and Fig 7.2.2 shows that for N=30. The widths of the ideal peaks in the N=30 curve are greater than that in the N=50. From Fourier theory, the width of the peaks is expected to be:-

$$w = \text{width} = \frac{4\pi}{N\, x_o\, k}$$

where k is the position of the peak in reciprocal space. In this case the difference in the spacing between the 1st order peaks of the N=50 and N=30 ideal curves is <0.5%, so for the purposes of calculation I shall ignore it. The equation for width of peak then simplifies to:-

$$w = \text{width} = \frac{c}{N}$$

where $c=4\pi/x_o k$, and is constant for both cases. The ratio of widths (w_{50}/w_{30}) is thus:-

$$\frac{w_{50}}{w_{30}} = \frac{30}{50} = 0.6$$

It should be noted that this is the ratio of the peak base widths. Measurement of the base widths of the ideal curves using calipers gives,

$$w_{50} = 1.86$$

$$w_{30} = 3.14 \text{ mm}$$

$$\text{so } \frac{w_{50}}{w_{30}} = 0.592$$

This measured value compares well with that predicted from Fourier theory.

Since the summation peaks in the relaxed condition were so sharp, this effect was significant in the analysis of the peaks (see Table 7.2.2), and to make the results compatible with the rest of the data, the 30 filament section was used for comparison. Table 7.1.1 with Figs 7.1.1, 7.1.2, 7.1.1.2 and 7.1.1.3 show that the effects on RMSD, mean spacing and local distortion are small compared to the large effect on the summation peak width of filament number (see Table 7.2.2).

In all cases the R_{hw} of both the first and second order peaks is well above 0.25, allowing both peaks to be analysed for $\Delta s/s$ with

Table 7.2.2. $\Delta s/s$ and R_{hw} values for frog sarcomeres in relaxed, contracted and rigor states at various S.

CONDITION	S (μm)	$\Delta s/s$		R_{hw}	
		1st peak	2nd peak	1st peak	2nd peak
Relaxed (50 filaments)	2.77	0.006	0.004	115	43
Relaxed (30 filaments)	2.77	0.010	0.009	59	17
Contracted	2.67	0.104	0.103	2.3	0.56
Contracted	2.06	0.140	0.166	2.5	0.56
Rigor	2.06	0.136	0.148	2.2	0.46

confidence. The Δs/s for the relaxed sarcomeres is significantly less than for the contracted or rigor sarcomeres. In the relaxed state the degree of bowing is very low compared to that seen in the contracted and rigor state. From Figs 7.1.1.3 → 7.1.1.5 it is clear that the increase in bowing is greater than the increase in local disorder, so it seems that this change in peak width is likely to be a result of bowing changes in the sarcomere.

Another feature of the results is the differing pattern in the relative widths of the first and second orders. In the relaxed state, the second peak Δs/s is lower than the first. This shows that the type of disorder present in the relaxed state is primarily of the first kind (due for example to thermal motion - see distortion discussion Section 9) resulting in a decrease in height, but not an increase in width. It would be expected that as Δs is constant and s doubles, the ratio Δs/s should halve, and the fact that it does not do so shows that some second type of disorder (which describes the local disorder) is present. By contrast, in the contracted and rigor states, Δs/s for the second orders are the same or greater than for the first order, indicating that there is a greater degree of disorder of the second type, which increases peak width with order number.

7.3. Comparison of EM results to X-ray results.

Table 7.2.1 gives measured spacing values from the four sarcomeres analysed. Since the sample size is so small (one sarcomere in each physiological state) and the sampling errors so uncertain (it is unlikely that the either the (1,0) or (1,1) plane will be sectioned precisely), only trends in spacing will be discussed. X-ray diffraction values for spacing in relaxed frog muscle all give values around 37-43 nm over the range of S of the sarcomeres used in this study

(Matsubara and Elliott (1972), Elliott et al (1963)). This value decreases when the muscle passes into the contracted or rigor state, in skinned fibres, the spacing on contraction is dependent on the tension generated (Brenner and Yu (1985), Matsubara et al (1985) in mice) but at short S falls from ~43-44 nm to ~39 nm at 100% activation. In rigor the value is also ~39 nm (Rome (1968). The electron microscope values for relaxed and contracted sarcomeres at S=2.77 and 2.67 μm are 20-25% lower than this, a figure comparable to the shrinkage seen in rabbit on EM preparation (see Table 5.4.1). The other two sarcomeres show a higher spacing than seen with X-ray diffraction, possibly due to error in the EM tracing caused by confusion between thick and thin filaments at such low S.

The Δd/d was measured from traces in various studies using X-ray diffraction in a manner similar to that described in methods Section 3.1, and the results are shown in Table 7.3.1.

Table 7.3.1 Δd/d values measured from various studies using X-ray diffraction.

AUTHORS	SPECIES + PREPARATION	CONDITION	Δd/d	COMMENTS
Matsubara et al (1975)	Intact frog Sartorius	Relaxed Contracted Rigor	0.118 0.169 0.182	IS of 170 mM and S=2.2 μm
Haselgrove et al (1976)	Frog	No spacing information given but (1,0) FWHM increases from 4.5 mm → 5.5 mm from relaxed to contracted.		
Brenner and Yu (1985)	Skinned rabbit psoas	Relaxed Contracted	0.099 0.111	IS of 170 mM and S=2.3 μm
Podolsky et al (1976)	Intact frog Sartorius	Relaxed Contracted	0.073 0.106	S=2.3 → 2.4 μm
Yu et al (1985)	Intact frog Sartorius	Relaxed Contracted	0.092 0.114	S=2.2 μm

By comparing the values for $\Delta d/d$ with those of $\Delta s/s$ given in Table 7.2.2, it is clear the decrease in sharpness seen in EM on the transition from the relaxed to the contracted state, is also occuring in the $\Delta d/d$ of the (1,0) X-ray reflections. As with rabbit psoas the values of the $\Delta s/s$ from the Fourier transform and the $\Delta d/d$ from X-ray diffraction fall in a similar range, though the $\Delta s/s$ for the relaxed state is much lower in the EM than in the X-ray diffraction. The single example of change in the rigor state also shows the decreased sharpness compared to the relaxed state.

7.4. Summary.

Analysis of EM pictures of frog muscle in various physiological states has shown that the relaxed state has a regular rectangular lattice with a very small degree of local disorder. On activation, the sarcomeres took on a more bowed appearance, and analysis showed the inversion of symmetry in the distortion graphs on changing lattice fit, and an improved RMSD value with truncated conical and elliptical models. This pattern was repeated for sarcomeres in the rigor state. Local distortion of the filaments in the A-bands of these sarcomeres increased compared to the relaxed state, but still did not appear to be as great as that seen in rabbit muscle. Fourier summation analysis of the sarcomeres showed extremely well defined peaks in the relaxed state, and analysis of two orders of the summation confirmed the very low level of second type of disorder. In contracted and rigor muscle, the widths of the peaks increased markedly reflecting the introduction of a degree of bowing, though the mean spacings of the experimental and ideal data varied very little indicating the low level of local disorder appearing in these sarcomeres.

The EM results were confirmed by X-ray analysis of traces from

various studies of contracting muscle, which in every case showed a decrease in sharpness when the muscle went from the relaxed to the contracted state. This decreased sharpness was also seen in the rigor state. It therefore would appear very likely that in the frog at the sarcomere lengths studied, changes in the width of X-ray reflections on contraction are due mainly to the introduction of bowing into the A-band thick filament lattice.

POSSIBLE STRUCTURAL ARTEFACTS ARISING FROM THE PREPARATION AND VIEWING OF STRIATED MUSCLE SAMPLES WITH TRANSMISSION ELECTRON MICROSCOPY.

Section 8.1.

Previous Sections (5,6 and 7) have dealt extensively with a description of the disorder seen with EM. Although the results have been treated on the assumption that changes seen in the micrographs are of a similar nature to those present in solution as sampled by X-ray diffraction, the possibility exists that the effects seen are due to artefacts introduced during preparation of samples for EM. This section deals with the preparative procedure in a critical way, from the viewpoint that the introduction of structural artefacts might lead to the types of disorder described. Each stage of the EM procedure is dealt with in the following sections:-

(a) Fixing and dehydration of the specimen.

(b) Embedding and polymerization of the samples.

(c) Sectioning and beam damage.

To gain some idea of structural changes during the procedure as a whole, the stages in the preparation are discussed with reference to studies where X-ray diffraction analysis and EM preparation have been run in parallel (eg. Reedy et al (1983a), Reedy and Barkas (1974)). Most of these parallel studies have used insect flight muscle (IFM). I have used a similar approach in a brief study of the equatorial spacings in rabbit psoas and have extended the analysis to include preliminary mesurements of reflection sharpness. Figs 8.1 → 8.3 show the effect on d(1,0) spacing and (1,0) sharpness of the various stages

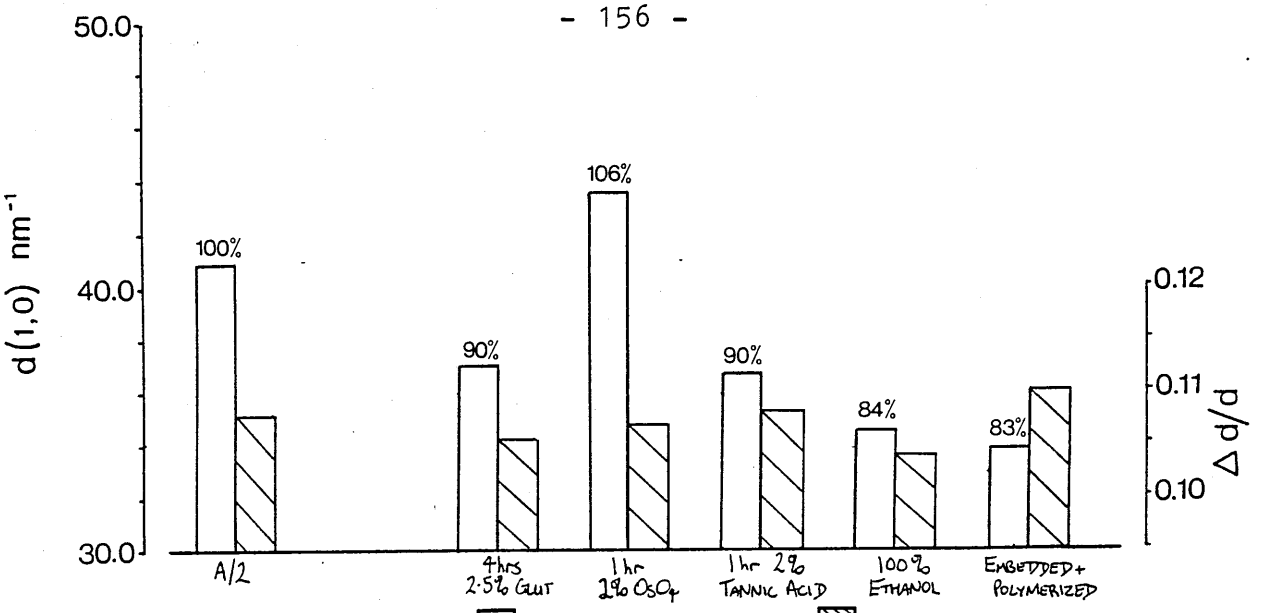

Fig 8.1. Changes in spacing □, and in sharpness ▨, in the rigor specimen.

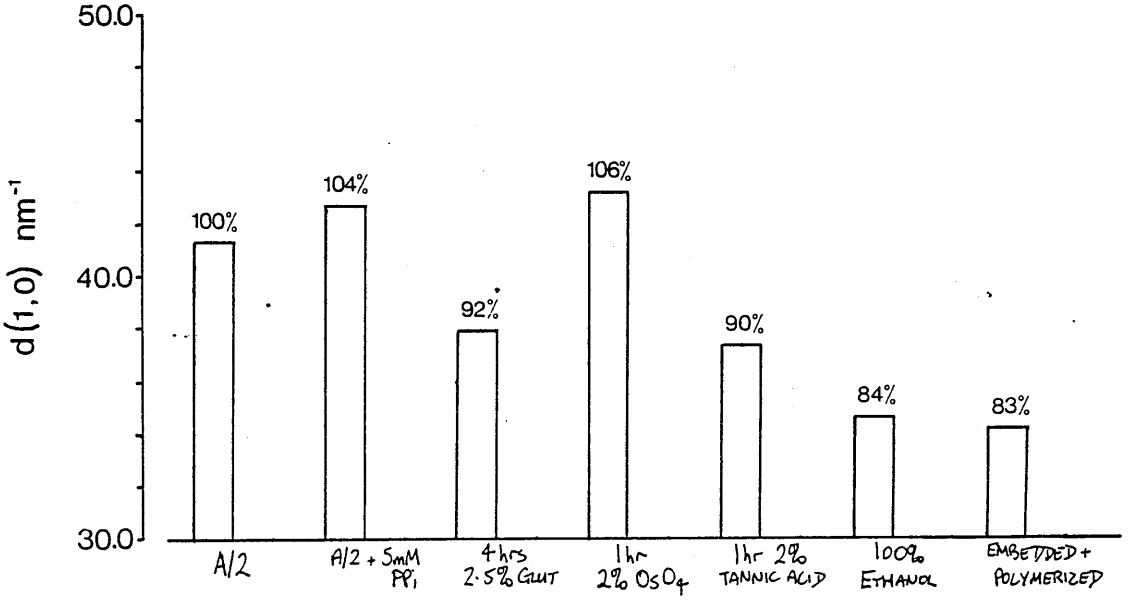

Fig 8.2 Changes in spacing in rigor (A/2) + 5mM PPi specimen.

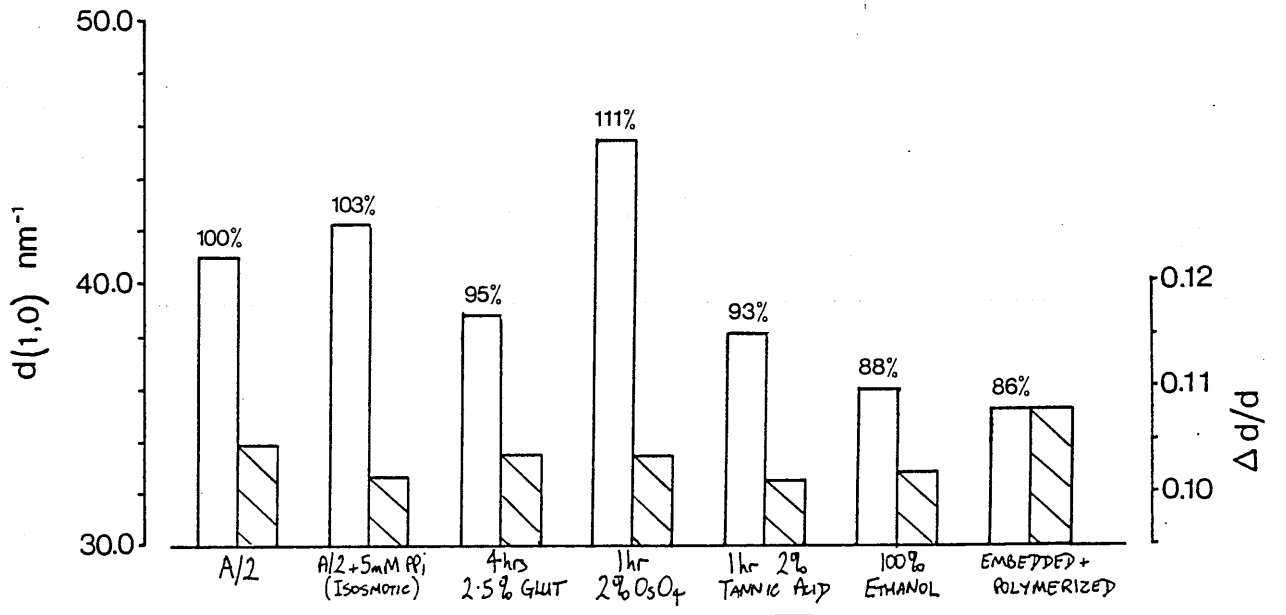

Fig 8.3. Changes in spacing □, and sharpness ▨, in isosmotic PPi specimen.

of EM preparation, starting from the control (A/2) solution, and ending with the polymerized block. A comparison of rigor (A/2), A/2+5mM PPi and isosmotic 5mM PPi solutions are shown. In all samples S≈2.05 → 2.1 μm. The overall shrinkage in the lattice is ~14 → 18%. This is a similar value to the 17 → 20% seen in IFM by Reedy et al (1983a) but somewhat less than the 25% estimated by Eisenberg and Mobley (1975) from single fibre diameter changes in frog. Taking each stage separately:-

(a) 8.2. Fixation and dehydration of the specimen.

(i) 8.2.1. Glutaraldehye fixation.

Primary fixation was performed using a 2.5% glutaraldehyde (GA) solution made up from dilution of a GA stock with experimental solution. Coetzee and Van der Merwe (1985) have shown that this is the optimum concentration for crosslinking bovine serum albumin - any lower and fixation time is prolonged, any higher and changes in osmolarity become a problem (more of this later).

Evidence for a structural disordering effect of GA in muscle is provided by the small tension developed over the course of the fixation. Bergman (1983) demonstrated the generation of a force ~5% that of an isometric tetanus during a 2 hr fixation of muscle in relaxing solution. Walker and Randolf-Schrodt (1969) have shown a 3% decrease in thick filament length and a larger length decrease in the thin filament, though they do assume an initial length of >1.6 μm for thick filaments. This implies that not only are crossbridges becoming firmly attached to thin filaments during fixation, but also that the cross-linking action of GA causes the generation of tension. Tsukita and Yano (1985), using rapidly frozen muscle, have seen cross-bridge

attachment in the relaxed state at similar ionic strength to my solutions, but see no tension prior to fixation by freezing, implying that S1 heads may be in the vicinity or even bound at the ionic strengths used, but no tension is generated. So although S1 heads may be attached in the relaxed state, GA causes the tension to increase.

Further evidence of structural change comes from X-ray spacing changes. Figs 8.1 → 8.3, together with other spacing measurements of fixed psoas muscle show a spacing change from 40.2 ± 0.7 nm to 36.8 ± 0.3 nm, a decrease of 9-10%. This is similar to the 10% seen by Reedy at al (1983a) for rigor IFM, though Eisenberg sees a rather larger decrease in diameter of frog fibres on GA fixation. Structural changes were implicated further by Reedy at al (1983a) who also saw a loss of resolution of layer lines and reflections on the meridian and equator in IFM. However previously Reedy and Barkas (1974) reported that GA is the least disruptive of the primary fixatives since layer lines in relaxed and rigor states were preserved to a good extent.

Given the spacing and reported resolution changes, the question still remains, could GA cause the distortion effects seen? Habeeb and Hiromoto (1968) showed GA reacts predominantly with the ϵ-amino groups of lysine to form intermolecular cross-links, though tyrosine and histidine also showed some reactivity. Addition of GA to protein would therefore be expected to reduce its isoelectric pH (pI) as the $-NH_3^+$ groups react. Tonimatsu et al (1971) observe a rapid initial aggregation of α-chymotrypsin with GA, the rate of which increases with increasing pH. They argue that the pI of α-chymotrypsin is high, so the increased pH lowers the net charge and so reduces the electrostatic repulsion, allowing aggregation. A second rapid rise in aggregation is seen 1 → 3 hrs later, the rate of this decreases with increasing pH. They explain this by a fall in pI, so now the higher

pH increases the net charge on the protein, increasing the electrostatic repulsion, and decreasing the rate of aggregation. This process relies on a pI shift from 8.2 → 4.0 which is produced by reducing the pK_a of lysine by its reaction to GA. This effect was similar to that seen by Coetzee and Van der Merwe (1985) using bovine serum albumin, where increases in the pH slightly increased the time taken to form a gel - here again the pI of the protein is fairly high.

However, Bishop and Richards (1968) found with β-lactoglobin, that although the pK_a of lysine fell from 10 → 8.5, the pI of the protein remains fairly constant at ~5.2 → 5.4. They concluded that although the reaction with lysine groups was complete, the GA-lysine complex was protonated at lower pHs, so that the shift in pI was too small for them to detect with the coarse measurement method they were using.

It therefore seems possible that proteins with a high pI are more affected by GA reacting with the ε-amino group on lysine than are those with a low pI, where the charge on the protein is more determined by $-COO^-$ groups. Thick filaments are composed largly of myosin, which has a low pI (~4.2 → 4.5 see Naylor et al (1985)) and so it would be expected that the thick filament charge due to amino acids is only slightly affected by reaction with GA. However, the thick filament charge is also determined by ion binding, particularly of negative ions (Naylor et al (1985)), and the modification of $-NH_3^+$ groups will certainly affect this. Overall it is likely that the charge on the thick filaments will fall, and this could account for the reduced spacing seen on fixation with GA. Worthy of note is that Reedy et al (1983a) use a technique developed by Reedy (1976) in which carboxyl groups are reacted with carbodiimide and diamine, so adding an $-NH_3^+$ group to what was previously a -COOH group. These new amino groups are then cross-linked with GA. This treatment will remove $-COO^-$

groups and so would be expected to raise the pI of the myosin, so reducing its charge at pH7. It would be interesting to see if the lattice shrank with the modification alone, but it certainly does shrink by a further 7-10% on reaction with GA, probably the result of a change in pI of myosin in the thick filaments.

Possible charge changes become important when considering the ΔpH experiments, and although the shift in pI is likely to be small, it is possible that different rates of reaction may be present in the different samples. Changing buffer is known to alter the reaction rate of GA, though Coetzee and Van der Merwe (1985) have shown that the $-PO_4$ and citrate buffers used in pH7 and pH5 experiments are similarly good vehicles for fixation (I was unable to trace any data concerning borate buffers, which were used for the pH9 experiment). Changing pH does not alter the concentration of GA, since King et al (1974) showed that the free GA available for reaction is constant at a wide range of pHs.

However, a major effect of changing pH will be to change the availability of ϵ-amino groups as the thick filament either increases its charge with increasing pH, or decreases charge with decreasing pH. This change in reactive side chain availability could affect the cross-linking. McLachlan (1984) demonstrates that the sequence of myosin rod is typical of that of an extended coiled-coil structure, ie. a regular repeat of hydrophobic amino acid side chains in positions pointing inwards and charged side chains in positions pointing outwards. In particular he notes the predominance of lysine and arginine in this latter group, so it would appear that ϵ-amino groups are at evenly spaced intervals along the molecule and oriented outwards. These side chains would be expected to be susceptible to changes in the pH of the solution.

Ueno and Harrington (1981) suggest from proteolytic cleavage

studies, that the "short-S2" is weakly associated with the rod backbone, raising pH from 7 to 8.5 is enough to dissociate the S2 and rod. This dissociation would result in the S2 parting from the rod. Extending the argument, at lower pH the rod and S2 would still be bound, but $-NH_3^+$ groups would be more plentiful, so more fixative cross-links could form between S2 and rod, thereby drawing more regions of the S2 into closer proximity with lysine side groups on the rod. These too could become cross-linked, and so the S2 and rod would be "zipped" up by the chemical cross-links resulting in an induced bowing. Bowing introduced in this manner would be a mechanochemical effect as opposed to the spacing change which would be an electrostatic effect.

However if this model were true, then it would be expected that a decrease in bowing would be seen at pH9 since most of the S2 would be dissociated and $-NH_3^+$ groups would be less available. In fact, little difference is seen at high pH (if anything there is a slight increase in bowing). This effect could account for the local disorder changes which have been observed, since at pH5 the S2-rod interaction would be maximized and so once chemical cross-linking starts there would be less scope for local movement of the thick filament as a whole. At pH9, with S2 free from the rod backbone, more movement of the less constrained thick filaments would be possible, allowing for an increased local disorder.

However, this explanation of local disorder fails to account for the differences between local disorder between rigor and PPi experiments where pH and so the expected $-NH_3^+$ group availability is constant. Furthermore, Rasmussen and Albrectsen (1973) have shown that at pH5 the rate of polymerization of GA under storage is slower than at pH7. If this is true of the situation in fixation, then although $-NH_3^+$ groups are more available, the formation of an extended GA

polymer network may be impaired at low pH, which would be expected to reduce the mechanical effect described. My own observation of muscle in fixative solutions is that at pH7 and 9 the specimens appear to have a pale orange tinge, whereas at at pH5 they have a pale yellow appearance, perhaps this a result of a differing degree of polymerization within the tissue.

A further effect to consider is that the ionic strength of the fixative solution is greater than the experimental solution, due to the addition of GA. Even the 2.5% solution used in these studies would be enough to raise the osmolarity of the solutions from ~0.07 to ~0.30 (the ionic concentrations in the solutions will be very similar however, since only a 5-10% diluting effect occurs on addition of GA). Hopwood (1972), in his review, mentions several studies where the osmolarity of the fixative solutions is changed, and notes that hypotonic solutions tend to swell and hypertonic fixative solutions tend to shrink specimens.

Increasing osmotic pressure has been shown to decrease the d(1,0) (eg. Millman et al (1983), Maughan and Godt (1981)), so it is possible that changes in osmolarity could distort the lattice. This effect supposes that the penetration of GA is significantly less than the efflux of water, that is that the GA would encounter a partial osmotic barrier at the surface of the A- or I-band. Chambers at al (1968) and Theissen et al (1970) have studied penetration rates into relatively large blocks of tissue (5-20 mm minimum dimension), and the studies show that the outer edges fix very well (Chambers et al), but that material is free to diffuse out of the centre of the tissue after fixation (Theissen et al). This highlights the need to minimize the distance GA must diffuse through a specimen for even fixation, but offers little information about the rate of diffusion relative to water.

Morel et al (1971) observed distortions induced in red blood cells

at various osmolarities and showed that at very high osmolarities caused by high GA concentrations, the cells showed extreme distortion, but at low GA concentrations and low osmolarity they show little change. The authors conclude that the diffusion of GA into cells is rapid, but not as fast as the efflux of water. Therefore at high GA concentration the water leaves rapidly, and the high GA levels result in rapid fixation of the distorted cell. Note that in the red blood cell, the cell membrane is probably very important in determining cell volume and so cell shape, consequently the system is highly sensitive to osmotic change. The muscle samples used had a minimum dimension of 0.5 → 1mm and no plasma membrane, so it is likely that GA rapidly diffuses throughout the sample resulting in an even fixation. This is supported by the observation that the bowing effects seen are consistent at the edges as well as at the centre of the specimens examined.

(ii) 8.1.2. The effects of OsO_4, Uranyl acetate, tannic acid and dehydration.

After rinsing in the experimental solution, secondary fixation was carried out using a 1:1 mixture of 4% aqueous OsO_4 and s-collidine, this gives a 2% OsO_4 solution at pH ~7.2 → 7.4. Some samples were treated at 4°C since Maupin-Szamier and Pollard (1979) found that actin filaments were preserved better at these low tempertures. No difference was seen between these samples and those fixed at room temperature. The presence of tropomyosin is suggested by these authors to stabilize the actin filaments in skeletal muscle.

Evidence for futher disruption of the filament structure comes from both X-ray and EM. Figs 8.1 → 8.3 show that the d(1,0) increases with OsO_4 to a value 5-11% higher than the initial value. Eisenberg at

al (1975) show that the diameter of the filaments also increases with OsO_4. The action of OsO_4 with proteins is at present unclear, but the increased spacing and diameter are possibly the result of a charge increase on the filaments when they bind OsO_4. Behrman (1985) has reviewed the reaction of OsO_4 and has suggested that it can react with a number of amino acids. The reaction with tryptophan involves the osmate ion, so raising the possibility of a charge change at this site. Alternatively, Dr A.Glauert (personal communication) has suggested that reaction with the cross-linked GA, or possible changes in protein conformation, could cause the effects seen.

Further X-ray evidence for disordering with OsO_4 is provided by Reedy and Barkas (1974) who note that layer lines preserved in GA fixation disappear on treatment with OsO_4. Comparison of EM pictures of samples fixed in both GA only and GA followed by OsO_4 show that OsO_4 causes a shortening of the thick filaments by 12 → 15% in rat (Walker and Randolph-Schrodt (1969)) and slightly less in frog (6 → 8% Page and Huxley (1963)). The shortening effect of OsO_4 is a likely source of the 6 → 8% decrease in spacing of the 14.4 nm reflection between X-ray pictures of muscle in solution and those of embedded material (see Section 5.4, Table 5.4.3). This shortening effect is likely to be due to the chemical reaction of OsO_4 with proteins in the thick filaments to form cross-links. Page and Huxley (1963) also showed that S is constant with OsO_4 when the muscle is restrained, whereas the filament length change still occurs. This brings in the possibility that internal rearrangement of filaments could "take up the slack" and so result in the disappearance of layer lines seen by Reedy.

Bergman (1983) has shown that in frog, OsO_4 fixation in the relaxed state results in the A-bands, as viewed in longitudinal section, having rectangular lattices; any reordering is not apparent as a change in bowing. This does not exclude the possibility that in the

rigor state the bowing is the result of a shortening of the filaments, which are constrained by actomyosin cross-bridges, in combination with the swelling seen. However Walker and Randolph-Schrodt (1969) also used $KMnO_4$ as fixative and reported a very large decrease in thick and thin filament lengths of ~30 → 35%, yet little change in bowing is seen in the pictures they present of these sections. Furthermore, Reedy et al (1983b) comment that the structure they see after image reconstruction in IFM using no OsO_4 or other heavy metal stains is the same as that seen with OsO_4 treatment, indicating that at least at the fine structure level, OsO_4 has no effect on the result.

Uranyl acetate (UAc) was used as en bloc stain, and was found to increase greatly the the intensity of the equatorial peaks, but to decrease the d(1,0) spacing (result not shown) to a value similar to that seen after GA fixation. Eisenberg and Mobley (1975) also saw a decrease to the level seen with GA in the diameter of the muscle fibres. Lee et al (1979) have shown that not only does UAc have a staining action, it also protects unfixed smooth muscle cells from drastic volume changes under scanning electron microscopy, so some fixative properties are also probable. Boyde and Boyde (1980) suggest this may be due to the strong charge on the acetate being involved in stabilizing the structure. It is unclear, however, whether the lattice shrinkage seen is a charge or mechanochemical effect.

Treatment with tannic acid (TA) had little effect on spacing. When this treatment was omitted, subsequent lead staining had a much reduced effect, illustrating well the mordant property of TA. (A mordant is a compound that acts as a bridge between a stain and the structure to be visualised). The powder used as the TA is a mixture of several compounds, which have been shown to be the gallic acid monomer,dimer and trimer. In low concentration aqueous solution, the dimer has been shown to be the dominant form (Haslam (1966)). The

varied side groups of the dimer enable the reaction with arginine and lysine side groups, and also the formation of hydrogen bonds with -CO-NH- bonds in the peptide chains of proteins, so it is possible that TA has a cross-linking effect between side groups. In this study it was used primarily as a mordant for lead stain, and its fixative properties appear to have little effect.

Dehyration has been shown to cause considerable shrinkage in muscle fibres. Page and Huxley (1963) showed a 9% decrease in fibre length on dehydration. Lee et al (1979) and Boyde and Boyde (1980) show that the effect of dehydration is minimised by starting the procedure in a 70% alcohol solution. Figs 8.1 → 8.3 show the effect of dehydration on the d(1,0) spacing starting in a 30% and ending in a 100% alcohol solution, and show a small decrease (a further 4-6% shrinkage). This compares well with IFM (Reedy et al (1983a) which show a 3-5% decrease on dehydration. This small change in spacing also correlates with the results of Eisenberg and Mobley (1975) who saw a small decrease in fibre diameter on dehydration. Reedy et al (1983a) note that there is a small increase in contrast in X-ray pictures in the dehydrated state as compared to those from the same fibres after fixation, and in an earlier paper (Reedy (1976)) notes that layer line detail is preserved by a gradual dehydrating procedure. These results would indicate that the disordering effect of dehydration is slight.

(b) 8.3. Embedding and polymerization.

Figs 8.1 → 8.3 also show the change in d(1,0) when the samples are embedded and polymerized in resin. The d(1,0) spacing shows a 1-2% decrease, which is somewhat less than the diameter of frog fibres seen by Eisenberg and Mobley (1975) who reported a 9-10% decrease

with embedding, and a slight increase in diameter on polymerization, leading to a 5-6% decrease in diameter over the whole embedding/polymerization step.

Reedy et al (1983a) observed a very small (0-2%) increase in spacing on embedding. In all three cases the spacing change is small. However, Reedy (1976), using a heavy metal free fixation and slow deydration, managed to preserve layer line reflections in parallel X-ray/EM studies on the same fibres. On embedding, these reflections are much weakened or abolished completely, indicating that a disordering effect has occured. It is possible that this disordering arises from the inhomogeneous or incomplete polymerization of the resin; however with thorough infiltration and patient polymerization this should not be a problem. My own samples were infiltrated for at least 24 hrs, and polymerized at 40°C for 1 day, 60-70°C for another day (different resins required different polymeriation temperatures) and were finally left to cure at 30-40°C for 1 day. Even with this procedure it was noted that the volume of the blocks decreased. The shrinkage appeared to be restricted to the depth of the block in the EM mould, since the fixed block was not loose when removed. This indicates the small change in resin volume could be due to evaporation of the more volatile components of the resin, an idea supported by the observation that (a) the effect was minimized by the initial low temperature treatment, and (b) there is little change in equatorial thick filament spacing on polymerization. Such a change would tend to concentrate the less volatile resin constituents, and so would not be expected to cause a bowing type distortion, though local changes in viscosity or polmerization rate could produce local disorder. The possibility of changes in volume as an effect of chemical changes in the resin cannot be dismissed, and these too will have a disordering effect.

Further disordering may occur due to the interaction of the resin chemicals with side groups of proteins. Causton (1985) suggests that the cyclohexene dioxide in Spurr resin reacts with -OH side groups, so potentially serine, threonine and tyrosine residues can be cross-linked. Other reactions with the anhydride in resin involve modification of side groups. It is unlikely that at this stage either of these reactions have much effect as seen by the small change in d(1,0) spacing. A potentially greater effect is from the physico-chemical interaction between the polymer chains of GA associated with the thick filament, and the polymer chains of the resin. These two polymers will be separate but intertwined, raising the possibility of distortion on polymerization. Again this would be unlikely to introduce a bowing disorder, but might produce a local disorder.

Both shrinkage and polymer chain disorders would be expected to be of the local type, and each specimen might be expected to be subject to these disorders irrespective of prior treatment, so similar levels of local disorder could be expected as a result. The differences in local disorder with PPi tend not to support the local disorder artefact, though the possibility exists that changes in local disorder with increased S may be slightly enhanced by embedding and polymerization.

(c) 8.4. Sectioning and Electron Beam Damage.

In most specimens, a diamond knife was used to cut sections, this eliminated many of the routine artefacts often encountered eg. chatter,uneven sections, though in practice, no difference between these sections and those cut with a glass knife was found. However, the problem of compression of sections still remained. This was overcome to a large extent by using chloroform vapour to relax the

sections once cut, though mechanical differences in the sections at the sarcomere level caused by the different protein assemblies in the A- and I- band, crossbridge attachment and uptake of fixative etc may cause differences in the compression/relaxation, leading to a bowing type distortion. However, the constant bowing for any given treatment, together with the differences in bowing between treatments, would point to this not being the case.

A more likely source of artefact would be if the fibre axis were not parallel to the edge of the knife, the result of this would be to introduce a bowed appearance into the sections of a perfectly cylindrical sarcomere. This effect was evident when aligning blocks to the knife, and frequent adjustments to the angle the knife edge made to the axis of the fibre were neccesary to achieve 15-20 sarcomeres in the same fibre all of equal width, which was the criterion used to minimize this angle.

It was assumed that once the sections were on grids, subsequent staining with heavy metals had no disordering effects on the sarcomere, and that storage in EM grid boxes also caused no structural changes. With these assumptions, the final source of artefact is the extreme conditions imposed on the sections in the electron microscope. Stenn and Bahr (1970) have reviewed the effects of electron beam damage in vacuum of EM specimens.

The high vacuum in EM causes any water bound to the specimen to be removed, this probably has no effect in these studies since there will be low levels of hydration anyway. Of more importance are the effects of the electron beam, even at low intensities and low magnification the electron beam delivers an energy of $\sim 10^3$ J g^{-1} s^{-1} to the specimen. Stenn identified four sources of damage:-

(i) Contamination.

(ii) Charge effects.

(iii) Ionizing radiation.

(iv) Heat effects.

The contamination effect will be small over the time taken to choose a sarcomere and photgraph it, this small effect might be relevant in some studies, but here no structural change is likely, so the discussion will concentrate on the other three.

(i) 8.4.1. The ionization and charge effects.

Damage to the specimen will result from the inelastic collisions of incident electrons with those of the specimen. This results in the absorption of energy by the specimen, an increase in the intensity of the beam results in more inelastic collisions and more damage, as does low voltage/high current operating conditions. Consequently high voltage/low current operation with the intensity kept to a minimum, was used. The damage involves the formation of ions, free radicals or the emission of secondary X-rays. C–H bonds are very susceptable to damage since they do not reform, whereas C-C bonds are damaged but reform rapidly, so it is possible that ionization could result in local rearrangement of polymer chains within the specimen, giving rise to a local distortion due to C–C bonds breaking and reforming. Such interactions between broken chains and nearby side groups is the basis of beam fixation, though it is unlikely that this or the mass loss of the species formed by ionization is significant on the time scale used in these experiments.

The charge effect is another consequence of ionization. Interaction of high energy electrons with the specimen will produce

charged species which can cause electric fields of 10^{-1} V nm^{-1}. Although C–C bonds are stable under these conditions, the effect may enhance the ionization effects previosly described. Other bonds may not be so stable, so possibly these too could be involved in cross-linking.

The ionization effect, and so the charge effect, will increase as the specimen thickness increases since the path length the electrons traverse is greater, so the thinner the sections used, the more this effect is reduced.

(ii) 8.4.2. Heat effect.

In the present study, bearing in mind the time of exposure, magnification and intensity used, the heating effect of the electron beam is most likely to distort the sections to a significant degree. In sections where the intensity of the beam was accidentally raised too high, the sections showed a rapid shrinkage resulting in a gross distortion of the area of grid under examination. Important in reducing this is the minimization of temperature gradients through the section. The temperature reached by the specimen during routine operation is probably <60°C, and increasing heat conduction away from the section will cause this temperature to be lower. By increasing the area of the section in contact with the grid, a high heat transfer is achieved. The sections cut in this study were picked up on G400 grids of Cu/Pd which has a higher thermal conductivity than Cu alone, so this too should help reduce the temperature. Reducing the diameter of the beam also reduced the heating effect. This could be achieved by using a small objective aperture which had the disadvantage of slightly reducing image contrast. Using minimum intensity for all operations (eg focussing and photography) also minimized the temperature rise in

specimen.

The area of the grid under examination was illuminated at low magnification/low intensity prior to higher magnification as routine. Whether this actually completed polymerization of the resin, or served to bring that part of the grid to a thermal equilibrium is unclear, but the practical result was to remove the "drift" in the specimen at higher magnification and to preserve the low magnification image. The heating effect should be much reduced by using carbon coated grids, and if distortions were being introduced by this effect, it would be predicted that they would be reduced with carbon coated grids. A few earlier experiments were tried using such grids and no effect on bowing was seen between these and uncoated grids, indicating that the heating effect was not important. This was supported by meridional spacing measurements of embedded X-ray specimens prior to sectioning and OD measurement of analagous reflections after EM examination, which showed no shrinkage.

8.5. Resumé.

The results from my own X-ray work together with that of others has shown that the preparation of samples for EM causes a weakening of reflections and a weakening or disappearance of layer lines in meridional patterns. By following the changes in the reflections the degree of disordering has been followed (eg Reedy and Barkas (1974), Reedy (1976), Reedy et al (1983a)) and these have shown that the changes are greatest at the OsO_4 and embedding stages. In all the steps discussed, comparison between samples and different preparative techniques have shown that it is unlikely that the artefact causing the X-ray effects is the introduction of bowing. To gain some insight as to the nature of this disordering, a sharpness analysis on the (1,0)

equatorial reflections of pictures used in Figs 8.1 → 8.3 was performed. The results of this analysis are presented next and correlated to previous data, the artefact discussion and a discussion of EM results from rapid freeze fixation experiments from striated muscle.

8.6. Assessment of the degree of structural preservation with EM preparation.

The previous sections have discussed extensively the possible introduction of structural artefact to produce the results seen. In this section I will assess the degree to which the structure seen with EM resembles that in the filament under conditions used for X-ray diffraction.

Figs 8.1 and 8.3 show the sharpness ($\Delta d/d$) for the (1,0) reflection at various stages during the EM preparation. These pictures were taken using GX13 rotating anode, and show higher values for sharpness, like those noted earlier in the pH results (section 4.2.2). Given the limitations of the sharpness data from the GX13, small changes in sharpness will not be detected. The results show that the peak sharpness remains fairly constant throughout the preparation for EM. The simplest interpretation of this is that the degree of disorder within the specimen remains constant, though there is a possibility that the contribution from different sources of disorder change, and that the sum of these remains constant (see Section 9).

Perhaps a small decrease in sharpness occurs on embedding and polymerization; this is in agreement with Reedy and Barkas (1974) and Reedy (1976) where layer line resolution preserved through the previous processing is much reduced. Reedy and Barkas (1974) note that OsO_4 post-fixation also reduces layer line clarity, but it would appear that although it increases d(1,0) dramatically and shortens

thick filament length by 6-8%, it has little effect on filamentary lateral disorder. Another potential measurement of disorder is provided by the degree of continuous scatter round the backstop of X-ray pictures (Poulsen and Lowy (1983). However in the EM preparation series it would be extremly difficult to use this as a measure of disorder since as the sample is prepared, more mass is added by way of fixatives,stains etc, so the scatter seen in the X-ray pictures is probably due to this, and any filamentary disorder will have a comparatively minor effect.

Reedy et al (1983a) show pictures using a heavy metal free preparative method. The X-ray pictures they present have a constant continuous scatter up to the point of embedding, whereupon there is a slight increase. In this case this may be indicating an increased disorder. Since it is thought this scatter comes from the S1 heads, and in the rigor state these will be highly ordered round the thin filament, so an increased scatter would imply a disordering of the thin filament, which may or may not reflect changes in the thick filament order. As noted earlier, changes in the order between filaments on embedding are likely to be in the random disorder and not in bowing. The simplest explanation of the X-ray data is that preparation of specimens for EM causes a slight increase in the degree of disorder in the specimen at the point of embedding/polymerization, even though the changes in lattice spacing are extreme.

A direct check of this interpretation can be made by comparing the EM pictures from conventionally prepared specimens with those prepared by rapid freezing fixation. This latter technique involves rapidly cooling a specimen at $\sim 10^6$ °C s^{-1} to bring about the formation of water ice in its amorphous state. The result of this is to eliminate the use of chemical fixatives and, if the freezing is rapid enough, to preserve the structure unchanged. By using cryomicrotomy and

cryoelectronmicroscopy, the freeze fixed section can be studied unstained at the magnifications provided by EM. Dudochet and McDowall (1984) and McDowall et al (1984) have provided such pictures of glycerinated IFM in the rigor state, and the sarcomeres shown exhibit bowing. These compare well to pictures of IFM prepared by conventional techniques (eg Reedy (1968)) which also show a bowing in rigor sarcomeres.

8.7. Summary.

The conclusion of this section is that conventional EM does not introduce major changes to the degree of disorder in striated muscle. It does, however, cause a large decrease in the equatorial spacing and a smaller shrinkage of the meridional spacings. The former can be attributed to changes either in electrostatic or mechanochemical effects between filaments, and the latter is probably due to the effect of OsO_4. Although the meridional spacings seen with EM decrease, the trends in filament spacing seen with EM (Brandt et al (1967)) and X-ray (Elliott et al (1963)) are similar in frog. Both show a decreased spacing with increased S, a result confirmed in rabbit in this study (see Section 5.4 Table 5.4.1). It is a surprising observation that even with these extreme changes in spacing, the equatorial (1,0) reflection sharpness shows little fluctuation. The preservation of the in vitro disorder is confirmed by cryo-EM which shows bowing in both conventionally prepared and in rapidly frozen thin sections.

THE EFFECTS OF THE DISTORTION SEEN IN THE ELECTRON MICROGRAPHS ON THE X-RAY DIFFRACTION PICTURES - LINKING THEORY WITH PRACTICE.

Section 9.1.

This section will introduce the theoretical types of distortion found in imperfect crystal structures. These will be discussed with reference to the thick filament arrangement in the specimens studied. The objective is to extend the correlation between the detailed EM observations of distortion from the ideal lattice and X-ray diffraction pictures and to arrive at a more complete understanding of thick filament disorder in the rabbit psoas A-band. To this end, this discussion will use a more theoretical approach, backed up by the EM results, to account for the X-ray pictures observed. The theory used in this section has been laid out fully in both Vainshtein (1966) and Guinier (1963).

Imperfections in crystal lattices occur when the scattering centres within that lattice are perturbed from their ideal or perfect periodicities. These perturbations may be divided into two types called:-

(a) Disorder of the first type. Here the long-range order between atoms or molecules is preserved. A more complete description of this is given later.

(b) Disorder of the second type. This is characterised by short-range order, the structures here having no long range order. This second type is often called liquid type disorder.

To illustrate this more clearly, Fig 9.1 shows a series of schematic 2D A-band lattices based on the perfect hexagonal lattice shown in Fig 9.1.1. Fig 9.1.2. shows the effect described by the first

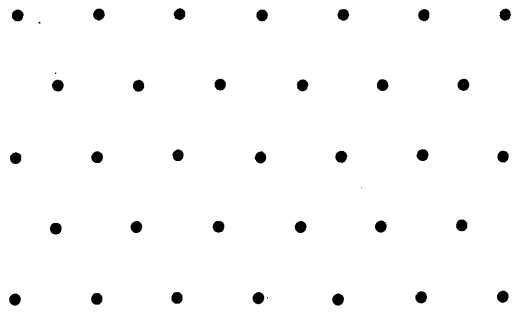

Fig 9.1.1 Cross section of filaments in an ideal lattice - all filaments are equally spaced.

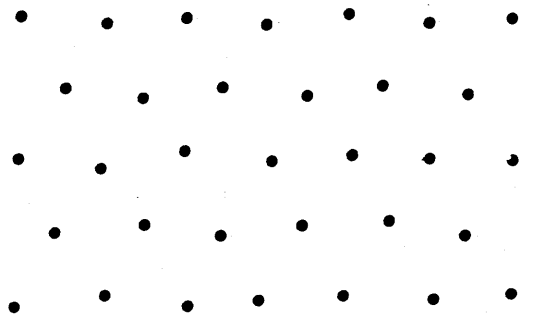

Fig 9.1.2 Lattice in Fig a showing distortion of the first kind - the filaments vary randomly from their equilibrium positions.

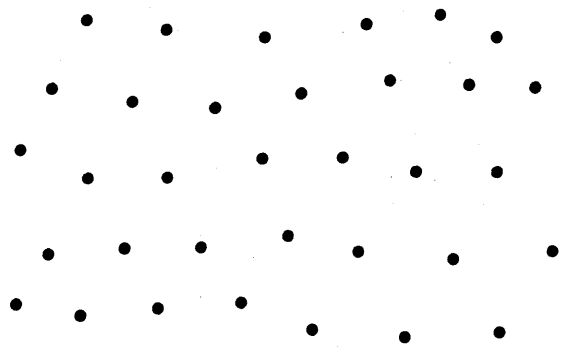

Fig 9.1.3 Lattice in Fig a showing distortion of the second kind - the spacing between neighbours varies, and there is no equilibrium position.

type of disorder. Here the position of the scattering centres (in this case thick filaments) are perturbed randomly (but not necessarily) by a small amount. The result is that the mean positions of the filaments remain unchanged, but the actual position of each filament is subject to a (small) displacement. This system therefore preserves long range order. In crystal lattices this effect is typical of disorder introduced by thermal agitation, or by substitution of one atom for another. In the A-band lattice, this type of disorder produces the small random variations in thick filament curve seen, for example, in Figs 6.2.3.1 → 6.2.3.3 (best seen by tilting the pictures away from you and viewing along the filaments at a highly oblique angle). This type of disorder affects the integrated intensity of the peak only, the shape of the peak remains the same for all reflections. As the intensity falls, the height of the peak also decreases, and in a lattice such as the A-band, the intensity lost from the reflection maxima goes to the minima, so that at high scattering angles the refections merge into the background.

Fig 9.1.3 shows the effect of the second type of disorder - the scattering centres in this case are spaced only to approximately the same distance, and as the distance from any given filament is increased, the degree of perturbation from the ideal situation of equal spacings is also increased. In this case there is no average lattice position, so any averaging of spacing is a measure of the separation of immediate neighbours, and this second type of disorder is concerned solely with short range order. The effect on X-ray reflections of this second type of disorder is to increase the width of the peaks in successive orders, and so changes in the degree of this disorder are a likely source of the sharpness change effects seen in X-ray pictures with S, PPi and pH.

To complete the theory, the idea of the statistical lattice is

included. Whereas the EM pictures capture a 2D section of a single sarcomere, in which each point on the thick filament can be assigned an X/Y coordinate, the result of the X-ray experiments show the reflection from a statistical lattice.

In the first type of disorder, there are the mean positions of the filaments from which the actual positions of the thick filaments vary, so any single filament will, in theory, be in an equilibrium about a given position, so the spacing between nearest neighbours will be constantly varying. This variation of distances between nearest neighbours, taken over the lattice as a whole, means there will be a range of spacings. There will therefore be a probability of any two atoms being separated by a given amount, and so the whole range of spacings can be described by a probability function, which in this case is Gaussian. As a result of this distribution, there will be a mean spacing (which corresponds to the fixed position about which the filaments are in equilibrium) and a root mean square distortion from that position. At any given time, the distribution of spacings will be constant, assuming that the number of filaments is very large (which in practice it is).

With the second type of disorder, the statistical lattice sampled by the lattice is now an average value of the spacing between immediately neighbouring filaments in the section, and no equilibrium position for the filament exists, so at any given time the range of spacings will again be constant for a large number of filaments. Note that for a small filament sample, the differences between the two types of disorder become less clear.

Since in both cases some sort of spatial averaging (a) is possible, and in each case some measure of the mean deviation (Δ) from this position can be made, a figure for Δ/a or the ratio of perturbation to the spacing can be derived. I shall return to this

later.

9.2. Bowing as a disorder.

Of the two types of disorder considered so far, the second type will increase the widths of the peaks. Vainshtein and Guinier have both shown that the width of the peak is proportional to both $(\Delta/a)^2$ and to the square of the order, $(n)^2$. If the bowing were of this type it would be predicted that the relative widths of the peaks would increase according to column 4 of Table 9.2.1.

Table 9.2.1. Relative peak widths (W_{rel}) from the first four orders of the Fourier summations of ideal truncated conical and elliptical lattices used to generate distortion graphs of rigor half-sarcomeres at S=2.1 μm.

ORDER	W_{rel} CONICAL	W_{rel} ELLIPTICAL	PREDICTED
1	1.00	1.00	1.00
2	1.98	2.00	4.00
3	2.93	3.00	9.00
4	3.89	4.00	16.00

Columns 2 and 3 are width measurements taken from Figs 5.3.5 and 5.3.6 and show the increase is proportional to the order number, not its' square. This shows the bowing seen is not a distortion of the second kind. The result highlights the different sources of the disorder, the type two disorder arises from the statistical fluctuation of nearest neighbour distance. The bowing disorder also arises from the variation in spacing, but in a predictable manner in which spacing decreases towards the A/I junction, from this it is expected that the change in peak width is proportional to the change in spacings over

the length of the filaments.

Figs 5.3.5 and 5.3.6 also show differences in the profile of the peak. As would be expected, the truncated conical lattice has a uniform distribution of spacing along the filament and so gives rise to a rectangular profile, whereas the truncated elliptical lattice in which the filament separation decreases more rapidly toards the tip has an asymmetric distribution, with a higher peak at shorter distance in reciprocal space, corresponding to the more uniform filament spacing nearer the M-line. This different distribution will affect the sharpness, since the half-width will be altered. As the disorder due to bowing depends so much on the shape of the filament lattice, it is perhaps more appropriate to call this type of disorder a geometric disorder.

From this analysis, it appears that the type two disorder and the geometric disorder both contribute to increased width of the peaks. Though the type two disorder is proportional to the $(\Delta/a)^2$, both the A-band shape and degree of filament bowing contribute to the geometric disorder.

9.3. Comparison of theory with practice.

Consider the situation at short and long S. At short S (eg Fig 5.2.4.1, control rigor solution at S=2.1 μm), the two sources of disorder which cause the changes seen in the widths of the peaks can be described.

(i) A variation in spacing similar to the situation as shown in Fig 9.1.3. Spacing distributions of this type are characteristic of the type two disorder, and correspond to the local disorder seen with EM.

(ii) The second source is a consequence of bowing, and is not so much caused by filament disorder as by filamentary distortion. The more distal ends of the filaments show a change in spacing in which

the filaments at the edges of the sarcomere are more closely spaced than those in the centre. An examination of Fig 5.2.4.1(ii) shows this change in spacing is related to distance from the centre of the sarcomere. Fig 5.2.9.1 confirms this: at the M-line there is a small fluctuation in filament position, whereas at the A/I junction the perturbation is larger, and clearly the distortion arises from a series of changes in the spacings between neighbouring filaments. This is the geometric disorder.

At the longer S (eg Fig 5.2.4.3), the bowing effect is not present, however now the variation in spacing at any given level is much greater ie the effect described by Fig 9.1.3 is increased. This corresponds to the increase in local disorder seen under EM. So changes in local disorder correspond to changes in type two disorder, whilst changes in bowing change the geometric disorder. The geometric disorder will be predominant at lower S, and the type two disorder at longer S (see Figs 5.2.4.1 and 5.2.4.3). The width due to the geometric disorder is determined by the regular decrease in spacing along the filament length. Halving the degree of bowing from ~8% in rigor at S=2.1 μm to ~4% in 5mM PPi reduces the $\Delta d/d$ of the (1,0) peak from ~0.065 to ~0.055. From Fig 4.2.3, increasing the bowing at S=2.6 μm from ~7% to ~11% increases the $\Delta d/d$ by 0.01→0.02 (though in this case there was also a decrease in local disorder). The type two disorder will increase the (1,0) peak width in proportion to $(\Delta/a)^2$, so a smaller degree of disorder will have a larger effect. The increase in the disorder may account for the rapid rise in peak width seen with S (see Figs 3.3.4 and 3.3.5). The two types of disorder can be separated to some extent by considering changes in another consequence of type two disorder, namely interaction radius, which changes with Δ/a (the statistical filament separation) and so would not be expected to change with geometric disorder.

As introduced in Section 9.1, the filament lattice will be statistically constant, although individual filaments may be subject to changes in position. Consider a filament within an extended lattice exhibiting a high degree of the second type of disorder; the probability that its nearest neighbours lie on or near a certain radius given by the mean spacing of the filaments is fairly high, even for a heavily distorted lattice. However, the probability that the second nearest neighbours lie on or near a radius twice that of the mean filament spacing is less, due to the variation in spacing between first and second neighbours which is the inherent property of this type of disorder. This decrease in probability of finding a filament at a given radius continues until there comes a point beyond which this probability becomes constant, this point prescibes a radius round the chosen filament within which is the short range region of order that characterises the second type of disorder. This radius is called the interaction radius (x_m).

The X-ray reflections from such a spacing distribution show a point where the half maximum intensity of one reflection (order m) is at a distance ma+a/2 from the origin and so overlaps with the intensity from the next reflection, the sum of these is then almost constant. An estimate of x_m can be found from the X-ray diffraction picture by finding the point where the intensity from adjacent reflections becomes constant. If a is known then an estimate of Δ/a can be found using eqn 82 in Vainshtein chapter V:

$$M = \frac{1}{(2.5\Delta/a)} \qquad \text{and } x_m = Ma$$

where M is the highest order expected to be resolved. Examining the equatorial reflections from specimens at short and long S in control and PPi solutions (Figs 9.2.1 → 9.2.4), then at S=2.32 μm although in

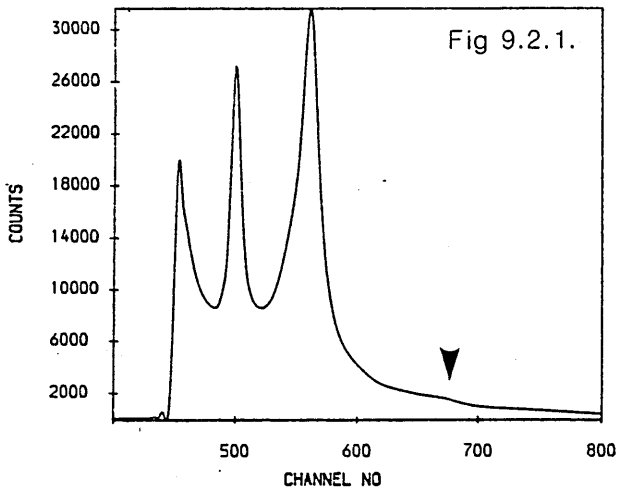

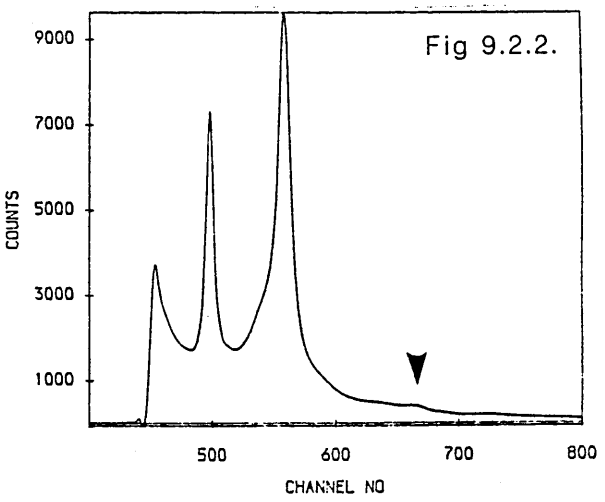

Figs 9.2.1. and 9.2.2. Equatorial reflections from rabbit psoas at S=2.32 μm. Fig 9.2.1 is in rigor solution, and 9.2.2 in 5mM PPi solution. There is a small spacing shift from the one to the other (the PPi has the lesser spacing in the graphs), but more noticable is the change in sharpness of the reflections. Note also that the (2,1) reflection (arrowed) becomes clearer. This indicates the interaction radius has increased. (See text for details).

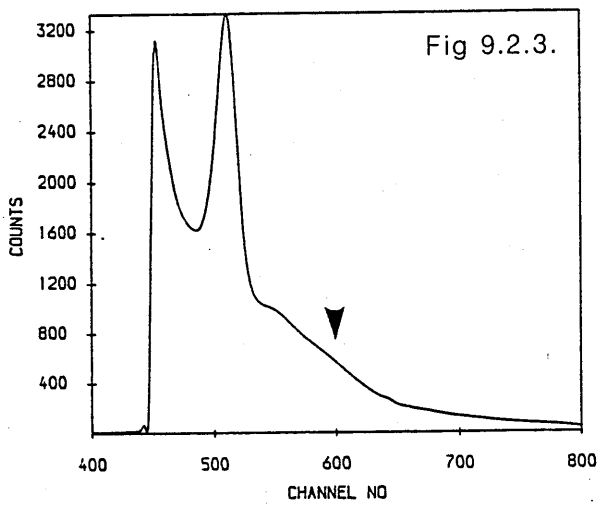

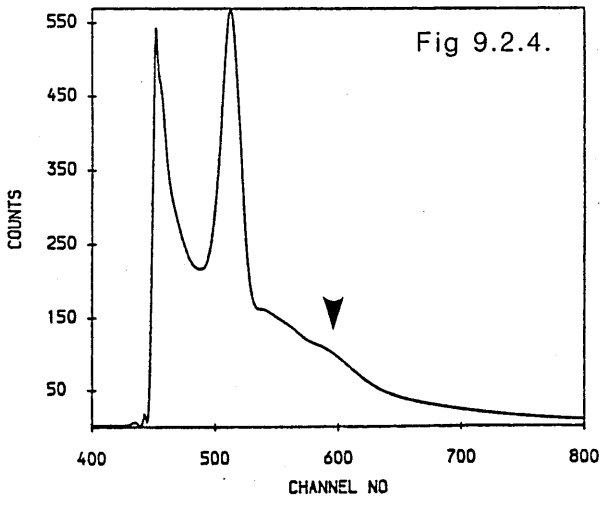

Figs 9.2.3. and 9.2.4. Equatorial reflections from rabbit psoas at S=3.25 μm. Fig 9.2.3 is in rigor solution, and Fig 9.2.4 in a 5mM PPi solution. Note the spacing has decreased and the reflections have broadened considerably. A slight sharpening effect is still seen in the (1,0) reflection, but the (2,0) reflection (arrowed) becomes more clearly defined. This again indicates an increase in the interaction radius.

rigor the (2,1) reflection is just visible, in PPi it is more clearly resolved, this gives M=2 or 3. Assuming an average d(1,0) spacing of ~40 nm this gives an x_m of ~100-150 nm and a Δ/a of between 0.23 and 0.28. Table 5.4.1 column 6 in section 5.4 of the EM results gives mean ± SD of measured spacings of thick filaments. The sd/mean value at short S of the EM measured spacings is 0.23 → 0.26 and at longer S 0.28 → 0.36. The values at short S correlate reasonably well with the Δ/a estimate from X-ray diffraction.

The EM values are taken at the M-line, and not over the whole half-sarcomere, so although they will not include distortion due to the bowing, the possible restraining action of the M-line will lead to an underestimate. Also the differences in sampling between EM and X-ray diffraction suggest that the comparison of these numbers be treated as a first approximation only. At longer S, although the X-ray diffraction reflections are less well defined in the (1,1) region of the pattern, slight humps corresponding to the positions of the (2,0) reflections can be made out indicating the x_m is ~80 nm or just under. This would tend to support higher values of Δ/a, though not as high as 0.36 (this implies an x_m of ~50 nm). These observations support the idea that EM processing enhances the local disorder, since the EM results give higher disorder values than do X-ray measurements. However this must be viewed with caution since sampling errors may also be a factor here.

9.4. Summary.

The width of reflection is dependent on the degree of the second type of disorder as measured by Δ/a, which is represented by local disorder, and the geometric disorder which is determined by both shape and degree of bowing. In the A-band, changes in either of

these types of disorder will alter peak width. The changes seen in the EM pictures can be correlated with different degrees of the disorders between the samples used in the X-ray experiments, and it remains to discuss the mechanisms and forces giving rise to these filamentary distortions and disorders.

SECTION 10. DISCUSSION.

In the introduction (Section 1), the radial forces acting on thick filaments in the A-band lattice were reviewed, and the concept of the balance of forces was introduced. This balance of forces dictates that the filaments will occupy a position at the point where the resultant force on the filament is zero. In the simplest case, where the forces on the filaments are assumed to be the same along their whole length, then changes in the individual attractive and repulsive forces will result in changes in spacing.

If the forces along the length of the filament are not constant, then the equilibrium positions of successive points along the filaments differs giving rise to bending couples and resulting in the bowing effect seen. More localised differences in the balance of forces of the A-band filaments would result in local distortions. This discussion will examine the relative contributions of the various forces involved in the balance, and will work towards an explanation of the effects seen.

10.1. An appraisal of the repulsive force between filaments.

In the introduction, repulsive forces between the filaments were described as being either electrostatic or the result of compressive resistance of myofilament components. Umazume et al (1986) have measured the radial stiffness of relaxed frog fibres using high molecular weight polymers and have shown that at a myosin/myosin filament separation (referred to as "spacing" from hereon) of ~40 nm there is a sharp increase in radial stiffness. This is accompanied by a decrease in the rate of shrinkage of d(1,0) with increased polymer concentration. Millman et al (1983) saw a similar effect at a spacing of ~40 → 42 nm. Gulati and Babu (1985) measured the force produced by

similarly compressed frog fibres and found that above a spacing ~40 nm the force production was constant, whereas below this figure the force production decreased rapidly. Clearly some effect inhibiting contraction starts at this filament separation; Gulati accounts for this decrease in force with the suggestion that there is a restriction of some contractile component, though at the thick/thin filament separations where this occurs he concludes that this is unlikely to be a large rocking or tilting of cross-bridges.

This explanation based on mechanical constriction agrees in part with Umazume et al's (1986) conclusions from their results, which they explain entirely as being due to S1 heads colliding with thin filaments and becoming momentarily attached. They further suggest that this interaction of S1 with thin filaments results in the observed increase in axial stiffness. Gulati and Babu (1985), however, measured axial stiffness in the compressed fibre and found this increased in the rigor state, where no increase in the number of attatched S1 heads would be expected. This indicated that the number of attached cross-bridges alone do not wholly determine stiffness under these conditions.

A discontinuity in the lattice spacing with applied osmotic pressure has been seen in crayfish by Hawkins and April (1981) at the lower spacing of ~35 nm. In rabbits, Krasner and Maughan (1984) have seen a non-linear decrease in force with fibre diameter, similar to that observed by Gulati and Babu (1985) in frogs. Assuming that the relationship between fibre diameter to lattice spacing is similar under high compression in rabbits and frogs, then the calibration curve given for frog by Umazume et al (1986) suggests that the decrease in force in rabbits would occur at a d(1,0) of ~33 nm. This is the d(1,0) at which the minor dislocation in the phase 2 line occurs in the d(1,0) vs S graphs at lower ionic strengths (see Figs 2.2.2, 2.2.3 and Table

2.2.8), and corresponds to a thick filament spacing of ~38 nm. The agreement between the effects in the two species suggests that the change in repulsive forces at these two spacings in frog and rabbit are similar in nature.

Any critical assessment of these mechanical compressive models has to take into account the dimensions of the thick and thin filaments, and the shape and size of the S1 head. Estimates of frog thick filament sizes vary widely. Huxley and Brown (1967) estimated the diameter at between 10 → 15 nm. From various studies using two dimensional Fourier syntheses of equatorial data, the thick filament appears to have a diameter of ~20 nm (eg Haselgrove et al (1976), Yu et al (1985)), though these results depend largely on the phases used in the analyses and do not resolve thick filament structure beyond doubt. Charge measurements indicate the diameter is larger still, at 25 → 30 nm (eg Elliott and Bartels (1982), Naylor (1982)). This is the effective charge diameter, which may well be larger than the physical diameter of the thick filament backbone and be due, for example, to a highly charged HMM-S2 portion of the myosin molecule extending out into the interfilament space. As such this value should be taken as the maximum diameter. Bearing in mind this three-fold range in thick filament diameter estimates, an *ad hoc* diameter of 15 → 20 nm is often adopted (eg Gulati (1982)) and will be used in this discussion. In crayfish, Hawkins and April (1983a) have estimated by direct observation under EM that the thick filament diameter is 18 nm, whereas from equatorial intensity X-ray measurements Yagi et al (1977) estimate the diameter to be 15 nm and the thick filaments to be hollow. In the discussion in this thesis a diameter range of 15 → 20 nm will be assumed for crayfish thick filaments.

Thin filament diameter estimates fall within a much narrower range. Huxley and Brown (1967) give a value of 7.5 → 8 nm and more

recently, Edelman and Padron (1984) estimated from the profile of the 59 A layer line that thin filament diameter is ~10 nm. Hawkins and April (1983a) from EM measurement give the diameter of thin filaments in crayfish as 8 nm, a similar value to that in frog.

The S1 dimensions have been estimated using EM by Knight and Trinick (1984), who show evidence for a pear-shaped flexible ellipsoid of mean length ~19 nm and mean maximum width of 6.5 nm. Kretchmer at al (1978), using X-ray scattering of S1 solutions, conclude the elliptical head is of the somewhat smaller dimensions of 10 → 13 nm on the long axis and 4 → 5 nm along the shorter axis. The discrepancy between the two values has been ascribed to either a confusion over length measurements, which would favour the lower X-ray value (Mendelson (1985)) or as an insensitivity by the X-ray diffraction technique to the long, thin regions of the S1 head which would favour the longer value measured with EM (Craig et al (1986)). Winkelmann et al (1985) using measurements from X-ray crystallography of S1 crystals reported a length of at least 16 nm and diameter of ~6 nm. Parallel studies with EM yield a very similar structure to that seen with X-ray in terms of the size and shape of the S1, and support the longer dimension of the myosin head.

10.1.1. The interaction of lattice components under compression.

In frog, a thick filament spacing of 40 nm (the point at which the force and radial stiffness effects occur) corresponds to a thick/thin filament spacing of ~23 nm. This is the spacing at which (according to Umazume et al (1986)), the compression, leading to the effects seen, begins. In crayfish, the thin filaments occupy positions directly between two thick filaments rather than the trigonal point between three as in frog, but the dimensions of the components under

compression are similar. From the geometry of the lattice, and assuming the collision radii in frog and crayfish are similar, the thick filament spacing at which compression starts would be predicted to be 2×23=46 nm if the interaction was between thick and thin filaments. This estimate is over 10 nm greater than that seen in practice. The low experimental spacing observed is all the more unusual since the values assumed for crayfish thick filaments diameter are possibly low. Stewart et al (1985) report a diameter of ~24 nm for *Limulus*, implying larger diameters for invertebrate thick filaments.

In addition to inconsistencies in collision radii, the binding of S1 to the thin filaments which Umazume et al (1986) use to explain the axial stiffness increase would be expected to cause the intensity ratio I(1,0)/I(1,1) to decrease. Matsubara et al (1985) find no significant change in intensity ratio on compression. Finally, Brenner et al (1982), using a rapid stretch technique, later corroborated using X-ray diffraction (Brenner et al (1984)) showed that S1 is largly unattached to thin filaments at the ionic strength used in Umazume et als' control curve. They also showed that at the lower ionic strength used (0.06 M) significant attachment is present. Under these low ionic strength conditions, it would be expected the attachment of S1 would cause an increase in radial stiffness; in practice little change is seen (Umazume et al (1986)).

An alternative explanation of the change in radial stiffness might be the compression of the counterions in the double layers surrounding the thick and thin filaments as the lattice dimensions decrease. A double layer (Verwey and Overbeek (1948)) is an electrochemical system in which a large molecule or particle (in this case thick and thin filaments) carrying a fixed charge and in an electrolyte solution becomes surrounded by a cloud of oppositely charged ions. This double layer forms by the attraction of counter

ions to the fixed charges and the repulsion of the co-ions. This will result in modified concentrations of these ions round the filament, and an equilibrium is established at the point where ions entering the double layer equal those leaving by diffusion. The double layer in equilibrium is a diffuse cloud of opposite charge surrounding a more sharply defined layer of fixed charge. Verwey and Overbeek (1948) examined the theoretical effects of bringing together two or more double layers, and have shown the compression of ions in the double layer system results in a decrease in the negative electrical free energy of the system, meaning that work must have been done in the compression. This work corresponds to the repulsion experienced in forcing the two double layers together. The repulsion will depend on the charge on the filament and the concentration of ions in the solution which is in equilibrium with the double layer.

Naylor et al (1985), using microelectrode measurements, have shown that the filament charge shows a significant decrease on changing from pH7 to pH6, but shows little change over the ionic strength range used by Umazume (0.06 → 0.20 M). These observations of charge on the filaments would be expected to have an effect on radial stiffness by the model under consideration. With lowered pH, the radial stiffness curve is shifted to the right corresponding to a decrease in osmotic pressure needed to bring about a given lattice shrinkage, and the point at which the rapid increase in stiffness occurs decreases from a d(1,0) of ~35 nm to ~34 nm. The gradients of the lines before and after the dislocation were also reduced, indicating the rate of stiffness increase with applied pressure was reduced, which again would be expected with a decreased charge on the filament. Furthermore, where little change in radial stiffness over the ionic strength range used is predicted, little change is observed. Umazume also reported that an increased [Mg^{2+}] further decreased the

spacing at which the dislocation occured (this point is so much reduced that it does not fall within the range of the graph). In addition, the gradient before the dislocation was certainly reduced. This too is predicted since Naylor (1977) found that even a small increase in $[Mg^{2+}]$ caused a decrease in charge on the filaments.

This alternative model, although it is attractive, in many respects does not account for all of the observations. Electrostatic models cannot explain changes in axial stiffness under compression, nor the rapid fall in force seen by Gulati and Babu (1985) at a compression similar to that seen for the rapid increase in stiffness. The rapid stiffness change itself clearly does not exhibit an exponential increase with decreased filament spacing as would be predicted by electrostatic theory (Elliott (1968), Elliott and Bartels (1982)).

10.1.2. Suggestion as to the nature of the repulsive force.

The degree of compression used in these studies corresponds to the separation at which the exponential rise in potential between filaments is increasing rapidly (Bartels and Elliott (1982)). A mechanical interaction between the filaments would be expected to exert no influence on stiffness until a certain point where components collide, below this point the radial stiffness would increase rapidly. Evidence for such a collision involving thin filaments comes from X-ray equatorial reflection ratios. Magid and Reedy (1980) reported that compression causes an increase in the (1,0) intensity relative to the (1,1). Using the interpretation of Elliott et al (1963), they concluded that thin filaments were being displaced from the (1,1) lattice planes so as to weaken the (1,1) reflection. Such an interaction would cause a rapid rise in radial stiffness at a certain filament spacing, and this interpretation is also that offered by Umazume et al (1986) (note that

Umazume went further and proposed actual attatchment rather than just collision - see earlier).

At this spacing, the electrostatic repulsive contribution from the exponential increase will also begin to become significant, and this increased contribution could account for the decreased gradients of Umazume et al's pH5 and [Mg^{2+}] data, as well as the small changes seen with ionic strength.

Having established that both electrical and mechanical repulsive forces need to be invoked to explain all the effects seen by Umazume et al (1986), the decrease in the spacings at which mechanical compression begins must be accounted for. A decrease in physical dimensions of one or more components could explain this changed spacing. Alternatively, the dimensions of the components could remain constant and the position they occupy within the lattice could change. The site of possible mechanical compression is the S1 head, since no other component has the "reach" to be compressed at the spacings under consideration. If the radial position of the S1 were changed, for instance by an altered affinity of the long S2 with the thick filament backbone, then the spacing at which collision with thin filaments or other S1 heads would alter. If this affinity were charge dependent in a manner similar to that implicated by Ueno and Harrington (1974), then a decrease in charge might be expected to increse the S2-backbone affinity and so decrease the radius of the S1 position, thereby lowering the spacing at which compression starts.

In conclusion then, it appears that at thick filament spacings of ~40 nm or greater in frog and ~38 nm in rabbit the repulsion between filaments is electrostatic. Below this value, mechanical compression of lattice components begins to add significantly to the rapid exponential increase in repulsion from the charge on the filaments, to produce the rapid rise in radial stiffness and the decrease in rate of spacing fall

seen experimentally by Umazume et al (1986) and Gulati and Babu (1985).

10.2. Towards an explanation of sarcomere bowing.

The analysis of reflections in other studies has been concentrated on spacing changes between filaments under various conditions, and description of the effects of these changes on reflection width have been limited to scattered comments in the literature. Yagi and Matsubara (1977) report a loss of sharpness in the outer reflections of crab muscle on going from the relaxed to the rigor states. Magid and Reedy (1980) have seen "weakened reflections" on skinning, especially in the higher orders, this effect is reversed to some extent by PVP. Matsubara et al (1985) report that reflections are "broadened and weakened" by compression with polyvinylpyrrolidone (PVP) or with high ionic strength bathing solution. Changes in meridional reflection widths have also been reported; the reflections become broader both axially and laterally on going from relaxed to rigor (eg Huxley and Brown (1967)). These authors also notice a decreased sharpness in the meridional reflections on stretching muscle.

In all the above examples, the reason for the decreases was suggested to be lattice disorder. The work in this thesis has been directed at unravelling the nature of this disorder and to relate this to changes in the equatorial reflection width observed (see Section 5.5, 6.4 and 7.4).

Consider first the effects of pH. The Introduction reviewed the radial forces operating in the lattice, the first part of this Discussion gave further consideration to the repulsive forces, and tentatively concluded that in rabbit at a thick filament spacing of ~38 nm the radial collision between lattice components begins to have an effect.

This exerts what amounts to a repulsive force at a thick filament spacing corresponding to a d(1,0) of ~33 nm. Examination of Fig 4.2.1 shows that the d(1,0) fell to around this level at pH5 at S≤2.9 μm. At longer S under these conditions d(1,0) fell just below ~33 nm. Assuming that the changes in the point at which compression becomes important are small, then at the spacings seen over the range of pH used it would appear that compressive forces are not important. This implies that the electrostatic repulsive force dominates in these experiments; and Naylor et al (1985) and Elliott et al (1985) have shown that thick filament charge increases with increasing pH. This increased charge is reflected in spacing changes in the filament lattice, raising pH from 5 to 9 increases both charge and spacing. Fig 4.2.1 confirms this observation and shows that the effect occurs over a wide range of S. Fig 4.2.3 shows that sharpness decreases rapidly with decreased pH. Raising pH also decreases the sharpness but to a lesser degree, and these changes are correlated with changes in bowing and local disorder seen with EM. Since changes in charge and spacing are so closely parallel (though this is not always the case) and since at constant S (2.6 μm in the EM experiments) the number of cross-bridges in the rigor state can be assumed to be constant, the pH changes offer the simplest system to begin an explanation of bowing.

As the pH is lowered from 7 to 5, the experimental observation is that there is a decrease in the local disorder and an increase in the bowing. This change is accompanied by a 9-10 nm decrease in thick filament spacing, a decrease in sharpness and a fall in the charge on the filaments. This reduction in the charge will reduce the repulsion between filaments in the lattice, and so Van der Waals attractive forces together with elastic constraints, such as cross-bridges, M- and Z-lines and any lateral intermediate filaments, cause the lattice to

shrink. This explains the spacing changes, but not the bowing increase. Table 6.2.1 shows that the bowing has increased from 7% to 11%, and Fig 6.2.3.1 shows this to be an increased curvature of filaments towards the sarcomere centre along their length. It is this curvature that causes the best ideal lattice fit to be that of an ellipse. The interpretation of this bowing depends on whether the filament is taken to be a rigid uniform body (ie a high Youngs modulus) or to have a variable stiffness along its length. In either case the mechanics of the bending of a rigid body can be applied.

To bend a thick filament, a bending couple must be applied. This comprises two equal and opposite forces separated by a given distance. In the A-band lattice, as a first approximation, it will be assumed that the cross-bridge exert an inward force at some point between M-line and A/I juction, and that the electrostatic repulsion exerts the equal and opposite force at the M-line. These two forces are at different points along the filament and so constitute a bending couple. The attractive and repulsive forces in the couple will be equal and opposite, and so the resultant force must be zero. If either force is changed then the filaments will experience a net force and so move to either a larger or smaller spacing at which the resultant force is again zero, and since the points at which the two opposing forces act are still separated, the bending couple and so the bowing will still be present.

This model is consistent with the idea that filament spacing is determined by the separation at which the resultant force is zero, and also provides a basis for an explanation of the bowing seen. To expand the model, consider the two types of filament mentioned above.

(a) 10.2.1. Bending of filaments with high uniform stiffness.

When a lateral force is applied to a filament which is held at the M-line, then for a filament to bend a bending couple must be established by an equal and opposite reaction at the M-line. In muscle, both the applied force and the equal and opposite reaction are the resultants of forces described in the first part of this Discussion and in the Introduction. For the filament in the bent state there must be an equilibrium between this bending couple and the internal couple due to the compression and extension of the filaments on either side of the neutral surface within the filament. The internal couple is equal but in the opposite rotation sense to the externally applied bending couple.

In the following discussion it will be assumed that the electrostatic forces on the thick filament act through the centre of mass of the filament (ie at the M-line). Attractive forces such as Van der Waals forces which also act over the whole filament are also considered to act at the M-line. Mechanical attractive forces such as M- or Z-line constraint, cross-bridge constraint and intermediate filament elasticity are considered to act at the site of the mechanical interaction. Since the filament is considered to be a rigid body, the filament spacing change effects will be dependent on the forces over the whole length of the filament; this is in keeping with the balance of forces.

Using the assumptions above, the interpretation of the pH result is that at fixed S of 2.6 μm the reduced charge at pH5 results in the reduced electrostatic repulsion acting at the M-line. The elastic forces of M-line, cross-bridges and intermediate filaments together with the Van der Waals forces (which will be collectivly called attractive forces) cause the lattice to shrink. The individual elastic elements, particularly

the cross-bridges in rigor, will exert their attractive component forces predominantly towards the ends of the filaments, and this together with the equal and opposite force at the M-line will constitute a bending couple.

To produce the large bowing seen at pH5, this bending couple must be larger than that at pH7 for example (assuming, of course, that the stiffness of the filaments is constant with pH). This is explained by the fact that the forces in the couple are resultant forces, the outward repulsive force at the M-line has an electrostatic contribution from the whole thick filament, whereas the attractive cross-bridge force is less opposed by the reduced electrostatic repulsion at the filament ends, so the attractive resultant force is high causing the lattice to shrink to the spacing where the overall force balance is satisfied. Under these circumstances the forces in the bending couple are large, explaining the high degree of bowing.

On raising the pH to 7, the charge on the filament increases, and so the electrostatic repulsion also increases. There is considerably more repulsion between thick and thin filaments, and although the cross-bridges are more strained, the observed reduction in bowing shows that this increase in the electrostatic repulsion overides the cross-bridge strain. The resultant attractive force in the cross-bridge region is reduced, so that the high charge causes the lattice to swell. This reduced cross-bridge attractive force also results in a decrease in the bending couple. This effect continues as pH is raised even further to 9. At the higher spacing seen at this pH, the attractive elastic forces in the M-line and the intermediate filaments are possibly significant, and this will act to reduce the resultant force at the M-line. The lower resultant cross-bridge attraction, relative to the electrostatic repulsion, towards the filament ends might result in a reduction of the bending couple expected from this high charge state,

but the bowing results indicate the difference between pH7 and pH9 is small.

This increased electrostatic repulsion compared to the attractive forces is responsible for the increase in local disorder of the filaments as they become less constrained under the changing conditions, and it will be seen that wherever conditions of high charge or reduced elastic constraint prevail, the degree of local disorder seen is high. This is equivalent to saying that the energy well in which the filaments lie is more shallow (see Verwey and Overbeek (1948)).

(b) 10.2.2. Filaments in which stiffness varies with length.

In this model the stiffness of the thick filament is considered to decrease towards the A/I junction. In the mechanical sense this corresponds to a decrease in Youngs modulus of the filament nearer the tip. Although a bending couple is still required to distort the filament, the magnitude is less for a given distortion, due to the reduced overall stiffness. Such a decrease in stiffness would be expected to bring about a more elliptical bowing to the filament (to a first approximation, the constant stiffness model will result in a bowing which fits the radius of a circle), since the ends will bend inwards more per unit bending couple than the central portion of the filament. Note that in this model forces acting on the filament tip will still be considered as acting at the M-line when considering spacing changes, so the idea of the balance of forces is maintained, and the attractive forces still provide a bending couple, however this couple need not be as great as in the uniform stiffness model to account for the bending seen.

Such a flexibility change along the filament would require either a decrease in myosin concentration or a change in the packing of

myosin molecules towards the filament tip. Squire ((1981),(1973)) and Pepe (1979) have considered models of myosin packing and filament assembly in which the thick filament tapers over the last 0.2 → 0.3 μm of its length, though the rest of the filament is of constant myosin concentration and possibly stabilised by C-protein. This agrees with the observations of Huxley (1963) who saw thick filament taper at a similar point.

A better model, therefore, would take elements from both situations and assume that the first 60-70% of the thick filament has a relatively high stiffness, and in the remainder, the taper in the filament causes a decrease in stiffness. This type of filament not only fits the theoretical and observed structure of thick filaments, but would also account for the improved fit with the "ideal" elliptical lattice of the bowed filaments seen in the pH experiments (see Table 6.2.2), the PPi experiments (Table 5.2.2) and the rigor state in the contraction analysis (Table 7.1.1). The taper also explains the "pinching" in of the filaments at the tip seen in some sarcomeres in rigor muscle (see Figs 5.2.4.1 and 6.2.3.3, for example). This lowered stiffness could also explain the bulbous swelling of filament tips at longer S (eg Figs 5.2.4.3 and 5.2.4.4) as being due to a local electrostatic swelling and cross-bridge attraction phenomenon exerted through a filament section of lowered stiffness.

The explanation of the bowing has relied on the assumption that the cross-bridge radial force acts at the mid-point of the thick/thin filament overlap zone. The true situation has these forces acting over the whole overlap region, so the distributed forces may also act to bring about the elliptical A-band shape.

The model can also be used to explain the decreased bowing (Table 5.2.1) and spacing (eg Fig 2.2.2) seen with increasing S. To develop the model to fit these data it is neccesary to consider the

Fig 10.1. Long S.

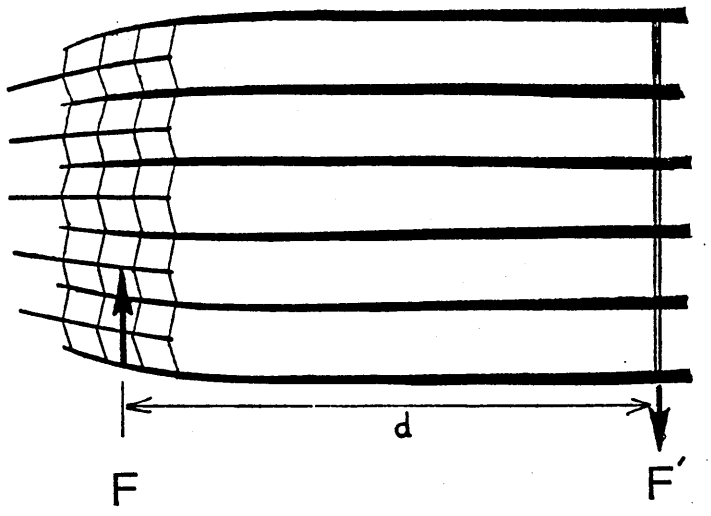

Bending couple = Fd

Fig 10.2. Short S

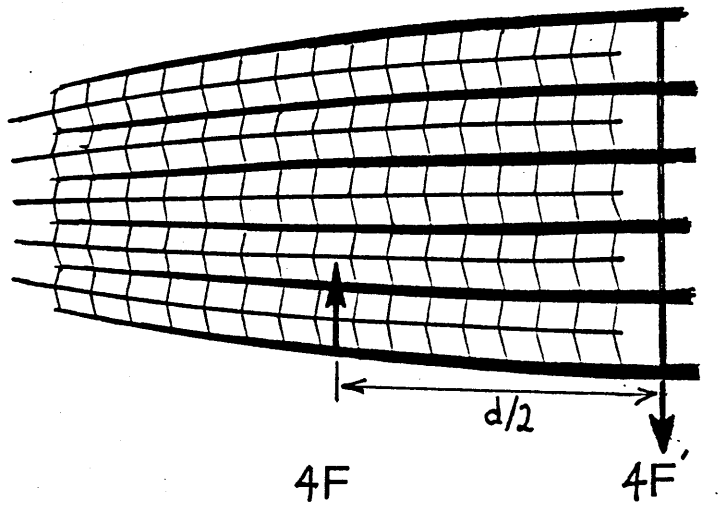

Bending couple = 2Fd

nature of the resultant forces acting to bring the filament tips together. In explaining the pH data it was assumed that the major inward elastic force arose from the elasticity of the cross-bridges. As a first approximation, it will be assumed that the force exerted per cross-bridge is constant, so the total force exerted by the cross-bridges will be directly proportional to their number. Since the cross-bridge population, and so the cross-bridge forces, act over a range of distances from the M-line (the range is determined by the degree of overlap), for the purposes of assessing their contribution to the bending couple, the total force is considered to be acting at a point in the centre of the overlap region.

At long S (eg Fig 10.1), the number of cross-bridges is small so the total force (F) is small, and the distance (d) of the mid-overlap zone to M-line is large. However the electostatic repulsion is largely thick/thick filament so the overall repulsion (F') is low, leading to the attractive forces lowering the filament spacing and also resulting in a small bending couple, so little bowing is expected. As noted previously the lowered tip stiffness in the region of the high thick/thin filaments repulsion leads to a bulging of the filaments towards their ends. This local bulging will mask any bowing if present.

Consider now the case at short S, where the overlap has increased fourfold (see Fig 10.2). The attractive elastic cross-bridge force is now four times as strong, but the mid-overlap zone to M-line distance has only halved. The electrostatic repulsion is now largly thick/thin and so the large electrostatic component acting at the M-line causes the lattice to expand. Thus the forces have increased, so the bending couple increases (though by a relativly smaller amount due to the geometry of the mid-overlap zone/M-line distance) so an increased bowing is seen. Notice also that the local disorder also increases on increasing S; rather than a charge change, this is most

likely due to a decrease in cross-bridge constraint of the thick filaments.

As noted in Sections 5.2 and 5.5, the decreased bowing with increasing S seen in this study is contrary to that seen by Bergman (1983), who saw an increased bowing with increassed S. A possible explanation of this is suggested in Section 10.4.

This explanation is rather simplistic, since other radial forces will come into play at various spacings and alter the resultant forces F and F'. Examination of Figs 2.2.1 to 2.2.3 show the variation of spacing with S at various ionic strengths, Fig 4.2.1 shows d(1,0) vs S at a variety of pH values, and Fig 3.3.4 shows the variation of sharpness with S at I=0.071. None of these graphs is a straight line, as would be expected from the description of the model so far. The sharpness change with S can be explained by a transition from a shape disorder due to the 8-9% bowing seen at short S to a high degreee of local disorder at long S (see X-ray discussion Section 9.1), and the forces affecting the type of disorder predominating are better understood by considering their effect on the spacing changes.

10.3. Forces influencing the filament spacing in the A-band.

The filament spacing is determined by more than the simple balance of electrostatic repulsive, cross-bridge and other restraining forces that have so far been considered. It has already been mentioned that at a thick filament spacing of ~38 nm the lattice components start to collide, and it is suggested this is the source of the minor dislocation in phase 2 of the lower ionic strength graphs (see Figs 2.2.1 → 2.2.3). When the gradient of the line after this dislocation was subtracted from the main phase 2 line, the gradient of the resulting line was the same, indicating that this effect is caused

by a common force which is unaffected by the ionic strength change. These are properties which might be expected from structures under mechanical compression. In no case did the thick filament spacing measured fall below ~34-35 nm, and in the plot of d(1,0) vs S for low ionic strength where the filament spacing approached this value at long S, the curve levelled off to give phase 3 of Figs 2.2.1 → 2.2.3. In the low I experiments this minimum is reached at the point of zero thick/thin overlap, and so it could be considered that the decrease seen in phase 2 is due to withdrawal of thin filaments from the A-band and consequent reduction in thick/thin filament electrostatic repulsion.

It would appear that this minimum spacing is the limit at all S, since with lowered pH the spacing decreases little (~1-2 nm) with increasing S, implying the minimum spacing is largly independent of S. This suggests that the collision is an interaction of thick filaments in some way, a suggestion supported by Millman (1981) who finds that at shorter S in relaxed muscle, the minimum value reached by osmotic compression is ~34 nm. If the interaction is thick/thick filament, it is likely that at the separation observed that the S1 heads are involved. A thick/thick filament interaction would also explain the lower spacing than expected for the dislocation in the lattice spacing vs compression graph for crayfish mentioned in Section 10.1. For solutions at pH>5 at values of S shorter than the point of zero overlap, the lattice swells rapidly.

Table 2.2.3 shows that the straight line of phase 2 (neglecting the effect of the minor dislocation) is steeper in lower ionic strength solutions. The reason for this could be that the decreased concentration of counter ions in the solution fail to mask the charges on the thick filaments as effectively, so repulsion between the filaments is increased. Decreasing the ionic strength will cause a small

decrease in charge on the myosin filaments (Naylor et al (1985)) and so a slight fall in electrostatic repulsion would be expected, so if this is true, the shielding has more effect than the charge effect on changing ionic strength. This might be expected since changing ionic strength is unlikely to alter the charge due to the amino-acid side groups, so reducing the double layer will cause the increased charge interaction. However, thin filaments could be acting differently compared to the thick filaments with changing I, so the thick/thin filament repulsion may be increased at low I.

Alternatively, a decrease in cross-bridge elasticity would account for the increase in phase 2 gradient. For instance in the pH experiments, the phase 2 gradient increases with pH. This could be explained by the increased charge at the increasing pH or by changing cross-bridge elasticity due to a dissociation of the S2 from the filament backbone in a manner similar to that proposed by Ueno and Harrington (1974).

A further factor affecting the rapid increase may also be a Donnan osmotic effect due to an increase in the concentration of fixed charges in the A-band with increasing thick/thin filament overlap. As suggested by Elliott (1973b), this will cause a movement of ions into the A-band lattice and so cause water to enter the lattice. This will cause a swelling and increased filament spacing. This Donnan osmotic effect acts as a repulsive force, and so might be expected to affect the bowing. Since it acts over the whole A-band the site of action, as with the electrostatic repulsion, can be considered at the M-line. So a decrease in S would be expected to enhance the electostatic repulsive force to increase the bending couple.

In the ionic strength and pH experiments the phase 2 increase levels off; the lower the ionic strength the more sharply defined the dislocation with the phase 1. Similar dislocations in the d(1,0) vs S

graphs have been seen in frog rigor by Magid and Reedy (1980) and Shapiro et al (1979) in relaxed frog muscle. Their presence in the relaxed state makes it unlikely to be due to cross-bridges reaching their limit of extension. This change is therefore more likely to be due to M-line or intermediate filament elastic constraint, and preliminary experiments using conditions under which M-line material is known to be removed causes an increase in the lattice spacing at these short S. The test will be if no such increase is seen at longer S.

The spacing at which the dislocation occurs increases with decreasing ionic strength (see Table 2.2.6) indicating that decreasing ionic strength inceases the "cut-in" spacing. The slight negative gradients of the phase 1 (which increase with increasing ionic strength) implies that the restraining links are not inelastic. A qualitative summary of the spacing changes with changing pH in this region shows that increasing the pH increases the gradient of the phase 1, but pin-pointing a spacing at which the dislocation occurs is not possible.

10.4. The nature and effect of the cross-bridge constraint.

This discussion has so far assumed that under a given condition the elasticity of the cross-bridges remains constant. Over a spacing range of ~34 to ~46 nm, the possibility exists that the elasticity is not constant. Tawada and Kimura (1986) have estimated from cross-linking studies that of the compliance in the cross-bridge, 65% resides in the S1 head, and 35% in the S2 region. Changes in the angle of S2 to the S1 may occur and so effectively alter the elasticity of the cross-bridge by altering the radial component of the lateral force exerted. Podolsky et al (1982) have suggested that a constant short S2 length is present in muscle in rigor under a wide range of pH, though

Ueno and Harrington (1974) suggest that at higher pH, more S2 dissociates from the thick filament backbone. This introduces the possibility that the functional length of the S2 may change with pH. Together with the change in charge the S2 will experience, it might be surprising to find the elasticity unchanged. A change in elasticity of the cross-bridges, although not affecting the presence of an attractive force *per se* will have an effect on its magnitude, and therefore on the balance of forces. The lattice spacing and bending couple may well be affected in this way.

An experiment which will alter cross-bridge restraint is the addition of PPi or moving from the relaxed to contracted state. PPi is known to have a pseudo-relaxing effect (e.g. White (1970), Schoenberg and Eisenberg (1985)), and a decreased stiffness with decreased rate of stretch is also seen, indicating that the cross-bridge is in rapid equilibrium with thin filaments (Schoenberg and Eisenberg (1984)). This rapid equilibrium causes a reduction in the attractive force exerted by cross-bridges. Bartels and Elliott (1983) show that with PPi in phosphate buffer, the A-band potential falls to just under half its rigor value, and the I-band potential to ~2/3. These reflect the decreased charge on the filaments, and so it is expected that the electrostatic repulsion will fall markedly. With a fall in both the attractive cross-bridge and repulsive electrostatic forces, and at any given value of S, the distance between the sites of action of the two forces being constant, the bending couple is reduced. This leads to a reduction in bowing. There is also a decrease in local disorder - this reflects the change from the high charge (in rigor) to the lower charged state.

As a point of note, this dual reduction in bowing and local disorder might be expected to have its greatest effect on sharpness at intermediate S, where there is still a degree of bowing, but where

local disorder in the rigor state is increasing. This effect is a possible source of the differing shapes of the rigor and PPi curves (Figs. 3.3.4 and 3.3.5). A subtraction of the PPi curve from the rigor curve does show an increased difference between the two over the range S~2.5 → 3.0 μm.

Figs 3.3.1 and 3.3.2 show the effect of 1 and 5 mM PPi causes the d(1,0) to increase in both cases. This lattice expansion is also reflected in the observation of Offer and Trinick (1983), who saw an increase in myofibril diameter on exposure to PPi. The shape of the Δ(1,0) vs S graphs strongly suggests the change in spacing is proportional to filament overlap, Table 3.3.1 shows the increase in spacing is zero at around no overlap, and greatest at maximum overlap. Since the lattice is swollen and the repulsive force has decreased, the conclusion drawn is that the removal of crossbridge constraints has a greater effect than the reduction of charge. A titration curve of charge on a filament versus [PPi] shows that at 1 mM the charge decrease is complete, so the increased swelling effect at 5 mM must be due to the increased weakness of the crossbridges.

The reverse effect, where cross-bridge attachment increases, is the situation found when muscle changes from the relaxed to the contracting state. In the relaxed state there are no cross-bridges attached, and the repulsion of the filaments, although low, is unrestrained except for M-line forces, Van der Waals forces and possible intermediate filament constraints. The fact that a spacing of 50 nm is possible with low charge shows that at least in the relaxed state these forces come into play only at large spacings. As a result there is no bending couple and this leads to the near perfect rectangular lattices seen by Bergman (1979) under these conditions.

On contraction, cross-bridges move to attach to thin filaments and in these circumstances, the increased attractive cross-bridge force

is augmented by the radial component of the axial force the muscle is generating, so the force per cross-bridge is likely to be higher in the contracting sarcomere. Against this increase attractive force is an increased electrostatic repulsion due to increased charge (Bartels and Elliott (1984a)(1984b)) acting at the M-line, so the bending couple is established and bowing increases. Dr A.J.Rowe (personal communication) has suggested this increased radial component due to the axial force may be involved in the explanation of the increased bowing seen with increasing S by Bergman (1983), in apparent contradiction to my own results. In the contracting state (which is very different from the rigor state of my own data), the distance component of the bending couple may be increasing more rapidly than the decrease in the radial cross-bridge force as filament overlap diminishes.

Although it is not very clear from the Figs 7.1.1 and 7.1.2, it appears that a slight increase in local disorder also occurs on contraction (again, this is a high charge state). Yu et al (1985) came to the conclusion that the liquid type disorder in frog muscle increased with contraction, and suggested that the filaments were moved off their lattice planes by irregular cross-bridge attatchment. This would correspond to a local type disorder, and although this is a factor, the major distortion is a bowing.

The attaching cross-bridges must exert enough force to overcome the increased repulsion, and the balance of forces causes the spacing of contracting muscle to decrease at short S (Brenner and Yu (1985), Matsubara et al (1984a), Matsubara et al (1984b)). Shapiro et al (1979) report that the decrease in a spacing diminishes with increasing S, further indicating that the numbers of crossbridges attached are important in determining the balance of forces.

In rigor sarcomeres the degree of bowing is increased, indicating that the bending couple is greater in magnitude. This is probably the

result of the number of cross-bridges being greatly increased over the situation in contraction, so even though the force per crossbridge may be lower, the increased numbers more than compensate for this and the resultant force inwards increases. The charge on the filaments, however, is increased in rigor and this increases the repulsive electrostatic force acting at the M-line; the result is an increased bowing. The spacing difference between contracting and rigor states in frog muscle at shorter S is similar. Millman (1981) reports a thick filament spacing of ~45 nm for rigor, and Brenner and Yu (1985) observed the slightly lower spacing of ~44 nm at maxiumum contraction. The high electrostatic force in rigor would be expected to be very sensitive to thick/thin filament overlap, and Figs 2.2.1 → 2.2.3 of d(1,0) versus S show this is the case. More evidence comes from Umazume and Kasuga (1984) who show a large decrease in radial stiffness with increasing S in the rigor state, indicating as overlap decreases the repulsive electrostatic force is reduced significantly.

There are, however, some data available which appear not to fit the model proposed. Dr K. Edman (Personal Communication) has provided pictures of rapidly frozen sarcomeres in relaxed and contracted conditions, and the pictures show a bowed relaxed and less distorted contracted state, the direct opposite of the Bergman observation. Bergman continued his experiments to very short S, and here the bowing effect was reversed. The diameter of the sarcomere at the tip of the filaments was found to be grater than that at the M-line. This effect is similar to that seen by Kreuger and London (1985) in cardiac muscle, also at very short S. Under these conditions the M-line will have two sets of thin filaments and one thick filament traversing it as opposed to one thick filament at longer S, and this may disrupt the structure somehow leading to the effect seen. These observations show that the model proposed in this thesis should be

taken as a first order approximation only, and that it is by no means complete.

10.5. Predictions from the model and suggested further work.

The reduction of either bowing or local disorder would also be expected to produce sharper meridional reflections. An examination of the effect of PPi on meridional spacings has shown that this is the case, with sharpness increasing in both the axial and lateral directions (see Section 3.2.). This effect occurs at all S studied so a reduction in local disorder appears to also enhance the meridional pattern. The sharpness analysis of the d(1,0) does not distinguish between disorder due to bowing and that due to local disorder. A possible method of resolving the two to some extent may be achieved by either (a) an analysis of the 144 nm layer line - a bowing would cause the layer line to open (fan out) in the axial direction as distance from the meridian increases - or (b) using a spot focused X-ray beam to measure a similar increase in axial width of the equatorial (1,0) and (1,1) reflections which would be expected from a bowed sarcomere. This would be a better method since the widths of the two reflections per specimen are measured, and it would be expected that the (1,1) axial width change would be a relatively large effect. Increases in either one of these, together with decreased equatorial sharpness, might indicate a more bowed structure, whereas a decreased sharpness with little axial increase may indicate local disorder. Preliminary measurements of the 14.4 nm layer line with PPi and in rigor are inconclusive due largely to a weakness of these reflections in the pictures so far discussed.

Another prediction from the model is that under any condition, decreasing S will cause increased electrostatic repulsion and increase

in cross-bridge restraint, so an increased bowing with decreased S would always be expected. Further measurements of changing S under various conditions will check this prediction, though the preliminary sharpness data from the pH experiments (See Figs 4.2.4 and 4.2.5) show that the sharpness decreases with increasing S, similar to the situation observed in the control at pH7. Electron microscopy studies should show whether the bowing changes. The synchrotron data so far obtained at pH5 indicate that the sharpness changes are not linear, and more measurements will be needed to define accurately the nature of the sharpness changes with S at every pH.

Ionic strength changes have a smaller effect on charge, and on spacing, so it would be expected that it would have little effect on the bending couple, and so little bowing would be seen. At shorter S, preliminary synchrotron data would suggest this is in fact the case, though again more pictures are needed to assess this fully.

The dislocation between phase 1 and phase 2 has been suggested to be due to the restraining action of the M-line, and extraction of M-line material has been shown to swell the lattice in this region, though a more thorough series of experiments over a larger range of S together with a biochemical analysis of other structures which may be extracted with M-lines is needed.

10.6. Summary and conclusions.

Data have been presented from the X-ray diffraction and EM studies which have shown that the structural distortions of bowing and local disorder in the A-band of rabbit psoas muscle seen with EM have a direct effect on the sharpness of the (1,0) equatorial reflection seen with X-ray diffraction. These changes are correlated with microelectrode studies of charge changes, and a first approximation

model based on a mechanical bending of thick filaments has been developed. The model has been used to correlate the sharpness and bowing/local disorder changes as well as to support the existence of a balance of attractive and repulsive forces which explains the changes in spacing seen under the various conditions. The model can be summarised as follows;

(a) The thick filaments have a constant, high stiffness over the first 2/3 of their length, and the taper in the last 1/3 towards the tips causes a reduction in the stiffness in that region. This decreased stiffness accounts for the elliptical shape in the more bowed sarcomeres, and is a basis for an explanation of various filament tip effects (eg pinching in, or bulging of, filaments in this region).

(b) The attractive and repulsive forces under any given conditions are in equilibrium, and this balance of forces determines the spacing as measured in X-ray diffraction.

(c) The individual attractive and repulsive forces are considered to act at different points along thick filaments in the A-band. Electrostatic repulsive and Van der Waals attractive forces act as if at the centre of the thick filament (the M-line), whereas attractive cross-bridge forces act at the centre of the overlap region. M-line elasticity will of course act at the M-line. The site of action of any attractive forces due to the intermediate filament network is uncertain. Higuchi and Umazume (1986) suggest attachments along the whole thick filament, in which case the site of action would be the M-line, whereas Wang (1984) suggests a model where the interaction is at a specific site on the thick filament. Because of such uncertainties the contribution from this network has been borne in mind, but not

considered in detail. The repulsive compressive force is suggested to come into play at a thick/thick spacing of ~38 nm in rabbit and ~40 nm in frog. Above this spacing, this effect is considered to be negligible, and the repulsion of filaments taken to be purely electrostatic.

(d) Although there are differences in the points of action of the forces, the attractive forces will still be in opposition to the repulsive, so the balance of forces is maintained.

(e) Differences in the points of action will result in a bending couple at a certain spacing where the overall attractive and repulsive forces are balanced. This couple will cause the filament to bow. Changes in conditions of charge, cross-bridge number, stability of attachment or stretch, degree of thick/thin filament overlap and so thick/thin filament repulsion etc, all alter both balance of forces and the bending couple, so altering the spacing and bowing seen.

(f) Local disorder is apparent under conditions where the repulsive force is high or the restraining forces are weak, eg at long S or under conditions of high charge.

APPENDICES.

APPENDIX I - Computer algorithms and programs.

All programs were written in either;

(1) Tektronix 4051 basic.

(2) Tbasic (Transera Incorporated. A Unix based version of basic run on Tektronix 6130).

(3) ANSI BASIC (as run on Tektronix 6130).

(4) TOPS 10/20 Fortran (an upgraded version of ANSI Fortran 77 run on DEC-20).

(5) In addition, some data analysis was performed using the computing facilities at Daresbury via the JANET network. The data processing program OTOKO was used as run on the VAX 11-750.

The range of languages used reflects the problems encountered due to one machine not supporting all the functions required, so a certain amount of data manipulation between machines was necessary. The diverse computing facilities available at the time of writing resulted in the adoption of a modular approach to the numerical manipulations. Separate routines were run on different machines usually culminating in a graphics output on the Tektronix 6130. This proved to be the easiest way of obtaining a hard copy, since segments could be defined and plotted simply by creating macros addressing the terminal graphics mode. An advantage of the modular system was its adaptability. The situation arose where a series of cubic spline fits with slightly different applications were needed, changing one program

slighly to accommodate this was both quick and safe. The algorithms fell into two broad categories, those used in X-ray analysis and those used for EM. Each algorithm was composed of one or more separate programs. Program listings for actual code, and flow charts are included, but the overall combinations of programs used to achieve the various data analyses are as follows:

X-ray diffraction data analysis.

(a) 38 nm layer line and equatorial comparison.

The X-ray digitization and curve fitting program. This contained all the routines needed.

(b) Sharpness curves.

Data files were created with MAKFIL.FOR (including dummy points), and fitted with the spline by SHARPFIT.FOR.

(c) PPi curves.

Data files created with MAKFIL.FOR, and the spline fitted with FITDAT.FOR.

EM picture analysis.

(i) Analysis of bowing data.

Two programs were used:

(a) 3dplot. This generates the means ± SD (eg Fig 5.2.1), opens a file and writes these figures for later analysis by "bowing" program.

(b) Bowing. This reads the file containing the mean ± SD values written by 3dplot, plots them out and fits a theoretical curve based on a trucated conical model to the data (eg figs 5.2.2 and 5.2.3).

(ii) Analysis of distortion of filaments.

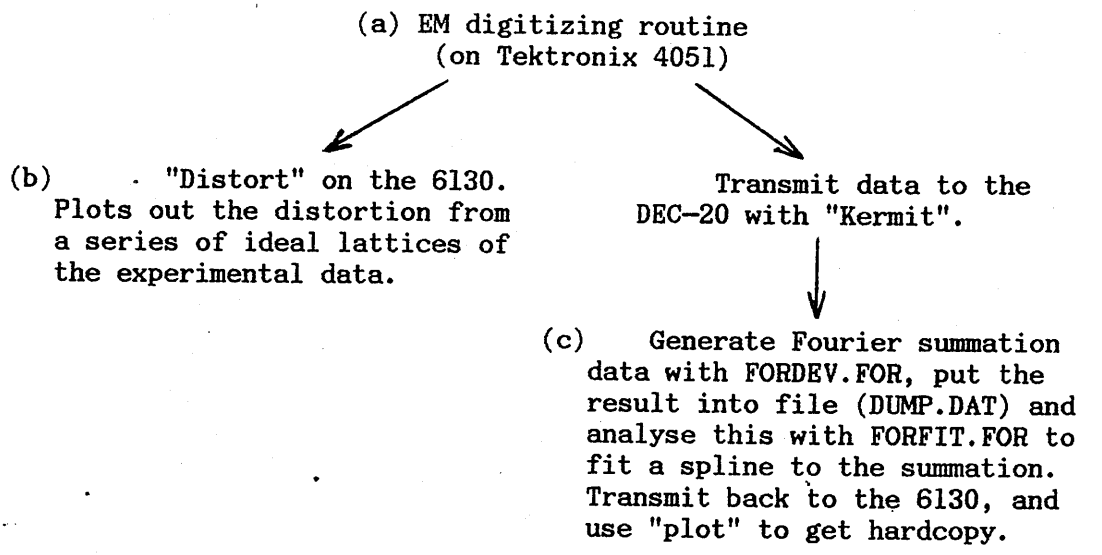

Although the algorithms divided into two groups, the actual programs defining the manipulations could not be grouped so easily, since as already mentioned, a certain degree of interchangability resulted from the methodology used. Consequently, each program will be treated separately with respect to program notes, flow diagrams and listings.

X-RAY ANALYSIS PROGRAMS.

(a) X-ray digitization and curve fitting program.

This is written in 4051 basic and is the only "stand alone" routine used. The flow diagram shows the steps used in the algorithm. A few brief notes explaining the steps taken will be useful.

Although pictures from both GX13 and synchrotron were analysed, the separation of peaks from synchrotrom pictures together with the high signal/noise ratio favoured the use of these pictures. Pictures were digitized out to distance of ~1/10 nm, which usually corresponded to 6-7 cm along the equator from the origin of the picture. The pictures were densitometered using an LKB Ultrascan and the optical density versus distance plotted on line printer. The two halves of the trace were treated independently.

A background was fitted by eye and both the original trace and background digitised. This procedure involved fixing the densitometer pattern to a Tektronix 4662 digital plotter, and defining the centre of the trace. A set of crosshairs could then be controlled by the computer to move 0.4 mm along the X-axis of the trace, the Y-axis movement was achieved by moving the crosshairs manually with the joystick. By pre-defining the number of points, then the number of 0.4 mm steps, and so the filament distance moves could be controlled. Use of the joystick led to a small amount of "drift" of the defined plotter area. To a first approximation, this was assumed to be linear over the range digitised, by measuring the distance the initial point had moved, a straight line could be subtracted to allow for this small effect.

The background could be subtracted by either taking the whole series of points again, or by a rapid method involving taking a series

of points over the curves and interpolating by straight lines the points in between. Subtraction of the background points' values from the densitometer trace point values gave the convoluted peak trace, which was dominated by the (1,0) and (1,1) peaks. The option of digitizing the opposite side of the trace was given, and if chosen the output gave the average of the two halves. Note that the background trace was not corrected for plotter drift, so as a result, the convoluted peak trace has a small, measurable and regular background that is again removed with a simple straight line correction. At this point the data were in a form where manipulation could begin, the data could be treated in various ways. These are summarised below:

(1) Trace smoothing using a 1:2:1 weighted mean.

(2) Scale alteration. This allows normalisation of peak heights.

(3) Averaging of several traces.

(4) Curve fitting. This used the least mean squares method based round Gaussian distributions to de-convolute the trace and find the standard deviation of the best fit Gaussian curves.

(5) Hard copy of trace.

Flow diagram for x-ray digitizing and curve fitting program

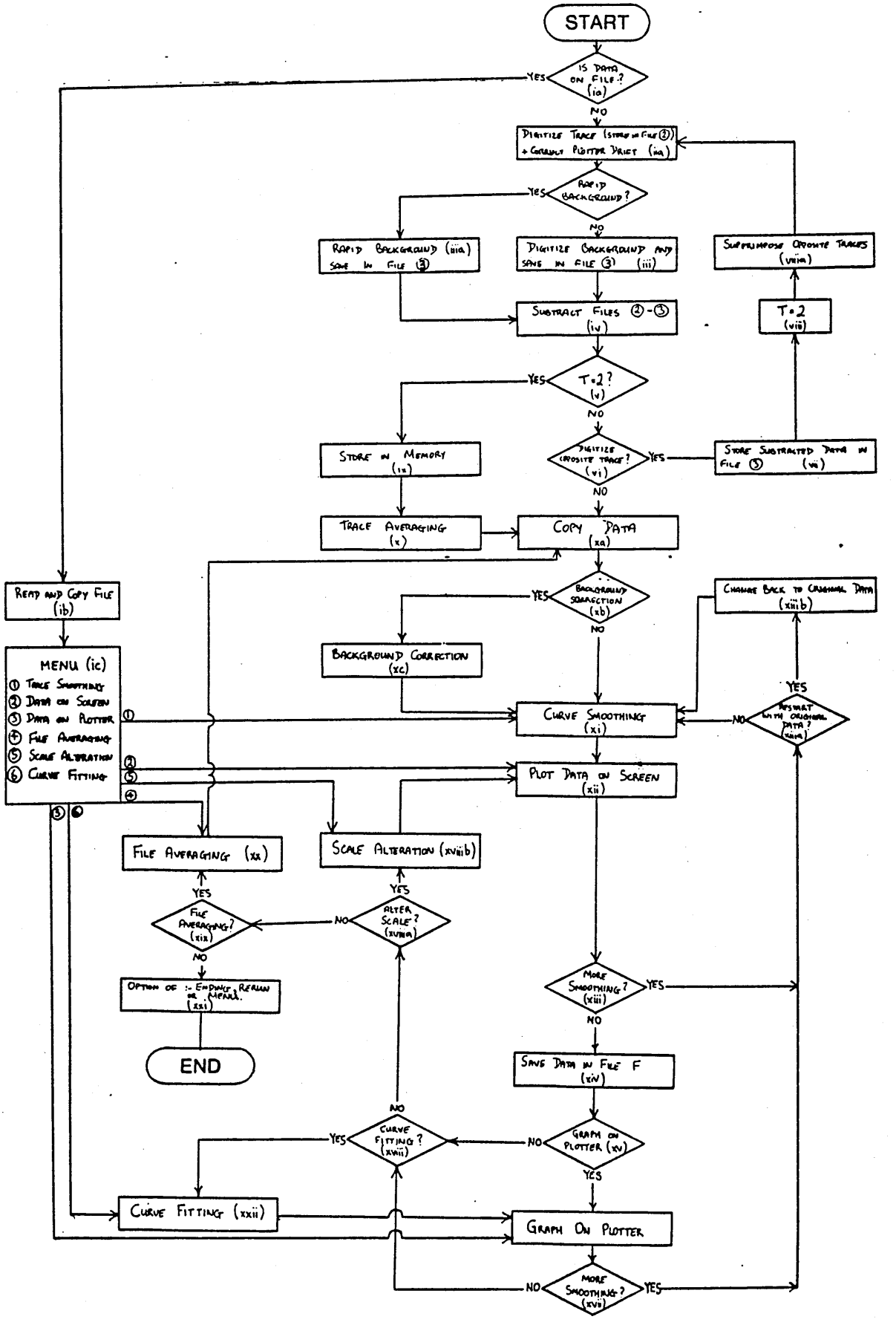

X-RAY DIGITIZATION AND CURVE FITTING PROGRAM.

```
10 INIT
20 RENUMBER 10,10,10
30 Q=0
40 P=0
50 P1=0
60 PRINT @32,26:2
70 REM is data on file ? (ia)
80 PRINT "J IS THE DATA YOU WANT ON FILE ?  ...(Y/N) ";
90 INPUT A$
100 IF A$="N" THEN 320
110 REM input file no,read data & make data copy (ib)
120 PRINT "J INPUT FILE NUMBER OF REQUIRED DATA    ";
130 INPUT F
140 FIND F
150 READ @33:B$,S1
160 DIM X(S1),Y(S1)
170 FOR N=1 TO S1
180 READ @33:X(N),Y(N)
190 NEXT N
200 GOSUB 3190
210 T=0
220 REM deceide where to join program (ic)
230 PRINT "JJ INPUT THE NUMBER WHERE DATA IS TO BE SENT"
240 PRINT "J TRACE SMOOTHING                1"
250 PRINT "J GRAPH ON SCREEN                2"
260 PRINT "J GRAPH ON PLOTTER               3"
270 PRINT "J AVERAGE SEVERAL FILES          4"
280 PRINT "J ALTER SCALE OF TRACE           5"
290 PRINT "J CURVE FITTING                  6"
300 INPUT Z
310 GO TO Z OF 1820,1940,2420,2860,2700,3410
320 REM digitizing routine (ii)&(iii)
330 T=1
340 L$=CHR(7)
350 F=2
360 PRINT "J INPUT NUMBER OF DATA POINTS  ";
370 INPUT S1
380 S2=20*S1
390 IF F=3 THEN 450
400 IF T=2 THEN 430
410 PRINT "J SET L.LEFT + U.RIGHT ON PRINTER, THEN PRESS RETURN ";
420 INPUT A$
430 PRINT "J DIGITIZE TRACE"
440 IF F=2 THEN 510
450 PRINT "J DO YOU WANT RAPID BACKGROUND METHOD ? ...(Y/N) ";
460 INPUT A$
470 IF A$="Y" THEN 490
480 GO TO 500
490 Q=1
500 PRINT "J DIGITIZE BACKGROUND"
```

```
510 FIND F
520 KILL F
530 FIND F
540 P=1
550 PRINT "J INPUT X-ORIGIN AT PRINTER @@@"
560 PRINT @1,26:1
570 INPUT @1,27:X1,Y1
580 PRINT @1:L$;
590 PRINT @1,26:0
600 IF Q=1 THEN 690
610 PRINT " 1",X1,Y1
620 WRITE P,Y1
630 X3=X1
640 Y2=Y1
650 FOR N=1 TO S1-1
660 P=P+1
670 X1=X1+0.2
680 MOVE @1:X1,Y2
690 REM move crosshairs down
700 PRINT @1,26:1
710 INPUT @1,27:X2,Y2
720 PRINT @1:L$;
730 PRINT @1,26:0
740 IF Q=1 THEN 880
750 REM check movement during Y adjustment
760 MOVE @1:X1,Y2
770 PRINT @1,26:1
780 INPUT @1,27:X2,Y2
790 PRINT @1:L$;
800 PRINT @1,26:0
810 ON EOF (0) THEN 1020
820 WRITE @33:P,Y2
830 PRINT @32,26:2
840 PRINT P,X2,Y2
850 NEXT N
860 REM - Quick background interpolation (ends at ln 1050)(iiia)
870 IF Q=0 THEN 1080
880 P2=INT((X2-X1)/0.2)
890 M=(Y2-Y1)/(X2-X1)
900 I=Y2-M*X2
910 PRINT X1,X2,Y1,Y2,I
920 X2=X1+0.2
930 FOR N=P TO P+P2
940 IF N<>1 THEN 960
950 X2=X2-0.2
960 Y2=M*X2+I
970 PRINT N,X2,Y2
980 WRITE @33:N,Y2
990 IF N=>S1 THEN 1080
1000 X2=X2+0.2
1010 NEXT N
1020 PRINT "@@@@@@"
1030 P=N
1040 X1=X2-0.2
1050 Y1=Y2
1060 MOVE @1:X1,Y1
1070 GO TO 690
1080 PRINT "J END OF RUN"
1090 IF F=3 THEN 1210
1100 F=3
1110 REM correct for plotter drift (iia)
```

```
1120 PRINT "J CORRECT FOR PLOTTER DRIFT GGGGG"
1130 MOVE @1:X3,Y1
1140 PRINT "INPUT THIS POINT AT PLOTTER "
1150 PRINT @1,26:1
1160 INPUT @1,27:X2,Y2
1170 PRINT @1:L$;
1180 PRINT @1,26:2
1190 B2=Y2-Y1
1200 GO TO 390
1210 REM sUbtraction routine (iv)
1220 Q=0
1230 DIM X(S1),Y(S1)
1240 FIND 2
1250 ON EOF (0) THEN 1290
1260 FOR N=1 TO S1
1270 READ @33:X(N),Y(N)
1280 NEXT N
1290 FIND 3
1300 ON EOF (0) THEN 1350
1310 FOR N=1 TO S1
1320 READ @33:A1,B1
1330 Y(N)=Y(N)-B1-B2
1340 NEXT N
1350 REM end of subtraction routine - (v)&(vi)
1360 IF T=2 THEN 1720
1370 PRINT "J DO YOU WANT THE OPPOSITE TRACE ?   ...(Y/N) ";
1380 INPUT A$
1390 IF A$="N" THEN 3190
1400 PRINT "J WAIT WHILST PREVIOUS DATA IS STORED"
1410 REM storage of subtracted data (vii)--> T=2 (viii)
1420 FIND 4
1430 KILL 4
1440 FIND 4
1450 ON EOF (0) THEN 1600
1460 FOR N=1 TO S1
1470 WRITE @33:X(N),Y(N)
1480 NEXT N
1490 PRINT "GGGGG O.K"
1500 REM alignment so opposite traces superimpose (viiia)
1510 PRINT "J INPUT L.RIGHT + U.LEFT AT PRINTER "
1520 PRINT "J WHAT VALUE OF N AT CENTRE OF PEAK ?"
1530 INPUT N
1540 M=N*0.2
1550 PRINT "J INPUT AT PRINTER CENTRE OF OPPOSITE PEAK"
1560 PRINT @1,26:1
1570 INPUT @1,27:M1,Y2
1580 PRINT @1,26:0
1590 PRINT @1:L$;
1600 MOVE @1:M1-M,Y2
1610 PRINT "J ADJUST VERTICAL POSITION OF CROSSHAIRS TO TRACE LINE
1620 PRINT "  AND INPUT THE POINT AT PRINTER"
1630 PRINT @1,26:1
1640 INPUT @1,27:M2,Y2
1650 PRINT @1,26:0
1660 PRINT @1:L$;
1670 MOVE @1:M1-M,Y2
1680 PRINT "GGGGG O.K"
1690 F=3
1700 T=2
1710 GO TO 340
1720 REM subtracted trace in RAM (ix)--> averaging routine starts
```

```
2340 FOR N=1 TO S1
2350 WRITE @33:X(N),Y(N)
2360 NEXT N
2370 REM graph on peripheral plotter ? (xv)
2380 PRINT "J DO YOU WANT A HARD COPY OF THE TRACE ?   ...(Y/N) ";
2390 INPUT A$
2400 IF A$="N" THEN 2620
2410 IF T=2 THEN 3360
2420 REM hardcopy on plotter (xvi)
2430 VIEWPORT 20,100,20,100
2440 WINDOW 0,250,0,100
2450 AXIS @1:10,10
2460 MOVE @1:100,95
2470 PRINT @1:B$
2480 MOVE @1:X(1),Y(1)
2490 FOR N=1 TO S1
2500 DRAW @1:X(N),Y(N)
2510 NEXT N
2520 IF P=0 THEN 2580
2530 IF P=0.5 THEN 3560
2540 IF P=5 THEN 4890
2550 IF P=6 THEN 4940
2560 IF P=7 THEN 5000
2570 IF P=8 THEN 2660
2580 REM more smoothing ? (xvii)
2590 PRINT "J DO YOU WANT MORE SMOOTHING ?   ...(Y/N) ";
2600 INPUT A$
2610 IF A$="Y" THEN 3080
2620 REM Curve fitting wanted ? (xviii)
2630 PRINT "J DO YOU WANT CURVE FITTING ? ...(Y/N) ";
2640 INPUT A$
2650 IF A$="Y" THEN 3410
2660 REM data scale altered ? (xviiia)
2670 PRINT "J DO YOU WANT TO ADJUST THE TRACE SCALE ? ...(Y/N) ";
2680 INPUT A$
2690 IF A$="N" THEN 2820
2700 REM trace amplitude adjustment (xviiib)
2710 PRINT "J WHAT AMPLITUDE IS THE TRACE TO BE ?   ";
2720 INPUT H3
2730 S2=1
2740 PRINT "JFINDING PRESENT (1,0) AMPLITUDE"
2750 P=9
2760 GOSUB 5110
2770 H4=Y(N1)
2780 FOR N=1 TO S1
2790 Y(N)=Y(N)*(H3/H4)
2800 NEXT N
2810 GO TO 1940
2820 REM more than two files to be averaged ? (xix)
2830 PRINT "J DO YOU WANT FILE AVERAGING ?   ...(Y/N) ";
2840 INPUT A$
2850 IF A$="N" THEN 3270
2860 D=2
2870 REM file averaging routine (xx)
2880 PRINT "J INPUT NUMBER OF FILE ";D;" TO BE AVERAGED   ";
2890 INPUT F
2900 FIND F
2910 READ @33:B$,S3
2920 PRINT "J SIZE OF ORIGINAL FILE = ";S1
2930 PRINT "J SIZE OF NEW FILE      = ";S3
2940 FOR N=1 TO S1
```

```
2950 READ @33:X2,Y2
2960 Y(N)=Y(N)+Y2
2970 NEXT N
2980 PRINT "J DO YOU WANT ANOTHER FILE ? Y/N ";
2990 INPUT A$
3000 IF A$="N" THEN 3030
3010 D=D+1
3020 GO TO 2870
3030 FOR N=1 TO S1
3040 Y(N)=Y(N)/D
3050 NEXT N
3060 GO TO 1820
3070 REM changing data back to the original ?  (xiiia)
3080 PRINT "J WILL YOU CONTINUE OR RESTART WITH ORIGINAL DATA ? (C
3090 INPUT A$
3100 IF A$="C" THEN 1820
3110 REM change data back to original  (xiiib)
3120 FOR N=1 TO S1
3130 X(N)=A(N)
3140 Y(N)=B(N)
3150 NEXT N
3160 IF A$="R" THEN 3180
3170 RETURN
3180 GO TO 1820
3190 REM routine for copying original data in memory (xa)
3200 DIM A(S1),B(S1)
3210 FOR N=1 TO S1
3220 A(N)=X(N)
3230 B(N)=Y(N)
3240 NEXT N
3250 IF F=3 THEN 1820
3260 RETURN
3270 REM end of program (xxi)
3280 PRINT "GGGJ YOU ARE AT THE END OF THE PROGRAM - DO YOU:"
3290 PRINT "J      (a) WANT TO EXIT     ...(INPUT 1)"
3300 PRINT "       (b) RETURN TO MENU   ...(INPUT 2)"
3310 PRINT "       (c) RERUN PROGRAM    ...(INPUT 3)"
3320 INPUT Z
3330 GO TO Z OF 3350,220,10
3340 PRINT @32,26:0
3350 STOP
3360 REM reset plotter l.left & u.right
3370 PRINT "J RESET PLOTTER L.LEFT & U.RIGHT, THEN KEY RETURN "
3380 INPUT A$
3390 T=1
3400 GO TO 2420
3410 REM New straight line BGND subtracted from data (xc)
3420 PRINT "JINPUT X VALUE FOR TROUGH BETWEEN PEAKS  ...";
3430 INPUT S2
3440 M=(Y(S1)-Y(1))/S1
3450 S=Y(1)
3460 FOR N=1 TO S1
3470 Y(N)=Y(N)-S
3480 Y(N)=Y(N)-(M*X(N)+M)
3490 NEXT N
3500 IF Y2=1 THEN 3520
3510 GO TO 3540
3520 Y2=0
3530 GO TO 1940
3540 P=0.5
3550 GO TO 2420
```

```
3560 GOSUB 3190
3570 REM Find peak (1,1)
3580 P1=1
3590 P=0
3600 GOSUB 5060
3610 REM Start curve fitting (xxii)
3620 DIM X4(6),Y4(6)
3630 M=-5
3640 FOR L=1 TO 6
3650 P1=1
3660 IF P1=1 THEN 3700
3670 GO TO 3740
3680 M=-1
3690 GO TO 3740
3700 IF L=1 THEN 3740
3710 N2=N3
3720 N2=N4
3730 H2=S1
3740 REM Find sum of squares of difference (R.H.S. of (1,1) )
3750 GOSUB 3110
3760 S=0
3770 T=0
3780 IF P<2 THEN 3850
3790 IF P=>5 THEN 3830
3800 N2=N4
3810 H2=S1
3820 GO TO 3850
3830 N2=N3
3840 H2=S1
3850 IF M=>0 THEN 3870
3860 H2=H2-M
3870 N2=N2+M
3880 FOR N=N2 TO H2
3890 IF N>S1 THEN 3980
3900 S=S+(X(N)-X(N2))^2*Y(N)
3910 T=T+Y(N)
3920 IF P1<>1 THEN 3960
3930 N=N+1
3940 NEXT N
3950 GO TO 3980
3960 N=N
3970 NEXT N
3980 REM Find standard deviation (1,1)
3990 S=SQR(2*S/(2*T-1)-0.0833)
4000 IF P=5 THEN 4020
4010 GO TO 4040
4020 MOVE @1:106,80
4030 PRINT @1:"STAN.DEV (1,1) = ";INT(S*100)/100
4040 REM Generate Gaussian + subtract from original data
4050 DIM G1(S1)
4060 FOR N=1 TO S1
4070 T=-1*(X(N)-X(N2))^2/(2*S^2)
4080 IF T<-10 THEN 4110
4090 G1(N)=Y(N2)*EXP(T)
4100 GO TO 4120
4110 G1(N)=0
4120 NEXT N
4130 REM Subtract generated curve from data
4140 FOR N=1 TO S1
4150 Y(N)=Y(N)-G1(N)
4160 NEXT N
```

```
4170 REM Find peak (1,0)
4180 P1=0
4190 GOSUB 5060
4200 REM Find standard deviation (1,0)
4210 S=0
4220 T=0
4230 FOR N=N1 TO H2
4240 S=S+(X(N)-X(N2))^2*Y(N)
4250 T=T+Y(N)
4260 NEXT N
4270 IF S/(T-1)-0.0833<=0 THEN 4290
4280 S=SQR(S/(T-1)-0.0833)
4290 IF P=5 THEN 4310
4300 GO TO 4330
4310 MOVE @1;106,75
4320 PRINT @1:"STAN.DEV (1,0) = ";INT(S*100)/100
4330 REM Generate gaussian curve for (1,0)
4340 DIM G(S1)
4350 FOR N=1 TO S1
4360 T=-1*(X(N)-X(N2))^2/(2*S^2)
4370 IF T<-10 THEN 4400
4380 G(N)=Y(N2)*EXP(T)
4390 GO TO 4410
4400 G(N)=0
4410 NEXT N
4420 REM Subtract gaussian and find sqr.root of sum of diff. squa
4430 Y1=0
4440 FOR N=1 TO S1
4450 Y1=Y1+SQR((Y(N)-G(N))^2)
4460 NEXT N
4470 PRINT Y1
4480 IF P=>2 THEN 4700
4490 REM Prepare for next loop (see ln 3180)
4500 X4(L)=N4+M
4510 Y4(L)=Y1
4520 M=M+2
4530 IF M<=0 THEN 4550
4540 H2=H2+M
4550 NEXT L
4560 REM Find lowest difference between calculated and data curve
4570 Y2=Y4(1)
4580 FOR L=1 TO 6
4590 IF Y2>Y4(L) THEN 4620
4600 NEXT L
4610 IF L=>6 THEN 4660
4620 Y2=Y4(L)
4630 N3=X4(L)
4640 IF L=>6 THEN 4660
4650 NEXT L
4660 REM Try values either side of optimum
4670 P=2
4680 N4=N3
4690 GO TO 3680
4700 IF Y1>Y2 THEN 4730
4710 N3=N3+M
4720 Y2=Y1
4730 IF P=>4 THEN 4770
4740 M=M+1
4750 P=P+1
4760 GO TO 3740
4770 IF P=5 THEN 4840
```

```
4780 REM Now have a value for centre of best fit curve
4790 REM Generate two gaussians
4800 M=0
4810 P=5
4820 N2=N3
4830 GO TO 3740
4840 REM Plot out both curves
4850 FOR N=1 TO S1
4860 Y(N)=G(N)
4870 NEXT N
4880 GO TO 2420
4890 FOR N=1 TO S1
4900 Y(N)=G1(N)
4910 NEXT N
4920 P=6
4930 GO TO 2480
4940 REM Add both curves together , and plot result
4950 FOR N=1 TO S1
4960 Y(N)=Y(N)+G(N)
4970 NEXT N
4980 P=7
4990 GO TO 2480
5000 REM Subtract composite curve from original data, and plot re
5010 FOR N=1 TO S1
5020 Y(N)=B(N)-Y(N)
5030 NEXT N
5040 P=8
5050 GO TO 2480
5060 REM Peak finding routine
5070 IF P1=1 THEN 5110
5080 H1=1
5090 H2=S2
5100 GO TO 5130
5110 H1=S2
5120 H2=S1
5130 Y2=0
5140 FOR N=H1 TO H2
5150 IF Y(N)>Y2 THEN 5170
5160 GO TO 5190
5170 Y2=Y(N)
5180 N1=N
5190 NEXT N
5200 IF P1=1 THEN 5260
5210 IF P=9 THEN 5260
5220 H2=2*N1
5230 N2=N1
5240 N1=1
5250 RETURN
5260 N3=N1
5270 N4=N1
5280 N2=N1
5290 RETURN
```

(b) MAKFIL.FOR.

This is a Fortran program which creates and manipulates data file. The options available are:

(1) Create a new data file This reads data in X/Y format from keyboard and saves data in a given file.

(2) Append an existing data file. This adds data to a file that already exists.

(3) Correct an existing data file. This corrects data already on file.

The program is fairly "User Friendly" but note that the unit number requested with the file name is normally 20, this gives access to the hard disk on DEC-20. The program is divided into the main program, which opens the various file types and calls the sub-routines which perform the various tasks such as reading or writing the data. All operations are conducted on the X and Y arrays, which are read or created first using XYREAD or XYWRITE manipulated with XYAPP and XYCHEK and finally written back to hard disk in the file named at the end of XYCHEK.

FLOW DIAGRAM FOR MAKFIL.FOR

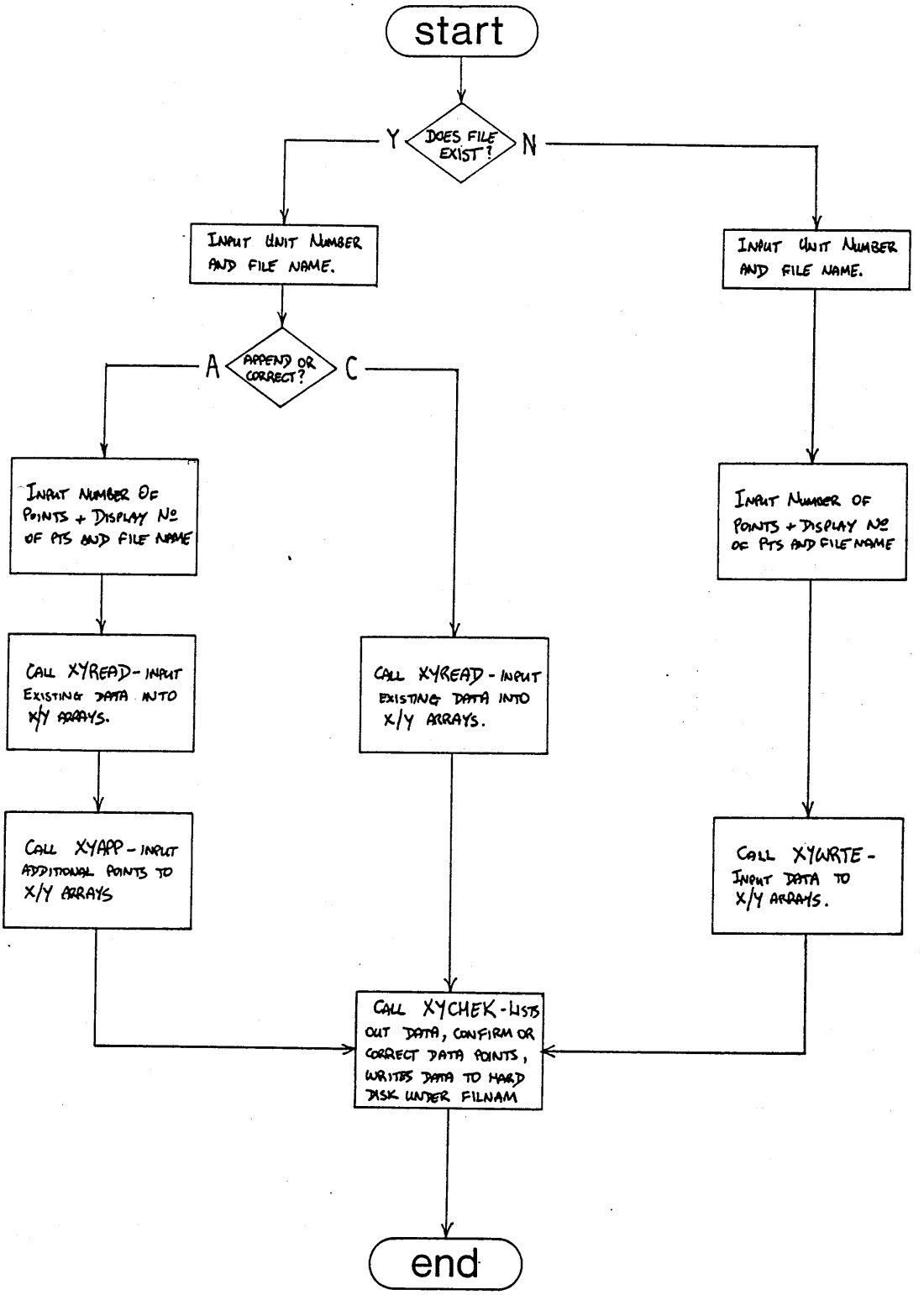

MAKFIL.FOR

```
C       This is a program to create a data file, FILNAM, which must be
C       inputted in the format:

C                                       ******.DAT

        PROGRAM CORE

C       Set up type of constants

        REAL XARRAY,YARRAY
        INTEGER ACCESS,L,N,NOPTS,TOTPTS
        CHARACTER*10 FILNAM,AORC*1,YORN*1

        COMMON /COMM1/ NOPTS,XARRAY(1000),YARRAY(1000) /COMM2/ TOTPTS

C       Does the file alredy exist, and if so run APPEND subroutine

        WRITE (5,5)
 5      FORMAT(/2X,'DOES FILE EXIST',5X,'(a) Y',/22X,'(b) N',
     2 /2X,'Input answer (Y/N) ... ',$)
        READ (5,6) YORN
 6      FORMAT (A1)

C       Input value for unit to be accessed (usually 20 for disk).

        WRITE (5,10)
 10     FORMAT (/2X,'INPUT UNIT NUMBER [SPACE] AND FILE NAME :',$)
        READ (5,20) ACCESS,FILNAM
 20     FORMAT (I2,1X,A10)

C       If file does exist, will you append or correct it ?

        IF ((YORN.EQ.'N').OR.(YORN.EQ.'n')) GOTO 22
        WRITE (5,21)
 21     FORMAT (/2X,'WILL YOU APPEND OR CORRECT FILE ? ... (A/C) ',$)
        READ (5,6) AORC
        NOPTS=0
        IF ((AORC.EQ.'C').OR.(AORC.EQ.'c')) GOTO 60

C       Input the number of point-pairs to be entered.

 22     WRITE (5,25)
 25     FORMAT (/2X,'INPUT NUMBER OF POINTS YOU WILL ENTER ... ',$)
        READ (5,*) NOPTS

C       Display input data on screen

        WRITE (5,30) ACCESS,FILNAM,NOPTS
 30     FORMAT (/2X,'UNIT ACCESSED  =    ',I2,/2X,'FILE',10X,' =    ',A10,
     2  /2X,'NO OF POINTS   =    ',I$,/1X)

C       Access relevant unit

        IF ((YORN.EQ.'Y').OR.(YORN.EQ.'y')) GOTO 40

C       Call subroutine to write data to file (XYWRTE)
```

```
C*************************************************************

      SUBROUTINE XYAPP (ACCESS,FILNAM,N)
      REAL XARRAY,YARRAY
      INTEGER ACCESS,L,N,TOTPTS
      CHARACTER *(*) FILNAM,YORN*1

      COMMON /COMM1/ NOPTS,XARRAY(1000),YARRAY(1000)
      COMMON /COMM2/ TOTPTS

      DO 40,L=N+1,TOTPTS
        WRITE (5,30)
 30     FORMAT (/2X,'INPUT DATA PAIR      ',$)
        READ (5,*) XARRAY(L),YARRAY(L)
 40   CONTINUE

      RETURN
      END

C*************************************************************

      SUBROUTINE XYCHEK (ACCESS)
      REAL XARRAY,YARRAY
      INTEGER ACCESS,NOPTS,L,TOTPTS,TOPPGE,ENDPGE
      CHARACTER*1 CORL,CORD,LOOP

      COMMON /COMM1/ NOPTS,XARRAY(1000),YARRAY(1000)
      COMMON /COMM2/ TOTPTS

C     Set up parameters for data checking

      TOPPGE=1
      ENDPGE=20
      LOOP='C'

C     Start checking and correcting routines

      DO WHILE (LOOP.EQ.'C')

      WRITE (5,20)
 20   FORMAT (//15X,'DATA IN FILE')
      DO 40,L=TOPPGE,ENDPGE
        IF (L.GT.TOTPTS) GOTO 160
        WRITE (5,30) L,XARRAY(L),YARRAY(L)
 30     FORMAT (/1X,I5,3X,2F9)
 40   CONTINUE

 50   WRITE (5,60)
 60   FORMAT (//2X,'CHANGE DATA, LIST ANOTHER PAGE OF DATA,
     2 OR LEAVE THE PROGRAM ? ...  (C/P OR L) ',$)
      READ (5,65) CORL
 65   FORMAT (1A)
      IF ((CORL.EQ.'L').OR.(CORL.EQ.'l')) GOTO 100
      IF ((CORL.EQ.'P').OR.(CORL.EQ.'p')) GOTO 140

      WRITE (5,70)
 70   FORMAT (/2X,'INPUT THE PAIR NUMBER  ... ',$)
      READ (5,75) NOPTS
 75   FORMAT (I5)

C     Choose correction or deletion of specified data
```

```
      WRITE (5,67)
 67   FORMAT (/2X,'WILL YOU CORRECT OR DELETE DATA ? ...(C/D) ',$)
      READ (5,65) CORD
      IF (.(CORD.EQ.'D').OR.(CORD.EQ.'d')) GOTO 90

C     Start correction routine

      WRITE (5,80)
 80   FORMAT (/2X,'INPUT CORRECT VALUES (GIVE THE PAIR) ... ',$)
      READ (5,*) XARRAY(NOPTS),YARRAY(NOPTS)
      GOTO 95

C     Deletion routine starts here

 90   DO L=NOPTS,TOTPTS
        IF (L.EQ.TOTPTS) THEN
          XARRAY(L)=0
          YARRAY(L)=0
        ELSE
          XARRAY(L)=XARRAY(L+1)
          YARRAY(L)=YARRAY(L+1)
        END IF
      END DO

      TOTPTS=TOTPTS-1
      ENDPGE=ENDPGE-1

C     Loop back to start of correction loop

 95   END DO

C     Store data file

 100  REWIND ACCESS

      WRITE (ACCESS,*) TOTPTS
      DO 120,L=1,TOTPTS
        WRITE (ACCESS,*) XARRAY(L),YARRAY(L)
 120  CONTINUE

      RETURN

 140  TOPPGE=TOPPGE+20
      ENDPGE=ENDPGE+20
      GOTO 95

 160  WRITE (5,165)
 165  FORMAT (/15X,'END OF DATA')
      GOTO 50

      END
@
```

(c) SHARPFIT.FOR, FITDAT.FOR and FORFIT.FOR.

These three routines are all very similar, they all involve fitting a cubic spline to a series of points defined in X/Y co-ordinates, evaluating the spline and plotting out the result. The overall structure of the program is the same for these routines, and all three versions used NAG library routines E02BAF to find the β/spline co-efficients E02BCF to evaluate the co-efficients. The result is stored in X/Y arrays. The differences lie in the number and method of positioning of the knots, the degree of evaluation of splines and the plotting of the data. The flow chart indicates with dashed lines where these differences occur, a dashed line to the right indicates the path taken by the FORFIT.FOR, and to the left by SHARPFIT.FOR.. FITDAT.FOR always takes the central path. The name with the line gives the program which differs at this point. A summary of these programs is as follows.

In the case of SHARFIT.FOR. and FITDAT.FOR, hard copies of the graphs were generated by "Simpleplot", a graphics package provided by the Academic Computing Service at the Milton Keynes campus. The graphs were captured on the screen by using segments, these could be plotted out on a Tektronix 4662 later on. With FOR.FITDAT the data was transmitted back to the 6130 from DEC-20 and the tbasic program "plot" run to generate the graphics, these two were captured by segments and plotted. Note in this case the three different colours had to be captured by three different segments, each segment was plotted separately and the pen changed between each. The differences between the three programs are as follows.

FORFIT.FOR. This is used for fitting a cubic spline to Fourier summation data (eg Fig 5.3.1). It takes input from DUMP.DAT, calculates

the first derivative of the cumulative data (DUMP.DAT is a cumulative file), plots out the ideal curve and first derivative of the spline of the experimental data. The resulting fitted data are put in the file FITFOR.DAT for transmission back to the 6130 using the "tip" command.

FITDAT.FOR. Used to fit a curve to the $\Delta d(1,0)$ seen with addition of PPi (Figs 3.3.1 and 3.3.2). Reads data from a data file compiled using MAKFIL.FOR, calculates the cubic spline together with its first and second derivatives. Plots out the original points along with the fit and the first derivative.

SHARPFIT.FOR. Used to fit a curve to the sharpness vs S data (eg Figs 3.3.4 and 3.3.5). Reads data from a data file created using MAKFIL.FOR. Note all dummy point weights are set to 1 by the program, but the option to change these is given, and in practice the weights used were 0.3. The routine calculates the spline with the first and second derivatives, but only the fit and first derivative are plotted.

FLOW DIAGRAM FOR ✱ FIT.FOR

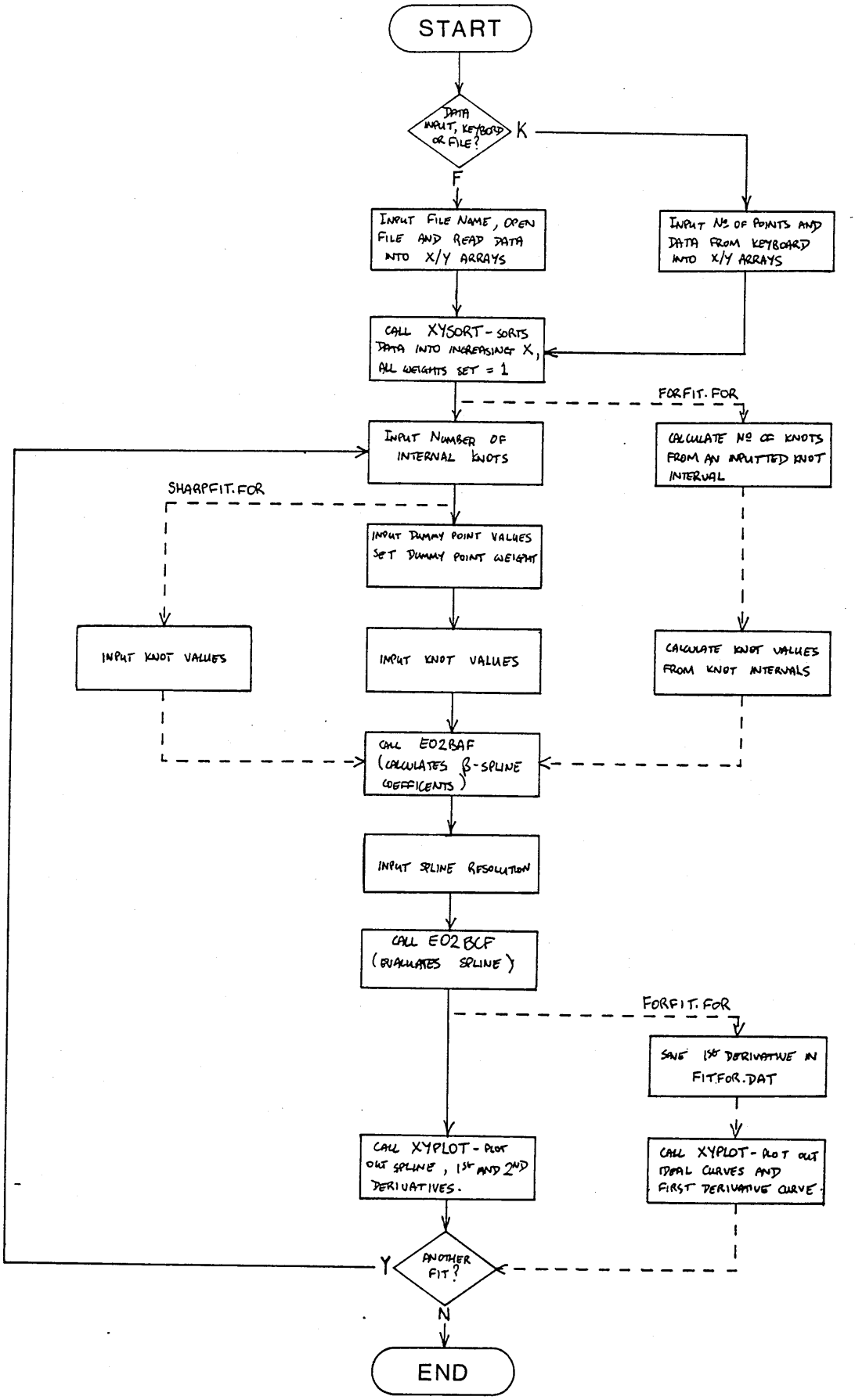

FITDAT.FOR

```
C       This is a program to fit a cubic spline to a series of inputs
C       in (x,y) format, taken either from keyboard or diskfile.

        PROGRAM CORE

        REAL C(100),SS,WORK1(1000),WORK2(4,100),K(100),
     2   W(1000),X(1000),Y(1000),XMIN,XMAX,XINCRE,XSPLIN(5),XEVAL,
     3   XRES(1000),YRES(1000),XDER(1000),YDER(1000),XDER2(1000),
     4   YDER2(1000),XVAL,YVAL,WEIGHT
        INTEGER ALTRET,IFAIL,L,L2,M,NCAP,NCAP2,NCAP3,NCAP7,NOKNOT,
     2  LEFT
        CHARACTER*1 FORK,FILNAM*10

        COMMON /ARRAY1/ W,X,Y
        COMMON /ARRAY2/ XRES,YRES,XDER,YDER,XDER2,YDER2


C       Will data input be from keyboard or diskfile ?

        WRITE (5,20)
 20     FORMAT (/2X,'INPUT DATA FROM KEYBOARD OR DISKFILE ? (K/F) ',$)
        READ (5,40) FORK
 40     FORMAT (A1)

C       Either read from keyboard or file.

        IF ((FORK.EQ.'F').OR.(FORK.EQ.'f')) GOTO 100

        WRITE (5,60)
 60     FORMAT (/2X,'INPUT NUMBER OF DATA POINTS.  ',$)
        READ (5,*) M

        DO 80,L=1,M
          WRITE (5,70)
 70       FORMAT (/2X,'INPUT DATA PAIR ... ',$)
          READ (5,*) X(L),Y(L)
 80     CONTINUE
        GOTO 200

C       File opened and data read

 100    WRITE (5,120)
 120    FORMAT (/2X,'INPUT DATA FILE TO BE FITTED.  ',$)
        READ (5,140) FILNAM
 140    FORMAT (A10)
        OPEN (UNIT=20,FILE=FILNAM,STATUS='OLD')

        READ (20,*) M
        READ (20,*) (X(L),Y(L),L=1,M)

C       Call subroutine XYSORT which arranges data sequentially w.r.t X
```

```
 200    CALL XYSORT (M)

        IF ((FORK.EQ.'K').OR.(FORK.EQ.'k')) GOTO 240

 220    CLOSE (20)

C       Input number of internal knots, define total no of knots.

 240    WRITE (5,241)
 241    FORMAT (/2X,'INPUT NUMBER OF INTERNAL KNOTS.  ',$)
        READ (5,*) NOKNOT

        WRITE (5,243)
 243    FORMAT(/2X,'INPUT FIRST & LAST POINT WEIGHTINGS.    ',$)
        READ (5,*) WEIGHT
        DO 244,L=1,3
          W(L)=WEIGHT
          W(M-L+1)=WEIGHT
 244    CONTINUE

        ALTRET=0
        NCAP=NOKNOT+1
        NCAP2=NCAP+2
        NCAP3=NCAP+3
        NCAP7=NCAP+7

        IF (NOKNOT.EQ.0) GOTO 300

C       Input to array K the values of the internal knots.

        WRITE (5,245)
 245    FORMAT (//3X,'INPUT INTERNAL KNOT VALUES.')
        TYPE *,'  ============================='
        WRITE (5,250)
 250    FORMAT (/2X,'THESE MUST LIE IN THE RANGE   Xmin < VALUE < Xmax'

        DO 280,L=5,NCAP3
          WRITE (5,260)
 260      FORMAT (/2X,'INPUT KNOT VALUE ... ',$)
          READ (5,*) K(L)
 280    CONTINUE

C       Set IFAIL=0 and call spline fitting routine

 300    IFAIL=0

        CALL E02BAF(M,NCAP7,X,Y,W,K,WORK1,WORK2,C,SS,IFAIL)

        IF (IFAIL.NE.0) THEN
          CALL MESSGE (IFAIL,XINCRE)
        END IF

        L=1
        WRITE (5,*) L,J,C(1)
        DO 360,L=2,NCAP2
          L2=L+2
          WRITE (5,*) L,K(L2),C(L)
 360    CONTINUE
        WRITE (5,*) NCAP3,J,C(NCAP3)

C       Evaluate spline at a resolution of XINCRE
```

```
      WRITE (5,370)
370   FORMAT (/2X,'RESOLUTION OF SPLINE EVALUATION.   ',$)
      READ (5,*) XINCRE

       XMIN=X(1)
       XMAX=X(M)
      L=1

      OPEN(UNIT=20,FILE='SPLINCON.DAT',STATUS='NEW',DISPOSE='SAVE')
      WRITE(20,*)  (X(M-4)-X(4))/XINCRE

      DO 400,XVAL=XMIN,XMAX,XINCRE
        XEVAL=XVAL
        IFAIL=0
        LEFT=1

        CALL E02BCF  (NCAP7,K,C,XEVAL,LEFT,XSPLIN,IFAIL)

        IF  (IFAIL.NE.0)  THEN
          CALL MESSGE  (IFAIL,XINCRE)
        END IF

        IF  ((XVAL.GT.X(3)).AND.(XVAL.LT.X(M-3)))  THEN
          WRITE(20,*)  XEVAL,XSPLIN(1)
        END IF

        XRES(L)=XEVAL
        YRES(L)=XSPLIN(1)
        XDER(L)=XEVAL
        YDER(L)=XSPLIN(2)
        XDER2(L)=XEVAL
        YDER2(L)=XSPLIN(3)
        L=L+1

400   CONTINUE

      L=L-1

C     Call graph plotting subroutine, XYPLOT.

      CALL XYPLOT  (M,L,ALTRET,*240)

      STOP

      END

C*********************************************************************

      SUBROUTINE XYSORT  (M)

      REAL W(1000),XVAL,X(1000),YVAL,Y(1000)
      INTEGER C,M,P,POINT

      COMMON /ARRAY1/ W,X,Y

C     Start sorting data.

      DO 100,POINT=1,M
        XVAL=X(POINT)
        YVAL=Y(POINT)
        W(POINT)=1 ! All weights set equal to 1 by this line
         DO 80,P=1,POINT
```

```
            IF (XVAL.LE.X(P)) THEN
                DO 60,C=POINT,(P+1),-1
                  X(C)=X(C-1)
                  Y(C)=Y(C-1)
60              CONTINUE
              X(P)=XVAL
              Y(P)=YVAL
              C=0
              GOTO 100
            END IF
80        CONTINUE
        X(POINT)=XVAL
        Y(POINT)=YVAL
100   CONTINUE


      RETURN

      END

C*****************************************************************

      SUBROUTINE XYPLOT (M,L,ALTRET,*)

      REAL W(1000),X(1000),Y(1000),XRES(1000),YRES(1000),
     2  XDER(1000),YDER(1000),XDER2(1000),YDER2(1000)
      INTEGER ALTRET,L,M,XVAL
      CHARACTER*1 RORE

      COMMON /ARRAY1/ W,X,Y
      COMMON /ARRAY2/ XRES,YRES,XDER,YDER,XDER2,YDER2

      XVAL=L

C     Define plot axes (limits and type)

        CALL SCALES(1.7,4.0,1,-0.5,0.5,1)

        CALL AXES('SARCOMERE LENGTH',16,'d(1,0)/d(1,0)',13)

         DO 20,L=4,M-3
           CALL MARK PT(X(L),Y(L),1)
20       CONTINUE

C     Plot fitted curve.

         CALL CV TYPE(1)
         CALL DRAW CV(XRES,YRES,XVAL)
         CALL DRAW CV(XDER,YDER,XVAL)
         CALL DRAW CV(XDER2,YDER2,XVAL)

C     End plotting routine.

         CALL ENDPLT

C     Will you end fitting,or try again?

      WRITE (5,40)
40    FORMAT (/2X,'RETRY USING DIFFERENT KNOTS, OR END ? ...(R/E) ',$)
      READ (5,60) RORE
60    FORMAT (A1)
```

```
      IF ((RORE.EQ.'R').OR.(RORE.EQ.'r')) THEN
        ALTRET=1
        CALL DEVNO(4)
      END IF

      RETURN (ALTRET)

      END

C*****************************************************************

      SUBROUTINE MESSGE (IFAIL,XINCRE)

      REAL XINCRE
      INTEGER IFAIL

      TYPE *,'ROUTINE FAILED'

C     Read appropriate error message for value of IFAIL

      IF ((IFAIL.EQ.2).AND.(XINCRE.NE.0)) GOTO 400

      GOTO IFAIL,(100,200,300,400,500)

 100  WRITE (5,110)
 110  FORMAT (/2X,'The values you gave for the internal knots are not,
     2 within the constraints of the routine. They must be:,
     3  (a) In non-decreasing order,
     4  (b) Of a value that falls within the data range')
      GOTO 600

 200  WRITE (5,210)
 210  FORMAT (/2X,'The weights are not all positive in value')
      GOTO 600

 300  WRITE (5,310)
 310  FORMAT (/2X,'The depedent variable data array has data within,
     2 it that is in descending order, check XYSORT subroutine,
     3 for a logical error.(Good luck!)')
      GOTO 600

 400  WRITE (5,410)
 410  FORMAT (/2X,'The number of interior knots you have chosen,
     2 is less than zero. There is no unique solution under these,
     3 conditions. I suggest you re-run the program.')
      GOTO 600

 500  WRITE (5,510)
 510  FORMAT (/2X,'You have violated the Schoenberg-Whitney con-,
     2 ditions (naughty,naughty). You MUST have a sequence in the,
     3 data where the value of the knot is:,
     4  (a) At least greater than the previous knot value,
     5  (b) Such that it lies in a range of five data points.,
     6  This in effect means that there are regions where there,
     7 are too many knots relative to the data.')
      GOTO 600

 600  RETURN

      END
```

@

SHARPFIT.FOR

```
C       This is a program to fit a cubic spline to a series of inputs
C       in (x,y) format, taken either from keyboard or diskfile.

        PROGRAM CORE

        REAL C(100),SS,WORK1(1000),WORK2(4,100),K(100),
     2   W(1000),X(1000),Y(1000),XMIN,XMAX,XINCRE,XSPLIN(5),XEVAL,
     3   XRES(1000),YRES(1000),XDER(1000),YDER(1000),XDER2(1000),
     4   YDER2(1000),XVAL,YVAL,WEIGHT
        INTEGER ALTRET,IFAIL,L,L2,M,NCAP,NCAP2,NCAP3,NCAP7,NOKNOT,
     2   LEFT
        CHARACTER*1 FORK,FILNAM*10

        COMMON /ARRAY1/ W,X,Y
        COMMON /ARRAY2/ XRES,YRES,XDER,YDER,XDER2,YDER2


C       Will data input be from keyboard or diskfile ?

        WRITE (5,20)
 20     FORMAT (/2X,'INPUT DATA FROM KEYBOARD OR DISKFILE ? (K/F) ',$)
        READ (5,40) FORK
 40     FORMAT (A1)

C       Either read from keyboard or file.

        IF ((FORK.EQ.'F').OR.(FORK.EQ.'f')) GOTO 100

        WRITE (5,60)
 60     FORMAT (/2X,'INPUT NUMBER OF DATA POINTS.  ',$)
        READ (5,*) M

        DO 80,L=1,M
          WRITE (5,70)
 70       FORMAT (/2X,'INPUT DATA PAIR ... ',$)
          READ (5,*) X(L),Y(L)
 80     CONTINUE
        GOTO 200

C       File opened and data read

 100    WRITE (5,120)
 120    FORMAT (/2X,'INPUT DATA FILE TO BE FITTED.  ',$)
        READ (5,140) FILNAM
 140    FORMAT (A10)
        OPEN (UNIT=20,FILE=FILNAM,STATUS='OLD')

        READ (20,*) M
        READ (20,*) (X(L),Y(L),L=1,M)

C       Call subroutine XYSORT which arranges data sequentially w.r.t X.

 200    CALL XYSORT (M)
```

```
      IF ((FORK.EQ.'K').OR.(FORK.EQ.'k')) GOTO 240

  220 CLOSE (20)

C     Input number of internal knots, define total no of knots.

  240 WRITE (5,241)
  241 FORMAT (/2X,'INPUT NUMBER OF INTERNAL KNOTS.  ',$)
      READ (5,*) NOKNOT

      WRITE (5,243)
  243 FORMAT(/2X,'INPUT FIRST & LAST POINT WEIGHTINGS.   ',$)
      READ (5,*) WEIGHT
      DO 244,L=1,3
        W(L)=WEIGHT
        W(M-L+1)=WEIGHT
  244 CONTINUE

      ALTRET=0
      NCAP=NOKNOT+1
      NCAP2=NCAP+2
      NCAP3=NCAP+3
      NCAP7=NCAP+7

      IF (NOKNOT.EQ.0) GOTO 300

C     Input to array K the values of the internal knots.

      WRITE (5,245)
  245 FORMAT (//3X,'INPUT INTERNAL KNOT VALUES.')
      TYPE *,'  ============================'
      WRITE (5,250)
  250 FORMAT (/2X,'THESE MUST LIE IN THE RANGE   Xmin < VALUE < Xmax'

      DO 280,L=5,NCAP3
        WRITE (5,260)
  260   FORMAT (/2X,'INPUT KNOT VALUE ... ',$)
        READ (5,*) K(L)
  280 CONTINUE

C     Set IFAIL=0 and call spline fitting routine

  300 IFAIL=0

      CALL E02BAF(M,NCAP7,X,Y,W,K,WORK1,WORK2,C,SS,IFAIL)

      IF (IFAIL.NE.0) THEN
        CALL MESSGE (IFAIL,XINCRE)
      END IF

      L=1
      WRITE (5,*) L,J,C(1)
      DO 360,L=2,NCAP2
        L2=L+2
        WRITE (5,*) L,K(L2),C(L)
  360 CONTINUE
      WRITE (5,*) NCAP3,J,C(NCAP3)

C     Evaluate spline at a resolution of XINCRE
```

```
      WRITE (5,370)
370   FORMAT (/2X,'RESOLUTION OF SPLINE EVALUATION.  ',$)
      READ (5,*) XINCRE

      XMIN=X(4)
      XMAX=X(M-3)
      L=1

      DO 400,XVAL=XMIN,XMAX,XINCRE
        XEVAL=XVAL
        IFAIL=0
        LEFT=1

        CALL E02BCF (NCAP7,K,C,XEVAL,LEFT,XSPLIN,IFAIL)

        IF (IFAIL.NE.0) THEN
          CALL MESSGE (IFAIL,XINCRE)
        END IF

        XRES(L)=XEVAL
        YRES(L)=XSPLIN(1)
        XDER(L)=XEVAL
        YDER(L)=XSPLIN(2)
        XDER2(L)=XEVAL
        YDER2(L)=XSPLIN(3)
        L=L+1

400   CONTINUE

      L=L-1

C     Call graph plotting subroutine, XYPLOT.

      CALL XYPLOT (M,L,ALTRET,*240)

      STOP

      END

C*********************************************************************

      SUBROUTINE XYSORT (M)

      REAL W(1000),XVAL,X(1000),YVAL,Y(1000)
      INTEGER C,M,P,POINT

      COMMON /ARRAY1/ W,X,Y

C     Start sorting data.

      DO 100,POINT=1,M
        XVAL=X(POINT)
        YVAL=Y(POINT)
        W(POINT)=1 ! All weights set equal to 1 by this line
         DO 80,P=1,POINT
            IF (XVAL.LE.X(P)) THEN
                DO 60,C=POINT,(P+1),-1
                  X(C)=X(C-1)
                  Y(C)=Y(C-1)
60              CONTINUE
              X(P)=XVAL
              Y(P)=YVAL
```

```
                C=0
                GOTO 100
              END IF
 80         CONTINUE
          X(POINT)=XVAL
          Y(POINT)=YVAL
 100    CONTINUE

        RETURN

        END

C*****************************************************************

        SUBROUTINE XYPLOT (M,L,ALTRET,*)

        REAL W(1000),X(1000),Y(1000),XRES(1000),YRES(1000),
     2  XDER(1000),YDER(1000),XDER2(1000),YDER2(1000)
        INTEGER ALTRET,L,M,XVAL
        CHARACTER*1 RORE

        COMMON /ARRAY1/ W,X,Y
        COMMON /ARRAY2/ XRES,YRES,XDER,YDER,XDER2,YDER2

        XVAL=L

C       Define plot axes (limits and type)

          CALL SCALES(1.7,4.0,1,-0.5,0.5,1)

          CALL AXES('SARCOMERE LENGTH',16,'d(1,0)/d(1,0)',13)

           DO 20,L=4,M-3
             CALL MARK PT(X(L),Y(L),1)
 20        CONTINUE

C       Plot fitted curve.

           CALL CV TYPE(1)
           CALL DRAW CV(XRES,YRES,XVAL)
           CALL DRAW CV(XDER,YDER,XVAL)
           CALL DRAW CV(XDER2,YDER2,XVAL)

C       End plotting routine.

           CALL ENDPLT

C       Will you end fitting,or try again?

        WRITE (5,40)
 40     FORMAT (/2X,'RETRY USING DIFFERENT KNOTS, OR END ? ...(R/E) ',$)
        READ (5,60) RORE
 60     FORMAT (A1)

        IF ((RORE.EQ.'R').OR.(RORE.EQ.'r')) THEN
          ALTRET=1
          CALL DEVNO(4)
        END IF

        RETURN (ALTRET)

        END
```

```
C*************************************************************************

      SUBROUTINE MESSGE (IFAIL,XINCRE)

      REAL XINCRE
      INTEGER IFAIL

      TYPE *,'ROUTINE FAILED'

C     Read appropriate error message for value of IFAIL

      IF ((IFAIL.EQ.2).AND.(XINCRE.NE.0)) GOTO 400

      GOTO IFAIL,(100,200,300,400,500)

 100  WRITE (5,110)
 110  FORMAT (/2X,'The values you gave for the internal knots are not.
     2 within the constraints of the routine. They must be:,
     3  (a) In non-decreasing order,
     4  (b) Of a value that falls within the data range')
      GOTO 600

 200  WRITE (5,210)
 210  FORMAT (/2X,'The weights are not all positive in value')
      GOTO 600

 300  WRITE (5,310)
 310  FORMAT (/2X,'The depedant variable data array has data within,
     2 it that is in descending order, check XYSORT subroutine,
     3 for a logical error.(Good luck!)')
      GOTO 600

 400  WRITE (5,410)
 410  FORMAT (/2X,'The number of interior knots you have chosen,
     2 is less than zero. There is no unique solution under these,
     3 conditions. I suggest you re-run the program.')
      GOTO 600

 500  WRITE (5,510)
 510  FORMAT (/2X,'You have violated the Schoenberg-Whitney con-,
     2 ditions (naughty,naughty). You MUST have a sequence in the,
     3 data where the value of the knot is:,
     4  (a) At least greater than the previous knot value,
     5  (b) Such that it lies in a range of five data points.,
     6  This in effect means that there are regions where there,
     7 are too many knots relative to the data.')
      GOTO 600

 600  RETURN

      END
@
```

FORFIT.FOR

```
C       This is a program to fit a cubic spline to a series of inputs
C       in (x,y) format, taken either from keyboard or diskfile.

        PROGRAM CORE

        REAL C(200),SS,WORK1(2000),WORK2(4,200),K(200),
     2  W(2000),X(2000),Y(2000),XMIN,XMAX,XINCRE,XSPLIN(5),XEVAL,
     3  XRES(2000),YRES(2000),XDER(2000),YDER(2000),XDER2(2000),
     4  YDER2(2000),KI(2000),XVAL,YVAL,WEIGHT
        INTEGER ALTRET,IFAIL,L,L2,M,NCAP,NCAP2,NCAP3,NCAP7,NOKNOT,
     2  LEFT,KADD,KINT
        CHARACTER*1 FORK,FILNAM*10

        COMMON /ARRAY1/ W,X,Y
        COMMON /ARRAY2/ KI,XRES,YRES,XDER,YDER,XDER2,YDER2

C       File opened and data read

  100   WRITE (5,120)
  120   FORMAT (/2X,'INPUT DATA FILE TO BE FITTED.  ',$)
        READ (5,140) FILNAM
  140   FORMAT (A10)
        OPEN (UNIT=20,FILE=FILNAM,STATUS='OLD')

        READ (20,*) M
        READ (20,*) (X(L),Y(L),KI(L),L=1,M+1)

C       Call subroutine XYSORT which arranges data sequentially w.r.t X

  200   CALL XYSORT (M)

        IF ((FORK.EQ.'K').OR.(FORK.EQ.'k')) GOTO 240

  220   CLOSE (20)

C       Define total no of knots.

  240   WRITE (5,241)
  241   FORMAT (/2X,'INPUT KNOT INTERVAL.  ',$)
        READ (5,*) KINT

        NOKNOT=INT((1000/KINT)+1)
        K(5)=10
        K(6)=20
        KADD=KINT

        ALTRET=0
        NCAP=NOKNOT+1
        NCAP2=NCAP+2
        NCAP3=NCAP+3
        NCAP7=NCAP+7

C       Input to array K the values of the internal knots.
```

```
      DO 280,L=7,NCAP3
        K(L)=K+ADD
        KADD=KADD+KINT
280   CONTINUE

C     Set IFAIL=0 and call spline fitting routine

300   IFAIL=0

      CALL E02BAF(M,NCAP7,X,Y,W,K,WORK1,WORK2,C,SS,IFAIL)

      IF (IFAIL.NE.0) THEN
        CALL MESSGE (IFAIL,XINCRE)
      END IF

C     Evaluate spline at a resolution of XINCRE

      WRITE (5,370)
370   FORMAT (/2X,'RESOLUTION OF SPLINE EVALUATION.  ',$)
      READ (5,*) XINCRE

       XMIN=X(1)
       XMAX=X(M)
      L=1

      OPEN(UNIT=20,FILE='FITFOR.DAT',STATUS='NEW',DISPOSE='SAVE')
      WRITE(20,*) M/XINCRE

      DO 400,XVAL=XMIN,XMAX,XINCRE
        XEVAL=XVAL
        IFAIL=0
        LEFT=1

        CALL E02BCF (NCAP7,K,C,XEVAL,LEFT,XSPLIN,IFAIL)

        IF (IFAIL.NE.0) THEN
          CALL MESSGE (IFAIL,XINCRE)
        END IF

        WRITE(20,*) XEVAL-1,XSPLIN(2)

        XRES(L)=XEVAL
        YRES(L)=XSPLIN(1)
        XDER(L)=XEVAL
        YDER(L)=XSPLIN(2)
        XDER2(L)=XEVAL
        YDER2(L)=XSPLIN(3)
        L=L+1

400   CONTINUE

      CLOSE (20)

      L=L-1

C     Call graph plotting subroutine, XYPLOT.

      CALL XYPLOT (M,L,ALTRET,*240)

      STOP

      END
```

```
C*************************************************************************

      SUBROUTINE XYSORT (M)

      REAL W(2000),XVAL,X(2000),YVAL,Y(2000)
      INTEGER C,M,P,POINT

      COMMON /ARRAY1/ W,X,Y

C     Start sorting data.

      DO 100,POINT=1,M
        XVAL=X(POINT)
        YVAL=Y(POINT)
        W(POINT)=1 ! All weights set equal to 1 by this line
         DO 80,P=1,POINT
            IF (XVAL.LE.X(P)) THEN
                DO 60,C=POINT,(P+1),-1
                  X(C)=X(C-1)
                  Y(C)=Y(C-1)
60              CONTINUE
              X(P)=XVAL
              Y(P)=YVAL
              C=0
              GOTO 100
            END IF
80        CONTINUE
        X(POINT)=XVAL
        Y(POINT)=YVAL
100   CONTINUE


      RETURN

      END

C*************************************************************************

      SUBROUTINE XYPLOT (M,L,ALTRET,*)

      REAL W(2000),X(2000),Y(2000),XRES(2000),YRES(2000),
     2  XDER(2000),YDER(2000),XDER2(2000),YDER2(2000),KI(2000)
      INTEGER ALTRET,L,M,XVAL
      CHARACTER*1 RORE

      COMMON /ARRAY1/ W,X,Y
      COMMON /ARRAY2/ KI,XRES,YRES,XDER,YDER,XDER2,YDER2

      XVAL=L

C     Define plot axes (limits and type)

        CALL SCALES(0,XRES(M),1,0,KI(1),1)

        CALL AXES ('nm',2,'y',1)

C     Plot fitted curve.

         CALL CV TYPE(1)
         CALL DRAW CV(X,KI,XVAL)
         CALL DRAW CV(XDER,YDER,XVAL)
```

```
C       End plotting routine.

           CALL ENDPLT

C       Will you end fitting,or try again?

        WRITE (5,40)
 40     FORMAT (/2X,'RETRY USING DIFFERENT KNOTS, OR END ? ...(R/E) ',$)
        READ (5,60) RORE
 60     FORMAT (A1)

        IF ((RORE.EQ.'R').OR.(RORE.EQ.'r')) THEN
          ALTRET=1
          CALL REVNO(4)
        END IF

        RETURN (ALTRET)

        END

C*************************************************************

        SUBROUTINE MESSGE (IFAIL,XINCRE)

        REAL XINCRE
        INTEGER IFAIL

        TYPE *,'ROUTINE FAILED'

C       Read appropriate error message for value of IFAIL

        IF ((IFAIL.EQ.2).AND.(XINCRE.NE.0)) GOTO 400

        GOTO IFAIL,(100,200,300,400,500)

 100    WRITE (5,110)
 110    FORMAT (/2X,'The values you gave for the internal knots are not,
     2 within the constraints of the routine. They must be;,
     3   (a) In non-decreasing order,
     4   (b) Of a value that falls within the data range')
        GOTO 600

 200    WRITE (5,210)
 210    FORMAT (/2X,'The weights are not all positive in value')
        GOTO 600

 300    WRITE (5,310)
 310    FORMAT (/2X,'The depedant variable data array has data within,
     2 it that is in descending order, check XYSORT subroutine,
     3 for a logical error.(Good luck!)')
        GOTO 600

 400    WRITE (5,410)
 410    FORMAT (/2X,'The number of interior knots you have chosen,
     2 is less than zero. There is no unique solution under these,
     3 conditions. I suggest you re-run the program.')
        GOTO 600

 500    WRITE (5,510)
 510    FORMAT (/2X,'You have violated the Schoenberg-Whitney con-,
     2 ditions (naughty,naughty). You MUST have a sequence in the,
     3 data where the value of the knot is;,
```

```
     4   (a) At least greater than the previous knot value,
     5   (b) Such that it lies in a range of five data points.,
     6   This in effect means that there are regions where there,
     7  are too many knots relative to the data.')
        GOTO 600

600     RETURN

        END
@
```

(2) EM ANALYSIS PROGRAMS.

(a) EM digitizing routine.

This is written in 4051 basic, and converts tracings of thick filaments (eg Fig 5.2.4.1) into a series of X/Y co-ordinates which are sent to a Tektronix 6130 file. The program is a low resolution digitising routine, the choice of 10 steps per half thick filament was chosen since this usually gave between 250 and 300 points, enough for acceptable resolution of thick filament position in the distortion graphs, and yet not too time consuming to input (the routine is largely non automatic and each tracing took about 15 - 20 minutes to digitize). The flow diagram shows the main steps taken in the program, the sarcomeres were selected on two criteria.

(1) M-line must be reasonably straight, large deviations will result in the distortion graphs appearing to have high local disorder.

(2) The number of filaments in the section was 25-30.

Lines 200-350 establish the communications link with the 6130 machine, where once logged on and in the relevant directory, terminal mode is changed back to basic mode, and the perameters of the sarcomere needed to reproduce ideal calculated lattices found. These are number of filaments (N) (found by direct input), filament length (L) (found by subtraction from the filament tip of the M-line X/Y co-ordinates), the angle of the M-line to the horizontal (A1), and the angle of the filaments to the M-line and (A2), the angle of the filaments to the M-line. The digitization of the traces was started by inputting on the first filament the position of the M-line, the

crosshairs were moved by the computer 1/10th of the filament length and adjusted to intercept the trace by moving them in a one or five degree arc centred on the previous point, by activating the relevant loops using the user defined keys. This was repeated 10 times for each filament and repeated for every filament in the trace. Counting the initial M-line position, this made a total of 11 x N points for the whole trace. This value too was transmitted to the 6130. Note that line 1510 transmits D$ which is defined in line 360 as end of transmission. If this is not sent (eg if the wrong button is pressed during digitisation) then re-establishing communications with the 6130 can only be done by issuing a reset command.

FLOW DIAGRAM FOR THE EM DIGITIZING ROUTINE ON 4051.

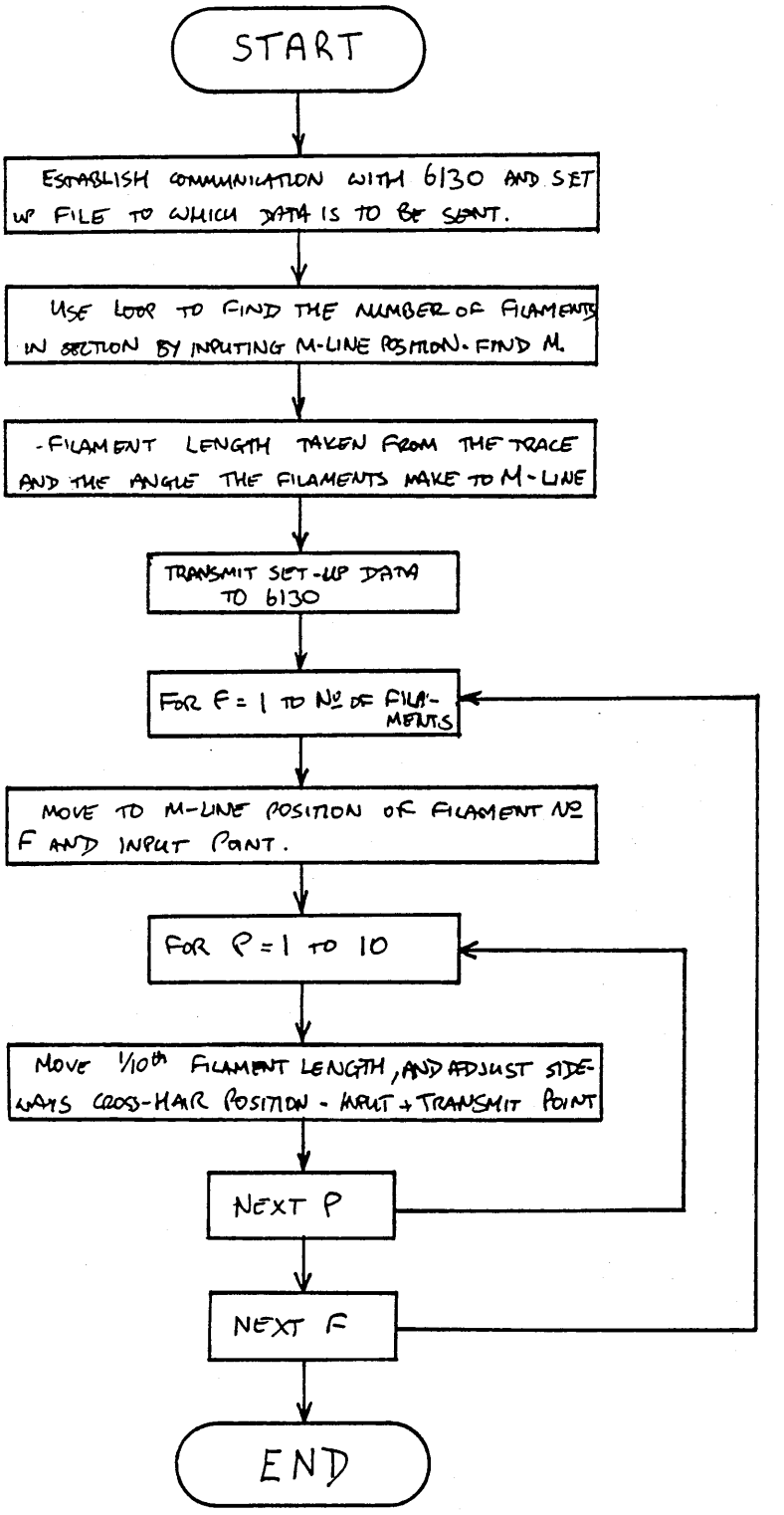

EM Digitizing Program.

```
1 GO TO 100
2 REM *** Control of arc stepping in ins 4 to 22
4 T=1
5 GOSUB 2000
7 GO TO 1215
8 T=1
9 GOSUB 2050
11 GO TO 1215
12 T=5
13 GOSUB 2000
15 GO TO 1215
16 T=5
17 GOSUB 2050
19 GO TO 1215
20 REM set K1=1
21 K1=1
22 GO TO 1215
100 REM E.M digitzing program
150 INIT
160 SET DEGREES
200 PRINT "Hit 'RETURN TO begin' key once logged in"
300 CALL "rate",2400,0,0
310 CALL "margin",0,0,0,0
330 CALL "termin"
350 REM return to this point in the program
351 INIT
352 SET DEGREES
353 SET KEY
360 D$=CHR(4)
370 E$=CHR(7)
372 S$=CHR(0)
375 DIM X(100),Y(100),A(10)
380 F=1
385 PRINT "Input the name for data file - KEEP IT SHORT ! ... ";
390 INPUT N$
392 PRINT "Input title for data (stored in the file) ... ";
394 INPUT T$
400 REM find no of filaments in the section
410 PRINT "Terminate loop by inputting (0,0) at plotter."
415 ON SRQ THEN 500
420 PRINT @1,26:1
430 INPUT @1,27:X(F),Y(F)
440 PRINT @1,26:0
450 IF Y(F)<Y(1) THEN 480
460 F=F+1
470 GO TO 410
480 X(F)=0
485 Y(F)=0
490 F=F-1
495 PRINT @1:E$;
500 REM Arrive here from filament no loop, start digitizing picture.lis
520 PRINT "There are ";F;" filaments in the section"
540 REM Calculate the mean filament separation
550 T=0
560 FOR N=1 TO F
570 IF N+1>F THEN 620
```

```
580 T=T+SQR((X(N+1)-X(N))^2+(Y(N+1)-Y(N))^2)
600 NEXT N
620 M=T/(F-1)
630 M=INT(M*1000)/1000
635 P=F*11
640 PRINT M
700 REM Find filament length
710 PRINT "Digitize points from M-line and A-band tip"
720 PRINT @1,26:1
725 PRINT "Press Input point at M-line"
730 INPUT @1,27:X1,Y1
740 PRINT "Press Input point at A-band tip"
750 INPUT @1,27:X2,Y2
760 PRINT @1,26:0
765 PRINT @1:E$;
770 L=SQR((X2-X1)^2+(Y2-Y1)^2)/10
800 REM Find angle which M-line makes to filament perpendicular.
805 PRINT "Digitize points either side of M-line. First the one side then"
806 PRINT "the point on the same filament on the opposite side. Take 10"
807 PRINT "filaments evenly distributed across the section."
812 T=0
815 FOR N=1 TO 10
820 PRINT @1,26:1
830 INPUT @1,27:X1,Y1
835 INPUT @1,27:X2,Y2
837 PRINT @1:E$;
840 PRINT @1,26:0
850 H1=SQR((X1-X2)^2+(Y1-Y2)^2)
855 A1=X1-X2
860 A(N)=ACS(A1/H1)
865 T=T+A(N)
870 NEXT N
875 A2=T/10-90
880 H2=SQR((X(F)-X(1))^2+(Y(F)-Y(1))^2)
885 A1=ACS((X(F)-X(1))/H2)-A2
900 REM Input data from plotter and transmit to RS-232.
910 PRINT "Start at lower left filament and digitize"
920 PRINT "Press Press"
930 REM Transmit filename, no points, no filaments and mean spacing
940 PRINT @40:"cat >";N$
941 PRINT @40:T$
942 PRINT @40:P
944 PRINT @40:F
946 PRINT @40:M
947 PRINT @40:L
948 PRINT @40:A1
950 PRINT @40:A2
1000 REM Move along filaments and adjust for land
1010 C1=L*COS(90+A2)
1020 C2=L*SIN(90+A2)
1100 FOR Q=1 TO F
1110 PRINT "Move to filament no ";Q;" and digitize"
1125 MOVE @1:X(Q),Y(Q)
1130 PRINT @1,26:1
1140 INPUT @1,27:X1,Y1
1150 PRINT @1,26:0
1160 PRINT @40:X1
1170 PRINT @40:Y1
1200 FOR R=1 TO 10
```

```
1205 X2=X1
1206 Y2=Y1
1207 A3=A1
1208 K1=0
1210 C=0
1211 MOVE @1:X1+C1,Y1+C2
1215 REM return here after udk routines
1218 PRINT @1,26:1
1220 IF K1=0 THEN 1310
1230 X1=X2
1240 Y1=Y2
1250 IF C=1 THEN 1280
1260 X1=X1+C1
1270 Y1=Y1+C2
1280 GO TO 1350
1310 REM wait for udk
1320 IF K1=0 THEN 1310
1350 PRINT @40:X1
1360 PRINT @40:Y1
1370 PRINT @1:E$;
1380 PRINT @1,26:0
1490 NEXT R
1500 NEXT Q
1510 PRINT @40:D%
1520 PRINT "END OF RUN"
1600 STOP
2000 X2=X1+L*COS(90+A3+T)
2010 Y2=Y1+L*SIN(90+A3+T)
2020 MOVE @1:X2,Y2
2030 A3=A3+T
2035 C=1
2040 RETURN
2050 X2=X1+L*COS(90+A3-T)
2060 Y2=Y1+L*SIN(90+A3-T)
2070 MOVE @1:X2,Y2
2080 A3=A3-T
2085 C=1
2090 RETURN
```

(b) Distort.

This generates the graphs of the distortion of the experimental lattices from the ideal rectangular, conical and elliptical lattices using digitised data from the trace filaments as sent by the EM digitizing program. The data needed for the generation of the ideal lattices are input at line 160 (the same data are used here as are sent from the 4051 EM digitizing routine), and the digitized data are input into the X/Y input arrays from file. The choice of assessing the distortion from rectangular, conical or elliptical arrays is available. All three result in the co-ordinates of the chosen lattice in the X/Y CALC array, the distortions of the experimental data in X/Y INPUT arrays from the ideal data X/Y CALC arrays and placed in the X/Y DIST arrays. Finally the data are converted to X/Y co-ordinates for the terminal screen (X/Y plot arrays) and plotted out (Lines 1320 - 2300). A hard copy is obtained by opening, closing and plotting segments with the 6130 terminal.

FLOW DIAGRAM FOR "DISTORT" - GENERATE DISTORTION FROM LATTICE GRAPHS.

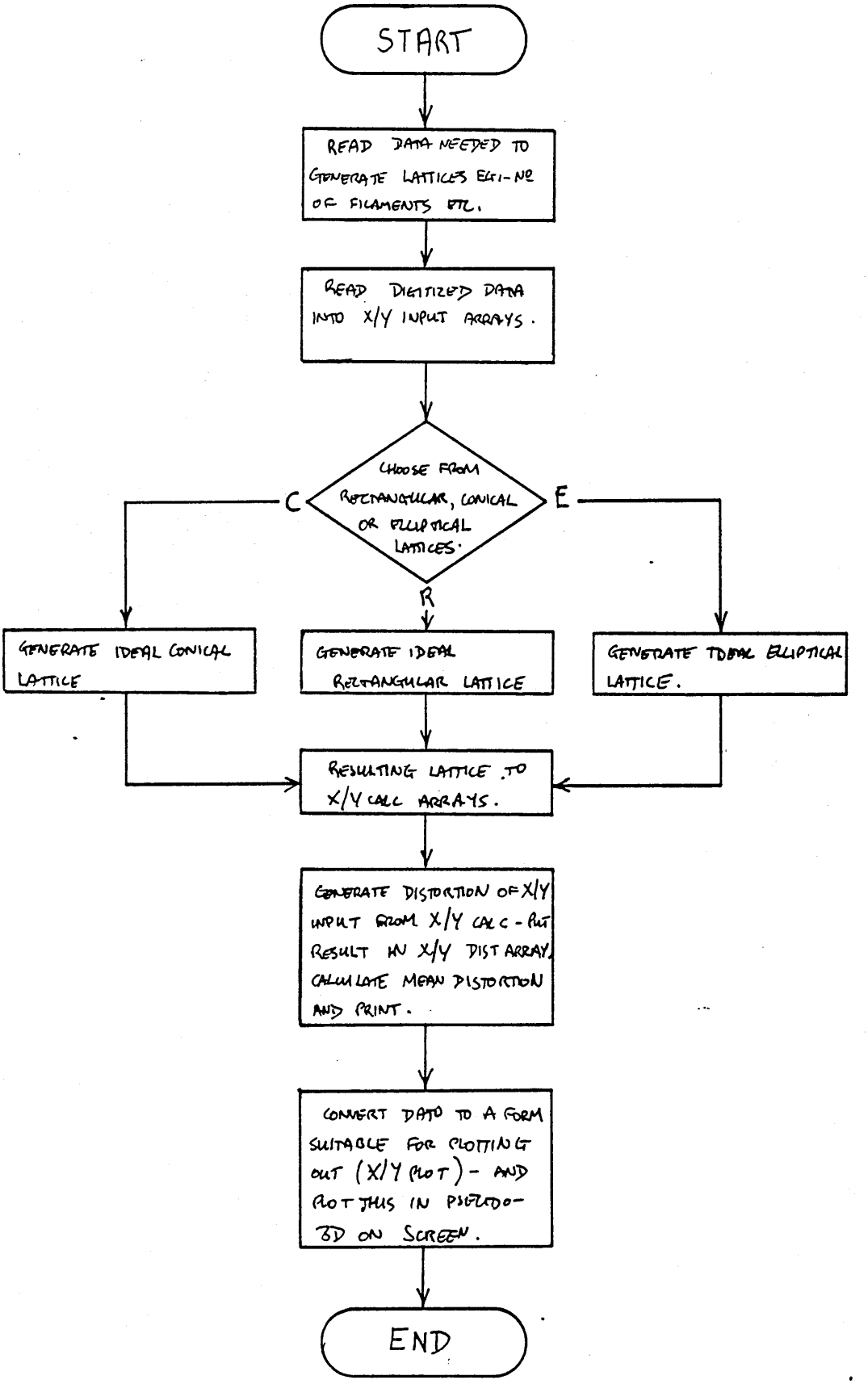

DISTORT.

```
100 INIT
110 OPTION ANGLE DEGREES
120 PRINT "Input file for analysis.    ";
130 INPUT A$
140 OPEN #2:A$,"R"
150 INPUT #2:Title$
160 INPUT #2:Nopts,Noflmts,Mnspcng,L,Mu1,Mu2
170 N1 = Noflmts
180 N2 = Nopts/Noflmts
190 REM
200 REM *** Input values from data files into X/Yinput arrays ***
210 REM
220 DIM Xinput[N1,N2],Yinput[N1,N2]
230 FOR Filno = 1 TO Nopts/11
240   FOR Filong = 1 TO 11
250     INPUT #2:Xinput[Filno,Filong],Yinput[Filno,Filong]
260   NEXT Filong
270 NEXT Filno
275 CLOSE #2
280 PRINT "Input correction angle.    ";
290 INPUT Corrang
300 Mu1 = Mu1+Corrang
310 Mucalc = Mu1+(Mu2-Mu1)
320 REM
330 REM *** Calculate ideal lattice ***
340 REM
350 DIM Xcalc[N1,N2],Ycalc[N1,N2]
360 Xadd = L*COS(90+Mucalc)
370 Yadd = L*SIN(90+Mucalc)
380 PRINT "Rectangular, truncated cone or elliptical lattice ? ...(r,
390 INPUT Ans$
400 IF Ans$="c" OR Ans$="C" OR Ans$="e" OR Ans$="E" THEN 500
410 FOR Filno = 1 TO Noflmts
420   Xcalc[Filno,1] = Xinput[1,1]+Mnspcng*(Filno-1)*COS(Mu1+Mu2)
430   Ycalc[Filno,1] = Yinput[1,1]+Mnspcng*(Filno-1)*SIN(Mu1+Mu2)
440   FOR Filong = 2 TO 11
450     Xcalc[Filno,Filong] = Xcalc[Filno,1]+(Filong-1)*Xadd
460     Ycalc[Filno,Filong] = Ycalc[Filno,1]+(Filong-1)*Yadd
470   NEXT Filong
480 NEXT Filno
490 GOTO 1100
500 REM
510 REM *** Truncated cone/ellipse lattice generation ***
515 REM
520 Thlen = SQR((10*Xadd)^2+(10*Yadd)^2)
530 Xmidm = Xinput[1,1]+Noflmts/2*Mnspcng*COS(Mu1+Mu2)
540 Ymidm = Yinput[1,1]+Noflmts/2*Mnspcng*SIN(Mu1+Mu2)
550 Xmidai = 10*Xadd+Xmidm
560 Ymidai = 10*Yadd+Ymidm
570 Dxai = (Xinput[Noflmts,11]-Xinput[1,11])^2
580 Dyai = (Yinput[Noflmts,11]-Yinput[1,11])^2
590 Mnspcngai = SQR(Dxai+Dyai)/Noflmts
600 IF Ans$="e" OR Ans$="E" THEN 700
610 FOR Filno = 1 TO Noflmts
620   Dxm = Xmidm+10*Xadd-Mnspcng*(Noflmts/2-Filno+0.5)*COS(Mu1-Mu2)
630   Dym = Ymidm+10*Yadd-Mnspcng*(Noflmts/2-Filno+0.5)*SIN(Mu1-Mu2)
640   Dxai = Xmidai-(Noflmts/2-Filno+0.5)*Mnspcngai*COS(Mu1-Mu2)
```

```
  650    Dyai = Ymidai-(Noflmts/2-Filno+0.5)*Mnspcngai*SIN(Mu1-Mu2)
  660    Dx = Dxai-Dxm
  670    Dy = Dyai-Dym
  680    D = SQR(Dx^2+Dy^2)
  690    IF Dxai<Xmidai THEN D = -1*D
  700    Mu3 = 2*ASIN(D/2/Thlen)
  710    Xcalc[Filno,1] = Xinput[1,1]-Mnspcng*(Filno-1)*COS(Mu1+Mu2)
  720    Ycalc[Filno,1] = Yinput[1,1]+Mnspcng*(Filno-1)*SIN(Mu1+Mu2)
  730    FOR Filong = 2 TO 11
  740      Xcalc[Filno,Filong] = Xcalc[Filno,1]+(Filong-1)*L*COS(90+Mucal
  750      Ycalc[Filno,Filong] = Ycalc[Filno,1]+(Filong-1)*L*SIN(90+Mucal
  760    NEXT Filong
  770  NEXT Filno
  780  GOTO 1100
  800  REM
  810  REM *** Elliptical lattice generation ***
  820  REM
  830  Xconst = Mnspcng*COS(Mu1-Mu2)
  840  Yconst = Mnspcng*SIN(Mu1-Mu2)
  850  FOR Filno = 1 TO Noflmts
  860    Dxm = Xconst*(Noflmts/2-Filno+0.5)
  870    Dym = Yconst*(Noflmts/2-Filno+0.5)
  880    Dxai = (Noflmts/2-Filno+0.5)*Mnspcngai*COS(Mu1-Mu2)
  890    Dyai = (Noflmts/2-Filno+0.5)*Mnspcngai*SIN(Mu1-Mu2)
  900    B = SQR(Dxm^2+Dym^2)
  910    Y = SQR(Dxai^2+Dyai^2)
  920    IF Y=B THEN B = B+0.0001
  930    A = SQR((10*L)^2/(1-Y^2/B^2))
  940    Xcalc[Filno,1] = Xinput[1,1]+Xconst*(Filno-1)
  950    Ycalc[Filno,1] = Yinput[1,1]+Yconst*(Filno-1)
  960    FOR Filong = 2 TO 11
  970      Xcomp = (Filong-1)*L*COS(90+Mucalc)
  980      Ycomp = (Filong-1)*L*SIN(90+Mucalc)
  990      Y = SQR(B^2-((Filong-1)*L*B/A)^2)
 1000      Dx = Y*COS(Mu1+Mu2)
 1010      Dy = Y*SIN(Mu1+Mu2)
 1020      IF Filno>Noflmts/2 THEN
 1030        Dx = -1*Dx : Dy = -1*Dy
 1040      END IF
 1050      Xcalc[Filno,Filong] = Xcalc[Filno,1]+Dxm+Xcomp-Dx
 1060      Ycalc[Filno,Filong] = Ycalc[Filno,1]+Dym+Ycomp-Dy
 1070    NEXT Filong
 1080  NEXT Filno
 1100  REM
 1110  REM *** Calculate X/Ydist arrays ***
 1115  REM
 1120  DIM Xdist[N1,N2],Ydist[N1,N2]
 1130  Xdistot = 0
 1140  FOR Filno = 1 TO Noflmts
 1150    FOR Filong = 1 TO 11
 1160      Dx = Xinput[Filno,Filong]-Xcalc[Filno,Filong]
 1170      Dy = Yinput[Filno,Filong]-Ycalc[Filno,Filong]
 1180      IF Dx=0 THEN
 1190        Xdist[Filno,Filong] = 0
 1200        Ydist[Filno,Filong] = 0
 1210      ELSE
 1220        Xdist[Filno,Filong] = SQR(Dx^2+Dy^2)*COS(Mu1-ATAN(Dy/Dx))
 1230        Ydist[Filno,Filong] = SQR(Dx^2+Dy^2)*SIN(Mu1-ATAN(Dy/Dx))
 1240      END IF
```

```
1250      IF Dx<0 THEN Xdist[Filno,Filong] = -1*Xdist[Filno,Filong
1260      IF Dy<0 THEN Ydist[Filno,Filong] = -1*Ydist[Filno,Filong
1270      Xdistot = Xdistot+SQR(Xdist[Filno,Filong]^2)
1280    NEXT Filong
1290 NEXT Filno
1300 PRINT "Mean distortion from ideal lattice in nm = ";Xdistot/Nopts*
1310 REM
1320 REM *** Calculate X/Yplot arrays ***
1330 REM
1340 DIM Xplot[N1,N2],Yplot[N1,N2]
1350 PRINT "Input viewing angle (normally between 20 and 30 degrees)."
1360 INPUT Viewang
1370 L = 2
1380 Zhori = L*COS(Viewang)
1390 Zvert = L*SIN(Viewang)
1400 FOR Filno = 1 TO Noflmts
1410   FOR Filong = 1 TO 11
1420     Xplot[Filno,Filong] = Filno+(Filong-1)*Zhori
1430     Yplot[Filno,Filong] = Xdist[Filno,Filong]+(Filong-1)*Zvert
1440   NEXT Filong
1450 NEXT Filno
1460 REM
1470 REM *** Plot axes for 3D plot ***
1480 REM
1490 SET VIEWPORT 10,130,10,100
1500 SET WINDOW -7,Noflmts+15+10*Zhori,-3,7+15*Zvert
1505 REM *** Plot X-axis ***
1510 FOR Xaxis = 1 TO Noflmts+1
1520   PLOT LINE Xaxis-1,0;Xaxis,0
1530   PLOT LINE Xaxis,0;Xaxis,-0.1
1540 NEXT Xaxis
1550 REM *** Plot Z-axis ***
1560 FOR Zaxis = 1 TO 10
1570   PLO LIN N1+1+(Zaxis-1)*Zhori,(Zaxis-1)*Zvert;N1+1+Zaxis*Zhori,Z
1580   PLOT LINE N1+1+Zaxis*Zhori,Zaxis*Zvert;N1+1+Zaxis*Zhori,Zaxis*Z
1590 NEXT Zaxis
1600 REM *** plot y-axis ***
1610 FOR Yaxis = -1 TO 5
1620   PLOT LINE 0,Yaxis;0,Yaxis+1
1630   PLOT LINE 0,Yaxis+1;-0.25,Yaxis+1
1640 NEXT Yaxis
1650 Xpoint = 10*Zhori+Noflmts+1
1660 Ypoint = 10*Zvert
1670 FOR Yaxis = -6 TO 5
1680   PLOT LINE Xpoint,Yaxis+Ypoint;Xpoint,Yaxis+1+Ypoint
1690   PLOT LINE Xpoint,Yaxis+1+Ypoint;Xpoint+0.25,Yaxis+1+Ypoint
1700 NEXT Yaxis
1710 REM
1720 REM *** Plot graph - lines along filaments ***
1730 REM
1740 FOR Filno = 1 TO Noflmts
1750   FOR Filong = 2 TO 11
1760     PLO LIN Xplot[Filno,Filong-1],Yplot[Filno,Filong-1];Xplot[Fil
1770   NEXT Filong
1780 NEXT Filno
1790 REM *** plot lines across filaments ***
1800 FOR Filong = 1 TO 11
1810   FOR Filno = 2 TO Noflmts
1820     PLO LIN Xplot[Filno-1,Filong],Yplot[Filno-1,Filong];Xplot[Fil
```

```
1830    NEXT Filno
1840 NEXT Filorc
1850 REM
1860 REM *** Smarten up the graph (axes labels, title etc) ***
1870 REM
1880 SET TEXT SIZE 0.35
1890 PLOT TEXT AT 30,Ypoint+8:Title$
1900 PLOT TEXT AT 9,-3:"FILAMENT NUMBER"
1910 SET TEXT ANGLE 90
1920 PLOT TEXT AT 3+Xpoint,4.75:"DISTORTION"
1930 SET TEXT ANGLE Viewang*1.9
1940 PLOT TEXT AT N1+4,-3.5:"<-- M-LINE  A/I JNTN -->"
1950 SET TEXT ANGLE 0
1960 REM *** plot lines round graph ***
1970 Lastx = 0
1980 Lasty = 0
1990 FOR Tidy = 10 TO -1 STEP -1
2000   Plotx = Tidy*Zhori
2010   Ploty = Tidy*Zvert
2020   IF Ploty<Yplot[1,Tidy+1] THEN
2030     Lastx = Plotx
2040     Lasty = Ploty
2050     GOTO 2130
2060   ELSE IF Tidy=10 AND Ploty>=Yplot[1,Tidy+1] THEN
2070     Lastx = 10*Zhori
2080     Lasty = 10*Zvert
2090     GOTO 2110
2100   ELSE
2110     PLOT LINE 0,0;Lastx-0.3*Zhori,Lasty-0.3*Zvert
2120     EXIT TO 2170
2130   END IF
2140 NEXT Tidy
2150 REM *** Line at top of graph ***
2170 FOR Tidy = Noflmts TO 1 STEP -1
2180   IF Yplot[Tidy,11]<=Ypoint THEN
2190     PLOT LINE Zhori*10+Tidy,Ypoint;Zhori*10+Tidy+1,Ypoint
2200   END IF
2210 NEXT Tidy
2220 REM *** Line for Y-axis at top of graph
2230 Ydiff = Yplot[1,11]-Yplot[1,10]
2240 FOR Tidy = 6 TO 1 STEP -1
2250   IF Yplot[1,11]>=Ypoint+Tidy OR Tidy=1 THEN
2260     PLOT LINE Xpoint-(N1+1),Ypoint+1+Tidy-0.6*Ydiff;Xpoint-(N1+1
2270     EXIT TO 2300
2280   END IF
2290 NEXT Tidy
2300 END
```

(c) FORDEV.FOR.

This program wirtten on DEC-20 in TOPS 10/20 Fortran includes the Fourier transforms of the 11 separate transverse levels from the M-line to the A/I junction sampled by the digitising routine, averages then and puts them in the file DUMP.DAT. FORFIT.FOR reads this file and fits a cubic spline to the data it finds. The flow diagram of FORDEV.FOR is the same as for the tbasic programe "Fouriersum", but only the Fortran program is listed, since it was used almost exclusively. The digitised data was first sent to the DEC-20 using the "Kermit" file transfer routine. The first step loaded the data in a given file into the X/Y INPUT arrays. The original data are suitable for Fourier transform analysis and this is performed at the 11 levels at each half sarcomere. The amplitude at each point in reciprical is stored in the K array, and this is used to generate the average trace used, for example, in Figs 5.3.1 to 5.3.4, by taking an average of the 11 amplitudes at each position in reciprocal space and placing the result in the same position in the Kav array. The mean spacing of the thick filaments over the whole half-sarcomere is found, and using this value, the "ideal" Fourier transform is generated (ie the transform of the ideal rectangular lattice). The result gives the theoretical curve expected for an extended array of points. Both this theoretical transform and the experimental transform are stored together in DUMP.DAT. This file is transferred back to the 6130 using the "Tip" command, and plotted out using the tbasic program "Plot".

FLOW DIAGRAM OF "FORDEN.FOR" - FOURIER SUMMATION CALCULATION.

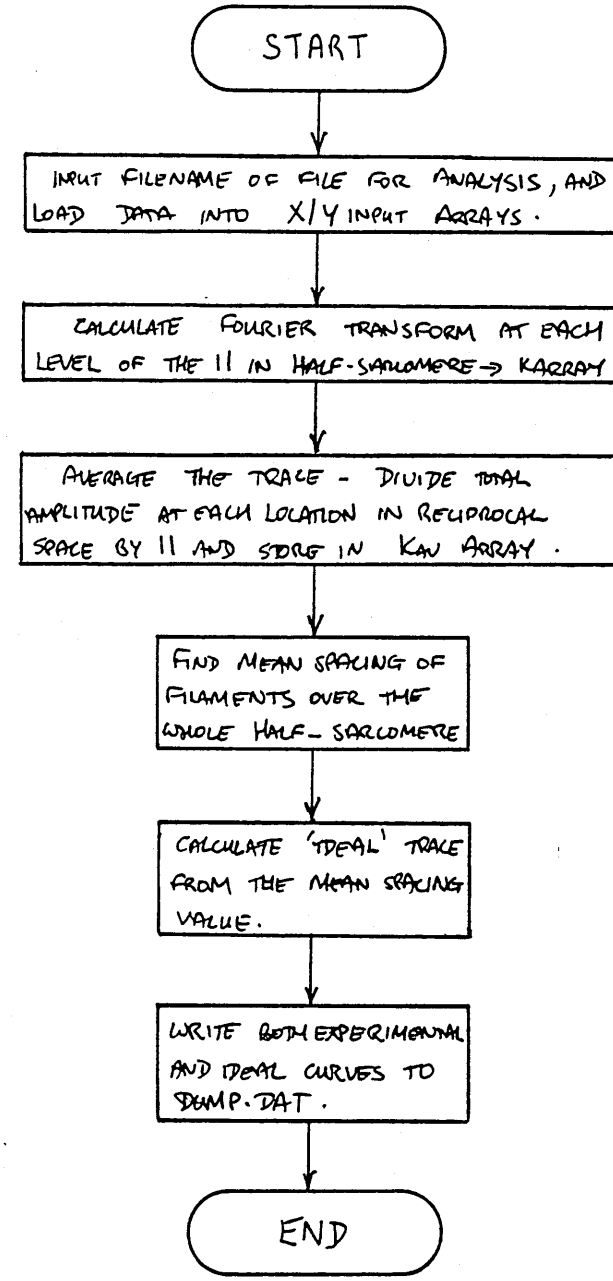

FORDEV.FOR

```
C       This program calculates a series of 11 Fourier transforms

        PROGRAM CORE

        REAL XINPUT(50,550),YINPUT(50,550),KVAL,XI,DX,DY,MNSPNG,
     2  L,MU1,MU2,SCLFAC,K(11,1001),KA/(1001),XISUM,KI(1001),
     3  X(1001),PI,KTOT

        INTEGER KLOOP,XPOS,IVAL,N1,N2,NOPTS,NOFLMT,AVLOOP,MNLOOP,
     2  MNSPN

        CHARACTER*20 TITLE,FILNAM

C       Input file for analysis

        WRITE (5,10)
 10     FORMAT (/2X,'Input file for analysis    ',$)
        READ (5,20) FILNAM

C       Load data into array X/Yinput

        OPEN (UNIT=20,FILE=FILNAM,STATUS='OLD',MODE='ASCII')

        READ (20,20) TITLE
 20     FORMAT(A20)
        READ (20,*) NOPTS,NOFLMT,MNSPNG,L,MU1,MU2
        SCLFAC=19.8
        PI=3.141593

        DO 60,N1=1,NOPTS/11
          DO N2=1,11
            READ (20,*) XINPUT(N1,N2),YINPUT(N1,N2)
          END DO
 60     CONTINUE

        CLOSE (20)

C       Summation starts here

        DO 80,XPOS=1,11
          KVAL=0
          DO KLOOP=1,1001
            DO XIVAL=1,(NOPTS/11)-1
              DX=(XINPUT(XIVAL+1,XPOS)-XINPUT(1,XPOS))**2
              DY=(YINPUT(XIVAL+1,XPOS)-YINPUT(1,XPOS))**2
              XI=SQRT(DX+DY)*SCLFAC
              K(XPOS,KLOOP)=K(XPOS,KLOOP)+COS(2*PI*KVAL*XI)
            END DO
            KVAL=KVAL+0.005
          END DO
 80     CONTINUE

C       Averaging of calculated traces

        KTOT=0
```

```
      DO 100,KLOOP=1,1001
        DO AVLOOP=1,11
          KAV(KLOOP)=KAV(KLOOP)+K(AVLOOP,KLOOP)^2
        END DO
        KAV(KLOOP)=SQRT(KAV(KLOOP)/11)
        KTOT=KTOT+KAV(KLOOP)^2
        KAV(KLOOP)=KTOT
  100 CONTINUE

C     Find mean spacing from data

      XISUM=0
      DO 120,MNLOOP=1,11
        DO MNSPA=1,(NOPTS/11)-1
          DX=(XINPUT(MNSPA+1,MNLOOP)-XINPUT(MNSPA,MNLOOP))^2
          DY=(YINPUT(MNSPA+1,MNLOOP)-YINPUT(MNSPA,MNLOOP))^2
          XISUM=XISUM+SQRT(DX+DY)
        END DO
  120 CONTINUE

      MNSPNG=XISUM/(11*((NOPTS/11)-1))
      TYPE*,MNSPNG

C     Calculate ideal trace from mean spacing

      KVAL=0
      DO 140,KLOOP=1,1001
        X(KLOOP)=KLOOP
        KI(KLOOP)=0
        DO XIVAL=1,(NOPTS/11)+1
          KI(KLOOP)=KI(KLOOP)+COS(2*PI*KVAL*(MNSPNG*(XIVAL-1)*SCLFAC))
        END DO
        KVAL=KVAL+0.005
        KI(KLOOP)=KI(KLOOP)^2
  140 CONTINUE

C     Plot out resulting traces, NOTE - NUMBER OF POINTS IN F(K)=1000


      OPEN(UNIT=20,FILE='DUMP.DAT',STATUS='NEW',MODE='ASCII')

      WRITE(20,*) 1000

      DO 220,KLOOP=1,1001
        WRITE(20,*) KLOOP-1,KAV(KLOOP),KI(KLOOP)
  220 CONTINUE

      CLOSE(20)

      END
```

(d) Plot.

This is written in 6130 tbasic, and plots out the files resulting from the Fourier analysis transmitted from the DEC-20. The program first loads data from the file transmitted from DEC-20 as DUMP.DAT, the result of the theoretical and experimental Fourier analysis on the half-sarcomeres. The second file loaded is the result of the cubic spline fit to the experimental Fourier analysis as performed by FOURFIT.FOR and is transmitted from the DEC-20 as FITFOR.DAT. These two files are loaded into arrays. The choice of either a continuous X/Y plot or a histogram of any chosen resolution is available, and the routine plots at the theoretical transform in black, the experimental curve or histogram in green and finally the cubic spline fitted data in red.

To get hard copies of the graphs, each line plotted was placed in a separate segment, and each segment printed separately. The different colours in the copy were achieved by changing pens between the plotting of each segment.

FLOW DIAGRAM FOR "PLOT" - FOURIER SUMMATION CURVE PLOTTER.

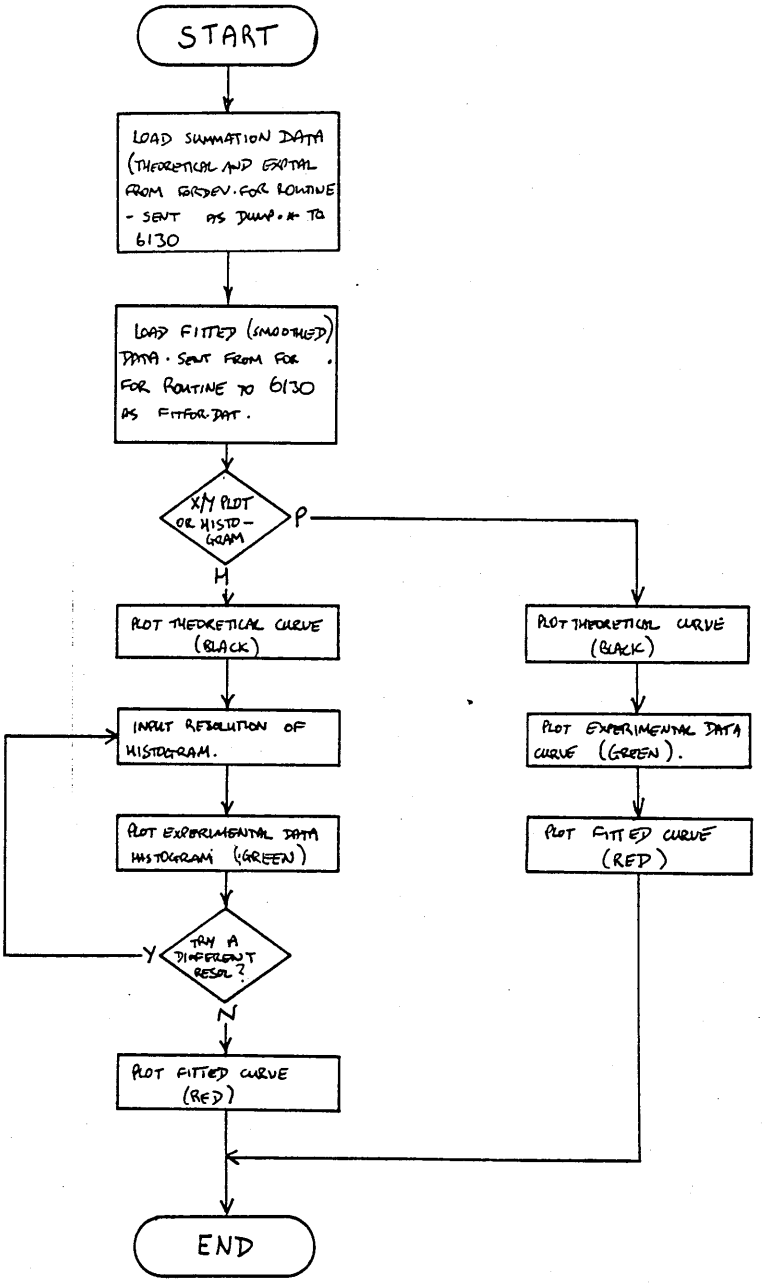

PLOT

```
100 INIT
110 DIM X(1000),K(11,3),Kav(1001),Kfit(1001)
115 REM
120 REM *** Load data from file ***
130 REM
135 PRINT "Loading summation and fit curves"
140 OPEN #2:"dump1","R"
150 Divtot = 0
155 INPUT #2:Nopts
160 FOR L = 1 TO 1001
180   X(L) = L
200   INPUT #2:Null,Kav(L),K(L,
205   Kav(L) = Kav(L)-Divtot
210   Divtot = Divtot+Kav(L)
220 NEXT L
230 CLOSE #2
232 PRINT "Loading fitted curve"
235 OPEN #2:"dump3","R"
240 INPUT #2:Nopts
245 FOR L = 1 TO 1000
250   INPUT #2:Null,Kfit(L)
255 NEXT L
257 Kfit(1001) = Kfit(1000)
260 CLOSE #2
300 REM
310 REM *** Plotting starts here ***
315 REM
320 REM Plot F(k)^2
330 PRINT "Do you want X/Y plot or Histogram ? ...(p/h) ";
340 INPUT Ans$
350 Esc$ = CHR$(27)
360 PRINT Esc$;"SOA0"
370 SET VIEWPORT 10,130,10,100
380 SET WINDOW 0,1010,0,K(1)
390 AXIS 20,100
395 REM
400 REM *** X/Y plot starts here ***
405 REM
410 FOR Ploop = 1 TO 3
420   IF Ploop=3 THEN
430     PRINT Esc$;"SOC0"
435     SET LINE COLOR 4
440     FOR Kloop = 1 TO 1000
450       PLOT LINE Kloop-1,Kfit(Kloop-1),Kloop,Kfit(Kloop+1)
460     NEXT Kloop
470     PRINT Esc$;"SC"
500   ELSE IF Ploop=2 THEN
510     IF Ans$="h" THEN GOSUB 680
520     PRINT Esc$;"SO3"
530     FOR Kloop = 1 TO 1000
540       PLOT LINE Kloop-1,Kav(Kloop-1),Kloop,Kav(Kloop+1)
550     NEXT Kloop
560     PRINT Esc$;"SC"
570   ELSE IF Ploop=1 THEN
580     SET LINE COLOR 2
590     FOR Kloop = 1 TO 1000
600       PLOT LINE Kloop-1,K(Kloop-1),Kloop,K(Kloop+1)
```

```
610       NEXT Kloop
620       PRINT Esc$;"SC"
630     END IF
640     SET LINE COLOR 15
650   NEXT Ploop
660   END
670   REM
680   REM *** histogram plot starts here ***
690   REM
700   PRINT "Input resolution of histogram   suggest 5 -> 20 ). ";
710   INPUT Xres
720   Xlast = -0.5 : Ylast = 0
730   PRINT Esc$;"S0R0"
740   FOR Kloop = 1 TO 1000 STEP Xres
750     Xsum = 0
760     FOR Xav = Kloop TO Kloop+(Xres-1)
770       Xsum = Xsum+Kav[Xav]
780     NEXT Xav
790     PLOT LINE Xlast,Ylast;Xlast,Xsum/Xres
800     PLOT LINE Xlast,Xsum/Xres;Xlast+Xres,Xsum/Xres
810     Xlast = Xlast+Xres
820     Ylast = Xsum/Xres
830   NEXT Kloop
840   PRINT Esc$;"SC"
850   PRINT "Plot with different resolution ? . . .(y/n) ";
860   INPUT Ans$
870   IF Ans$="n" THEN 900
880   PRINT Esc$;"SK80"
890   GOTO 680
900   RETURN TO 570
```

(e) 3dplot.

This is a graphics program originaly written in ANSI BASIC and translated to tbasic. The input is a set of raw bowing data, the output is either a bar chart, scatter plot, or mean bowing with standard deviations. The latter two options can have multiple files superimposed in different colours.

The file is loaded and sorted into increasing order of number of filaments in section (N) and decreasing bowing, so the array Zser has in its lowest location the highest value for bowing of the lowest value of N. The viewing angle (A) is input, and if the value is greater than 0 then a bar chart of all the points Zser array is printed sequentially, so resulting in a 3D graph as seen, for example, in Fig 6.2.2. The program ends at the end of each plot. If A=0,then the option of mean and standard deviation or scatter plot is available. The scatter plot is a 2D plot of bowing versus N for all points in the Zser array. The mean and standard deviation option calculates the mean bowing at all values of N, and prints out the mean plus or minus standard deviation error bars. The option of another file is available, and if chosen the variable "filecount" is made greater than 1 and a new file name requested, this file is read sorted and printed out. The output now gives the standard deviation error bars in the opposite direction and of different colour (eg Fig 5.2.1). With the mean and standard deviation option, the values calculated for the mean are stored in a separate file in the directory /4944/usr/dickie/embowing/meanbow for later curve fitting analysis using the tbasic program "bowing".

Hard copies were made by using the Tektronix 4695 screen copier, hence the rather poor quality of Figs 5.2.1 and 6.2.2.1 to 6.2.2.3.

FLOW DIAGRAM FOR '3DDEV' - EM GRAPHICS ROUTINE.

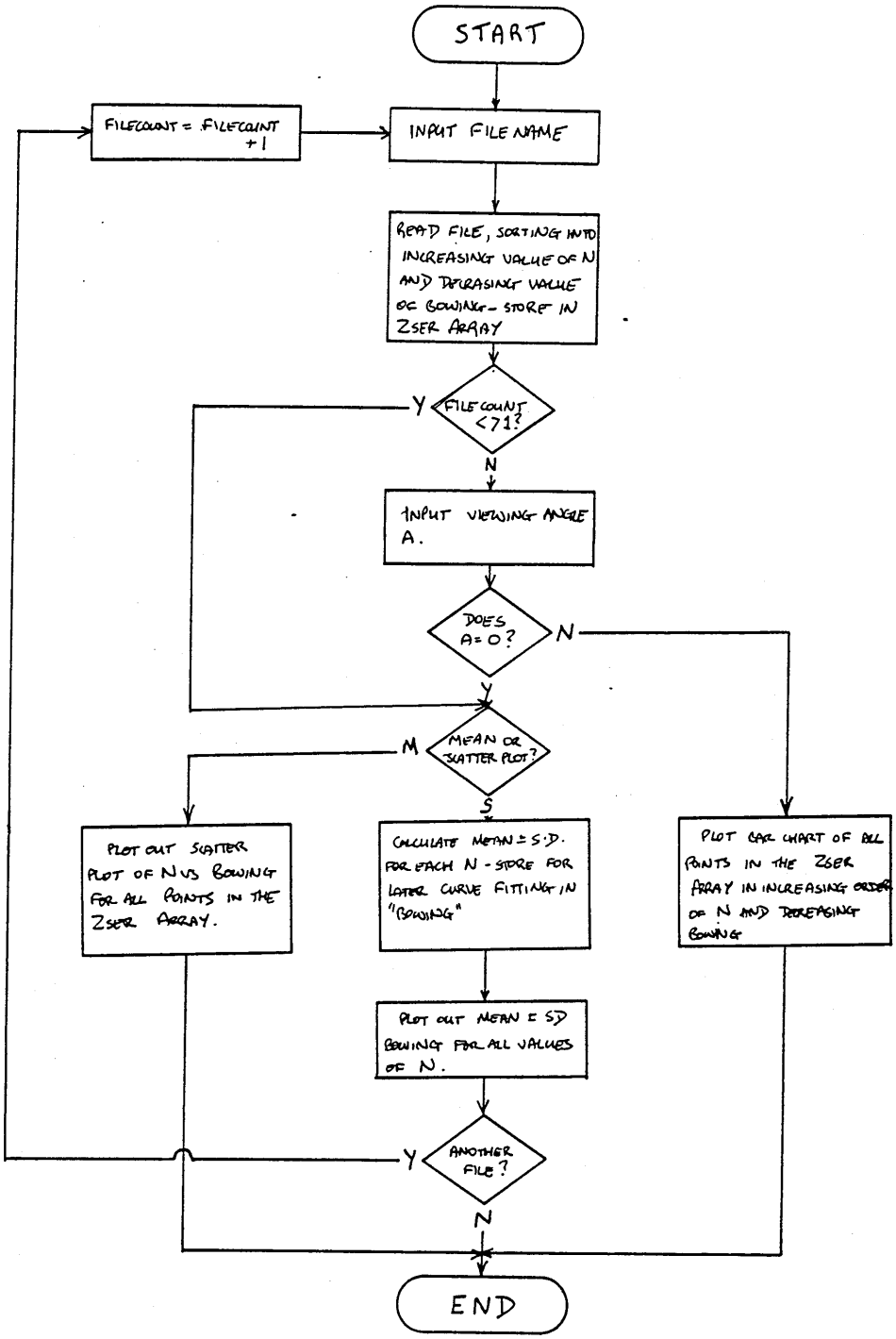

3DROT

```
 50 INIT
100 Zmax = 1
110 Zmin = 9
120 Filecount = 1
130 CLEAR
140 PRINT "Input data file name";
150 INPUT A$
155 Sega$ = SEG$(A$,5,3)
160 OPEN #2:A$,"R"
170 READ #2:A$,N
180 DIM X1[N],Y1[N],Z1[N],Xser[N],Yser[N],Zser[N]
190 FOR L = 1 TO N
200   READ #2:X1[L],Y1[L]
250   Z1[L] = 1
260   FOR R = 1 TO L
270     IF R=L THEN EXIT TO 630
280     IF X1[L]>Xser[R] THEN 310
290     IF X1[L]=Xser[R] THEN EXIT TO 520
300     EXIT TO 520
310   NEXT R
320   FOR C = R TO L
330     IF C=L THEN 340 ELSE 370
340     Z1[C] = Z1[C]-1
350     R = C
360     EXIT TO 630
370     IF X1[L]<>Xser[C] THEN Z1[L] = Zser[C-1]-1 ELSE 400
380     R = C
390     EXIT TO 520
400     IF Y1[L]>=Yser[C] THEN EXIT TO 420
410   NEXT C
420   LET Addx = 0
430   FOR Q = C TO L
440     IF Q=L THEN EXIT TO 470
450     IF X1[L]=Xser[Q] THEN Addx = Addx+1 ELSE EXIT TO 470
460   NEXT Q
470   FOR S = C TO C+(Addx-1)
480     Zser[S] = Zser[S]-1
490   NEXT S
500   IF C>R THEN Z1[L] = Zser[C-1]-1
510   R = C
520   Lsift = L-1
530   Xshift = 0
540   FOR M = R TO Lsift
550     Reset = M
560     Xshift = Xshift+1
570     M = L-Xshift
580     Xser[M+1] = Xser[M]
590     Yser[M+1] = Yser[M]
600     Zser[M+1] = Zser[M]
610     M = Reset
620   NEXT M
630   Xser[R] = X1[L]
640   Yser[R] = Y1[L]
650   Zser[R] = Z1[L]
```

```
660 NEXT L
670 IF filecount<1 THEN 1030
690 FOR Zminfind = 1 TO N
695   Zmin = MIN(Zser(Zmin+inc),Zmin
700 NEXT Zminfind
710 IF Zmin>=1 THEN 750
720 FOR R = 1 TO N
730   Zser(R) = Zser(R)+(1-Zmin)
740 NEXT R
750 Zmax = Zmax+(1-Zmin)
760 Zmost = Zmax
770 Zmax = Zmax+1
780 REM draw axes in 3 dimensions
790 PRINT "input viewing angle (normally between 30 and 45 degrees)"
800 INPUT A
810 OPTION ANGLE DEGREES
820 READ #2:Xmin,Xmax,Ymax
830 Ymax = MAX(Ymax,10)
840 Ymin = 0
850 Zhori = SIN(A)*(Zmax+1)+COS(A)
860 Zvert = SIN(A)*(Zmax+1)*SIN(A)
880 SET VIEWPORT 10,130,10,100
890 IF A=0 THEN
893   SET WINDOW Xmin-4,Xmax+2,Ymin-2,Ymax+7
896 ELSE
900   SET WINDOW Xmin-4,Xmax+15,Ymin-2,Ymax+Zmax+Zvert
905 END IF
910 PLOT LINE Xmax+2,0;Xmin-2,0;Xmin-2,INT(Ymax+2);Xmin-2,0
915 IF A=0 THEN PLOT LINE Zhori+Xmin-2,Zvert
920 SET TEXT SIZE Ymax/50
940 FOR X = Xmin-2 TO Xmax+2
950   PLOT LINE X,0;X,-0.15
960   PLOT LINE X,0;X+Zhori,Zvert
965   B$ = STR$(X)
970   IF X/5-INT(X/5)=0 THEN PLOT TEXT AT X-0.75,-0.85:B$
980 NEXT X
1000 FOR Y = 0 TO Ymax+2
1005   B$ = STR$(Y)
1010   PLOT LINE Xmin-2,Y;Xmin-2.15,Y
1015   IF A<>0 THEN
1020     PLOT LIN Xmax+2+Zhori,Zvert;Xmax+2+Zhori,Y+Zvert;Xmax+2.15+Zho
1030     PLOT TEXT AT Xmax+2.5+Zhori,Y+Zvert:B$
1031   ELSE
1035     PLOT TEXT AT Xmin-3.5,Y:B$
1038   END IF
1040 NEXT Y
1050 F = Xmin-2
1060 IF A=0 THEN 1160
1070 FOR Z = 1 TO Zmost+1
1080   PLOT LIN Z*(Zhori/Zmax)+F,Z*(Zvert/Zmax);2*(Zhori/Zmax)+F,Z*(Zve
1090   PLOT LIN Z*(Zhori/Zmax)+F,Z*(Zvert/Zmax);2*(Zhori/Zmax)+Xmax+2,Z
1100   Zprint = Zmax-Z
1110   IF Zprint=0 THEN 1130
1115   B$ = STR$(Zprint)
1120   IF Z/2-INT(Z/2)=0 THEN PLOT TEXT AT Z*(Zhori/Zmax)+Xmax+2.2,Z*(Zve
1130 NEXT Z
1160 PLOT TEXT AT (Xmin+Xmax)/2-5.6,-1.5:"Number of filaments in secti
1170 SET TEXT ANGLE 90
1180 IF A=0 THEN
```

```
 1182    PLOT TEXT AT Xmax+4,(Zvert/2)/Y-2:"100-(T/M-100)"
 1186 ELSE
 1190    PLOT TEXT AT Xmax+5+Zhori,Zvert/2:"100-(T/M*100)"
 1200    SET TEXT ANGLE 0
 1210    PLOT TEXT AT Xmax+4.5+Zhori/2,Zvert/2:"frequency"
 1215 END IF
 1220 REM
 1230 PRINT "Do you want mean with S.D, or a scatter plot ? ...(m/s) ";
 1235 SET TEXT ANGLE 0
 1240 INPUT Plot$
 1250 IF Plot$="m" THEN 1480
 1260 FOR L = 1 TO N
 1270    X = Xser[L]
 1280    Y = Yser[L]
 1290    Z = Zser[L]
 1300    X = X-0.3
 1310    Z = Z-0.3
 1320    IF A=0 THEN 1450
 1330    Xplot = X+Z*Zhori/Zmax
 1340    Yplot = Y+Z*Zvert/Zmax
 1350    SET AREA COLOR 2
 1360    PLOT ARE Xplot,Yplot;X+(Z+0.6)*Zhori/Zmax,Y+(Z+0.6)*Zvert/Zmax;X+
 1370    SET AREA COLOR 3
 1380    PLOT AREA Xplot,Yplot;Xplot+0.6,Yplot;Xplot+0.6,Yplot-Y;Xplot,Yp
 1390    SET AREA COLOR 4
 1400    PLOT ARE Xplot+0.6,Yplot-Y;Xplot+0.6,Yplot;X+0.6+(Z+0.6)*Zhori/Z
rt/Zmax
 1410    SET LINE COLOR 0
 1420    PLOT LINE Xplot,Yplot;Xplot,Yplot-Y
 1430    PLOT LIN X+0.6+(Z+0.6)*Zhori/Zmax,Y-Y-(Z+0.6)*Zvert/Zmax;X+0.6+(
 1440    IF A>0 THEN 1470
 1450    SET LINE COLOR 1
 1460    PLOT LINE X,Y;X+0.6,Y
 1470 NEXT L
 1475 GOTO 1845
 1480 REM stats routine
 1481 PRINT "Input filename for means + SD  ";
 1482 INPUT B$
 1485 SET DIRECTORY "/usr/dick1-/amboning/maunbow"
 1486 OPEN #4:B$,"w"
 1487 WRITE #4:B$
 1488 L = 1
 1490 Start = 1
 1495 DO WHILE L<=N
 1500    Count = 1
 1510    FOR L = Start TO N
 1520       IF L=N THEN EXIT TO 1550
 1530       IF Xser[L]=Xser[L+1] THEN Count = Count+1 ELSE EXIT TO 1550
 1540    NEXT L
 1550    Total = 0
 1560    FOR Mean = Start TO L
 1570       IF Mean=N+1 THEN EXIT TO 1600
 1580       Total = Total+Yser[Mean]
 1590    NEXT Mean
 1600    Mean = Total/Count
 1610    SET POINT COLOR 4
 1620    IF S-ga$="CON" THEN 1640 ! Sets colour for lines of control lat
 1630    SET POINT COLOR 1
 1640    PLOT POINT Xser[L],Mean
```

```
1650    Total = 0
1660    IF Count=1 THEN 1910
1670    FOR Var = Start TO L
1680      IF Var=N+1 THEN EXIT TO 1710
1690      Total = Total+(Yser[Var]-Mean)^2
1700    NEXT Var
1710    Standev = SQR(Total/Count)
1715    WRITE #4,Xser[L],Mean,Standev
1720    IF Sega$="COM" THEN
1730      SET LINE COLOR 4
1740      PLOT LINE Xser[L],Mean;Xser[L],Mean+Standev
1750      PLOT LINE Xser[L]-0.1,Mean+Standev;Xser[L]+0.1,Mean+Standev
1755      PLOT LINE Xmin,Ymax+6;Xmin+4,Ymax+6
1757      PLOT TEXT AT Xmin+6,Ymax+5.75;A$
1760    ELSE
1770      SET LINE COLOR 1
1780      PLOT LINE Xser[L],Mean;Xser[L],Mean-Standev
1790      PLOT LINE Xser[L]-0.1,Mean-Standev;Xser[L]+0.1,Mean-Standev
1795      PLOT LINE Xmin,Ymax+4;Xmin+4,Ymax+4
1797      PLOT TEXT AT Xmin+6,Ymax+3.75,A$
1800    END IF
1810    Start = L+1
1820    L = L+1
1830 LOOP
1840 SET DIRECTORY "/usr/dickie/embowing/bowda"
1842 CLOSE #4
1845 SET LINE COLOR 15
1850 PRINT "another file ? ... (y/n) ";
1860 INPUT File$
1870 IF File$="y" THEN
1880   CLOSE #2
1885   Filecount = Filecount+1
1890   GOTO 140
1900 END IF
1910 END
```

(f) Bowing.

This program is written in tbasic and fits a theoretical curve based on information given to a series of mean bowing values at various number of filaments (N) in the EM section using a truncated cone model. The values the routine needs are Mr, the cone radius at the M-line; Tr, the cone radius at the A/I junction; the increment used in the calculation of bowing and the file name containing the mean bowing data. This file will have been created when the "3dplot" routine was run.

The program plots the mean values out and then works out the theoretical values of bowing from the parameters given (see attached sheet for mathematical details), and plots the line superimposed over the points. Note the scaling factor, "Corr" (line 560) which allows for difference maximum values of N. The routine is not automatic, so repeated fits using various variables where necessary and so iteration and open "best fit" are left to the users discretion. Note that repeated loops only ask for Mr and Tr, and so could be completed in 15 - 20 seconds - curve fitting was a rapid process.

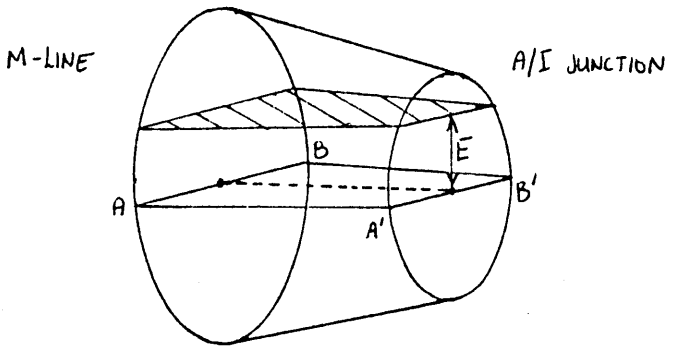

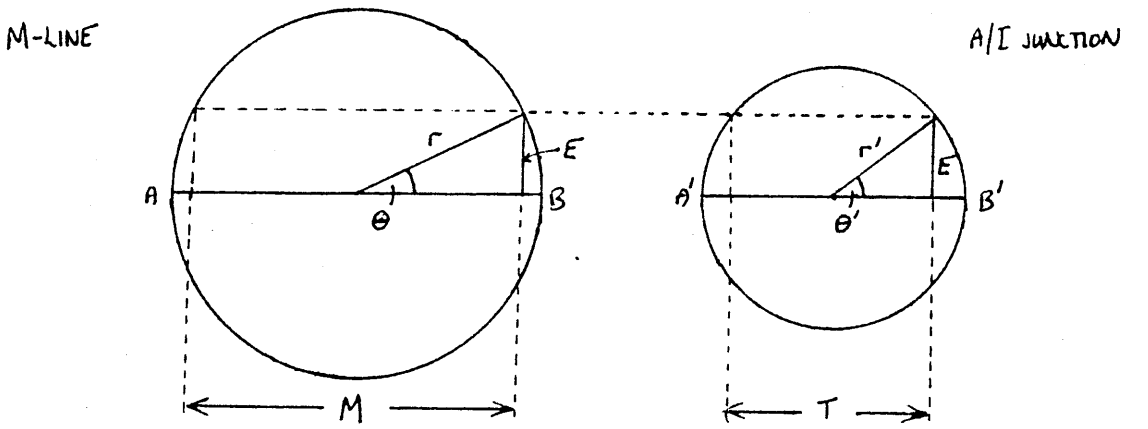

Consider filament F' at the surface of the myofibril. It will always occupy a position at a radius r from the centre of the M-line, and a radius r' from the centre of the A/I junction. r and r' are supplied as the radii of sarcomere at M-line and A/I junction.

For a section parallel to the plane AA'B'B the distance of the plane of cut will be E, therefore the angles at the M-line (θ) and A/I junction (θ') are:

$$\theta = \text{Asin}\left(\frac{E}{r}\right) \qquad \text{and} \qquad \theta' = \text{Asin}\left(\frac{E}{r'}\right)$$

The ratio of A/I junction to M-line width of this section is T/M where:-

$$M = 2r\cos\theta \qquad \text{and} \qquad T = 2r'\cos\theta'$$

Bowing is defined as:-

$$\text{Bowing} = 100-(100T/M)$$

Therefore theoretical bowing, B:-

$$B = 100-\left(\frac{r' \cos\theta'}{r \cos\theta} \times 100\right)$$

The solution to this equation is repeated for a range of increasing values of E, reprisenting sections cut further from the plane AA'B'B in the sarcomere (ie sections approaching the edge of the sarcomere).

FLOW DIAGRAM FOR "BOWING" - THEORETICAL BOWING CURVE FIT.

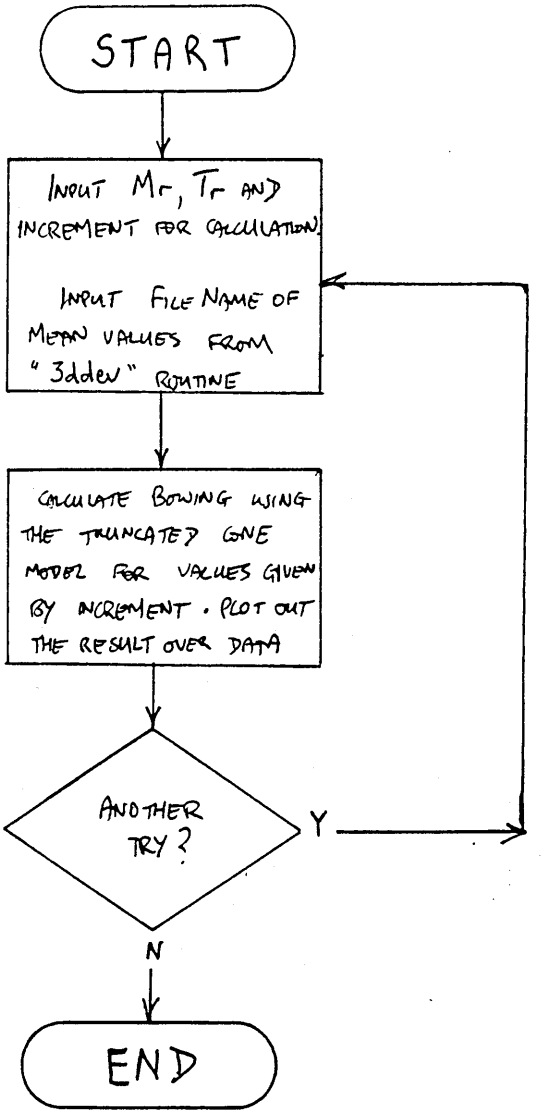

Bowing

```
100 INIT
105 Rerun = 0
107 Esc$ = CHR$(27)
110 REM Input parameters for fit
120 PRINT "INPUT Mr = ";
140 INPUT Mr
160 PRINT "INPUT Tr = ";
180 INPUT Tr
190 IF Rerun=1 THEN 270
200 PRINT "INPUT INCREMENT (NORMALLY = 1) = ";
220 INPUT Incre
240 PRINT "INPUT FILE NAME Or MEAN DATA  ";
260 INPUT B$
270 REM Plot axes, read data from file, plot axes and points
280 OPEN #2:B$,"R"
300 READ #2:A$
320 OPTION ANGLE DEGREES
330 PRINT Esc$;"SUA0"
340 SET VIEWPORT 10,130,10,100
360 SET WINDOW 10.50,0,30
380 AXIS 10,5,10,0
400 ON ECF(2) GOTO 520
420 SET POINT STYLE 4
440 DO WHILE Mr=Mr
460   READ #2:Xplot,Yplot,Sd
480   PLOT POINTS:xplot,Yplot
500 LOOP
505 CLOSE #2
510 REM Calculate bowing for various segment levels and plot curve
520 Lastx = Tr
540 Lasty = 100-Tr/Mr*100
560 Corr = Xplot/Tr
580 FOR A = Incre TO Tr STEP Incre
600   Theta = ASIN(A/Tr)
620   Dt = Tr*COS(Theta)
640   Theta = ASIN(A/Mr)
660   Dm = Mr*COS(Theta)
680   Bowing = 100-Dt/Dm*100
700   PLOT LINES:Lastx*Corr,Lasty;(Tr-A)*Corr,Bowing
720   Lastx = Tr-A
740   Lasty = Bowing
760 NEXT A
770 PRINT Esc$;"SC"
780 PRINT "Another try with same data ' ...(y/n) ";
800 INPUT Ans$
820 IF Ans$="n" THEN 900
840 PRINT Esc$;"SK!"
860 Rerun = 1
870 PRINT Esc$;"SK!"
880 GOTO 110
900 END
```

APPENDIX II - TENSION AND STIFFNESS MEASUREMENTS.

The mechanical studies presented here were done in collaboration with Dr Jonathan Kentish at the University College, London, to whom I am indebted for his enthusiasm and seemingly infinite patience.

The solutions used in the X-ray and EM experiments were all of a slightly lower ionic strength than those used in comparable studies (Schoenberg and Eisenberg (1985)), and were buffered using a phosphate system. Since these differences may have been sufficient to significantly change the physiological response of the muscle, studies were undertaken to asses tension development and stiffness under conditions similar to those used in the other experiments.

It is well known that glycerinated rabbit muscle is capable of generating force on exposure to MgATP and Ca^{2+}. Typically, maximal force developed is about 1.4 kg cm^{-2} (Brandt et al, Krasner et al) with a pCa of 4.5 → 5. Measurements of maximum force produced by my own samples showed a tension of ~1.5 kg cm^{-2} in a pCa of 4.8.

Two other effects were assessed in the samples. These were:-

(a) Pseudo-relaxation with PPi.

(b) Decreased apparent stiffness with decreased rate of stretch.

White (1970) has shown that 5mM PPi causes the tension in a rigor muscle to be reduced to a level 15 → 20% that of the initial tension in rigor, and Schoenberg et al (1985) also report a decrease to 10 → 20% initial tension with PPi. Results from my own studies show a somewhat smaller decrease to 30% in some experiments of initial tension (see Fig 2). This smaller change could be due to MgPPi concentration differences, in both White's and Schoenberg et al's studies, [MgPPi] was 3.8 mM whereas with the phosphate buffer I used addition of 5mM PPi gave a [MgPPi] of 2.3 mM.

Stiffness changes with addition of PPi were also assessed by

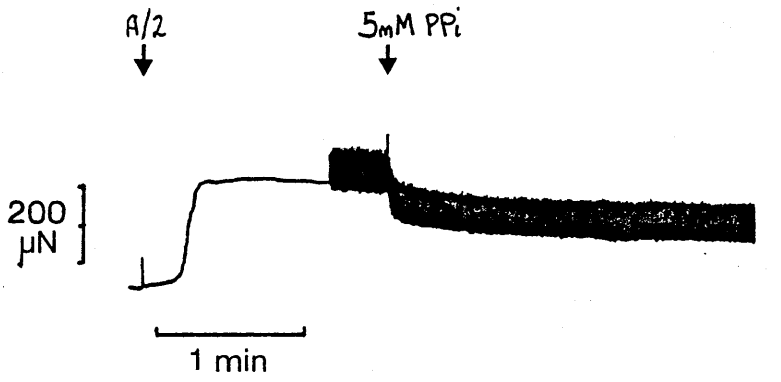

Fig 1. Pseudo-relaxing effect of PPi on rabbit rigor psoas fibre. Note the stiffness in response to 5μm stretches every 5 s remains constant.

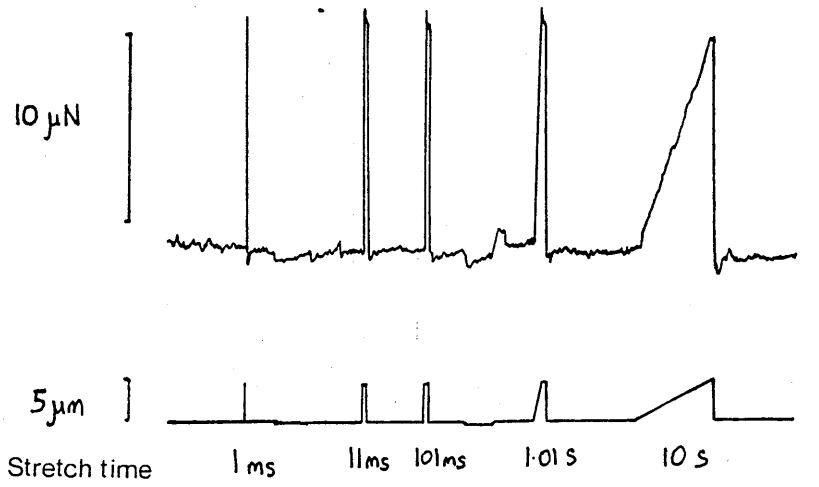

Fig 2a. Force (upper trace) and stretch (lower trace) at decreasing rates of stretch in rigor (A/2) solution.

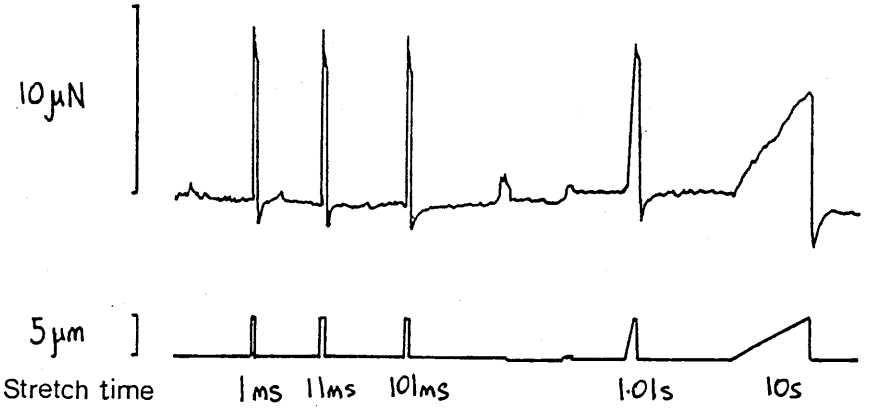

Fig 2b. Force (upper trace) and stretch (lower trace) at decreasing rates of stretch in 5mM PPi solution.

recording the force responses to rapid length changes. White (1970) reports a 60% decrease in apparent stiffness after addition of PPi, which after correction for decrease in force was found to give the same stiffness as in rigor, whereas Schoenberg et al (1985) report no change between PPi solution and rigor. My own samples showed a slight decrease in the stiffness as measured by imposing a series of rapid stretches on the muscle, though as already implied above, stiffness is related to tension. So the fall in tension could account for the change in stiffness in both this study and that of White (see Fig 10B of White (1970)). Note Schoenberg measured stiffness at nearly constant tension in his samples and saw no stiffness difference.

White (1970) also noted that at high rates of stretch the stiffness in PPi appeared to be at the higher value of 60% rigor stiffness. However, if the rate of stretch was decreased to a very low value (0.25% muscle length min^{-1}), then the stiffness decreased to a value similar to that seen with ATP. An experiment was performed in which decreasing rates of stretch were applied and the apparent stiffness measured in rigor (Fig 2a) and with 5mM PPi (Fig 2b). These too showed that the stiffness decreased very slightly with decreasing stretch rate in rigor, but this effect was greatly increased in the presence of PPi.

Both the decrease in stiffness with decreased rate of stretch and the fall in tension on exposure to PPi have been explained by a decrease in the affinity of S1 heads for the thin filaments, leading to the suggestion that the heads are in rapid equilibrium with thin filaments (White (1970), Schoenberg and Eisenberg (1985)).

In conclusion then, the glycerinated specimens used in the EM and X-ray diffraction studies show similar behaviour in terms of stiffness and tension on exposure to PPi as previous experiments reported in the literature. As such, the biochemical and mechanical

interpretations of these previous studies are considered to apply to the samples used in this thesis.

REFERENCES.

ALDOROTY R.A. and APRIL E.W. (1984). Donnan potentials from striated muscle liquid crystals - A-band and I-band measurements. Biophys.J. 46:769-779.

ALDOROTY R.A., GARTY N.B. and APRIL E.W. (1985). Donnan potentials from striated muscle liquid crystals - sarcomere length dependence. Biophys.J. 47:89-96.

APRIL E.W., BRANDT P.W. and ELLIOTT G.F. (1972). The myofilament lattice II. The effects of osmotic strength, ionic concentration and pH upon the unit-cell volume. J.Cell.Biol. 53:53-65.

APRIL E.W. and WONG D. (1976). Non-isovolumetric behaviour of the unit cell of skinned striated muscle fibres. J.Mol.Biol 101:107-114.

BAGSHAW C.R. (1982). Outline studies in Biology - Muscle Contraction. J.W. Arrowsmith Ltd, Bristol, U.K.

BARTELS E.M. and ELLIOTT G.F. (1981). Donnan potentials from the A- and I-bands of skeletal muscle, relaxed and in rigor. J.Physiol 317:105P.

BARTELS E.M. and ELLIOTT G.F. (1982). Donnan potentials in rat muscle: differences between skinning and glycerination. J.Physiol. 327:72-73P.

BARTELS E.M. and ELLIOTT G.F. (1983). Donnan potentials in glycerinated rabbit skeletal muscle: the effects of nucleotides and of pyrophosphate. J.Physiol 343:32-33P.

BARTELS E.M. and ELLIOTT G.F. (1984a). Donnan potentials from contracting muscle. J.Mus.Res.Cell.Motility. 5:227.

BARTELS E.M. and ELLOITT G.F. (1984b). Changes in the Donnan potential from the A- and I-bands of contracting skeletal muscle. Acta.Physiol.Scand 121(3):A20.

BARTELS E.M. and ELLIOTT G.F. (1985). Donnan potentials from the A- and I-band of glycerinated and chemically skinned muscle, relaxed and in rigor. Biophys.J. 48:61-76.

BEHRMAN E.J. (1985). The chemistry of Osmium tetroxide fixation. In "Science of biological specimen preparation" pp1-5. SEM Inc, AMF O'Hare (Chicago).

BERGMAN R.A. (1983). Ultrastructural configuration of sarcomeres in passive and contracted frog sartorius muscle. Am.J.Anatomy. 166: 209-222.

BENDALL.J.R. (1969). Muscles, molecules and movement. Heineman Educational books Ltd. London.

BISHOP W.H and RICHARDS F.M. (1968). Isoelectric point of a protein in the crosslinked crystalline state: β-Lactoglobulin. J.Mol.Biol. 33: 415-421.

BOYDE A. and BOYDE S. (1980). Further studies of specimen volume changes during processing for SEM: including some plant tissue. Scanning Electron Microscope II: 117-131.

BRANDT P.W., REUBEN J.P., LOPEZ.E. and GRUNDFEST.H. (1967). The relationship between myofilament packing density and sarcomerre length in frog striated muscle. J.Cell.Biol. 33:255-264.

BRANDT P.W., COX R.N., KAWAI M., and ROBINSON T. (1982). Regulation of tension in skinned muscle fibres. J.Gen.Physiol. 79: 997-1016.

BRENNER B., SCHOENBERG M., CHALOVITCH J.M., GREENE L.E. and EISENBERG E. (1982). Evidence for cross-bridge attatchment in relaxed muscle at low ionic strength. Proc.Natl.Acad.Sci.USA. 79:7288-7291.

BRENNER B., YU L.C., and PODOLSKY R.J. (1984). X-ray diffraction evidence for cross-bridge formation in relaxed muscle fibres at various ionic strengths. Biophys.J. 46:299-306.

BRENNER B. and YU L.C. (1985). Equatorial X-ray diffraction from single skinned rabbit psoas fibres at various degrees of activation. Biophys.J. 48: 829-834.

BRENNER B., YU L.C., GREENE L.E., EISENBURG E., and SCHOENBERG M. (1986). Ca^{2+} sensitive cross-bridge dissociation in the presence of magnesium pyrophosphate in skinned rabbit psoas fibes. Biophys.J. 50:1101-1108.

CARLSEN F., KNAPPEIS G.G. and BUCHTHAL F. (1961). Ultrastructure of the resting and contracted skeletal muscle fibre at different degrees of stretch. J.Biophys.Biochem.Cyt. 11: 95-117.

CAUSTON B.E. (1985). Does the embedding chemistry interact with tissue ? Science of Biologial Tissue Preparation (pp 209-214) SEM inc AMF O'Hare (Chicago).

CHAMBERS R.W., BOWLING M.C., and GRIMLEY P.M. (1968). Glutaraldehye fixation in routine pathology. Tissue and Cell 85: 18-30

COETZEE J. and VAN DER MERWE C.F. (1985). Penetration rates of Glutaraldehyde in various buffers into plant tissues and gelatin gels. J.Micros. 137(2): 129-136.

COLLINS E.W. and EDWARDS C. (1971). Role of the Donnan equilibrium in the resting potentials in glycerol-extracted muscle. Am.J.Physiol 4:1130-1133.

COOKE P. (1985). A periodic cytoskeletal lattice in striated muscle. In "Gene expression in muscle." pp 287-313. Ed Strohman R.C. and Wolf S.

CRAIG R., TRINICK J. and KNIGHT P. (1986). Discrepancies in lengths of myosin head. Nature 320:688.

DUBOCHET J., and McDOWALL A.W. (1984). Frozen hydrated specimens. Science of Biological Specimen Preparation 61-70. SEM inc AMF O'Hare (Chicago) USA.

EDELMAN H. and PADRON R. (1984). X-ray diffraction evidence that actin is a 100 A filament. Nature 307:56-58.

EISENBERG B.R., and MOBLEY B.A. (1975). Size changes in single muscle fibres during fixation and embedding. Tissue and Cell 7(2): 383-387.

ELLIOTT G.F., LOWY.J. and WORTHINGTON C.R. (1963). An X-ray and light diffraction study of the filament lattice of striated muscle in the living state and in rigor. J.Mol.Biol. 6: 295-305.

ELLIOTT G.F. (1967). Low-angle X-ray diffraction studies of living striated muscle during contraction. J.Mol.Biol. 25:31-45.

ELLIOTT G.F. (1968). Force-balance and stability in hexagonally packed polyelectrolyte systems. J.Theoret.Biol. 21:71-87.

ELLIOTT G.F., ROME E.M. and SPENCER.M. (1970). A type of contraction hypothesis applicalble to all muscles. Nature 226:417-420.

ELLIOTT G.F. (1973a). The muscle fibre: Liquid-crystalline and hydraulic aspects. Ann.N.Y.Acad.Sci. 204:564-574.

ELLIOTT G.F. (1973b). Donnan and osmotic effects in muscle fibres without membranes. J.Mechanochem.Cell.Motility. 2:83-89.

ELLIOTT G.F., GOODFELLOW J.M. and WOOLGAR A.E. (1980). Swelling studies of bovine corneal stroma without bounding membrane. J.Physiol. 298:453-470.

ELLIOTT G.F., SAYERS Z. and TIMMINS.P.A. (1982). Neutron diffraction studies of the corneal stroma. J.Mol.Biol 155:389-393.

ELLIOTT G.F. and BARTELS E.M. (1982). Donnan potential measurements in extended hexagonal polyelectrolyte gels such as muscle. Biophys.J. 38:195-199.

ELLIOTT G.A., BARTELS E.M. and HUGHES R.A. (1985). In "Electrical double layers in Biology". Ed Blank M., Plenum Publishing Corp, New York.

EREMIA D. (1985). Is there continuity of filaments in the sarcomere? J.Theor.Biol. 112:177-181.

FRANKS A. (1955). An optically focussing X-ray diffraction camera. Proc.Phys.Soc(London) B, 68:1054-1063.

GOLDMAN Y.E., MATSUBARA I. and SIMMONS R.M. (1979). Lateral filamentary spacing in frog skinned muscle fibres in the relaxed and rigor states. J.Physiol 295:80-81P.

GOLDSPINK G. (1972). Postembryonic growth and differentiation of striated muscle. In "The structure and function of muscle. Volume 1 part 1". Ed Bourne G.H. Academic press.

GUINIER A. (1963). In "X-ray diffraction". W.H.Freeman and Company pp 151-172 and 297-304.

GULATI J. and BABU A. (1985). Critical dependance of calcium activated force on width in highly compressed skinned fibres of the frog. Biophys.J. 48:781-787.

HABEEB A.F.S.A., and HIRAMOTO R. (1968). Reaction of proteins with Glutaraldehyde. Arch.Biochem and Biophys. 126: 16-26.

HANSON J. and HUXLEY H.E. (1955). The structural basis of contraction in striated muscle. Symp.Soc.Exp.Biol. 9:228-264.

HARRINGTON W.F. (1971). A mechanochemical mechanism for muscle contraction. Proc.Natl.Acad.Sci.U.S.A. 68:685-689.

HARRINGTON W.F. (1981). Muscle contraction. Oxford/Carolina Biology readers 114. Scientific Piblications Div., Carolina Biological Supply Co.

HASELGROVE J.C., STEWART M. and HUXLEY H.E. (1976). Cross-bridge movement during muscle contraction. Nature 261: 606-608.

HASLAM E. (1966). In " The Chemistry of vegetable tannins". Academic Press London.

HAWKINS R.J. and APRIL E.W. (1981). X-ray measurements of the bulk modulus of the myofilament liquis crystal in striated muscle. Mol.Cryst.Liq.Cryst. 75:211-216.

HAWKINS R.J. and APRIL E.W. (1983a). Liquid crystals in living tissues. Adv.Liq.Cryst. 6:243-264.

HAWKINS R.J and APRIL E.W. (1983b). The planar deformation behaviour of skinned striated muscle fibres. Mol.Cryst.Liq.Cryst. 101:315-328.

HIGUCHI H. and UMAZUME Y. (1986)- Lattice shrinkage with increased resting tension in stretched, single skinned fibres of frog muscle. Biophys.J. 50:385-389.

HOPWOOD D. (1972). Theoretical and practical aspects of glutaraldehyde fixation. Histochem.J. 4: 267-303.

HOROWITS R., KEMPNER E.S., BISHER M.E. nad PODOLSKY R.J. (1986). A physiological role for titin and nebulin in skeletal muscle. Nature 323:160-164.

HUXLEY A.F. and NIEDERGERKE R. (1954). Interferance microscopy of living muscle fibres. Nature 173:971-973.

HUXLEY A.F. and SIMMONS R.M. (1971). Proposed mechanism of force generation in striated muscle. Nature 233:533-538.

HUXLEY A.F. (1980). Reflections on muscle. Liverpool University Press, Liverpool.

HUXLEY H.E. and HANSON J. (1954). Changes in the cross-striations of muscle during contraction and stretch and their structural implications. Nature 173:973-976.

HUXLEY H.E. (1963). Electron microscope studies on the structure of natural and synthetic protein filaments from striated muscle. J.Mol.Biol. 7:281-308.

HUXLEY H.E. and BROWN W. (1967). The low-angle X-ray diagram of vertebrate striated muscle and its behaviour during contraction and rigor. J.Mol.Biol. 30:383-434.

HUXLEY H.E. (1969). The mechanism of muscular contraction. Science 164:1356-1366.

KING J.A., WOODSIDE W. and McGUCKEN P.V. (1974). Relationship between pH and antibacterial activity of Glutaraldehyde. J.Pharm.Sci. 63: 804-805.

KNIGHT P. and TRINICK J. (1984). Structure of the myosin projections on native thick filaments fron vertebrate skeletal muscle. J.Mol.Biol. 177:461-482.

KRASNER B.H. and KUSHMERICK M.J. (1983). Tension and ATPase rate in steady state contractions of rabbit soleus fibre segments. Am.J.Physiol. 245: C405-414.

KRASNER B.H. and MAUGHAN.D. (1984). The relationship between ATP hydrolysis and active force in compressed and swollen skinned muscle fibres of the rabbit. Pflug.Arch. 400:160-165.

KRETZSCHMAR K.M., MENDELSON R.A. and MORALES M.F. (1978). Investigation of the shape and size of myosin subfragment 1 using small-angle X-ray scattering. Biochemistry 17(12):2314-2318.

KREUGER J.W. and LONDON B. (1985). Morphological changes in the cardiac sarcomere during extreeme active and passive shortening. Biophys.J. 47:130a.

LEE R.M.K.W., GARFIELD R.E., FORREST J.B., and DANIEL E.E. (1979). The effects of fixation, dehydration, and critical point drying on the size of cultured smooth muscle cells. Scanning Electron Microscope III: 439-448.

LEE R.M.K.W. (1984). A critical appraisal of the effects of fixation, dehydration and embedding on cell volume. Science of Biological Specimen Preparation 61-70. SEM inc, AMF O'Hare (Chicago) USA.

LOEWY A.G., WILSON F.J., TAGGART N.M., GREENE E.A., FRASCA P., KAUFMAN H.S. and SORRELL M.J. (1983). A covalently cross-linked matrix in skeletal muscle fibres. Cell Motility 3:463-483.

MAEDA Y. (1978). Birefringence of oriented thin filaments in the I-bands of crab striated muscle and comparison with the flow birefrincence of reconstituted thin filaments. Eur.J.Biochem. 90:113-121.

MAGID A. and REEDY M.K. (1980). X-ray diffraction observations of chemically skinned frog skeletal muscle processed by an improved method. Biophys.J. 30:27-40.

MAGID A., TING-BEALL H.P., CARVELL M., KONTIS T. and LUCAVECHE C. (1984). Connecting filaments, core filaments and side-struts: a proposal to add three new load-bearing structures ot the sliding filament model. In "Contractile mechanisms in muscle." pp 307-328. Eds Pollack G.H. and Sugi H. Plenum Publishing Corp, New York.

MATSUBARA I. and ELLIOTT G.F. (1972). X-ray diffraction studies on skinned fibres ao frog skeletal muscle. J.Mol.Biol. 72:657-669.

MATSUBARA I., YAGI N. and HASHIZUME H. (1975). Use of an X-ray television for diffraction of the frog striated muscle. Nature 255: 728-729.

MATSUBARA I., GOLDMAN Y.E., and SIMMONS R.M. (1984a). Changes in the lateral filament spacing of skinned muscle fibres when cross-bridges attach. J.Mol.Biol. 173:15-33.

MATSUBARA I., UMAZUME Y. and YAGI N. (1984b). Lateral shrinkage of the myofilament lattice in chemically skinned muscles during contraction, In "Contractile mechanisms in muscle." pp711-720. Eds Pollack G.H. and Sugi H. Plenum Publishing Corp, New York.

MATSUBARA I., UMAZUME Y. and YAGI.N. (1985). Lateral filamentary spacing in chemically skinned murine muscles during contraction. J.Physiol. 360:135-148.

MAUGHAN D.W. and GODT R.E. (1981). Radial forces within muscle fibres in rigor. J.Gen.Physiol. 77: 49-64.

MAUPIN-SZAMIER P. and POLLARD T.D. (1979). Actin filament destruction by Osmium Tetroxide. J.Cell.Biol. 77: 837-851.

McDOWALL A.W., HOFMANN W., LEPAULT J., ADRIAN M. and DUBOCHET J. (1984). Cryoelectron microscopy of vitrified insect flight muscle. J.Mol.Biol. 178: 105-111.

McLACHLAN A.D. (1984). Structural implications of the myosin amino acid sequence. Ann.Rev.Biophys.Bioeng. 13: 167-189.

MENDELSON R. (1985). The length of myosin subfragment 1. Nature 318:20.

MILLER A. and WOODHEAD-GALLOWAY J. (1971). Long range forces in muscle. Nature 229:470-473.

MILLMAN B.M. and NICKEL B.G. (1980). Electrostatic forces in muscle and cylindrical gel systems. Biophys.J. 32:49-63.

MILLMAN B. (1981). Filament lattice forces in vertebrate striated muscle: relaxed and in rigor. J.Physiol. 320:118P.

MILLMAN B., WAKABAYASHI K., and RACEY J.R. (1983). Lateral forces in the filament lattice of vertebrate striated muscle in the rigor state. Biophys.J. 41: 259-267.

MOREL M.M., BAKER R.F., and WAYALND H. (1971). Quantation of human red blood cell fixation by Glutaradehyde. J.Cell.Biol. 48: 91-100.

NAYLOR G.R.S. (1977). X-ray and microelectrode studies of glycerinated rabbit psoas muscle. PhD thesis, Open University, Milton Keynes, UK.

NAYLOR G.R.S. (1982). Average electrostatic potential between the filaments in striated muscle and its relation to a simple Donnan potential. Biophys.J. 38:201-204.

NAYLOR G.R.S., BARTELS E.M., BRIDGEMAN T.D. and ELLIOTT G.F. (1985). Donnan potentials in rabbit psoas muscle in rigor. Biophys.J. 48:47-59.

OFFER G. and TRINICK J. (1983). On the mechanism of water holding in meat: the swelling and shrinking of myofibrils. Meat Science 8:245-281.

PAGE S.G. and HUXLEY H.E. (1963). Filament lengths in striated muscle. J.Cell.Biol. 19: 369-390.

PAGE S. (1968). Fine structure of tortoise skeletal muscle. J.Physiol. 197:709-715.

PEPE F.A. (1979). In "Motility and cell function." pp 103-116. Academic press.

PERRIN D.D. and SAYCE I.D. (1967). Computer calculation of equilibrium concentrations in mixtures of metal ions and complexing species. Talenta 14:833-842.

PODOLSKY R.J., St ONGE R., YU L.C. and LYMN R.W. (1976). X-ray diffraction of actively shortening muscle. Proc.Nat.Acad.Sci.USA. 73: 813-817.

PODOLSKY R.J., NAYLOR G.R.S., and ARATA.T. (1982). Cross-bridge properties in the rigor state. In "Basic biology of muscles" ed Twarog B.M., Levine R.J.C., and Dewey M.M. Raven press, New York pp 79-89.

POLLACK G.H. (1983). The cross-bridge theory. Physiol.Rev. 63(3):1049-1113.

POULSEN F.R. and LOWY.J. (1983). Small angle X-ray scattering from myosin heads in relaxed and rigor frog skeletal muscles. Nature 303: 146-152.

RASMUSSEN K.E., and ALBRECTSEN.J. (1974). Glutaraldehyde. The influence of pH, temperature and buffering on the polymeriation rate. Histochemistry 38:19-26.

REEDY M.K. (1968). Ultrastructure of insect flight muscle. I. screw sense and structural grouping in the rigor cross-bridge lattice. J.Mol.Biol. 31: 155-176.

REEDY M.K. and BARKAS A.E. (1974). Disordering of the myofibril structure due to fixation, dehydration and embedding. J.Cell.Biol. 63: 282a.

REEDY M.K. (1976). Preservation of X-ray patterns from frog sartorius muscle prepared for electron microscopy. Biophys.J. 16: 126a.

REEDY M.K, GOODY R.S., HOFMANN W., and ROSENBAUM G. (1983a). Co-ordinated electron microscopy and X-ray studies of glycerinated insect flight muscle. I.X-ray diffraction monitoring during preparation for E.M of muscle fibres fixed in rigor, in ATP and in AMPPNP. J.Mus.Res.Cell.Mot. 4: 25-53.

REEDY C.M., REEDY M.K. and GOODY R.S. (1983b). Coordinated electron microscopy and X-ray studies of insect flight muscle. II. Electron microscopy image reconstruction of muscle fibres fixed in rigor, ATP and in AMPPNP. J.Musc.Res.Cell.Mot. 4: 55-81.

ROME E. (1967). Light and X-ray diffraction studies of the filament lattice of striated muscle. PhD thesis, University of London.

ROME E. (1968). X-ray diffraction studies of the filament lattice of striated muscle in various bathing media. J.Mol.Biol. 37: 331-344.

SCHOENBERG M. (1980). Geometrical factors influencing muscle force development II. Radial forces. Biophys.J. 30:69-78.

SCHOENBERG M. and EISENBERG E. (1985). Muscle cross-bridge kinetics in rigor and in the presence of ATP analogues. Biophys.J. 48: 863-871.

SHAPIRO P.J., TAWADA K. and PODOLSKY R.J. (1979). X-ray diffraction of skinned muscle fibres. Biophys.J. 25:18a.

SJOSTROM M.M. and SQUIRE J. (1977). Fine structure of the A-band in cryosections. The structure of the A-band of human skeletal muscle fibres from ultra-thin cryo-sections negativly stained. J.Mol.Biol 109:49-68.

SQUIRE J. (1973). General model of myosin filament structure III. Molecular packing arrangements in myosin filaments. J.Mol.Biol 77:291-323.

SQUIRE J. (1981). In "The structural basis of muscular contraction". Plenum press, New York, USA.

STENN K., and BAHR G.F. (1970). Specimen damage caused by the beam of the Transmission Electron Microscope, a correlative reconsideration. J.Ult.Res. 31:526-550.

STEWART M., KENSLER R.W. and LEVINE R.J.C. (1985). Three dimensional reconstruction of thick filaments from Limulus and scorpion muscle. J.Cell.Biol. 101:402-411.

STROMER M.H., HARTSHORNE D.J. and RICE R.V. (1967). Removal and reconstruction of Z-line material in a striated muscle. J.Cell.Biol. 35:C23-C28.

TAWADA K. and KIMURA M. (1986). Stiffness of carbodiimide cross-linked glycerinated muscle fibres in rigor and relaxing solution at high salt concentrations. J.Mus.Res.Cell.Motility 7:339-350.

THEISSEN G., THEISSEN H., DOWIDAT H.J., LUCIANO L., and REALE E. (1970). Die differen der ^{59}Fe-markierten Hamoglobins, ein artefukt der Glutaraldehyde-fixierung. Histochemie 23: 171-175.

TONIMATSU Y., JANSEN E.F., GAFFIELD W., and OLSON A.C. (1971). Physical chemical observations on the α-chymotrypsin glutaraldehyde system during formation of an insolluble derivative. J.Colliod.Interface.Sci. 36: 51-64.

TREGEAR R.T. and MARSTON S.B. (1979). The cross-bridge theory. Ann.Rev.Physiol. 41:723-736.

TSUKITA S. and YANO.M. (1985). Actomyosin structure in contracting muscle detected by rapid freezing. Nature 317: 182-184.

UENO H. and HARRINGTON W.F. (1974). Cross-bridge movement and the conformational state of the myosin hinge in skeletal muscle. J.Mol.Biol. 149: 619-640.

UMAZUME Y. and KASUGA N. (1984). Radial stiffness of frog skinned muscle fibres in relaxed and rigor conditions. Biophys.J. 45:783-788.

UMAZUME Y., ONODERA S., and HIGUCHI H. (1986). Width and lattice spacing in radially compressed frog skinned muscle fibres at various pH values, magnesium ion concentrations and ionic strengths. J.Musc.Res.Cell Mobility 7:251-258.

VAINSHTEIN B.K. (1966). In "Diffraction of X-rays by chain molecules". Elsevier, pp 203-240.

VERWEY E.J.W. and OVERBEEK J.TH.G (1948). Lyophobic colloids. Elsevier Publishing Company.

WALKER E.M. and RANDOLPH SCHRODT G. (1969). Filament lengths and distribution of staining material in the I-bands of rat skeletal muscle. Am.J.Phys.Med. 48: 178-192.

WANG K. and RAMIREZ-MITCHELL R. (1983). A network of transverse and longitudinal intermediate filaments is associated with sarcomeres of adult vertebrate skeletal muscle. J.Cell.Biol. 96:562-570.

WANG K. (1984). Cytoskeletal matrix in striated muscle: the role of titin, nebulin and intermediate filaments. In "Contractile mechanisms in muscle." pp 285-305. Eds Pollack G.H. and Sugi H. Plenum Publishing Corp, New York.

WHITE D.C.S. (1970). Rigor contraction and the effect of various phosphate compounds on glycerinated insect flight and vertebrate muscle. J.Physiol. 208: 583-605.

WINKELMANN D.A., MEKEEL H. and RAYMENT I. (1985). Packing analysis of crystalline myosin subfragment-1. Implications for the size and shape of the Myosin head. J.Mol.Biol. 181:487-501.

WINTERTON R.H.S. (1970). Van Der Waals forces. Contemp.Phys 11(6):559-574.

YAGI N. and MATSUBARA I. (1977). The equatorial X-ray diffraction patterns of crustacean striated muscles. J.Mol.Biol. 117:797-803.

YU L.C., STEVENS A.C., NAYLOR.G.R.S., GAMBLE R.C. and PODOLSKY R.J. (1985). Distribution of mass in relaxed frog skeletal muscle and its redistribution upon activation. Biophys.J. 47: 311-321.